LEADING THE WAY
KHALĪFAH · AMĀNAH · IQRA' · RAHMATAN LIL-ĀLAMĪN
LEADING THE WORLD
AN INTERNATIONAL AWARD-WINNING INSTITUTION FOR SUSTAINABILITY
Kulliyyah of Engineering
for sustainable future

IIUM ENGINEERING CONGRESS 2023 (IEC '23)

PROCEEDINGS
Volume 1 Number 1 2023

IIUM Engineering Congress Proceedings Volume 1 Issue 1 2023

International Conference on Chemical Engineering & Sustainability 2023 (ICCHES 2023)

6th International Conference on Mechanical, Automotive and Aerospace Engineering (ICMAAE '23)

9th International Conference on Computer and Communication Engineering (ICCCE 2023)

6th International Conference on Engineering Professional Ethics and Education (ICEPEE '23)

e ISBN 978-967-25875-1-4

9 789672 587514

Kulliyyah of Engineering, International Islamic University Malaysia

IIUM Engineering Congress Proceedings

Volume 1 Issue 1 2023

Editors

AHM Zahirul Alam
Md Zahangir Alam
Mohd. Sultan Ibrahim Bin Shaik Dawood

Editorial Notes

Welcome to this issue of our engineering journal, where we celebrate the rich diversity of our field, encompassing chemical, aerospace, mechanical, automotive, computer and communication engineering, and Engineering Professional Ethics and Education.

With each discipline contributing its progress, in this issue, we explore the latest developments and achievements across these diverse engineering domains, highlighting the incredible impact engineers have on our world.

From the precise processes of chemical engineering to the soaring wonders of aerospace, the practical marvels of mechanical engineering, the sustainable strides in automotive engineering, and the digital frontiers of computer and communication engineering, we showcase the breadth of possibilities that engineering offers.

As you dive into the articles within, take a moment to appreciate the collective effort of engineers across these disciplines, and let's continue to celebrate the diversity that makes engineering such a vibrant and dynamic field.

Thank you for your unwavering support and engagement with IIUM Engineering Congress Proceedings (IIUMECP). Together, let us continue to explore the horizons of engineering excellence while upholding the ethical principles that guide our journey.

Published by

Kulliyyah of Engineering
International Islamic University Malaysia
P.O. Box 10, 50728 Kuala Lumpur, Malaysia

Web: https://kulliyyah.iium.edu.my/koe/

e ISBN 978-967-25875-1-4

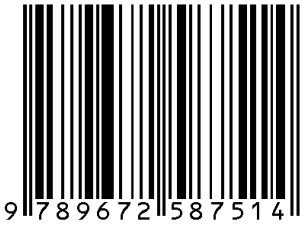

IIUM ENGINEERING CONGRESS PROCEEDINGS

Volume 1 Issue 1 2023

e ISBN 978 -967-25875-1-4

Copyright Notice

Consent to publish: The Author(s) agree to publish their articles with Faculty of Engineering, International Islamic University Malaysia.

Declaration: The Author(s) declare that the article has not been published before in any form and that it is not concurrently submitted to another publication, and also that it does not infringe on anyone's copyright. The Author(s) holds the Faculty of Engineering, International Islamic University Malaysia and Editors of the journal harmless against all copyright claims.

Transfer of copyright: The Author(s) hereby agree to transfer the copyright of the article to International Islamic University Malaysia, which shall have the non-exclusive and unlimited right to publish the article in any form, including in electronic media. For articles with more than one author, the corresponding author confirms that he/she is authorized by his/her co-author(s) to grant this transfer of copyright.

The IIUM Engineering Congress Proceedings follows the open access policy.

All articles published open access will be immediately and permanently free for everyone to read, download, copy and distribute even for commercial purposes.

Table of Contents

MESSAGE FROM THE PRESIDENT

YBhg. Tan Sri Samsudin Osman

President

International Islamic University Malaysia

Assalamu'alaikum wrt. wbt.

A very warm welcome to all participants of the IIUM Engineering Congress 2023 (IEC'23).

This event marks a significant milestone in our academic journey, as we come together to celebrate the remarkable achievements and advancements in the field of engineering.

This year the IIUM Engineering congress features four conferences in different fields of Engineering, namely, the 6th International Conference on Mechanical, Automative and Aerospace Engineering (ICMAAE '23), the 9th International Conference on Computer and Communication Engineering (ICCCE 2023), the 6th International Conference on Engineering Professional Ethics and Education (ICEPEE '23), and the International Conference on Chemical Engineering & Sustainability 2023 (ICCHES 2023).

Today, as we gather under the theme "Engineering for a Sustainable Future", we are reminded of the critical role engineers play in shaping our world. The challenges we face as a global community are unprecedented, from climate change and resource scarcity to rapid urbanization and technological disruption. These challenges demand innovative solutions and a concerted effort to create a sustainable future for generations to come.

At IIUM, we have always recognized the importance of engineering in driving societal progress and addressing pressing global issues. Our engineering programs have consistently produced graduates who possess not only technical competence but also a deep understanding of ethical responsibility and the need to contribute positively to society.

As we embark on this congress, I urge all participants to embrace the spirit of collaboration, exchange of ideas, and intellectual curiosity. This platform serves as an opportunity for us to engage in meaningful dialogue, challenge conventional thinking, and push the boundaries of knowledge. Let us seize this occasion to cultivate interdisciplinary partnerships, foster innovation, and explore new frontiers of engineering.

MESSAGE FROM THE PRESIDENT

Together, we can create a better world through our dedication to innovation, sustainability, and ethical engineering practices. I encourage each and every one of you to embrace the challenges that lie ahead, to push the boundaries of what is possible, and to remain committed to the pursuit of knowledge and excellence.

I would like to express my heartfelt gratitude to the organizing committee for their tireless efforts in putting together this exceptional congress IEC'23. Your dedication and commitment to fostering academic excellence and intellectual growth are truly commendable. I would also like to extend my appreciation to the faculty members, industry professionals, and guest speakers for gracing us with their presence and sharing their expertise.

Thank you once again to the organizing committee, the faculty members, the distinguished guests, and all the participants for making this congress a resounding success. May Allah bless our efforts, guide our paths, and grant us success in all our endeavors.

Wassalamualaikum warahmatullahi wabarakatuh.

Tan Sri Samsudin Osman
President of International Islamic University Malaysia

MESSAGE FROM THE RECTOR

Professor Emeritus Tan Sri Dato' Dzulkifli Abdul Razak
Rector
International Islamic University Malaysia

Assalamu'alaikum Warahmatullahi Wabarakatuh

A warm welcome to the IIUM Engineering Congress 2023 keynote speakers and participants.

The main objective of organizing this congress is to provide an international technical forum for engineers, academicians, scientists and researchers to present results of ongoing research in various engineering areas, through the four conferences, namely, the 6th International Conference on Mechanical, Automative and Aerospace Engineering (ICMAAE '23), the 9th International Conference on Computer and Communication Engineering (ICCCE 2023), the 6th International Conference on Engineering Professional Ethics and Education (ICEPEE '23), and the International Conference on Chemical Engineering & Sustainability 2023 (ICCHES 2023). This event serves as a testament to our commitment to academic excellence, innovation, and the pursuit of knowledge in the field of engineering.

The challenges we face as a global society demand innovative solutions, groundbreaking research, and the ability to adapt to a rapidly evolving technological landscape. At IIUM, we take great pride in our engineering programs, which have consistently produced graduates who possess not only technical expertise but also a deep sense of ethical responsibility, social consciousness, and a commitment to serving humanity. Our graduates are equipped with the skills and knowledge needed to address the complex challenges of our time and to contribute meaningfully to the sustainable development of our society.

I would like to express my deepest appreciation to the organizing committee in bringing this congress to fruition. Your hard work has created an exceptional platform for academic discourse, intellectual exchange, and the celebration of engineering achievements.

This congress provides an unparalleled opportunity for students, academics, and industry professionals to come together, collaborate, and share their research findings, innovative ideas, and practical experiences. It is a platform where minds can meet, where new partnerships can be formed, and where interdisciplinary collaborations can flourish.

I encourage all participants to make the most of this congress by actively engaging in discussions, attending the various sessions and workshops, and seizing the chance to learn from the wealth of knowledge and experience present here. This is an opportunity for us to expand our horizons, challenge conventional wisdom, and push the boundaries of what is possible in the field of engineering.

MESSAGE FROM THE RECTOR

As we navigate the complex challenges of our time, we must remember that our actions have far-reaching consequences. Our faith teaches us to be mindful of our responsibilities as stewards of the Earth, to strive for justice and fairness, and to seek solutions that uplift society as a whole. Let us be guided by these principles in our pursuit of engineering excellence and innovation.

In conclusion, I would like to extend my heartfelt gratitude to the organizing committee, the faculty members, the distinguished guests, and all the participants for their contributions to this congress 23. Your presence and active engagement demonstrate the collective commitment we share to advance the frontiers of knowledge and to create a better future for all.

May this congress serve as a catalyst for groundbreaking research, meaningful collaborations, and transformative ideas. May it inspire us to strive for excellence, ethical leadership, and responsible innovation. Together, let us engineer a future that is sustainable, inclusive, and in harmony with the values we hold dear.

I wish everyone a good deliberation and discussion and pray to Allah SWT for His blessing and guidance.

Wassalam,

Prof. Emeritus Tan Sri Dato' Dzulkifli Abdul Razak
Rector of International Islamic University Malaysia

MESSAGE FROM THE CONGRESS CHAIRMAN

Assoc. Prof. Dr. Sany Izan Ihsan
Dean
Kulliyyah of Engineering

Bismillahirrahmanirrahim
Assalamualaikum warahmatullahi wabarakatuh

It is my utmost pleasure to welcome all participants to the IIUM Engineering Congress 2023 (IEC'23). This year, in conjunction with the IIUM 40th Anniversary celebration, the IIUM Engineering Congress features four conferences in different fields of Engineering. These are 6th International Conference on Mechanical, Automotive and Aerospace Engineering (ICMAAE '23), the 9th International Conference on Computer and Communication Engineering (ICCCE 2023), the 6th International Conference on Engineering Professional Ethics and Education (ICEPEE '23), and the International Conference on Chemical Engineering & Sustainability 2023 (ICCHES 2023)

The main objective of organizing this congress is to provide a medium for institutions and industries to share ideas and knowledge, exchange information, innovations, and problem-solving techniques. With our tagline "For Sustainable Future", the Kulliyyah strive to play our role, particularly in engineering field, for the betterment and sustainability of future mankind, society, and the world at large. This congress would be a suitable avenue for us to showcase and share our knowledge and findings, besides providing an opportunity to expand our networking with colleagues for other places. We are proud to have good expertise in many engineering areas from all around the world and look forward to establishing meaningful collaborations for mutual benefits.

Since Covid-19 has become more manageable and online conference tools have been well established due to the pandemic situation, we decided to organize the congress in hybrid mode for the first time this year. We hope that this approach will provide us with both benefit of giving opportunity for participant from abroad to share their knowledge as well as providing the opportunity to have face-to-face discussions and networking opportunities, that has been missing in the past several years. Of course, we anticipate that conducting hybrid session will find new challenges, but we hope that the event will run smoothly to meet its objectives and all participants will be able to get full benefit.

I would like to take this opportunity to express my heartfelt appreciation to all parties who have directly and indirectly contributed towards the success of this auspicious event, especially the committed and passionate committee members. May Allah SWT reward you greatly for your good efforts.

Thank you very much for your participation and we welcome you again to IIUM Engineering Congress 2023.

Assoc. Prof. Dr. Sany Izan Ihsan
Chairman
IIUM Engineering Congress 2023

CONGRESS ORGANIZING COMMITTEE

CHAIRMAN	Sany Izan Ihsan
SECRETARY	Md. Hashim Selamat
SECRETARIAT	Nurhanina Rafa'i
	Ahmad Halfathuddin Yusof
TREASURER	Siti Zubaidah Mohamed Yusof
	Yun Eza Mohd. Radzi
CHAIRMAN OF ICCCE 2023	Md. Rafiqul Islam
CHAIRMAN OF ICCHES 2023	Mohammed Saedi Jami
CHAIRMAN OF ICMAAE 2023	Fadly Jashi Darsivan
CHAIRMAN OF ICEPEE 2023	Ani Liza Asnawi
PROMOTION AND WEBMASTER	Wan Mohd. Fazli Wan Nawawi
PUBLICATION	AHM Zahirul Alam
HEAD OF PROGRAMME	Md Zahangir Alam
HEAD OF REGISTRATION	Mohd Farid Aladdin
HEAD OF SOUVENIR	Nurhanina Rafa'i
HEAD OF SPONSORSHIP	Muhammad Saifuddin Mohamed Rehan
HEAD OF AUDIO VISUAL	Mohd Shahnan Zainal Abidin

KEYNOTE 1

HARMONIZING COMPUTER TECHNOLOGY, AI, AND ETHICAL ENGINEERING FOR A SUSTAINABLE FUTURES

Abstract: This keynote speech explores the intersection of computer technology, AI, and ethical engineering, emphasizing the need to address the ethical considerations that arise alongside technological advancements. It highlights the potential risks and benefits of these technologies and emphasizes the importance of ethical decision-making in their design and implementation. The speech emphasizes key principles of ethical engineering, interdisciplinary collaboration, and the role of education in nurturing a culture of ethical engineering. By harmonizing computer technology, AI, and ethical engineering, we can shape a sustainable future that aligns with our shared values and respects fundamental human rights.

Rafeek Ibrahim is a distinguished professional known for his remarkable contributions to the fields of engineering and management. With a diverse educational background and extensive experience in various leadership roles, he has made a significant impact on the global stage.

Rafeek's journey began with a solid academic foundation. He completed his undergraduate studies in Engineering, specializing in solid state physics. Driven by his passion for knowledge, he pursued a master's degree in the same field, delving deeper into the intricacies of solid state physics. However, he didn't limit himself to technical expertise alone. Recognizing the importance of business acumen in today's fast-paced world, Rafeek enrolled in an executive education program at Harvard Business School, focusing on data analytics, a crucial skill in the digital age.

Rafeek's professional career commenced in the field of IP Validation Engineering, where he honed his skills in ensuring the integrity and functionality of intellectual property. His expertise soon expanded to encompass Power Management, an area vital for optimizing energy usage and efficiency. With his extensive knowledge and experience in Power and Performance, Rafeek emerged as a subject matter expert in these domains.

Demonstrating his adaptability and leadership prowess, Rafeek held leadership positions in large engineering organizations across different countries. His expertise was sought after in the United States, Singapore, and Malaysia, where he led diverse teams of engineers and researchers. Through his strategic vision and effective management, Rafeek successfully steered these organizations towards groundbreaking achievements in research and development, as well as operational excellence.

As a testament to his contributions to the scientific community, Rafeek has published technical papers in prestigious journals such as IEEE and Springer. His research and findings have been shared and recognized in international conferences, further solidifying his reputation as an authority in his field. Moreover, Rafeek's commitment to innovation has resulted in the granting of two patents in the United States, highlighting his inventiveness and ability to translate ideas into tangible solutions.

Rafeek's dedication to fostering growth and knowledge extends beyond his own accomplishments. He actively participates as a mentor in the Intel Global Mentor Circle mentorship program, where he imparts his wisdom and guidance to senior leaders. Recognizing the importance of diversity and inclusion, Rafeek represents Malaysia in a global forum aimed at advocating for these values. As a member of the Intel Disability Leadership Council, he strives to create an inclusive environment that celebrates the unique contributions of individuals with disabilities.

In addition to his impressive professional achievements, Rafeek also serves as a consultant to the government, providing expertise on the Nation Robotics Roadmap. His valuable insights contribute to shaping policies and strategies in the field of robotics, furthering the nation's technological advancements. Moreover, Rafeek holds an advisory role at the Economic Planning Unit, where he helps shape R&D policies that drive innovation and economic growth.

Recognized for his expertise and leadership, Rafeek sits on the University Advisory Board for multiple universities globally. His involvement in these esteemed institutions allows him to contribute to educational and research initiatives, providing guidance and insight to shape the future workforce in engineering and technology.

Throughout his career, Rafeek Ibrahim has seamlessly blended his technical expertise with his management skills, making him a trailblazer who bridges the gap between engineering and business. His commitment to research and development, combined with his strategic leadership, has paved the way for innovation and growth in the organizations he has led.

KEYNOTE 2

THE TREND AND IMPACT OF COMPUTER TECHNOLOGIES TO TELECOMMUNICATION

Abstract: With the advancement of computer technologies, we see the increasing capabilities of telecommunication to connect, serve and impact lives of individuals and businesses. We will take a quick look on how we got here, and what impact has it made. Also looking forward, what we would be expecting computer technologies to have impact on how we deliver and use telecommunication.

Tan Cheng Peng, the Acting Chief Technology Strategy Officer, Maxis, is accountable for our technology strategy roadmap to ensure technology and network leadership in anticipation of industry trends and direction, with the right and optimum technologies, network features, capabilities, architecture to meet our current and future needs. He leads a team of technologists to develop technology strategy and long range network plan along the vectors of innovation, service quality, business objectives and customer experience by ensuring right technology & investment at the right time and right place with the view to increase network efficiency and performance while minimise cost, rework and single point of failure.

KEYNOTE 3

MALAYSIA RENEWABLE ENERGY ROADMAP

Abstract: Moving forward, Malaysia aims to achieve a higher RE growth, from the existing 23% or 8.45 GW RE in its power installed capacity. Malaysia Renewable Energy Roadmap (MyRER) projected to increase the share of RE to 31% or 12.9 GW in 2025, and 40% or 18.0 GW in 2035. The RE Initiatives under this roadmap are expected to support Malaysia's commitment to greenhouse gas (GHG) emission reduction under the Paris Agreement led by the United Nations Framework Convention on Climate Change (UNFCCC). Malaysia's global climate commitment is to reduce its economy-wide carbon intensity (against GDP) of 45% in 2030 compared to 2005 level. Realization of the Government's vision is crucial in supporting the nation to achieve its Nationally Determined Contributions (NDC) targets. This talk will describe the identified resource potential, strategies, key actions, opportunities, current and future scenarios.

Mr. Saiful Hakim bin Abdul Rahman, has been in the utility and energy related business for over 28 years. He started his career with Distribution TNB scholar and served the distribution division for 17 years which provides him with vast experience in Distribution Network business. He then moved to United Kingdom and worked with Scottish and Southern Energy (SSE), one of the big 6 utilities in the UK based in Glasgow. Whilst in SSE, he was involved in Business Planning, Regulatory Reporting and Compliance, Asset Management and supporting the grid connections for Renewable Energy under the Transmission business. He worked closely with OFGEM, the Regulator for the UK utilities during that period in developing the Regulatory Reporting for the RIIO-T1 Regulatory Period. He developed his interest and enthusiasm on Renewable Energy whilst working there. Later he joined Landis+Gys AG, a Swiss based energy management company developing business on energy management solution such as smart metering and smart grid. Mr. Saiful Hakim obtained his Bachelor of Engineering in Electrical & Electronic Engineering from University of Brighton, United Kingdom in 1993 and MBA (Strategic Management) from Aston University, United Kingdom in 2011. During his MBA time he also attended Audencia Business School, Nantes in France for lectures.

KEYNOTE SPEAKERS ICCHES 2023

DECARBONIZATION TECHNOLOGIES FOR THE NATURAL GAS PROCESSES AS THE TRANSITION ENERGY SOURCE

Abstract: Gas to Liquid (GTL) conversion of natural gas to synthetic fuels (Syncrude) expands the value-chain of natural gas utilization where plants like the Bintulu and the Pearl GTL plants are typical cases. However, the CO_2 emissions from GTL processes, estimated at 314 kgCO_2/bbl. Syncrude, negatively impact the carbon footprint of the ultra-clean fuels produced from the GTL plant. Natural gas reforming is the first-step in the GTL plant and emits up to 60% of the CO_2 emission of the entire process. Therefore, decarbonization of the reforming process is imminent to reduce the CO_2 footprint of the GTL products. CARGEN-based reformer unit demonstrated a 40% reduction in CO_2 footprint compared to the benchmark reforming processes and is therefore considered an attractive candidate for decarbonizing the GTL and other chemical process plants. CARGEN-based reformer comprises two integrated reactors that sequentially convert natural gas and CO_2 to multi-walled carbon nanotubes (MWCNTs) and downstream compatible syngas. The co-production of MWCNTs presents significant economic incentives unmatched by the benchmark reforming processes while bringing CO_2 sustainability. In this work, we present a retrofitting case study of state-of-the-art Autothermal Reformer (ATR)-based GTL plant that produces 50,000 bbl./day of Syncrude using CARGEN-based technology. We demonstrate that the implementation of the CARGEN technology results in a net CO_2 emission of 84 kg CO_2/bbl. Syncrude, which is a 73% reduction compared to the 314 kg CO_2/bbl. emission of the ATR-based GTL plant. CARGEN implementation also requires a 79% less oxygen than the ATR-based GTL plant. Also, the additional functionality of CO_2 abatement results in the co-production of 243 kg MWCNTs/bbl., however, at a 61% higher methane requirement. Nevertheless, our comprehensive economics assessment entails the opportunity for 1.2 M USD/day additional revenue generation upon CARGEN implementation. Ultimately, the outcome of this study encourages CARGEN-based chemicals and refinery plants that co-produces syngas, hydrogen, and MWCNTs from CO_2 and natural gas as an integrated decarbonization solution.

Prof. Nimir Elbashir
Texas A&M University, Qatar

Professor Elbashir holds a joint appointment as a professor in the Chemical Engineering Program and the Petroleum Engineering Program at Texas A&M University at Qatar. He is the director of Texas A&M's Engineering Experiment Station Gas and Fuels Research Center (GFRC), a major research center involving 30 faculty members from the College Station and Qatar campuses of Texas A&M University (http://gfrc.tamu.edu/). He has extensive research and teaching experience from four countries worldwide, including his previous position as a researcher at BASF R&D Catalysts Center in Iselin, New Jersey. His research activities focus on designing advanced reactors, catalysts, and conversion processes for natural gas, coal, and CO_2 to ultraclean fuels and value-added chemicals. He has established several unique global research collaboration models between academia and industry, with research funds exceeding thirteen million dollars during the past eight years. He holds several U.S. and European patents and many scientific publications in peer-reviewed journals, conference papers, technical industry reports, and invited talks and conference presentations. The scholarship of his research activities has been recognized by awards from the Qatar Foundation, BASF Corp., Texas A&M University Engineering Experiment Station, Texas A&M University Qatar, the American Institute of Chemical Engineers, Shell, ORYX GTL Co., and others. Professor Elbashir has been elected as a member of the Sudanese National Academy of Sciences (SNAS) since 2022.

KEYNOTE 1

INNOVATING IN MALAYSIAN INDUSTRIAL ECOSYSTEMS

Abstract:

Innovating in Malaysian industrial ecosystems involves a combination of government support, industry-academia collaboration, technology adoption, sustainable practices, industry clustering, startup ecosystem, and skills development. These elements work together to enhance competitiveness, promote sustainable growth, and ensure the country's industrial sectors remain at the forefront of innovation.

Mr. Naguib Mohd Nor
BEng. Aerospace Engineering - UMIST, MSc. Aerospace Vehicle Design – Cranfield.

Naguib is CEO of Strand Aerospace Malaysia and President of Malaysia Aerospace Industry Association (MAIA). Naguib holds a BEng. Aerospace Engineering from UMIST and a MSc. Aerospace Vehicle Design from Cranfield. He began his career growing a UK aerospace start-up, and then returned to Malaysia to build Strand Aerospace Malaysia into an organisation leading the design and analysis engineering services industry in Malaysia. Naguib has been active as an engineer, technologist and business developer in the global aerospace supply chain since 2000. He speaks frequently on aerospace and other technology subjects at global events. His deep understanding of technology comes through his 20 years' experience as an aerospace engineer supporting the design and development of commercial aircraft and aerospace companies.

KEYNOTE 2

RESEARCH TRENDS IN SUSTAINABLE MOBILITIES

Abstract:

Air pollution and climate change are significantly affected by the increase of greenhouse gases produced by burning fossil fuels. The transportation or mobility sector is considered the primary source of these emissions. Policymakers have imposed stricter legislation to reduce greenhouse gas emissions and implement new energy mobilities such as battery electric vehicles, fuel cell vehicles, and hydrogen internal combustion engine vehicles. For example, the European Parliament has agreed to ban new fossil fuel sales beyond 2030. The demand for cleaner and sustainable mobility has driven a drastic change in the way how mobilities are functioning today. However, the new energy mobilities pose several challenges such as range anxiety, lack of charging infrastructure, vehicle costs, and charging time, that are interrelated to each other. Many automotive manufacturers and researchers have developed more innovative system designs and solutions. In this topic, the trends in future mobilities will be covered to understand the research opportunities that can help to achieve the net zero emissions target.

Dr. Raja Mazuir Shah
Associate Dean, College of Engineering, University of Doha for Science and Technology, Qatar.

Dr. Raja Mazuir Shah is an Associate Dean at the College of Engineering, University of Doha for Science and Technology, Qatar. Dr. Mazuir has been working in academia and industry research settings in Automotive Engineering for more than 27 years, for example, Warwick University UK, Coventry University UK, Sakarya University Turkiye, Lotus Engineering UK, Arrival Limited UK. Dr. Mazuir has also collaborated with external stakeholders such as Jaguar Land Rover UK, Aston Martin Lagonda UK, and Bladon Jets UK to develop innovative solutions for propulsions and energy management systems. Dr. Mazuir is currently working on several research clean mobility projects to develop a sustainable and renewable green hydrogen EV charging infrastructure, a novel lithium-ion battery thermal management system for energy and thermal optimisation, a sustainable mobility system, and advanced sustainable mobility design and testing facilities. Dr. Mazuir was a visiting academic at Cranfield University, UK and Universiti Teknologi Petronas, Malaysia. Dr. Mazuir has published his works in high-impact journals and conferences.

KEYNOTE 1

ENGINEERING EDUCATION AND ETHICS TOWARDS SUSTAINABLE SOCIETY

Prof. Emeritus Tan Sri Dato' Dzulkifli Abdul Razak
Rector, International Islamic University Malaysia, Malaysia

Abstract: Education for Sustainable Development has been adopted globally as the overarching framework to transform education holistically in shaping the society of the future. It integrates the 3Ps of People, Planet and Prosperity in a balanced and harmonious way. In short, the same applies to the discipline of engineering. Taking into account transdisciplinary, inclusive as well as indigenous approaches to realise a sustainable society. The presentation will explain on how this could be systematically achieved.

KEYNOTE 2

PREPARING STUDENTS FOR INDUSTRY: BRIDGING THE GAP BETWEEN ACADEMIA AND THE REAL WORLD

Prof. Dr. Abdel Magid Hamouda

Professor, College of Engineering, Qatar University

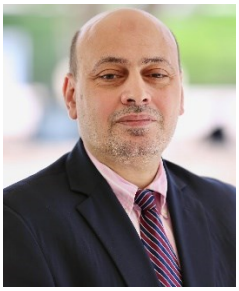

Abstract: In an ever-evolving technological landscape, the dynamic role of engineering education in preparing industry-ready graduates has gained paramount importance. The journey to bridge the gap between academia and the real world, aligning graduate attributes and skills with industrial needs, is influenced by various challenges and barriers. The involvement of industry professionals in curriculum design infuses programs with pertinent skills, technologies, and practices. Experiential learning, internships, and collaborative activities reveal profound insights to student about industries.

Industries are undergoing rapid transformations driven by technological breakthroughs and market dynamics. Automation, artificial intelligence, renewable energy, sustainable practices, and digitalization are reshaping the landscape of various sectors. By aligning with industry needs, universities ensure their engineering programs reflect these changes, enabling students to acquire the latest technical skills and knowledge. Graduates with up-to-date expertise become more relevant and valuable to employers, positioning themselves for career success.

Introducing the concept of innovation in engineering education as a bridge between academia and industry is crucial. The presentation will highlight methodologies such as project-based learning, problem-based learning, flipped classrooms, and experiential learning. Examples showcasing how these approaches engage students in practical, real-world scenarios, fostering critical thinking, collaboration, and problem-solving will be presented and discussed. The design of innovative classrooms that include space design (hubs) for experiential and hands-on learning mirroring industry landscapes is essential for foster critical thinking.

The presentation is also delves into the pivotal role of soft skills in graduate employability, such as communication, adaptability, and leadership. Integrating these skills into the curriculum empowers graduates to manage not just the details of their technical subjects, but also the complexities of different work environments. It will also illustrate the benefits of incorporating real-world projects within the curriculum, showcasing a successful projects that effectively embed and nurture the skills and attributes needed for students to excel in the real world.

The presentation will explore how fostering an entrepreneurial mindset can encourage innovation and adaptability among engineering graduates, and how to foster an entrepreneurial and innovative ecosystems within universities.

The presentation delves into the significant influence that accreditation holds on the employment prospects of university engineering graduates. The presentation will present and discuss how university ranking often hold a reputation for offering quality education and producing skilled graduates.

Employers may prioritize graduates from top-ranked universities due to their perceived higher competence.

Finally, looking toward the future, universities act as navigators. Their curricula must serve as a map, equipping graduates with the skills required to navigate this AI-driven job market.

KEYNOTE 3

RESEARCH IN ENGINEERING EDUCATION FOR TEACHING EXCELLENCE CAREER PATHWAY

Prof. Dr. Fatin Aliah Phang Abdullah
Professor, Universiti Teknologi Malaysia, Malaysia

Abstract: When the Ministry of Higher Education launched the Malaysia Education Blueprint 2015-2025 (Higher Education), one of the shifts is to achieve Talent Excellence. To support this shift, MOHE published the Orange Playbook to introduce the Differentiated Career Pathways for the promotion of academics. This opens up a few niches for academics to focus in developing their academic careers such as Teaching & Learning, Research, Professional Services and Leadership. Engineering educators at higher education institutes are given the opportunities to venture further into teaching, curriculum development, research in engineering education and engineering education related conferences and awards as a new pathway towards career promotion. This keynote will introduce the teaching excellence framework by the Royal Academy of Engineering as a foundation for engineering educators in planning their career towards the teaching & learning pathway. The keynote will also cover various levels of engineering educators ranging from good practices in teaching to conduct rigorous research in engineering education.

MESSAGE FROM THE CHAIRMAN OF ICCCE 2023

Prof. Dr. Md Rafiqul Islam
Assalamualaikum warahmatullahi wabarakatuh,

I would like to extend my warmest welcome to the participants of the 9th International Conference on Computer and Communication Engineering 2023 (ICCCE 2023) organized by the Department of Electrical and Computer Engineering (ECE), Faculty of Engineering, International Islamic University Malaysia (IIUM). The Department and the Faculty have been encouraged to organize bi-yearly ICCCE conferences by the enthusiasm and participation in the previous conferences which drawn from around the world. Our aim in establishing ICCCE series of IEEE supported and Scopus indexed conferences is to make it a landmark in the field of Computer and Communication Engineering, which provides a healthy atmosphere for intellectual exchange of thoughts and sharing of research findings among fellow colleagues, researchers, policy makers and students. The theme of the present conference is "Engineering Research for a Sustainable World".

The past ICCCE conferences, as well as the current one, has followed a strict regime of IEEE guidelines of blind-review process seconded by the experienced technical committee scrutiny to update the papers based on reviewers' comments and to comply with the template guidelines. The ICCCE2023 conference has achieved acceptance rates of around 71% out of 110 full paper submissions through EDAS from around 20 countries.

I would like to express my sincere gratitude to the organizing committee and everybody who has worked very hard to make this conference a reality and a success. I would like to express my deepest gratitude to the distinguished keynote speakers, International Advisory Board members and sponsors. I am also grateful to all the reviewers, as without their effort the high-quality standard for the conference could not have been maintained.

I wish all of you a pleasant hybrid experience and we hope that ICCCE 2023 will be a successful and enjoyable event for all participants. I would like to express my gratitude to the participants, members of the organizing committee, secretarial staff, and everyone who have worked hard to make this conference into reality. Finally, I hope that ICCCE 2023 will be successful and enjoyable to all participants.

Wassalam,

Prof. Dr. Md Rafiqul Islam
Electrical and Computer Engineering Department
Kulliyyah of Engineering
Chairman of ICCCE 2023

ORGANIZING COMMITTEE OF ICCCE 2023

CHAIRMAN
Md. Rafiqul Islam

VICE CHAIRMAN
Othman O Khalifa

SECRETARY
Mohd. Shahrin Abu Hanifah
Aliza 'Aini Bt. Md. Ralib @ Md. Raghib

TECHNICAL COMMITTEE
Nor Farahidah bt Za'bah (Chair)
Nurul Fariza Zulkurnain (Co-Chair)
Teddy Surya Gunawan
Rosminazuin Ab Rahim
Siti Hajar Bt Yusoff

FINANCE
Nur Shahida Bt Midi (Chair)
Faridah Bt Abdul Rahman (Co-chair)

REGISTRATION
Huda Adibah Mohd Ramli (Chair)
Norazlina Bt Saidin (Co-Chair)

SPONSORSHIP
Khaizuran Abdullah (Chair)
Azran Azhim Noor Azmi (Co-Chair)
Sr. Sharifah Junita (Engineer)

FOOD & LOGISTIC
Suriza Ahmad Zabidi (Chair)
Belal Ahmed Hamida (Co-chair)

WEBSITE
Malik Arman Morshidi (Chair)
Rashidah Funke Olanrewaju (Co-Chair)

PUBLICITY
S. M. A. Motakabber (Chair)

PUBLICATION/PROGRAMME
A.H.M. Zahirul Alam (Chair)
Noreha Abd Malik (Co-Chair)
Nurul Arfah Bt Che Mustafa

INTERNATIONAL ADVISORY BOARD & KEYNOTE SPEAKERS
Nurul Fadzlin Hasbullah (Chair)
Khairayu Badron (Co-chair)
Khairul Azami Bin Sidek

ORGANIZING COMMITTEE OF ICCCE 2023

COMMITTEE MEMBERS

Ahmad Fadzil Bin Ismail
Ahmad Zamani Bin Jusoh
Aisha Hassan Abdalla
Amelia Wong Bt. Azman
Ani Liza Bt. Asnawi
Anis Nurashikin Bt. Nordin
Athaur Rahman Najeeb
Farah Diyana Bt. Abdul Rahman
Hasmah Bt. Mansor
Mashkuri Bin Yaacob
Mohamed Hadi Habaebi
Mohd Shahnan Bin Zainal Abidin
Muhammad Ibn Ibrahimy
Nadirah Binti Abdul Rahim
Norazlina Bt. Saidin
Norun Farihah Bt. Abdul Malek
Nurul Fariza Bt. Zulkurnain
Rosminazuin Bt. Ab. Rahim
Sarah Yasmin Bt. Mohamad
Siti Norjannah Bt. Ibrahim
Yasser Asrul Bin Ahmad

INTERNATIONAL ADVISORY BOARD

Prof. Dr. Huseyin Arslan, Fellow IEEE, University of South Florida, USA
Prof. Dr. Muhammad Mustafa Hussain, fellow IEEE, University of California, USA
Prof. Dr. Emmanuel Oyekanlu, Drexel University, USA
Prof. Dr. Zakaria Hossain, Mie University, Japan
Prof. Dr. Shinji Tsuruoka, Mie University, Japan
Prof. Dr. Abul Lais M S Haque, Presidency University, Bangladesh
Prof. Dr. Mohammad Abdul Matin, North South University, Bangladesh
Prof. Dr. Nowshad Amin, Universiti Tenaga Nasional, Malaysia
Prof. Dr. Abiodun Musa Aibinu, Federal University of Technology, Nigeria
Prof. Dr. Rushan Ziatdinov, Keimyung University, South Korea
Prof. Dr. Jia Uddin, Woosong University, South Korea
Prof. Dr. Hasan Tinmaz, Woosong University, South Korea
Prof. Dr. Tumennast Erdenebold, Woosong University, South Korea

MESSAGE FROM THE CHAIRMAN OF ICCHES 2023

Prof. Ir. Dr. Mohammed Saedi Jami

Chairman

International Conference on Chemical Engineering & Sustainability 2023
(ICCHES 2023)

Assalamualaikum warahmatullahi wabarakatuh,

The International Conference on Chemical Engineering & Sustainability 2023 (ICCHES 2023) (Previously known as ICBioE) is being organized by the Department of Chemical Engineering and Sustainability at the Faculty of Engineering, International Islamic University Malaysia. The conference will take place on August 15th – 16th, 2023, and its theme is "Nurturing Innovation for Sustainable and Green Future". The conference will serve as an international platform for researchers to share their ideas, experiences, and latest research findings and innovations in various fields of chemical engineering, including bioenergy, materials, bio-chemical engineering, environmental engineering, and bioprocess engineering. The submissions will undergo a rigorous review process by at least two experts, including members and non-members of the organizing committee. The organizer eagerly looks forward to see you there as the members of the organizing committee, participants, members of the advisory committee, keynote speakers, and sponsors and be a part of this impactful pool of ideas and knowledge sharing.

To summarize, we would like to extend a warm invitation to you to join us at our upcoming conference. We have an exciting line-up of speakers and topics that we believe will be of great interest to you and your colleagues. We hope you will take advantage of this opportunity to network, learn, and engage with other professionals in your specific field. We look forward to seeing you at the conference and hope that you will find it to be a valuable and enlightening experience. Thank you for the impactful work that you do and we hope to see you soon.

Wassalam,

Prof. Ir. Dr. Mohammed Saedi Jami
Chairman, ICCHES 2023

ORGANIZING COMMITTEE OF ICCHES 2023

CHAIRMAN

Prof. Ir. Dr. Mohammed Saedi Jami

CO-CHAIRMAN

Assoc. Prof. Dr. Nor Fadhillah Mohamed Azmin

SECRETARY

Dr. Farah Ahmad (Secretary)
Assoc. Prof. Dr. Noor Illi Mohamad Puad (Co-Secretary)
Sr. Sharifah Bt. Hussain (Co-Secretary)

STEERING COMMITTEE

Prof. Ir. Dr. Mohammed Saedi Jami
All Chairpersons of Sub-committees

TECHNICAL COMMITTEE

Dr. Nurul Sakinah Engliman (Chairman)
Prof. Dr. Faridah Yusof
Prof. Dr. Ma'an Fahmi Al-Khatib
Assoc. Prof. Dr. Fazia Adyani Ahmad Fuad
Assoc. Prof. Dr. Fathilah Ali
Dr. Husna Ahmad Tajuddin
Dr. Munira Shahbudin
Dr. Nik Rashidah Nik Abdul Ghani

PUBLICITY

Assoc. Prof. Dr. Amanatuzzakiah Abd. Halim (Chairman)
Prof. Dr. Faridah Yusof
Assoc. Prof. Dr. Noor Illi Mohamad Puad
Dr. Ricca Rahman Nasaruddin

SPONSORSHIP

Assoc. Prof. Dr. Dzun Noraini Jimat (Chairman)
Assoc. Prof. Ir. Dr. Azlin Suhaida Azmi
Prof. Dr. Ts. Maizirwan Mel
Dr. Husna Ahmad Tajuddin
Dr. Mariatul Fazilah Mansor
Dr. Nik Rashidah Nik Abdul Ghani

WEBSITE

Dr. Wan Mohd Fazli Wan Nawawi (Chairman)
Br. Mohd Iznan Ab. Hamid

MULTIMEDIA

Dr. Mohd Firdaus Abd Wahab (Chairman)
Assoc. Prof. Dr. Dzun Noraini Jimat
Assoc. Prof. Dr. Noor Illi Mohamad Puad
Dr. Yusilawati Ahmad Nor
Dr. Wan Mohd Fazli Wan Nawawi

ORGANIZING COMMITTEE OF ICCHES 2023

Dr. Farah Ahmad
Br. Mohd Iznan Ab. Hamid
Br. Mohd Hafizul Shaibon
Br. Nasaruddin Mohd Sulaiman

PUBLICATION AND JOURNAL

Prof. Dr. Md. Zahangir Alam (Chairman)
Prof. Dr. Ma'an Fahmi Al-Khatib
Prof. Dr. Ts. Maizirwan Mel
Assoc. Prof. Ir. Dr. Sarina Sulaiman
Assoc. Prof. Dr. Dzun Noraini Jimat
Assoc. Prof. Dr. Fathilah Ali
Dr. Mohd Firdaus Abd Wahab
Dr. Ricca Rahman Nasaruddin

KEYNOTE/INVITED SPEAKERS/ADVISORY BOARD

Prof. Dr. Nassereldeen A. Kabbashi (Chairman)
Prof. Dr. Md. Zahangir Alam
Assoc. Prof. Dr. Dzun Noraini Jimat
Dr. Ricca Rahman Nasaruddin

REGISTRATION (INCLUDING TREASURER, DIGITAL PROGRAMME BOOK & CERTIFICATE)

Assoc. Prof. Ir. Dr. Azlin Suhaida Azmi (Chairman)
Dr. Yusilawati Ahmad Nor
Dr. Munira Shahbuddin
Dr. Mariatul Fadzillah Mansor
Dr. Nik Rashidah Nik Abdul Ghani
Br. Aslan Sarif Asrimon
Br. Anuar Ariffin
Sr. Siti Noradila Md Misri
Sr. Suharti Yahya

MESSAGE FROM THE CHAIRMAN OF ICMAAE ‘23

Fadly Jashi Darsivan

Chairman

6th International Conference on Mechanical, Automotive and Aerospace Engineering 2023 (ICMAAE ‘23)

Assalamualaikum warahmatullahi wabarakatuh,

Welcome to the International Conference on Mechanical, Automotive, and Aerospace 2023, ICMAAE ‘23. We gather here to celebrate the brilliance of engineering and technology, uniting researchers, professionals, and experts from across the globe.

Within these pages of the program book, a realm of knowledge awaits you—a testament to human ingenuity, innovation, and collaboration. From mechanics to automotive engineering, and aerospace exploration, we showcase the incredible achievements that have shaped our world.

As we delve into plenary sessions and technical presentations let us remember the power of collective wisdom. Together, we can overcome challenges and unlock opportunities that lie ahead. This conference not only heralds progress but also reminds us of our responsibility. Sustainable development and ethical practices must underpin every advancement we make. Let us steer our innovations toward a brighter and more inclusive future.

ICMAAE ‘23 is more than just an academic event; it embodies the spirit of community. Let us cherish the bonds formed here and leverage mentorship to nurture the next generation of visionaries. In conclusion, my gratitude goes to all whose dedication made ICMAAE ‘23 a reality. This program book serves as a beacon, inspiring us to explore new frontiers, guided by the principles of responsible innovation.

Thank you and enjoy the enriching experience of ICMAAE ‘23. Together, we shape a world of endless possibilities.

Wassalam,

Assoc. Prof. Dr. Fadly Jashi Darsivan
Chairman of ICMAAE ‘23

ORGANIZING COMMITTEE OF ICMAAE 2023

CHAIRMAN

Fadly Jashi Darsivan

CO-CHAIRMEN

Meftah Hrairi
Waqar Asrar
Masjuki Hassan

SECRETARY

Amelda Dianne Andan

TECHNICAL COMMITTEE

Jaffar Syed Mohamed Ali – Chairman
Sany Izan Ihsan
Sanisah Saharin
Hanan Mokhtar
MD. Ataur Rahman
Muhammad Abdullah
Tengku Nordayana Akma
Moumen Mohammed Idris

KEYNOTE/INVITED SPEAKERS/ADVISORY BOARD

Waqar Asrar – Chairman
Muhammad Hanafi Azami
Hilmi Hela Ladin
Dwi Pebrianti

FINANCIAL SPONSORSHIP, FOOD AND SOUVENIRS

Muhammad Saifuddin Rehan - Chairman
Salmiah Ahmad
Nabilah Ramli
Azweeda Dahlan

WEB, APPS AND SOCIAL MEDIA

Mohammed Aldheeb – Chairman
Norfazrina Mohd Yatim
Aiffa Najihah Binti Rosli
Ahmad Mursyid

PUBLICATION IN JOURNALS

Muhammad Abdullah – Chairman
Dwi Pebrianti
Hanan Mokhtar
Moumen Mohammed Idres
Sher Afghan Khan
Waleed Fekry Faris

AUDIO VISUAL AND TECHNICAL

Mohammed Aldheeb – Chairman

PROCEEDINGS AND PROGRAMME BOOK

Mohd Sultan Ibrahim – Chairman
Wan Luqman Hakim

REGISTRATION

Mohd Farid – Chairman
Syed Noh Syed Abu Bakar
Adib Hamdani
Sany Izan Ihsan
Foziah Baharom
Mohammad Azizudeen
Syazwani Mahmoodin
Nooryani Haji Ali

PUBLICITY

Nur Azam Abdullah – Chairman
Muhammad Hanafi Azami
Tengku Nordayana Akma
Mohd Azan Sapardi
Sher Afghan Khan
Waleed Fekry Faris
Masjuki Hassan
Ahmad Faris Ismail
Najihah Binti Abd Razak
Farhana Nur Danisyah
Raef Al-Fathoni
Fakhru Razee

INTERNATIONAL ADVISORY BOARD

Ashraf A Omar, UIR, Morocco
Yulfian Aminanda, UTB, Brunei Darussalam
Mirghani Ishaq Ahmed, IUM, Saudi Arabia
Tasneem Pervez, SQU, Oman
Raed Kafafy, HCT, UAE
Erwin Sulaeman, UAE University, UAE
Kassim Abdullah, UAE University, UAE
Mohamed Okasha, UAE University, UAE
Ari Legowo, HCT, UAE

MESSAGE FROM THE CHAIRMAN OF ICEPPE 2023

Assoc Prof. Dr. Ani Liza Asnawi

Chairman of 6th International Conference on Engineering Professional Ethics and Education 2023 (ICEPEE' 23)

Assalamualaikum waramatullahi wabarakuh

A warm welcome to the 6th International Conference on Engineering Professional Ethics and Education (ICEPEE'23), organized by the INTEGRATES (Integrative Engineering Education and Ethics for Sustainability) research group, Kulliyyah of Engineering, International Islamic University Malaysia (IIUM). We proudly present our conference theme this year, which focus on the "*Engineering Education and Ethics towards Sustainable Society*".

Globalization has led the whole world to be closely connected and interdependent economically, socially, and politically. This has led to increasing apprehension globally that many engineering advancements and scientific research lead to contentious breakthroughs and outcomes that are ethically unacceptable. In the era marked by rapid technological advancements and global challenges, the intersections of sustainability, ethics and engineering education have never been significant. Today, as engineers and educators, we carry profound responsibility not only to develop innovative solutions but also to perform it with a conscious understanding of their impact on our society, generations, and our ecosystem as well.

The ICEPEE'23 with its significant theme serves as a platform to bring the gaps between theory and practice, to share insights that inspired ethical considerations in engineering, and to foster a commitment to sustainability that echoes through our institutions, curriculum, and research. As we embark on this transformative journey over the coming days, it is important for us to take every opportunity to engage, learn and collaborate. The objective of this conference is to gather all related parties to exchange relevant ideas and findings to enrich their knowledge and views on the significance of the engineering education, and ethics in shaping our future generation.

I would like to take this opportunity to extend my heartfelt gratitude to our keynote speakers, authors, and presenters, who have dedicated their commitment to the accomplishment of this conference. Surely the insights and all the sharing will undoubtedly serve as beacons of inspiration for us to continue the journey in shaping our engineers and society. This conference also will not be possible without the tireless effort of our organizing committee particularly. For the organizing committee, thank you for your hard work and support that have turned this conference into a reality and success. May Allah grant the efforts tremendously.

Finally, on behalf of the organizing committee, I welcome all participants to the ICEPEE'23, may this platform bring a meaningful change and inspire us for shaping our engineering education and ethics towards a sustainable society. Thank you and let us embrace the challenges and opportunities that lie ahead.

Best Regard,

Assoc Prof. Dr. Ani Liza Asnawi
Chairman, ICEPEE'23

ORGANIZING COMMITTEE OF ICEPEE 2023

Chairman:	Assoc Prof Dr. Ani Liza Bt. Asnawi
Co-chairman:	Assoc. Prof. Dr. Siti Noorjannah Bt. Ibrahim Prof. Dr. Aisha Hassan Abdalla Hashim
Secretary:	Dr. Nurul Arfah Binti Che Mustapha Dr. Norazlina Saidin
Registration:	Assoc. Prof. Dr. Suriza Ahmad Zabidi Dr. Dwi Pebrianti
Technical Committee:	Dr. Adibah Amir (Head) Dr. Nur Shahida Binti Midi Dr Hazlina Md Yusof Assoc. Prof. Dr. Nurul Fariza Binti Zulkurnain
Publication Committee:	Dr. Ahmad Zamani Bin Jusoh (Head) Assoc. Prof. Dr. Nor Fadhillah Bt. Mohamed Azmin
Publicity and Promotion:	Dr. Siti Noratikah binti Che Deraman Dr. Wan Nur Firdaus Wan Hasan
Program Book & Certificates:	Dr. Azni Nabela Bt Wahid
Multimedia:	Dr. Suhaily Binti Mokhtar
Keynote Speakers:	Prof. Dr. Ir. Zuraida Bt. Ahmad
Website:	Assoc. Prof. Dr. Ali Sophian Br. Arselan Ashraf
Sponsorship:	Dr. Hasmawati Bt. Antong (Head) Ms. Sharifah Junita Syed Idrus

INTERNATIONAL ISLAMIC UNIVERSITY MALAYSIA (IIUM)

IIUM was established in 1983 to fulfill one of the major aspirations of the contemporary global Muslim community. This yearning of the Ummah is a key element in IIUM's vision statement: "To become a leading international center of educational excellence which seeks to restore the dynamic and progressive role of the Muslim Ummah in all branches of knowledge and intellectual discourse."

IIUM operates under the direction of a Board of Governors with representatives from the eight sponsoring governments and the Organization of Islamic Conference (OIC). Currently, IIUM is home to over 24,000 students (18,000 undergraduates and 6,000 Postgraduates) students including students from more than 117 countries and 3,000 teaching and administrative staff members.

The university's current physical facilities are located at five sprawling campuses in Gombak, Kuala Lumpur, Kuantan, Gambang and Pagoh. This was a far cry from its humble beginnings in 1983 when it operated from temporary quarters with 153 students and a handful of lecturers and administrators.

IIUM offers a wide range of academic programs through its faculties of Science, Laws, Medicine, Engineering, Islamic Revealed Knowledge and Human Sciences, Economics and Management, Nursing and Allied Health Sciences and Architecture and Environmental Design. These are geared towards both skill-building and scholastic attainments and designed by IIUM‟s philosophy, which is built upon the belief that knowledge must be pursued and propagated in the spirit of tawhid, as an act of worship, in full recognition that it is a trust which Allah has placed upon mankind. Malaysian graduates of IIUM have performed well in both the public and private sectors. Since 1987 IIUM has been producing about 3,000 graduates annually.

KULLIYYAH OF ENGINEERING, IIUM

The mission of the Faculty of Engineering is to provide quality engineering education, with sufficient scope to include fundamental and specialized knowledge and practice in engineering and a broad base in management, ethics, and humanities. This will enable our graduates to be ready to serve the current and emerging needs of the society.

Besides being professionally qualified and competent, the graduates will acquire spiritual, intellectual, moral and ethical characteristics towards the development of an integral and harmonious relationship with Allah (the Creator), fellow human beings and with the natural environment. The interdisciplinary approach to engineering education not only allows the graduates to solve industrial and human problems; it will also enable them to bring about and manage changes in conformity with the worldview based on the principles of Islam.

Currently, there are nine programs being offered: Aerospace Engineering, Chemical Engineering, Civil Engineering, Electrical and Electronics Engineering, Manufacturing Engineering, Materials Engineering, Mechanical Engineering and Mechatronics Engineering. The faculty is also offering postgraduate engineering programs leading to MSc. and Ph.D. degrees. At the moment the student population at the undergraduate level stands around 2200 and more than 200 at the postgraduate level.

Research and development are one of the primary activities in the Kulliyyah of Engineering which is harnessed by excellent facilities, qualified and competent academic staff, and holistic 'Garden of Knowledge and Virtue' ecosystem that elevate active participations in research activities in multi-disciplinary engineering areas. To foster research collaboration amongst faculty members, research units and research groups have been established towards broader Quintuple-Helix interactions for problem solving and solutions. Presently, there are three research units and fifteen research groups spanning over various areas of engineering, encompassing both conventional and emerging fields. There are also well equipped Advanced Laboratories to support research and development activities and postgraduate studies.

The Faculty of Engineering offers a wide range opportunity of postgraduate studies with Ph.D. and Masters degree programmes. With the Kulliyyah's philosophy that is based on systems approach, the engineering programmes offer an integrated and comprehensive education that transcends the boundaries of various disciplines. The Ph.D. programme is by research whereas the Master degree.

program is conducted in three different modes, namely, research only, mixed mode (equal number of credits for both taught courses and research element), and coursework mode.

The Mixed-mode and Coursework mode programmes are offered in the following nine (9) programmes respectively: Automotive Engineering, Biotechnology Engineering, Communication Engineering, Computer and Information Engineering, Electronic Engineering, Manufacturing Engineering, Material Engineering, Mechanical Engineering and Mechatronics Engineering.

In addition to its teaching role, the Kulliyyah has the responsibility to conduct strong research programmes that contribute to the advancement of knowledge. Fourteen (14) cutting edge specialisations are offered under the MSc in Engineering (Full Research) programme, that are Automotive Engineering, Biochemical Engineering, Biotechnology Engineering, Communication Engineering, Computer and Information Engineering, Chemical Engineering, Civil Engineering, Electronics Engineering, Engineering Mathematics, Engineering Science, Manufacturing Engineering, Material Engineering, Mechanical Engineering and Mechatronics Engineering.

ACKNOWLEDGEMENT

The organizing committee acknowledges the efforts of all those who have contributed their valuable time and efforts as reviewers in ensuring high-quality technical papers for the IIUM Engineering Congress 2023.

Deepest appreciation to all faculty members of the Kulliyyah of Engineering, International Islamic University Malaysia (IIUM) for their sincere cooperation in making the conference successful. Appreciation also goes to all parties who have contributed to the success of the IIUM Engineering Congress 2023.

Finally, the organizing committee would like to express their thanks to the following companies for sponsoring this congress:

ICESCO Chair in Sustainable Engineering (ICESCO CiSE) is a programme initiated by the Islamic World Educational, Scientific and Cultural Organization (ICESCO), for promoting capacities of the institutions of higher education by facilitating access to knowledge and taking parts in its activities e.g., motivation, training and research activities, academic exchange etc.

ICESCO CiSE is based at the Kulliyyah of Engineering, and focuses on youth training and capacity building and its sustainability. Our vision and action strategy dwell on three main domains : 1) Capacity building project for youth in national STEM Education at the primary and secondary level of schooling, 2) Project on the new outlook of the engineering programmes and 3) Contribution of engineering on sustainability of the society through capacity building.

Sonictron - An Award-Winning Company.
Sonictron Sdn Bhd is actively involved in the development, design, system construction, training, support for Industrial Precision Cleaning Solution. We have rich experience in standard, custom-made for all kinds of Industrial as specialist in Ultrasonic Cleaning tasks.

Modiezham Sdn. Bhd is a 100% bumiputra company which focuses on fulfilling the needs and requirements of our customers when it comes to supplying for healthcare, laboratory, engineering and IT equipment. The primary nature of business is supply equipment's as well as provide services in the field of research and study.

WNF Resources Sdn. Bhd. continues to explore the general trading opportunities, mainly R&D and lab equipment for government agency, universities and other higher learning institutes.

WinLi Technology Sdn. Bhd. provides electrical and electronics, chemical and lab products, education and training, communication and media, computer and information technology.

https://doi.org/10.31436/iiumecp.v1i1.2982

THE EFFECT OF COEFFICIENT OF FRICTION BETWEEN RAIL VEHICLE WHEELS AND RAIL TRACK ON OPERATION POWER CONSUMPTION

NUR SHAHIBRAHIM MAHAMUDIN *, FADLY JASHI DARSIVAN

Dept. of Mechanical and Aerospace Engineering, Kulliyyah of Engineering,
International Islamic University Malaysia,
Kuala Lumpur, Malaysia

**Corresponding author: shahibrahim.mahamudin@live.iium.edu.my*

ABSTRACT: The daily cost of rail operation is increasing due to increased rail network size. Therefore, reducing operation power consumption is important for rail operators to optimize daily operation costs. Operation power consumption in rail operation can be divided into 80% traction power, such as vehicle propulsion system, and 20% non-traction power, such as station electrical consumption. Much research has already been conducted on advanced traction systems, such as regenerative braking storage systems, hybrid batteries, and others, which aim to reduce operation power consumption. However, very few address the concern about track condition and maintenance. This research focuses on the interaction between the rail vehicle wheels and the rail track and how the coefficient of friction affects the rail operation power consumption. As rail grinding is an essential rail preventive maintenance to improve track surface, the indirect coefficient of friction has shown an improvement that reduces rail operation power consumption. Train resistance can be expressed in the Davis equation, which is the mathematical model used in rail industries to find train performance. Our findings indicate that the application of the rail grinding method had successfully reduced the track kinetic coefficient of friction, reducing 9% in operation power consumption.

KEYWORDS: *Rail operation, Power consumption, Coefficient of friction, Rail grinding, Davis equation.*

1. INTRODUCTION

The daily cost of rail operation is increasing due to the expanding size of the rail network nationwide [1]. Therefore, reducing energy consumption has played an important role in the urban rail industry, as electric energy is the main source of traction power systems [2]. Good track surface coefficient of friction and profile may improve vehicle wheel and rail track interaction and reduce running resistance, therefore reducing operation energy consumption. One of the methods and strategy is to control the coefficient of friction of the rail track surface by applying good track maintenance plan such as rail grinding. Train resistance compromises a major percentage of the overall traction power losses. In rail industry, the equation of train resistance is commonly known as the Davis equation [3], as the coefficients of the Davis equation are related to different resistance contributions, as train resistance can be expressed in following form,

$$R = A + Bv + Cv^2 \quad (1)$$

https://doi.org/10.31436/iiumecp.v1i1.2982

Where R is the train resistance in N, v is the train velocity, A is the resistance component independent to train speed such as rolling resistance in N, contacts between the wheel and track surface. B is the coefficient used to define train resistance dependent on train speed such as flange friction, wave action and oscillation and C is the streamlining and aerodynamic coefficient. Davis equation can be generalized into the following equation [4],

$$R = (c_1^r + \frac{c_3^r}{p} + 10i + c_2^r v)G + c_a^r a v^2 \quad (2)$$

Where the value of c_1^r is the coefficient of resistance on track surface or also can be represent as the track coefficient of friction, μ and G is the train weight. Values of c_2^r and c_3^r are the coefficient of resistance due to track alignment, p is the train axile loading in N and i is the track gradient percentage. The value of c_a^r is the coefficient of train body smoothness and the value a is the cross-sectional profile of the train frontal. Therefore, by summarizing the above equation (1) to equation (2) the value A can be represented in terms of the following equation.

$$A = mg\mu \quad (3)$$

Where m is the rail vehicle dry mass in kg. The value of g is the gravitational constant which is 9.81 m/s^2. The value μ is the kinematics coefficient of friction of the running track. Value B can be represented in term of the following.

$$B = (\frac{c_3^r}{p} + 10i + c_2^r v)\, G \quad (4)$$

Where coefficient c_3^r is 130 and coefficient c_2^r is 0.009 for rapid transit type of rail vehicle. The value i is the percentage of track gradient and the study took place in low gradient track, the value is 1. Meanwhile, the value C can be represented in the following term,

$$C = c_a^r\, a\, v^2 \quad (5)$$

Where c_a^r is the rail vehicle body smoothness coefficient in term of 0.013 for rapid transit. The value a is the cross-sectional profile of the rail vehicle frontal area.

2. RAIL OPERATION POWER CONSUMPTION WITH THE APPLICATION OF RAIL GRINDING

2.1. Test Methodology

Two sets reading of μ and v is taken for before rail grinding and after rail grinding being applied. The track coefficient of friction is taken and recorded using the weight balance method and train velocity profile is recorded from the train speedometer. Figure 1 is the schematic diagram,

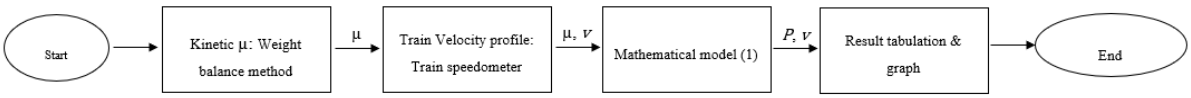

Fig. 1. Schematic diagram of the testing.

The variable for the analysis is the track coefficient of friction before the application of rail grinding and the track coefficient of friction after the application of rail grinding. Therefore,

https://doi.org/10.31436/iiumecp.v1i1.2982

the testing can be divided into two which are before the application of rail grinding (normal track coefficient of friction) and after the application of rail grinding (improved track coefficient of friction). Power consumption graph is constructed using the data from train tractive force, resistance, and velocity profile.

2.2 Test Result

Based on the application weight balance method to measure track coefficient of friction, the following is the measurement of track coefficient of friction before and after rail grinding is being applied for 15 measurement locations along the track,

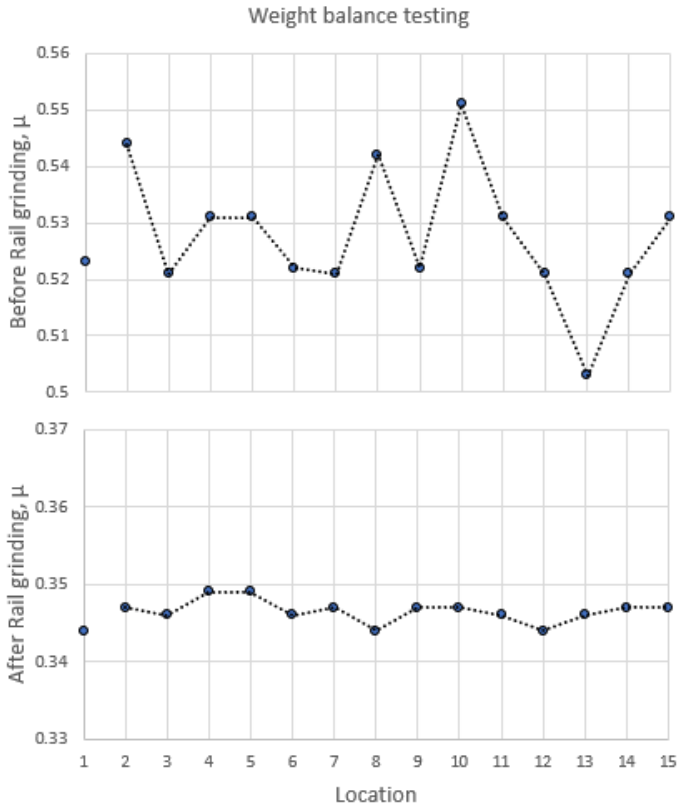

Fig. 2. Graph of weight balance testing for before and after the application of rail grinding to find μ.

Based on the finding, the track coefficient of friction before rail grinding is being applied is approximately μ=0.5 and after rail grinding being applied is approximately μ=0.3. Meanwhile, the following Figure 3 and Table 1 are the test result.

Table 1: Summary of experimental analysis of different of μ.

Coefficient of Friction, μ	Resistance (kN)		Tractive force (kN)		Power consumption (kW)		Travel time (s)
	Stage 1	Stage 2	Stage 1	Stage 2	Stage 1	Stage 2	
0.5	3021	3021	3403	3021	116	104	194
0.3	2749	2749	3157	2749	108	94	190
↓40%	**↓9%**	**↓9%**	**↓6%**	**↓9%**	**↓6%**	**↓9%**	**↓2%**

Where the value of resistance, tractive force, and power consumption is based on the maximum value and compromise two stages of station-to-station operation; Stage 1: acceleration, and Stage 2: constant speed. The difference in the result is shown in terms of percentage.

https://doi.org/10.31436/iiumecp.v1i1.2982

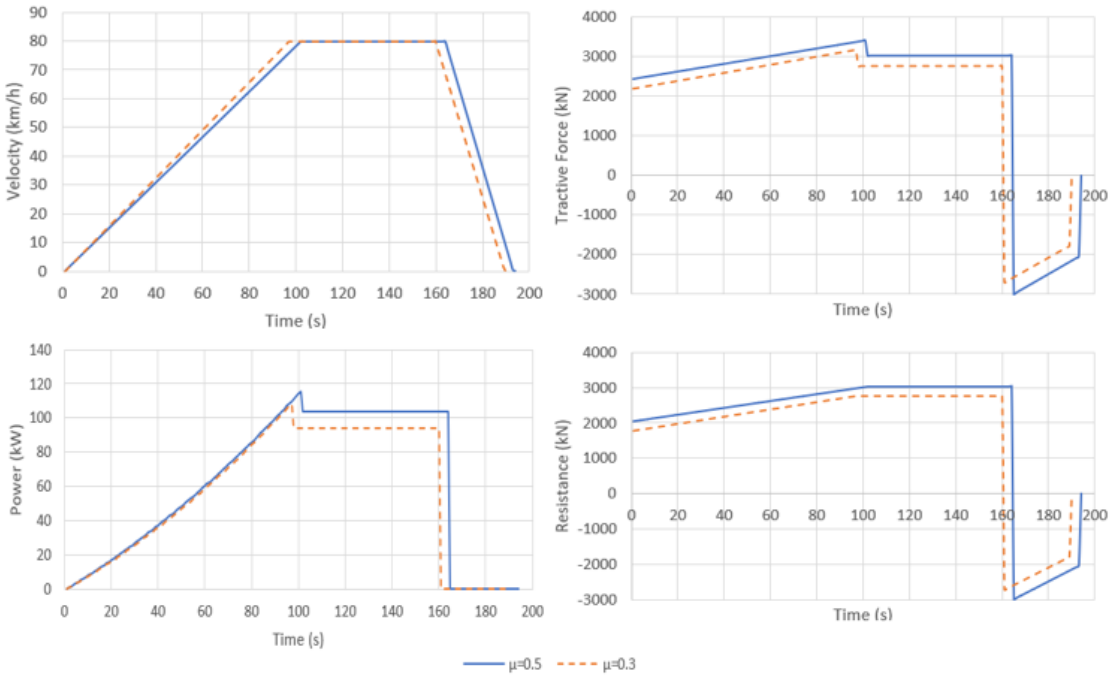

Fig. 3. Graph of velocity profile, resistance, tractive force, and power consumption before and after rail grinding.

2.3 Result discussion

During the first stage of the rail operation, the train moves with positive acceleration and the vehicle speed increases. During this stage of the operation, the train accelerates initially at its maximum rate; the acceleration rate increases for some period and decreases as it approaches its maximum velocity; acceleration starts to decrease as the train approaches its constant speed region. In the first stage of rail operation, μ=0.5 train operation increases its velocity at a rate of 0.21 km/h^2, and μ=0.3 increase its velocity at 0.24 km/h^2. Lower track friction coefficient produces a higher acceleration rate in the first stage of the train operation; therefore, the train operation enters the constant speed region faster. The differences in the μ affect the running resistance; a train with a lower μ achieved its constant speed region faster as its running resistance is lower, producing a higher acceleration rate on the first stage of operation. Therefore, the trip time in the acceleration region is reduced, producing lower operation power consumption as trip time always exerts influence on operation power consumption [4][5].

As the rail vehicle reaches its maximum velocity, it enters its second stage of the operation, which is constant speed operation, the net force is zero, and the tractive force is equal to resistance; the train reaches its constant speed regime, and acceleration is zero. The train operates with the lowest operation power consumption in this region, lower μ producing lower operation power consumption due to lower running resistance value and longer trip time.

In the third stage of operation, the braking operation start (deceleration stage) and the train start to decelerate until it stops momentarily at the station platform. According to the above experimental result, the train propulsion system is not exerting any tractive force due to braking operation. The fastest train operation that reaches the breaking point will produce lower station-to-station travel time. Meanwhile, according to the above finding, the reduction of μ from 0.5 to 0.3 reduced approximately 4 seconds of station-to-station trip due to higher acceleration rate to attain constant speed region; μ=0.3 achieved the breaking point faster

https://doi.org/10.31436/iiumecp.v1i1.2982

compared to μ=0.5. According to research in a metro, an average reduction of 5 seconds is recorded in their research in a decrease of 40% of friction coefficient [5].

The experimental result shows that operation power consumption during acceleration and constant speed stage decresed approximately linear with the decrease of μ from 0.5 to 0.3 from the effect of rail grinding procedure. According to the power consumption profile before and after rail grinding, reduction of $\mu = 0.5$ before rail grinding being applied to $\mu = 0.3$ after rail grinding being applied producing 9% lower operation power consumption rate in 40% reduction in track coefficient of friction. Meanwhile, according to research in Yizhuang Line China metro, that use tasimilar track gauge, type of rolling stock and maximum operation speed, on influnce of running resistance on operation power consumption rate, average of 3% of operation power consumption rate is reduced in every 20% reduction of track coefficient of friction [5]. Therefore, the results refect the finding of Shuai *et ai*., 2016 in China metro system as average reduction of 9% is recorded for 40% (μ =0.5 to μ=0.3) reduction of μ. In addition, according to research on top of rail friction modifier using rail lubrication, an average of 5.3% and 7.8% reduction of operation power consumption rate is recorded in the research for curve and tangent rail track [6].

3. CONCLUSION

According to the finding in the above section on operation power consumption before and after rail grinding being applied, it can be concluded that rail grinding had successfully lower the μ, therefore lower the resistance value in the Davis equation. The operation power consumption after rail grinding is about 9% lower compared to before rail grinding. The train station-to station trip time is also reduced due to the increase in acceleration rate during the first stage of the rail operation (acceleration region), therefore the rail operation enters the breaking point faster. The changes in μ from higher value to much lower value had successfully lower the operation power consumption by the decreasing of the traction force due to the reduction in resistance. In addition, changes in the A value of Davis equation using rail grinding method successfully lower the power consumption value in the study and it can be concluded that the A value of Davis Equation bring significant effect to operation power consumption by reduction of 4% of operation power consumption in μ=0.1 reduction in μ.

ACKNOWLEDGEMENT

The completion of this research project would not have been possible without the contribution and support of many individuals and organizations. We are deeply grateful to all those who played a role in the success of this project.

REFERENCES

[1] Anupiya Arupiya, Prateek Bansal, Daniel Graham (2020). Understanding the Cost of Urban Rail Transport Operation.

[2] Qing Gu, Toa Tang, Yong-duan Song (2010). A Survey on Energy-saving Operation of Railway Transportation system.

[3] Hansen, H. S., Nawaz, M. U., & Olsson, N. (2017). Using operational data to estimate the running resistance of trains. Estimation of the resistance in a set of Norwegian tunnels. Journal of Rail Transport Planning & Management, 7(1), 62-76.

[4] Vukan, R. (2007). Urban Transit Systems and Technology, John Wiley & Sons.

https://doi.org/10.31436/iiumecp.v1i1.2982

[5] Shuai Su, Tao Tang and Yihui Wang (2016). Evaluation of Strategies to Reducing Traction Energy Consumption of Metro Systems Using an Optimal Train Control Simulation Model.
[6] VanderMarel, J., Eadie, D. T., Oldknow, K. D., & Iwnicki, S. (2013). A predictive model of energy savings from top of rail friction control. Wear, 314(1), 155-161.

https://doi.org/10.31436/iiumecp.v1i1.2995

ENHANCING AND ENRICHING AN EXISTING 3-AXIS CNC MACHINE FOR TEACHING AND LEARNING: A CASE STUDY AT IIUM

DAKHEL ABDULRAHMAN, TANVEER SALEH*

Department of Mechatronics Engineering, International Islamic University Malaysia, Jalan Gombak, 53100, Kuala Lumpur, Malaysia

**Corresponding author: tanveers@iium.edu.my*

ABSTRACT: CNC machines are widely used in manufacturing, but their controllers are vulnerable to damage, which can render the entire machine inoperable. Repairing or replacing a damaged controller can be expensive and time-consuming, leading to significant downtime and lost productivity. This project aims to address these issues by developing a replacement controller for stepper motor-based CNC machines. The objective is to create a controller that can be easily installed and used to quickly restore machine operation in the event of controller damage, minimizing waste and lost productivity. The project utilizes a systematic approach, incorporating various key elements. An Arduino-based GRBL controller, known for its open-source firmware, is chosen for seamless integration with the CNC machine's stepper motor drivers, enabling precise control over axis movement. To provide users with a user-friendly interface for machine control, g-code file loading, and status monitoring, a graphical user interface (GUI) is developed using C# Windows Forms. A Raspberry Pi serves as the machine's computer due to its affordability and powerful capabilities. Running the GUI and necessary software, the Raspberry Pi enhances user interaction through a connected touch screen. Additionally, a protective case is constructed to house all components, ensuring their safety and facilitating device transportation and setup. To enable remote monitoring and receive alerts, the device incorporates IoT monitoring using AWS. This feature adds convenience and functionality for users. Rigorous testing is conducted to ensure the replacement controller performs reliably as expected. The developed replacement controller achieves a high level of precision for most CNC machines, with repeatability within +/- 0.01 mm for the X and Y axes and +/- 0.02 mm for the Z axis.

KEYWORDS: *CNC machine, Value addition, Retrofitting*

1. INTRODUCTION

In recent years, there has been a growing recognition of the environmental impact of our lifestyle, leading to an increased awareness of the need to shift from consumerism to minimalism. In light of these considerations, it is worth exploring the retrofitting of existing machines using off-the-shelf components and simple control strategies. This project focuses on developing a controller implemented on the Arduino platform to repurpose an existing CNC machine for milling operations. By utilizing available hardware components and open-source GRBL software, non-functional machines can be revitalized. Numerous CNC machines are left idle due to major component failures like the controller or motors. As a result, these machines occupy valuable space and become wasted resources. However, the structural integrity of these

https://doi.org/10.31436/iiumecp.v1i1.2995

machines remains intact. This project aims to offer a sustainable solution by reducing electronic and industrial waste through straightforward retrofitting operations.

The discussion in [1] revolves around the use of GRBL (pronounced as gerbil), an open-source high-performance software designed for controlling CNC machine motion. The software runs on ATmega328-based microcontrollers, and it effectively converts G-code instructions into corresponding motions. GRBL has been successfully employed in various CNC machines, allowing researchers to build advanced axis motion-based machines with motor control in a practical and seamless manner, resulting in high-performance CNC motions.

Recent developments, such as an Arduino-based GRBL-powered CNC laser cutting machine [2] and low-cost CNC routers [3], further demonstrate the potential of GRBL in creating CNC machines. Several other researchers have also utilized GRBL in the development of CNC machines [4]–[7] . Kolla et al. [8] proposed a methodology for retrofitting legacy machines by incorporating Industrial Internet of Things (IIoT) capabilities. Aebersold et al. [9] integrated IIoT systems into an existing industrial CNC machine, enabling control via mobile devices. Also GRBL based CNC system has also been utilized for mechanized rehabilitation system as well [10].

Building upon the current research trends, this study aims to provide a cost-effective solution for CNC machines with damaged controllers. To the best of the authors' knowledge no research has been carried out on the upgradation of the broken CNC system with the capability of IIoT based monitoring system. The objective is to develop a replacement controller that can be easily installed, thereby restoring the machine's functionality and promoting the reuse of otherwise discarded systems. Additionally, IIoT monitoring has been incorporated to enable remote monitoring of the machine's performance, enhancing overall efficiency.

2. MATERIALS AND METHODS

In this project, a replacement controller for stepper motor-based CNC machines was developed. The methodology employed several key elements to ensure the device's ease of installation, use, and upgrade. The first step involved utilizing an Arduino-based Grbl controller as the machine's control system. Subsequently, a Graphical User Interface (GUI) was developed using C# Windows Forms, simplifying machine control, g-code file loading, and status monitoring for users. A Raspberry Pi was employed as the machine's computer, providing a cost-effective and powerful platform for running the GUI and other software. To enhance user interaction and usability, a touch screen was connected to the Raspberry Pi, making the GUI more user-friendly. Additionally, a protective case was constructed to house all components, offering protection and facilitating device transportation and setup. The device was equipped with IoT monitoring using Amazon Web Service (AWS), enabling remote monitoring and receiving alerts in case of issues. Finally, comprehensive testing was conducted to ensure the device's expected functionality and reliability before its market release.

The CNC machine in this project offers two distinct operating modes. The first mode, known as "Computer Connection Mode" (shown in Fig. 1), involves directly connecting the device to a computer. By establishing this connection, the computer becomes the primary control interface for the CNC machine. It enables the user to send G-code commands to the machine, controlling its movements with precision. Additionally, the computer provides the ability to make adjustments to the machine's settings and parameters, granting greater flexibility in customization. Operating the CNC machine in Computer Connection Mode offers several advantages. Firstly, the computer's processing power allows for the execution of

https://doi.org/10.31436/iiumecp.v1i1.2995

complex programs and the performance of advanced operations. This means that intricate designs and intricate machining tasks can be achieved with ease. Furthermore, the user can benefit from the comprehensive control and monitoring capabilities offered by the computer, enabling real-time adjustments and ensuring optimal performance. In summary, Computer Connection Mode provides a versatile and powerful approach to operating the CNC machine. By connecting the device to a computer, users gain enhanced control, flexibility, and the ability to perform intricate machining tasks and advanced operations.

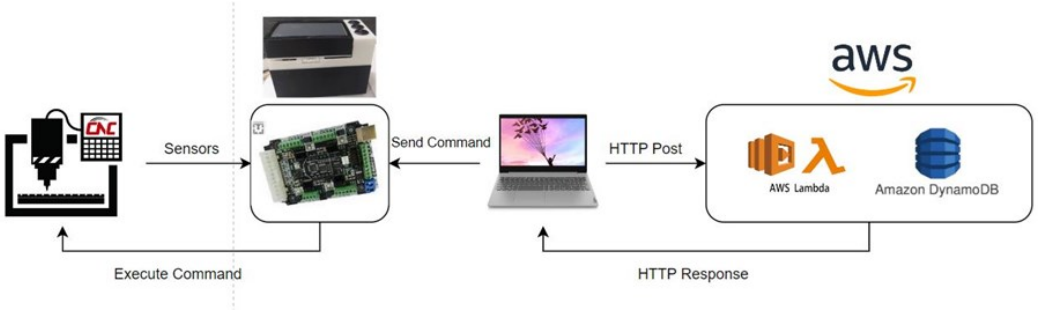

Fig. 1. Computer Connection Mode

The CNC machine in this project offers an alternative operating mode called "Onboard Interface Mode" (shown in Fig. 2). This mode allows users to operate the machine directly using the onboard computer and touch screen, eliminating the requirement for an external computer. Fig. 3 shows the developed onboard Raspberry PI based CNC controller. In Onboard Interface Mode, the machine's onboard computer and touch screen serve as a user-friendly interface for controlling the CNC machine and performing basic operations. This mode caters to users who prefer a streamlined and simplified approach to machine control. By utilizing the onboard computer and touch screen, users can conveniently navigate through menus, input commands, and adjust machine settings with ease. This approach offers several advantages. Firstly, it eliminates the need for an additional computer, reducing complexity and setup requirements. Users can simply power on the machine, access the onboard interface, and begin operating the CNC machine without any external dependencies. The touch screen provides an intuitive and user-friendly interaction, making it easy for both experienced and novice users to control the machine. Onboard Interface Mode is particularly well-suited for users who prioritize simplicity and efficiency. It offers a straightforward and accessible method of machine operation, allowing users to quickly perform basic operations and achieve their desired results without the need for advanced programming or complex setups. In summary, the Onboard Interface Mode provides a convenient and user-friendly alternative for operating the CNC machine. By utilizing the onboard computer and touch screen, users can enjoy a streamlined and intuitive experience, eliminating the need for an external computer and simplifying the control process.

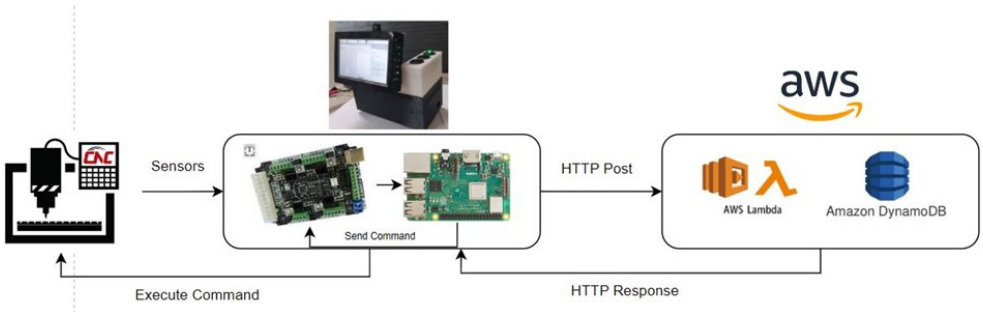

Fig. 2. Onboard Interface Mode

https://doi.org/10.31436/iiumecp.v1i1.2995

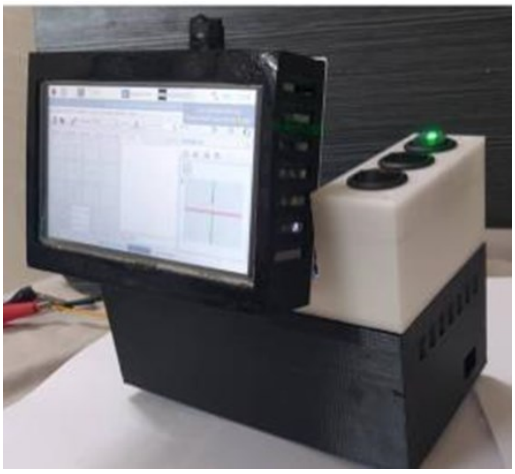

Fig. 3. Raspberry PI based onboard controller for the CNC system

Both of the aforementioned modes involved integrating the CNC system with the AWS system through the HTTP protocol, enabling remote monitoring of the machine's status via the Industrial Internet of Things (IIoT).

3. RESULTS AND DISCUSSIONS

The primary goal of this project was to create a replacement controller with a user-friendly graphical user interface (GUI) specifically designed for stepper motor-based CNC machines. The intended purpose of the controller is to effectively replace any malfunctioning controllers and restore the functionality of the machines. By offering a cost-effective solution, the project aims to cater to numerous users who possess older machines and wish to sustain their operations without the need to purchase new ones.

3.1. Functionality test of the machine using onboard controller

In order to evaluate the functionality of the modular controller, the CNC machine was connected to it, and all the necessary wiring was meticulously inspected to ensure proper connections, as illustrated in Fig.4.

Fig. 4. Modular controller hosting the GUI to operate the CNC machine

https://doi.org/10.31436/iiumecp.v1i1.2995

The modular controller was found to be fully operational, effectively executing commands specified by the G-Code program. Additionally, the performance of the modular controller was assessed while integrating it with IoT monitoring through AWS. Data including machine status, run time, estimated time, percentage of completion, as well as machine and work positions, were diligently recorded and transmitted via the internet to the AWS DynamoDB database for real-time monitoring. The IIoT monitoring system utilizing AWS performed as expected and was also tested with a mobile phone, as depicted in Fig.5, allowing for remote monitoring and prompt alerts in case of any machine-related issues. During the testing phase, the controller exhibited overall performance that aligned with the anticipated outcomes, without any encountered issues or errors. These findings affirm the controller's ability to function as intended and fulfill the requirements of the CNC machine.

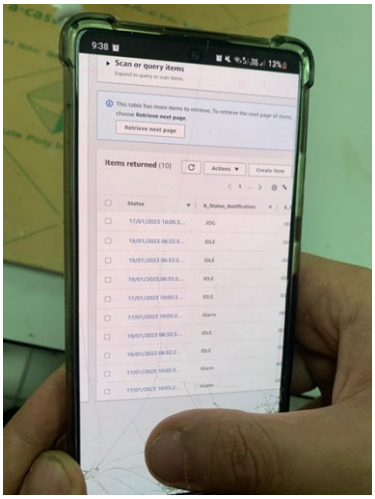

Fig. 5. AWS IIOT Monitoring of the machine status via mobile device.

3.2. Functionality test of the machine using windows based graphical user interface (GUI)

The CNC machine established a connection with the laptop's hosted GUI using a USB interface. The machine exhibited complete functionality comparable to that of the onboard controller. Furthermore, the IIoT system based on AWS performed according to expectations. Fig. 6 illustrates the laptop hosting the GUI responsible for controlling the machine, while Fig. 7 presents a snapshot of the AWS database capturing real-time machine status through the utilization of standard IIoT protocols.

Fig. 6. Laptop hosting the GUI to operate the CNC machine

Status	A_Status_Notification	B_Run_Ti...	C_Estimated_Time	D_Percentage_Done
17/01/2023 10:05:26 AM	Alarm	00:00:00:000	00.00.00	NA
17/01/2023 10:05:28 AM	Alarm	00:00:00:000	00.00.00	NA
17/01/2023 10:05:30 AM	Alarm	00:00:00:000	00.00.00	NA
17/01/2023 10:05:32 AM	IDLE	00:00:00:000	00.00.00	NA
17/01/2023 10:05:34 AM	JOG	00:00:00:000	00.00.00	NA

Fig. 7. Snapshot of the AWS database storing various machine related information in realtime

4. CONCLUSIONS

In summary, this project has successfully achieved the development of a user-friendly replacement controller that efficiently restores the functionality of old CNC machines. The integration of a dual approach to operating the CNC machine enhances flexibility and convenience for operators, enabling them to select the method that aligns with their needs and skill level. Additionally, the device incorporates an innovative IoT monitoring feature utilizing AWS, enabling remote monitoring and real-time alerts in the event of any issues, thus enhancing safety and security. Thorough functionality tests were conducted for both the GUI from the laptop and the modular controller, yielding positive results as everything performed according to expectations.

ACKNOWLEDGEMENT

Authors' express their gratitude to IIUM for the facilities provided to conduct the research. The corresponding author also acknowledges the use of CHAT GPT to improve the writing style of the manuscript.

REFERENCES

[1] S. S. Sarguroh and A. B. Rane, "Using GRBL-Arduino-based controller to run a two-axis computerized numerical control machine," in 2018 International Conference on Smart City and Emerging Technology (ICSCET), IEEE, Jan. 2018, pp. 1–6. doi: 10.1109/ICSCET.2018.8537315.

[2] M. Nasir Khan, A. Maheshwari, and H. Verma, "Study and Design of Arduino Based CNC Laser Cutting Machine," IOP Conf Ser Mater Sci Eng, vol. 1224, no. 1, p. 012008, Jan. 2022, doi: 10.1088/1757-899X/1224/1/012008.

[3] A.T. Suryawanshi, D. S. S. Sudhakar, and B. T. Patil, "Low cost and open source software-based CNC router for machining contours," IOP Conf Ser Mater Sci Eng, vol. 872, no. 1, p. 012084, Jun. 2020, doi: 10.1088/1757-899X/872/1/012084.

[4] M. Marsono, Y. Yoto, A. Suyetno, and R. Nurmalasari, "Design and Programming of 5 Axis Manipulator Robot with GrblGru Open Source Software on Preparing Vocational Students' Robotic Skills," Journal of Robotics and Control (JRC), vol. 2, no. 6, 2021, doi: 10.18196/jrc.26134.

[5] J. Veeramony and M. N. Osman Zahid, "A Customizable Controller for 3 Axis Modular CNC Machine," Journal of Modern Manufacturing Systems and Technology, vol. 6, no. 2, pp. 55–62, Sep. 2022, doi: 10.15282/jmmst.v6i2.8567.

[6] V. Lawson, M. Phister, and C. Rogers, "Automated Rotor Assembly CNC Machine," in 2020 Systems and Information Engineering Design Symposium (SIEDS), IEEE, Apr. 2020, pp. 1–5. doi: 10.1109/SIEDS49339.2020.9106641.

[7] Marsono, Yoto, A. Nafiah, and R. Nurmalasari, "Calibration the travel resolution stepper motor machines of CNC-based batik robot running GRBL firmware," 2023, p. 020011. doi: 10.1063/5.0106246.
[8] S. S. V. Keshav Kolla, D. M. Lourenço, A. A. Kumar, and P. Plapper, "Retrofitting of legacy machines in the context of Industrial Internet of Things (IIoT)," Procedia Comput Sci, vol. 200, pp. 62–70, 2022, doi: 10.1016/j.procs.2022.01.205.
[9] S. A. Aebersold, M. O. Akinsolu, S. Monir, and M. L. Jones, "Ubiquitous Control of a CNC Machine: Proof of Concept for Industrial IoT Applications," Information, vol. 12, no. 12, p. 529, Dec. 2021, doi: 10.3390/info12120529.
[10] A. Blanco Ortega et al., "CNC Machines for Rehabilitation: Ankle and Shoulder," Machines, vol. 10, no. 11, p. 1055, Nov. 2022, doi: 10.3390/machines10111055.

https://doi.org/10.31436/iiumecp.v1i1.2996

ANALYSIS AND MODELLING OF LASER-MICRO EDM-BASED HYBRID MICRO MILLING ON STAINLESS STEEL (SUS304) USING BOX BEHNKEN DESIGN

MIR AKMAM NOOR RASHID, TANVEER SALEH*, S.B ABDUL HAMID, MUHAMMAD MAHBUBUR RASHID

Department of Mechatronics Engineering, International Islamic University Malaysia, Jalan Gombak, 53100, Kuala Lumpur, Malaysia

**Corresponding author: tanveers@iium.edu.my*

ABSTRACT: Hybrid micro milling is drawing the attention of researchers and engineers to generate micro products with intense dimensional precision to use in discrete applications like aerospace, electronics, and optics. Laser milling is a faster machining process with a high material removal rate. It raises some problems like insufficient cutting depth, burrs, uneven edges, charred corners, and many more. On the other hand, the µEDM milling process is slower but produces a better surface finish with perfect alignment without compromising inaccuracy. This study aims to incorporate both machining advantages also to investigate the most substantial laser parameter that influences the output responses of µEDM milling time. In this hybrid micro-milling process, the stainless-steel (304) workpiece (0.5 mm thickness) was used to conduct laser micro-milling varying the laser input parameters such as scanning speed, power, pulse repetition rate, and loop. Sequentially the workpiece was shifted to the µEDM machine to continue µEDM milling with constant EDM parameters (Voltage 80 V, capacitance 1 nF, EDM milling speed 5 µm/sec) using a tungsten tool (0.5 mm thickness) and the total set of experiments (25) was run according to Box Behnken design (BBD). It was found that an increase in scanning speed (ss) factors (A) increases the µEDM milling time slightly. The laser power effect shows that a higher laser power machined slot channel consumes less µEDM milling time, which is quite significant compared to the scanning speed effect. A mathematical model was developed to correlate the laser input parameters and out responses of µEDM milling time. The optimization results reveal that power is the most significant factor affecting the µEDM milling time. Based on the Response Surface Methodology (RSM), the predicted optimized input laser parameter was scanning speed 1577.085 mm/sec, power 15.179 W, pulse repetition rate 8.42 KHz rate, and loop 5.959 nos in where the µEDM milling time would be lower 37.390 min.

KEYWORDS: *EDM, Laser, Milling*

1. INTRODUCTION

Recent advancements in micro-manufacturing enable the assembly of micro- and mesoscale structures in various engineering objects. Mechanical micro-milling, extensively researched recently, offers advantages over photolithography-based techniques [1, 2]. This process crafts small, precise components [3], used in biomedical devices, microsensors, etc., from polymer through microinjection molding [2]. Micromachining produces accurate, finely finished molds for this purpose [4]. While EDM and micro laser milling are alternatives, micro milling offers superior material removal rates and surface quality [5]. It's versatile, cost-effective, and user-friendly, making it a preferred choice [6].

https://doi.org/10.31436/iiumecp.v1i1.2996

Laser milling (LM) is advancing rapidly in micromanufacturing due to its ability to produce fine, precise 3D objects in various materials. In LM, a laser beam removes material layer by layer through ablation, heating it to vaporization [7]. The synergy between the laser ablation mechanism and the CNC program, derived from CAD data, is pivotal to its success. LM's advantages include machining tough materials like ceramics and graphite, no tool wear, superior surface finish, accuracy, and minute feature size [8, 9]. It excels in crafting detailed cavities or microfluidic channels. While LM offers faster material removal, its edge quality and surface roughness are inferior to micro EDM.

Micro-electrical discharge milling (micro-EDM) is a non-contact method that removes material from conductive substances through a thermal technique. This process uses electrical discharges in an insulated area between a tool electrode and a workpiece. During the discharges, a high-temperature plasma channel forms, causing localized melting and evaporation of both the workpiece and the electrode [10]. Micro EDM capability has been discussed thoroughly in [11]. Micro-EDM forces are minimal compared to mechanical methods. The process has various configurations, including micro-EDM drilling, sinking, and milling. Specifically, micro-EDM milling employs microelectrodes, which are like thin cylindrical rods, to move in set paths while rotating. Depending on the electrode diameter and discharge energy, the material is removed layer by layer, with layers as thin as 0.1 m. While micro-EDM offers superior surface finish and accuracy, its machining time is longer than laser machining.

A hybrid process has been introduced to address the shortcomings of laser and micro EDM machining. This method mitigates environmental impacts, enhances manufacturing efficiency, and benefits components with intricate geometry. While µEDM milling is inherently slower, following laser milling, it proves faster than standalone EDM milling. The performance of µEDM is influenced by laser parameters, especially in 1-D drilling [12]. A dual-stage artificial neural network model was developed to refine the parameters of this hybrid micromachining [13]. Several optimization techniques, like the Taguchi method, ANOVA, RSM, and GRA, are utilized to fine-tune the process. The objective is to pinpoint the optimal parameters that influence outcomes, such as tool wear and surface roughness [14]. Rajesh [14] employed RSM for multi-response optimization in turning, focusing on parameters like spindle speed and feed rate. Similarly, Bhuvnesh Bhardwaj et al. [15] utilized RSM for carbide insert end milling of AISI1019 steel, deriving empirical models for surface roughness. Emel Kuram and Babur Ozcelik [16] used the Taguchi method to study micro-milling effects on AISI 304 steel, considering factors like spindle speed and feed rate. In multi-response optimization via RSM, each outcome receives equal weightage.

Laser-assisted milling is well-researched, with some studies exploring macro-scale laser-assisted machining of ceramics [1]. However, research on laser-EDM based hybrid micro milling remains sparse. This paper offers an experimental study and an RSM-based model analysis, focusing on the interplay between laser parameters and µEDM milling time outputs. The optimization and contributions of the model are detailed.

2. MATERIALS AND METHODS

This study was done based on the experimental investigation to determine the outcome of laser parameters and how they affect the output execution of µEDM milling operation and a mathematical model was developed. In this research, the workpiece material used was stainless steel (SUS 304) with dimensions of 22.5 mm x 22.5 mm x 0.5 mm. Stainless steel is widely used in various applications due to its corrosion resistance. As part of the laser-µEDM based micro milling process at first the laser milling was carried out on a fiber laser system as shown

https://doi.org/10.31436/iiumecp.v1i1.2996

in Fig. 1. Then, the workpiece was transferred to the (Fig. 2) to carry out the μEDM process for fine finishing. The machined slots were characterized using optical instrumentation.

Fig. 1. Laser setup [12]

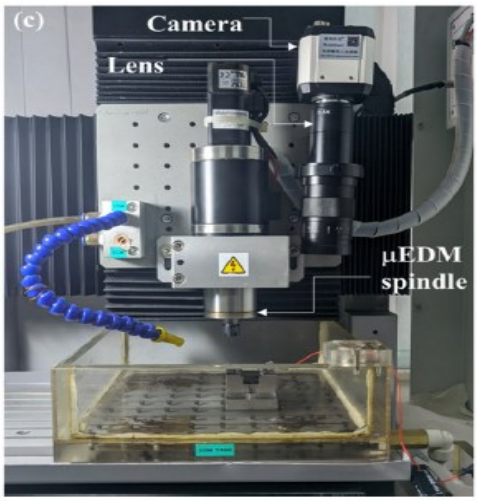

Fig. 2. μEDM setup.

3. RESULTS AND DISCUSSIONS

In this research, a prepatterned laser slot was machined using a variety of laser parameters and then finally, the slot was fine finished with constant total depth by the EDM process. Here we monitored the EDM time to see how laser parameters affected the EDM finishing time.

3.1 Dimensional Surface plot for μEDM milling time.

Here, experimental data were used to develop an empirical model (response surface method) of the EDM finishing time as a function of laser parameters. Fig. 3 shows the effect of laser power and scanning speed on the time required by the EDM process to carry out the fine finishing process. It can be seen from Fig. 3 that if higher power with lower scanning speed is used for the pilot machining process by laser, then the finishing time by the EDM process becomes shorter as most of the material is removed by the laser process due to the use of higher laser power with slower scanning speed.

https://doi.org/10.31436/iiumecp.v1i1.2996

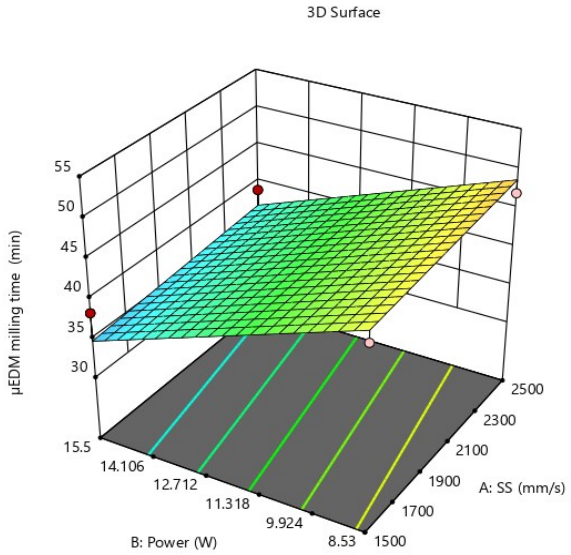

Fig. 3. Shows how EDM finishing time varies with laser machining parameters (laser power and laser scanning speed).

Fig.4, on the other hand, shows that pulse repetition rate does not have any significant effect on the final finishing time by the EDM process and loop count has an inverse effect on the machining time by the EDM process.

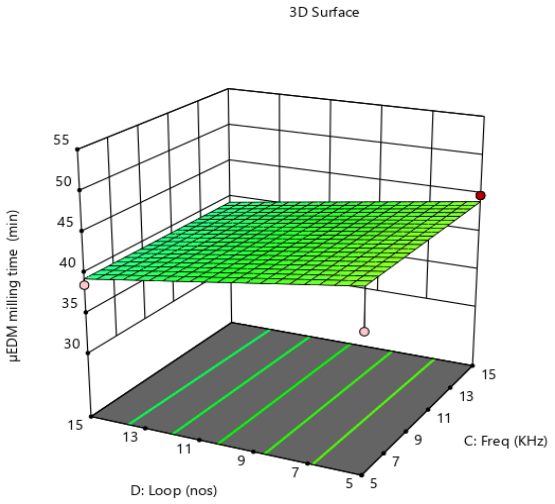

Fig.4. Shows how EDM finishing time is varied with laser machining parameters (loop count and pulse frequency).

4. CONCLUSIONS

In this study, the experimental table was designed using the Box-Behnken method, and ANOVA was employed for analysis. The µEDM milling time served as the response, with laser input parameters being the scanning speed, power, pulse repetition rate, and loops. It was observed that the laser power had the most significant impact on the µEDM milling time output responses.

The predicted optimal laser input parameters were a scanning speed of 1577.085 mm/sec, power of 15.179 W, pulse repetition rate of 8.42 kHz, and 5.959 loops, reducing µEDM milling time of 37.390 minutes.

ACKNOWLEDGEMENT

This project was funded by the FRGS grant (FRGS/1/2018/TK03/UIAM/02/2) funded by MOHE, Malaysia. The corresponding author also acknowledges the use of CHAT GPT to improve the writing style of the manuscript.

REFERENCES

[1] Melkote, S., Kumar, M., Hashimoto, F., & Lahoti, G. (2009). Laser-assisted micro-milling of hard-to-machine materials. CIRP annals, 58(1), 45-48.
[2] Masuzawa, T. (2000). State of the art of micromachining. Cirp Annals, 49(2), 473-488.
[3] Rao, D. B., Rao, K. V., & Krishna, A. G. (2018). A hybrid approach to multi-response optimization of micro milling process parameters using Taguchi method-based graph theory and matrix approach (GTMA) and utility concept. Measurement, 120, 43-51.
[4] Davim, J. P., & Jackson, M. J. (Eds.). (2009). Nano and micromachining (pp. 175-207). ISTE.
[5] Kuram, E., & Ozcelik, B. (2013). Multi-objective optimization using Taguchi-based grey relational analysis for micro-milling of Al 7075 material with ball nose end mill. Measurement, 46(6), 1849-1864.
[6] Thepsonthi, T., & Özel, T. (2014). An integrated toolpath and process parameter optimization for high-performance micro-milling process of Ti–6Al–4V titanium alloy. The International Journal of Advanced Manufacturing Technology, 75, 57-75. https://doi.org/ 10.1007/s00170-014-6102-2
[7] Campanelli, S. L., Casalino, G., Ludovico, A. D., & Bonserio, C. (2013). An artificial neural network approach for the control of the laser milling process. The International Journal of Advanced Manufacturing Technology, 66, 1777-1784.
[8] Pham, D. T., Dimov, S. S., Petkov, P. V., & Dobrev, T. (2005, June). Laser milling for micro tooling. In Proceedings of VIII LAMDAMAP Conference (pp. 362-371).
[9] Pham, D. T., Dimov, S. S., Ji, C., Petkov, P. V., & Dobrev, T. (2004). Laser milling as a 'rapid' micromanufacturing process. Proceedings of the Institution of Mechanical Engineers, Part B: Journal of Engineering Manufacture, 218(1), 1-7.
[10] Bissacco, G., Valentincic, J., Hansen, H. N., & Wiwe, B. D. (2010). Towards the effective tool wear control in micro-EDM milling. The International Journal of Advanced Manufacturing Technology, 47, 3-9.
[11] Rajurkar, K. P., Levy, G., Malshe, A., Sundaram, M. M., McGeough, J., Hu, X., ... & DeSilva, A. (2006). Micro and nano machining by electro-physical and chemical processes. CIRP annals, 55(2), 643-666.
[12] Rashid, M. A. N., Saleh, T., Noor, W. I., & Ali, M. S. M. (2021). Effect of laser parameters on sequential laser beam micromachining and micro electro-discharge machining. The International Journal of Advanced Manufacturing Technology, 114, 709-723.
[13] Noor, W. I., Saleh, T., Rashid, M. A. N., Mohd Ibrahim, A., & Ali, M. S. M. (2021). Dual-stage artificial neural network (ANN) model for sequential LBMM-µEDM-based micro-drilling. The International Journal of Advanced Manufacturing Technology, 117(11-12), 3343-3365.
[14] Bhushan, R. K. (2013). Multiresponse optimization of Al Alloy-SiC composite machining parameters for minimum tool wear and maximum metal removal rate. Journal of Manufacturing Science and Engineering, 135(2).
[15] Bhardwaj, B., Kumar, R., & Singh, P. K. (2014). Surface roughness (Ra) prediction model for turning of AISI 1019 steel using response surface methodology and Box–Cox transformation. Proceedings of the Institution of Mechanical Engineers, Part B: Journal of Engineering Manufacture, 228(2), 223-232.
[16] Kuram, E., & Ozcelik, B. (2016). Micro-milling performance of AISI 304 stainless steel using Taguchi method and fuzzy logic modelling. Journal of Intelligent Manufacturing, 27, 817-830.

https://doi.org/10.31436/iiumecp.v1i1.3000

NUMERICAL STUDY ON STABILITY OF OBLIQUE WING CONFIGURATION

J.S. MOHAMED ALI*, M.S. MUHAMMAD HAFIZ

Department of Mechanical and Aerospace Engineering, Kulliyah of Engineering, International Islamic University Malaysia, 53100, Kuala Lumpur, Malaysia

**Corresponding author: jaffar@iium.edu.my*

ABSTRACT: Oblique wing is one of the morphing wing configurations that offer a superior high speed aerodynamic performance. The mechanism in which a straight wing is being rotated by a pivot at the centre resulting swept back wing on one side and swept forward on the other side. It was proven that this configuration was able to reduce drag for a given lift at both supersonic cruise and subsonic; however, there are serious control issues. CFD analysis using SolidWorks software was performed to study and visualize the aerodynamic performance of an oblique wing for a high sweep angle. The results obtained were later used to compare with other swept configurations on its stability and control.

KEYWORDS: *Aerodynamics; Oblique wing; Asymmetric sweep; CFD; Stability*

1. INTRODUCTION

Modern-day high-speed aircraft are made of morphing wings to achieve high aerodynamic efficiency in all phases of flight. A morphing geometry wing is an aeroplane wing that can be adjusted during flight or on the ground. This configuration can provide aerodynamic advantages to an aircraft under low-speed and high speed conditions through the straight wing and swept wing respectively. During subsonic flight, a high aspect ratio wing is desired due to the fact that induced drag is inversely proportional to aspect ratio; however, during supersonic, drag is dominated by wave drag. Variable sweep and Oblique Wing aircraft are classes of aircraft that adopt such morphing wing concepts to achieve high aerodynamic efficiency.

The first oblique wing design was the Blohm and Voss P-202, designed in Germany by Richard Vogt in 1942 Hirschberg et al. [1]. Jones, the father of delta and swept wing proposed oblique wing as an alternative in his research papers during 1950s [2-3]. He proved analytically that at any flight Mach number, the minimum drag for a given lift could be achieved by an oblique swept wing with an elliptical planform. Jones proved that oblique wing configuration can minimize wave drag and induced drag with an elliptical lift distribution. For equivalent span, sweep and volume they distribute lift twice the length of conventional swept wing configuration during supersonic. This reduces wave drag by factor of 4 and volume dependent wave drag by a factor of 16. Jones also proved that the induced drag of an oblique wing at optimal sweep angle is half that of the delta wing with same span.

Kroo [4] later proved through wind tunnel experiment, oblique wings are very effective at reducing wave drag at supersonic flight. whereas years later, oblique wing configuration was rejected due to their control issue and flight complexity [1].

https://doi.org/10.31436/iiumecp.v1i1.3000

The desired feature of variable geometry wing aircraft is to maximize aerodynamics performances over wide range of Mach Numbers [5]. Comparing to the present Grumman F-14 Tomcat, additional masses are added for secondary system for variable wings of the aircraft, it emphasizes that, single pivot oblique wing is structurally advantageous compared to conventional swept wing and variable swept wing. For symmetric swept wing, the presence of bending moment results in additional mass of materials for the design. A straight through structure of oblique wing however does not experience bending moments, at the same time it is able to avoid torques by fuselage structure and it is easy to manufacture [5]. It was concluded that the majority of the wave drag advantages of the oblique wing are handicapped by the dominant volume wave drag of the fuselage, which lead to the idea of Flying Oblique Wing [5].

Stability and control of an oblique wing is complex and often discussed as its disadvantage. Bruce Larrimer [6] reported that, the NASA AD-1 pilots concluded that at or below sweep of 30°, the handling quality is satisfactory. Between 30° to 45°, the grade of handling quality decrease and worst control is at 45° to 60°. The evaluation is categorized in directional stability (yaw stability), unusual trim requirements, roll-pitch couplings, dynamic by aeroelastics and stall.

Kempel et al. [7] performed F-8 oblique research aircraft and they noted in general, as dynamic pressure and sweep angle increase, pilot ratings degraded. They noticed that in open-loop configuration (control system) there was significant pitch-to-roll coupling and an unacceptable amount of pitch-to-banking force coupling. At high dynamic pressure, a pilot described the pitching responses as “scary”.

At low sweep angles, an oblique wing aircraft can be controlled as conventional swept wing aircraft. Campbell et al. [8] noted that at sweep angles above 60°, ailerons become unsatisfactorily weak, and he theorized that aileron rolling effectiveness wasn’t reduced by skewing wing from 0° to 40° because damping in roll decreased approximately the same amount as aileron rolling moments.

Mushfiqul and Kashyapa [9] as well as Asif Shahriar et al [10] performed a numerical analysis of aerodynamic forces on an oblique wing, Wang et al [11] performed the dynamic characteristics analysis and flight control design for oblique wing aircraft. Recently Josuha [12] studied the effects of a bell shaped lift distribution on an Oblique flying wing and its impact on aerodynamic performance.

It can be noted that oblique wing has many advantages whereas it is found out that sweeping more than 45° causes instability and rolling control issue for the light aircraft. Most of the work carried out is on experimental, with the availability of modern CFD tools, it is easier and more cost effective to perform parametric analysis and to study the aerodynamic characteristics. In this work, the aerodynamic characteristics and hence the stability of an oblique wing is studied using SolidWorks CFD software and compared with the other swept wing configurations.

2. MODELLING AND SIMULATION

SolidWorks software was selected for CFD analysis to study the stability of the oblique wing. In this work, wing-only geometry stability was analysed by checking the six degree of freedom force/moment components (L, D, Z, M_x, M_y, M_z) of the wing at certain incoming air speed. As the objective of the work is to compare the stability of oblique wing with the other available wing configurations, SolidWorks modelling tool was used to model three different

https://doi.org/10.31436/iiumecp.v1i1.3000

wing configurations viz. Swept forward, swept back and oblique wing-only geometry as shown in Fig. 1. NACA 64(2)-415 was chosen as the wing section for all three configurations.

Ideal wall assumption was applied in the CFD analysis since the surface roughness and material are not defined and this assumption can be advantageous to save computational time. Errors are expected in the CFD analysis especially due to the geometry difference (scaling error), ideal wall assumptions, meshing and scheme (second order).

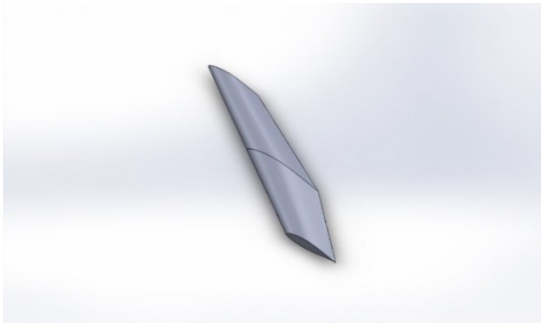

Fig. 1.1. 60° Oblique Wing

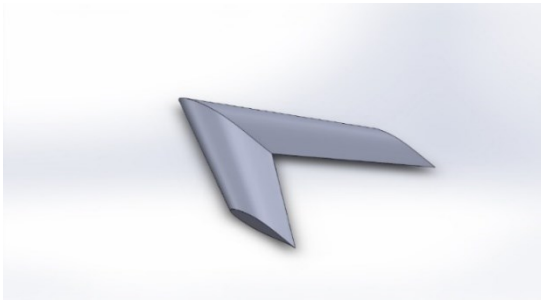

Fig.1.2. 60° Swept Back Wing

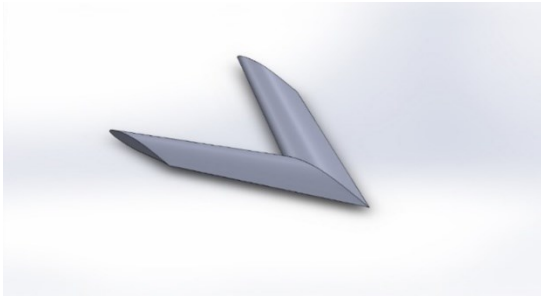

Fig.1.3. 60° Swept Forward Wing

Fig. 1. Geometry of three different swept wing configuration

Flow characteristics for the CFD analysis are listed below in Table 1.

Table 1: Inputs used for CFD analysis.

Parameter	Value
Fluid	Ideal Air
Mach number, M	0.5
Density	1.225 kg/m^3
Pressure	101325 Pa
Temperature	293.2 K
Wall	Ideal wall
Turbulence intensity	0.02%
Turbulence model	k-ω SST model

https://doi.org/10.31436/iiumecp.v1i1.3000

For meshing, a uniform structured mesh in SolidWorks was used. Although some accuracy penalty is known due to the inclination of incoming flow, it is inferred that it is reliable, and the expected error would be around 20% at most with low order scheme factor included. In SolidWorks, mesh refinement can be done simply by setting up the meshing space and increasing the meshing level of the domain. The figure below illustrates the meshing with that the Dark blue, Aqua and Green coloured region defines the meshing refinement as coarse, medium, and fine mesh region respectively. The medium mesh shown in Fig 2.was selected for analysis so that to balance the accuracy and the computational time.

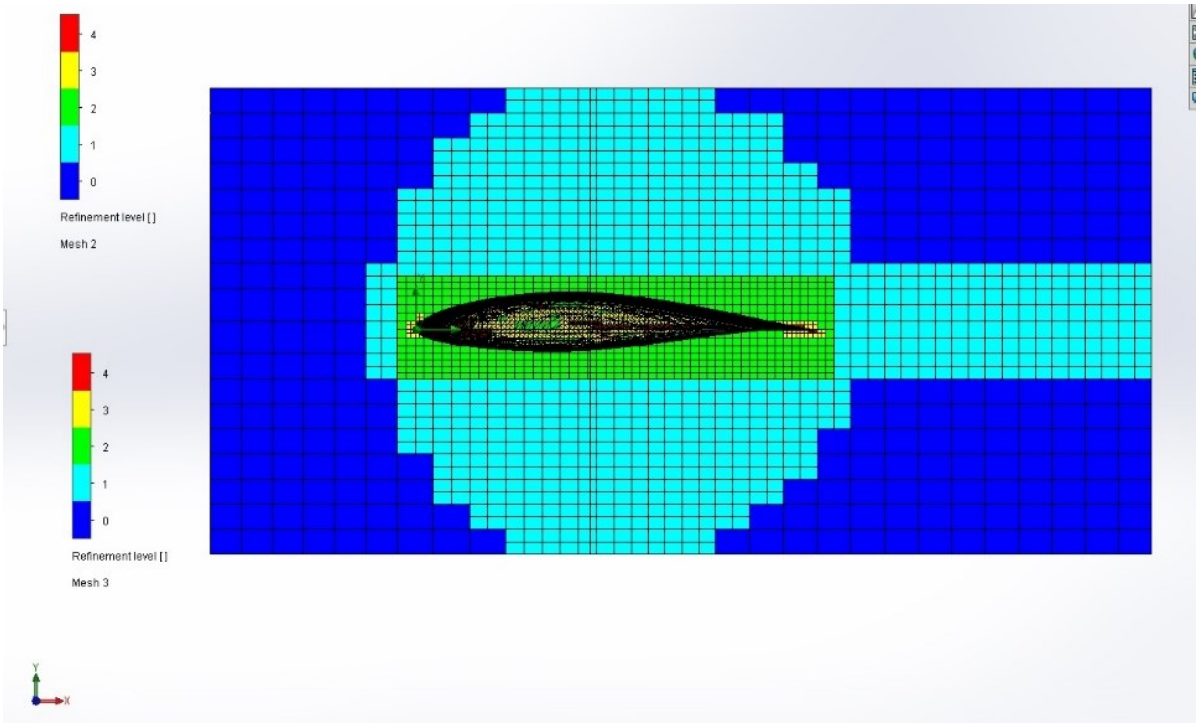

Fig. 2. Structured Medium Mesh

3. RESULTS AND DISCUSSION

Swept forward, swept back and oblique wing-only geometry stability are to be analyzed for stability by checking six degrees of freedom of force/moment components (L, D, Z, M_x,M_y,M_z) of the wing at a given incoming air speed. In this analysis, three wing configurations of equivalent span and sweep angle (60°) are analyzed with the geometric parameters as defined in Table 1. The objective of the analysis is to monitor, observe and compare forces and moments generated by three different wing configurations. As stated earlier, NACA 64(2)-415 is chosen as the wing section for all configurations.

Table 2: Geometric parameters for different wing configurations

Geometric Parameter	Value
Wing span, b	1.5m
Root chord, C_r	1m
Taper Ratio, λ	0.7
Aspect Ratio, AR	1.7647
Angle of attack, α	0°
Sweep angle, Λ_{LE}	60°

https://doi.org/10.31436/iiumecp.v1i1.3000

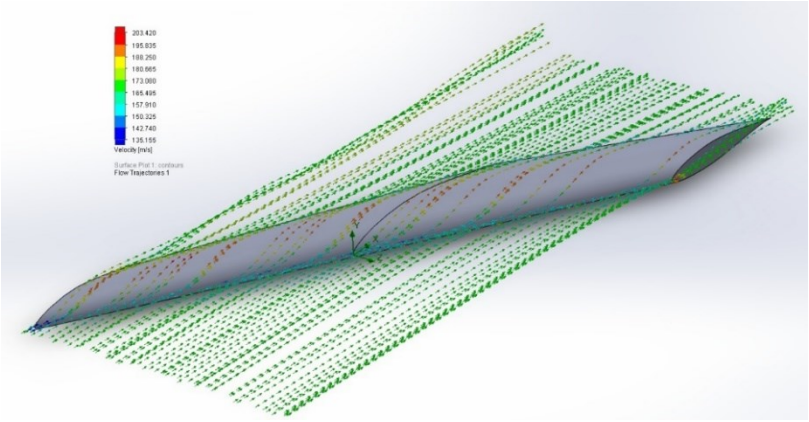

(a) Oblique Wing with 60º angle

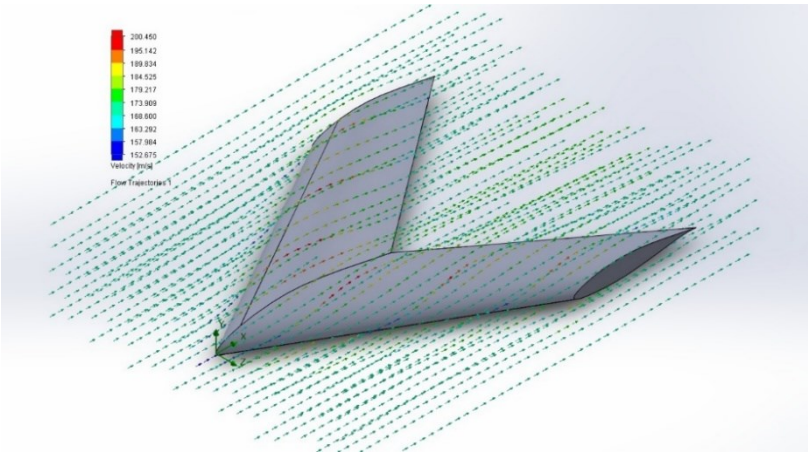

(b) Swept back Wing with 60º Sweep angle

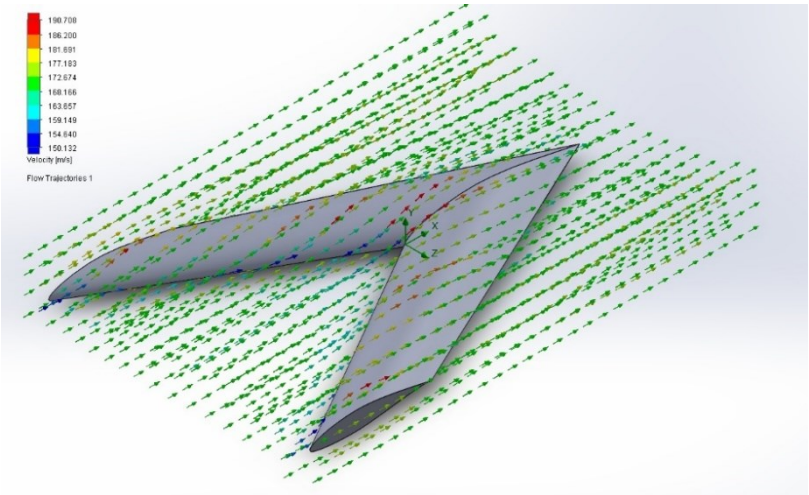

(c) Forward Swept Wing with 60º Sweep angle

Fig. 3. Velocity Vector plot for three different wing configuration

https://doi.org/10.31436/iiumecp.v1i1.3000

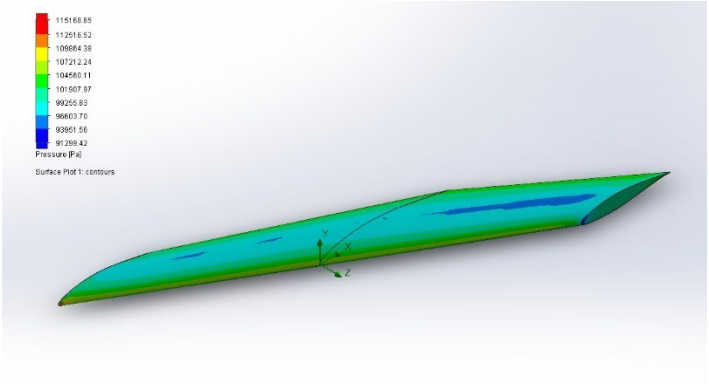

(a) Oblique Wing with 60º angle

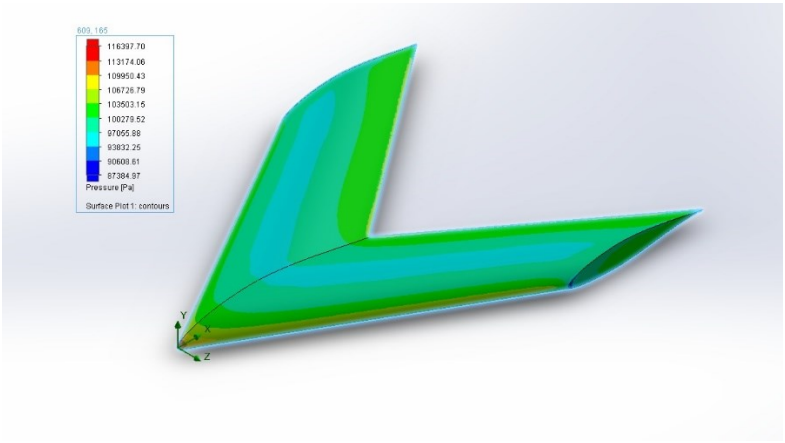

(b) Swept back Wing with 60º Sweep angle

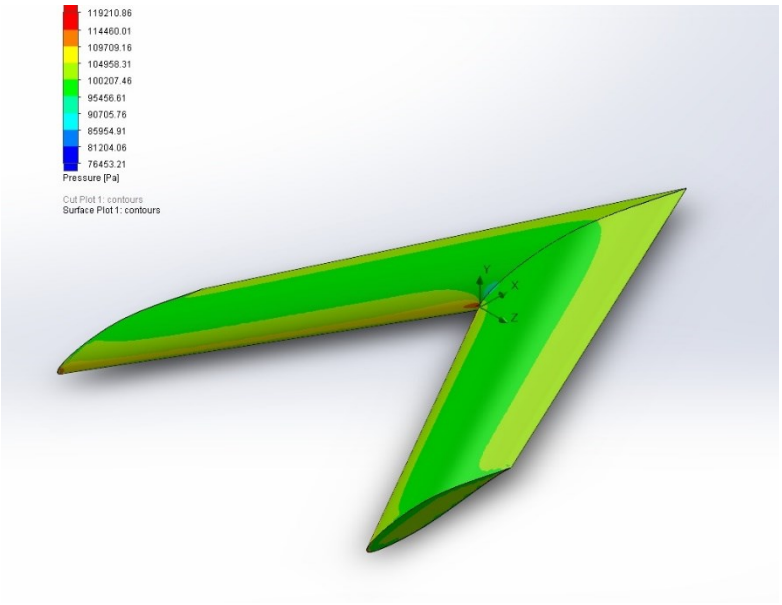

(c) Forward Swept Wing with 60º Sweep angle

Fig. 4. Surface Pressure Contour plot for three different wing configurations

https://doi.org/10.31436/iiumecp.v1i1.3000

Based on the CFD analysis, Fig. 3 and Fig. 4 shows the velocity contour and the pressure contour plot respectively for all the three wing configurations considered.

CFD results for stability observation is as follows. To simplify the analysis, all six components are equivalent to:-

- *X force = Drag*
- *Y force = Lift*
- *Z force = Sideslip force*
- *Moment about x-axis,* M_x *= Rolling moment*
- *Moment about y-axis,* M_y *= Yawing moment*
- *Moment about z-axis,* M_z *= Pitching moment*

Table 3: Forces and Moments on Different Wing Configurations

Force/Moment	Unit	60° Oblique	60° Swept Back	60° Swept Forward
D	N	83.609	88.041	67.275
L	N	1587.834	1692.756	1005.036
Z	N	-135.722	1.233	-1.526
M_x	N.m	-147.155	2.263	1.56
M_y	N.m	-304.626	-2.282	-1.045
M_z	N.m	1215.06	2164.471	143.634

All six components of forces and moments shown in Table 3 above were all subjected to origin (which is about the root leading edge). The Table 3 shows all six components of forces and moments for all 3 wing configurations considered in this analysis. Firstly, to observe whether the data is qualitatively reliable, the $\frac{L}{D}$ ratio of each of the wing configuration is checked as follows. From the Table 3 we can note that

- Oblique Wing, $\frac{L}{D}$ = 18.9911
- Swept Back, $\frac{L}{D}$ = 19.2269
- Swept Forward, $\frac{L}{D}$ = 14.9392

which is acceptable and within the range of expectation at Mach number = 0.5 for subsonic wing profile and it can be noted that aerodynamic performance of swept forward wing configuration is lower than sweptback wing as reported by Xue et al [13]. Moreover, it can be noted that oblique wing configuration has almost same $\frac{L}{D}$ value as compared to swept back wing which may not be true, it is expected to perform better than sweptback wing, this error may be due to quality of meshing.

It can be seen that for swept forward and swept back configuration sideslip force, Z, moment of x-axis, M_x, and moment of y-axis, M_y have low values of force and moments which can be neglected comparing to oblique wing which has significant value that obviously cannot be neglected. Thus, the oblique wing has a side slip and rotates about both x and y axis at the same time, thus causing serious stability problem making oblique wings highly unstable. The CFD analysis results obtained for high sweep angle of 60° confirms the flight experience reported by the experimental oblique wing aircraft pilots [6], that the flight performance dropped as sweep angle increased and also encountered serious lateral and directional instability. Thus, for high sweep angle at 60°, it can be noted that swept back and forward swept wings are better than oblique wings from the point of view of stability.

https://doi.org/10.31436/iiumecp.v1i1.3000

All wing configurations pitches as it is expected and known that wing is longitudinally unstable (pitching) which is countered by horizontal tail in complete aircraft. Surprisingly, it can be noted that swept forward wing has the lowest amount of all, followed by oblique wing and swept back respectively.

4. CONCLUSION

The aerodynamic performance and hence stability analysis was carried out for swept forward, swept back and oblique wing-only using SolidWorks software. Aerodynamic efficiency of Oblique wing is compared with other sweptwing configurations. From the present CFD analysis, it can be concluded that the flight performance of oblique wing drops at high sweep angle of 60^o coupled with high lateral and directional instability. Thus, for high sweep angle of 60^o, it can be noted that the sweptback and forward swept wings are better than oblique wing, as oblique wings are highly unstable. It is one of the prime reasons why oblique wing configuration could not be employed until recently, but the present day modern automatic control system may be able to control such unstable aircraft.

REFERENCES

[1] Hirschberg MJ, Hart DM, Beutner TJ. (2007) A Summary of a Half-Century of Oblique Wing Research, I 45th AIAA Aerospace Sciences Meeting, Reno.
[2] Jones RT. (1972) New Design Goals and a New Shape for SST, American Institute of Astronautics and Aeronautics, vol. 10, no. 12, pp. 66-70.
[3] Jones RT and Nisbet JW. (1974) Transonic Transport Wings-Oblique or Swept, American Institute of Astronautics and Aeronautics, vol. 12, no.1, pp. 40-47.
[4] Kroo IM. (1986) The Aerodynamics Design of Oblique Wing Aircraft, Proceedings of the AIAA/AHS/ASEE Aircraft Systems Design and Technology Meetings, CP 86-2624, AIAA, Washington D.C.
[5] Oblique Flying Wings: An Introduction and White Paper, (2005) Desktop Aeronautics, Inc., pg. 2-3, http://www.desktop.aero/library/whitepaper/.
[6] Bruce I. Larrimer. (2012) Thinking Obliquely, NASA Aeronautics Book Series.
[7] Kempel RW, McNeill WE, Maine TA. (1988) Oblique Wing Research Airplane Motion Simulation and Decoupling Control Laws, AIAA 26th Aerospace Sciences Meeting, AIAA-88-0402, 11-14 January 1988.
[8] Campbell JP, Drake HM. (1947) Investigation of stability and control characteristics of an airplane model with a skewed wing in the Langley free flight tunnel. NACA TN 1208.
[9] Mushfiqul A, Kashyapa N. (2014) Oblique Wing: Future Generation Transonic Aircraft, World Academy of Science, Engineering and Technology, International Journal of Mechanical, Industrial, Mechatronics and Manufacturing Engineering, Vol: 8, No: 5.
[10] Asif Shahriar Nafi, Shuvrodeb Barman, Anowar Sayef. (2015) An analysis of aerodynamic forces on an oblique wing" Proceedings of 10th Global Engineering Science and Technology Conference,2-3 January 2015, BIAM Foundation, Dhaka, Bangladesh.
[11] Wang L, Xu Z, Yue T. (2016) Dynamic Characteristics analysis and flight control design for oblique wing aircraft, Chinese Journal of Aeronautics, CSAA, Vol 29, No 6, 1664-1672.
[12] Joshua Patrick Deslich. (2020) Effects of a bell-shaped lift distribution on an Oblique flying wing and its impact on aerodynamic performance, MS thesis. University of Dayton.
[13] Xue Rongrong, Ye Zhengyin, Wang Gang. (2016) Aerodynamic characteristic comparison of the forward and backward-swept wings, ICAS 2016, 30th Congress of the International Council of the Aeronautical Sciences, Daejeon, Korea, Sept 25-30, 2016.

https://doi.org/10.31436/iiumecp.v1i1.2985

SURFACE RESISTIVITY OF CARBON NANOTUBE FILLED PRESSURE SENSITIVE ADHESIVE AFTER ANNEALING PROCESS

MAH HONG YEW[1], JAMAROSLIZA JAMALUDDIN[1*], NADIA ADRUS[1], LUQMAN ABDULLAH CHUAH[2]

[1]School of Chemical and Energy Engineering Faculty of Engineering
University Teknologi Malaysia, Johor Bahru, Johor, Malaysia
[2]Department of Chemical and Environmental Engineering, Faculty of Engineering,
Universiti Putra Malaysia, 43400 UPM, Serdang, Selangor, Malaysia

*Corresponding author: *jamarosliza@cheme.utm.my*

ABSTRACT: Pressure-sensitive adhesives (PSAs) exhibit adhesive properties upon applying light pressure. The light pressure adhesion of PSAs makes them suitable for potential applications in electronic packaging. However, to apply PSAs in electronic packaging, it is essential for them to possess electrostatic discharge (ESD) properties and high clarity. The attainment of ESD properties in PSAs can be achieved by either mechanically incorporating conductive fillers or chemically functionalizing the PSA compound. In this study, we aimed to achieve electrostatic discharge (ESD) properties in PSA using CNT as a conducting filler. CNT was selected for its strong conductivity compared to carbon black (CB). To accomplish this, CNT was mixed into the PSA formulation, which contained Chivacure 300 as a photoinitiator, silicone-urethane acrylate as an oligomer, and 2-ethyl-hexylacrylate and methyl methacrylate as monomers. The resulting PSAs were then coated onto polyethylene terephthalate (PET) film and cured with Ultraviolet light-emitting diode (UV-LED) light. However, the effect of CNT content on achieving a balance between ESD properties was insignificant. Therefore, an annealing process was introduced further to enhance the electrostatic discharge properties of the PSA. After the annealing process, it was found that PSAs with 0.75 phr of CNT achieved the desired electrostatic discharge (ESD) properties. Therefore, we examined the impact of the annealing process on the electrostatic properties and found that the inclusion of the annealing process significantly improved the electrostatic properties of pressure sensitive adhesives.

KEYWORDS*: Pressure Sensitive Adhesive, Multiwall Carbon Nanotube, Electrostatic Discharge, Ultra-Violet Light Emitting Diode, Annealing*

1. INTRODUCTION

Electrostatic Discharge (ESD) properties are one of the most important characteristics of pressure sensitive adhesive (PSAs) cover tape in order to prevent damage to electronic devices. In the context of the EOS/ESD Association (2008), material with different conductivity has been grouped according to their surface resistance. The requirement pertaining to ESD properties is very specific for packaging material, where it is mandated to achieve less than or equal to10^5 ohms to less than 10^{11} ohms by the International Electrotechnical Commission. To achieve surface resistance properties, various methods have been developed such as surface coating of static dissipative solutions, direct functionalization of filler onto matrix and compounding with filler. To our knowledge, compounding with filler is the most common technique, with several advantages over other methods, including stable surface conductivity, no environmental humidity effect, a more mature process, and lower cost. Conventionally, it is known that carbon black is the most common antistatic filler to use on PSA. Nonetheless, carbon black has several drawbacks, such aside requiring a higher amount of carbon

https://doi.org/10.31436/iiumecp.v1i1.2985

black to achieve the threshold level at which it exhibits the ESD properties(Antosik *et al.*, 2021). An studies has shown with inclusion of CB onto PSA tape would deteriorate the clarity and adhesion strength of the PSA (Park *et al.*, 2014). Threshold levels are often defined as the minimum content of the filler required to convert an insulative polymer to an antistatic polymer. Carbon nanotubes (CNT) discovered by Lijima in 1991 have emerged as one of the potential antistatic fillers. CNTs offer advantages such as higher conductivity, a higher surface ratio, better mechanical properties, and thermal resistance. However, the high surface ratio of CNTs often poses challenges when dispersing them into polymers. As a result, various techniques have been implemented to overcome the strong pi-bond between CNTs. These techniques can be broadly categorized into mechanical dispersion and functionalization dispersion methods. Mechanical dispersion involves physical mixing techniques such as sonification, calendaring, high-speed stirring, and extrusion, without altering the chemical properties of CNTs (Ma *et al.*, 2010). On the other hand, functionalization dispersion requires aggressive chemical reactions to change the surface properties of CNTs for better dispersion in polymers. However, even with physical mixing or chemical alteration, achieving a low percolation threshold (<1wt%) for effective dispersion of CNTs onto polymers, especially in PSA cover tape applications, is challenging due to the high percolation threshold (>2-3wt%) required. High percolation levels can result in deterioration of the host material's characteristics, such as transparency and peeling force, as reported in the literature (Czech *et al.*, 2011). Therefore, post-processing techniques, such as thermal annealing, have been introduced to further enhance the conductivity of CNTs in pressure-sensitive adhesive cover tape applications. Thermal annealing is associated with dynamic percolation, which refers to the network formation attribute through temperature changes resulting in self-assembly in quiescent melt. The focus of this paper is to understand and identify the impact of thermal annealing on carbon nanotube compounded on pressure-sensitive adhesive properties.

2. MATERIALS AND METHODS

2.1. Chemicals And Materials

Silicone urethance acrylate oligomer was obtained from Dymax Corporation, while 2-ethylhexylacrylate(2-EHA), methyl methacrylate(MMA),trimethlylopropane triacrylate (TMPTA), multiwall carbon nanotube, Sulphuric acid, and Nitric acid were purchased from Sigma Aldrich (Malaysia). The photoinitiator oligo[2-hydroxyl-2-methyl-1-[4-1(methylvinyl)phenyl]propanone] (Chivacure 300) was received from Chitec Sdn Bhd. Other chemicals were used without further purification.

2.2. Preparation of Pressure Sensitive Adhesive Filled Pristine CNT

The curable coating formulation was prepared by dissolving photoinitiator in the reactive monomers (2-EHA, MMA and TMPTA) for 1 hour at room temperature. Then, the oligomer and CNT of various compositions were added to the mixture and mixed mechanically for 1 hour, followed by ultrasound treatment for another hour. The prepared samples were then coated on PET film using a bar applicator with a coated thickness of 0.1mm and size of 130mm length X 80mm width. The samples prepared in such length and width are due to the minimal sizes required by the standard STM 11.11-2021. Lastly, the formulation was irradiated under UV LED radiation for 15 minutes.

2.3. Surface Resistance Analysis

In accordance with the standard STM 11.11 – 2021, the surface resistance of the static discharge pressure sensitive adhesive was measured by surface resistance meter (Prostat - 801). The coated adhesive sample was prepared with size of 130mm length X 80mm width. Then the electrode was placed on the middle of the coated surface and measured, for which this is a standard measurement that has been adopted by EOS/ESD Association for packaging material.

https://doi.org/10.31436/iiumecp.v1i1.2985

3. RESULTS AND DISCUSSION

To apply PSA to ESD products, it is necessary for the adhesive to possess a certain degree of surface resistance. The EOS/ESD Association specification mandates that the pressure-sensitive adhesive must have a minimum surface resistance of less than 10^{11} ohms. Hence, to meet this requirement, it is critical to incorporate a specific concentration of carbon nanotubes into the adhesive formula. The crucial concentration of carbon nanotubes required to meet the specification is commonly referred to as the percolation threshold. To achieve this threshold, various studies have explored the thermal effects of composite materials, which have shown a positive impact on the percolation threshold. Figure 1 shows the surface resistance of an annealing sample and non-annealing sample.

Figure1.0 Surface Resistance of Annealing Sample Vs Non Annealing Sample

Based on the result, it is observed that the sample without annealing treatment it unable to achieved static dissipative PSA on sample with annealing treatment it only required 0.75phr to achieve static dissipative ($8.1X10^{10}$ ohm). Based on the observations from the annealed sample, it can be concluded that the inclusion of conductive filler in an insulative material can lead to a transition in the material's behavior from being insulative to becoming static dissipative. This phenomenon is commonly referred to as the percolation threshold. In our study, it was observed that annealing the sample at 100°C resulted in a self-assembly process of carbon nanotubes, leading to their reorganization and closer proximity to each other, thereby forming a conductive network. In contrast, samples that did not undergo annealing showed carbon nanotubes remaining separated from each other, resulting in insulative behavior, despite the addition of conductive additives to the matrix. The similar conclusion has been made by McIntyre *et al.* (2020), annealing would cause reorganization of the CNT. Price *et al.* (2018) cited that CNT possess a high Van Der Waals forces; such forces are the barrier for which to disperse CNT evenly on the matrix. Hence, in this research, ultrasonification is applied to disperse CNT onto PSA material followed by annealing treatment to the sample. According to Frømyr *et al.* (2012), ultrasonification able create a high shear force to disperse CNT evenly onto the polymer matrix. Nonetheless, ultrasonification would cause the CNT farther apart from each other forming a random conductive network that causes an increase in electrical resistance (Pang *et al.*, 2014). Figure 2 below illustrates the ultrasonification dispersing CNT on PSA. As shown on Figure 2, the high Van der Waals forces cause the CNT to be lumped together, whereas dispersion via ultrasonification causes the CNT to be randomly dispersed, forming a random conductive network.

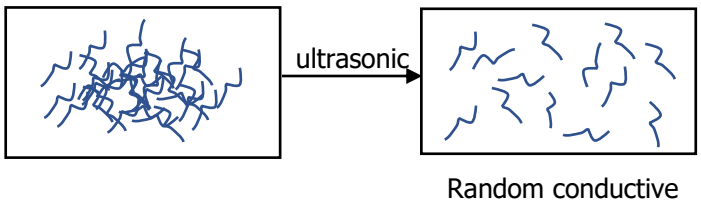

Figure 2.0 Ultrasonic Dispersing CNT on PSA

Upon annealing the sample, ultrasonification caused the CNTs to be dispersed further apart from each other. However, the thermal influence resulted in the re-aggregation of CNTs, forming a segregated

https://doi.org/10.31436/iiumecp.v1i1.2985

conductive network that led to a reduction in electrical resistance. This re-aggregation of CNT under 100ºC, is known as dynamic percolation, for which the factor causes the same concentration of CNT but behaves differently. In our study, the annealed sample containing 0.75 phr of CNT exhibited an electrical resistance of $8.1x10^{10}$ ohm, while the non-annealed sample had a higher resistance of $1.1x10^{11}$ ohm. Figure 3 shows a pictorial explanation of the random conductive network and segregated conductive network. It explained a schematic diagram where dispersion of CNT via ultrasonification followed by re-aggregation of CNT forming a conductive network.

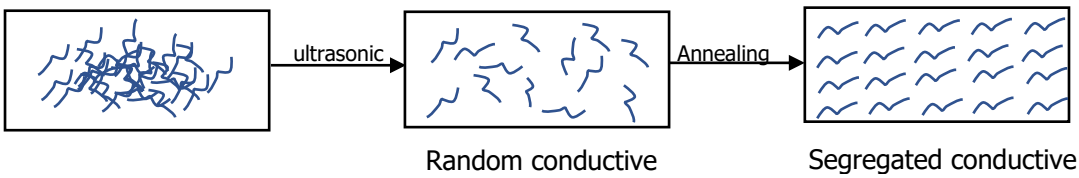

Figure 3.0 Schematic diagram of random conductive network and segregated conductive network.

According to Badard *et al.* (2017), the critical exponent (t) in the scaling law represents the dimensional structure of the carbon nanotubes within the pressure-sensitive adhesive. Based on our result shown that the critical exponent (t) value for the annealed sample was 2.26 with reference to the scaling law. Salaeh *et al.* (2020) have classified a universal critical value in which critical exponent less than or equal to two are represent a two dimensional structure and critical value greater than two are represents a three dimensional structure. According to this classification, it can be concluded that the annealed sample has a three-dimensional structure, which is likely to improve the conductivity of the PSA. Conversely, the non-annealed sample remained an insulating material as the concentration increased. Such a major dispute between the samples is due to two factors, where annealed samples undergo thermal expansion and dynamic percolation, whereas non-annealed samples depend on mechanical mixing to disperse CNT on the PSA. According to Zhang *et al.* (2015), thermal expansion increases the gap between CNTs, thereby reducing conductivity. This study observed thermal expansion in the annealed sample with 0.25 and 0.5 phr of CNTs, which resulted in higher electrical resistance compared to the non-annealed sample. As reference to Ansari *et al.* (2019) an thermal expansion of CNT reinforce material would happened within an material, hence in our studies it is proven that thermal expansion had occurred within the CNT and PSA. The second factor is the dynamic percolation event occurred within the PSA matrix which causes an increase in conductivity of 0.75 phr ($8.1X10^{10}$ ohm) in which with the application of the annealing the isolated carbon nanotube has been restructuring themselves into an infinite path because of the formation of the conductive network.

4. CONCLUSION

In conclusion, we have introduced annealing process to prepare pressure sensitive adhesive, whereby such methodology enables us to prepare a static dissipative pressure sensitive adhesive with a lower amount of CNT. The surface resistance reduction has been significantly reduced to 0.75 phr exhibiting static dissipative pressure sensitive adhesive after undergoing thermal annealing process at 100°C for which it led to a reaggregation of CNT on the PSA.

ACKNOWLEDGEMENT

The authors gratefully acknowledge the financial support of research funding from the Universiti Teknologi Malaysia: UTMFR vote no. 22H56, UTMFR vote no. 20H81 and Ministry of Higher Education Malaysia (MOHE): FRGS/1/2020/TKO/UTM/02/9 and FRGS/1/2017/TK05/UTM/02/16

REFERENCES

[1] Ansari, R., Hassanzadeh-Aghdam, M., & Darvizeh, A. (2019). Coefficients of thermal expansion of carbon nanotube-reinforced polyimide nanocomposites: A micromechanical analysis. Proceedings of the Institution of Mechanical Engineers, Part L: Journal of Materials: Design and Applications, 233(2), 169-179.

[2] Antosik, A. K., Mozelewska, K., Pełech, R., Czech, Z., & Antosik, N. A. (2021). Conductive Electric Tapes Based on Silicone Pressure-Sensitive Adhesives. Silicon, 13(3), 867-875.

[3] Badard, M., Combessis, A., Allais, A., & Flandin, L. (2017). Modeling the dynamic percolation of carbon nanotubes and revisiting critical exponents. Materials Chemistry and Physics, 191, 89-95.

[4] Czech, Z., Pełech, R., Kowalczyk, A., Kowalski, A., & Wróbel, R. (2011). Electrically conductive acrylic pressure-sensitive adhesives containing carbon black. Polish Journal of Chemical Technology, 13(4), 77-81.

[5] Frømyr, T. R., Hansen, F. K., & Olsen, T. (2012). The Optimum Dispersion of Carbon Nanotubes for Epoxy Nanocomposites: Evolution of the Particle Size Distribution by Ultrasonic Treatment. Journal of Nanotechnology, 2012, 545930.

[6] Ma, P.-C., Siddiqui, N. A., Marom, G., & Kim, J.-K. (2010). Dispersion and functionalization of carbon nanotubes for polymer-based nanocomposites: A review. Composites Part A: Applied Science and Manufacturing, 41(10), 1345-1367.

[7] McIntyre, D. J., Hirschman, R. K., Puchades, I., & Landi, B. J. (2020). Enhanced copper–carbon nanotube hybrid conductors with titanium adhesion layer. Journal of Materials Science, 55(15), 6610-6622.

[8] Pang, H., Xu, L., Yan, D.-X., & Li, Z.-M. (2014). Conductive polymer composites with segregated structures. Progress in Polymer Science, 39(11), 1908-1933.

[9] Park, G. H., Kim, K. T., Ahn, Y. T., Lee, H.-i., & Jeong, H. M. (2014). The effects of graphene on the properties of acrylic pressure-sensitive adhesive. Journal of Industrial and Engineering Chemistry, 20(6), 4108-4111.

[10] Price, G. J., Nawaz, M., Yasin, T., & Bibi, S. (2018). Sonochemical modification of carbon nanotubes for enhanced nanocomposite performance. Ultrasonics Sonochemistry, 40, 123-130.

[11] Salaeh, S., Thitithammawong, A., & Salae, A. (2020). Highly enhanced electrical and mechanical properties of methyl methacrylate modified natural rubber filled with multiwalled carbon nanotubes. Polymer Testing, 85, 106417.

[12] Zhang, H., Bilotti, E., Tu, W., Lew, C. Y., & Peijs, T. (2015). Static and dynamic percolation of phenoxy/carbon nanotube nanocomposites. European Polymer Journal, 68, 128-138.

https://doi.org/10.31436/iiumecp.v1i1.2991

REMOVAL OF CHLORAMPHENICOL COMPOUNDS USING HYDROCHAR FROM DRIED LEAVES

ISSWAR SENTHIL KUMEREN, NOORASHRINA A HAMID*

School of chemical engineering, Engineering campus, Universiti Sains Malaysia, 14300 Nibong tebal, Penang, Malaysia

**Corresponding author: chrina@usm.my*

ABSTRACT: Pharmaceutical industries' wastewater contains numerous contaminants including chloramphenicol (CAP) that harm human and aquatic lives which require the wastewater to be treated via adsorption. Hydrothermal carbonization (HTC) aids in producing hydrochar that can be converted into activated carbon at lower operating conditions to increase carbon porosity and decrease production costs. In this study, dry leaves were hydrothermally carbonized to produce hydrochar which was then activated into activated carbon prior to the removal of CAP. For CAP batch adsorption on resultant hydrochar, various operating parameters, including initial CAP concentration (10 mg/L to 50 mg/L) and solution pH (2 to 10) were utilized. Due to the high driving force for efficient mass transfer, the adsorption capacity of the initial CAP concentration increased as an increase in the adsorption capacity with a maximum value of 35.70 mg/g. The presence of the OH^- group enables the positive charge of CAP to attach easily to the adsorbent, thus making the basic conditions more favorable as opposed to the acidic conditions with maximum adsorption of 35.82 mg/g at pH 10. It was found that the Freundlich isotherm and pseudo-second order kinetic models suit well with the experimental data. Also, the rate-controlling step in this adsorption is chemical adsorption. According to the results, activated dried leaves derived hydrochar is a promising and cheap adsorbent for the removal of CAP from effluent wastewater.

KEYWORDS: *Adsorption, Characterization, Dried leaves, Hydrochar, Hydrothermal carbonization*

1. INTRODUCTION

In recent years, the potential threat of pharmaceuticals and personal care products to the environment has become a popular issue. Chloramphenicol (CAP), a broad-spectrum antibiotic discovered in 1947 in Streptomyces Venezuela is amongst the widely used in medical treatment of human and animals [1-2]. One way to treat the large amount of these compounds in pharmaceutical wastewater is by adopting adsorption techniques as these chemical compounds have high biological activity making biological treatment unsuitable to remove it. There are many sources of adsorbent including hydrochar derived activated carbon. Hydrochar derived from biomass waste via hydrothermal carbonization is an effective adsorbent for pollutant removal because of the abundance of surface oxygen-containing functional groups such as chloramphenicol (CAP) [3]. These functional groups play a crucial role in contaminant adsorption through electrostatic attraction, surface complexes, and ion exchange. Introducing new oxygen-containing functional groups, particularly carboxylate functional groups such as maleate and acetate, into hydrochar's structure and function can considerably increase its performance. As a result, the availability of surface functional groups in hydrochar can improve its adsorption effectiveness and expand the range of applications for which it can be used in

https://doi.org/10.31436/iiumecp.v1i1.2991

environmental clean-up [2-3]. Dried leaves are one of the potential biomass wastes that can be utilized as raw material for hydrochar as it's available abundantly with no cost. Utilizing dried leaves as source for hydrochar simultaneously solved the environmental issue related to waste management especially in urban area. Previously, Zahari and Hamid recorded 98.25% removal of methylene blue using 2.0 g of absorbent from dried leaves [4]. Meanwhile, Hamid and Thineswaren found that dried leaves that have been hydrothermally carbonized possessed unique characteristics ideally suitable to tuned into adsorbent [5]. Assessing this information earlier, dried leaves hydrochar has been proposed to solve the pharmaceutical wastewater containing chloramphenicol by activating it with phosphoric acid to enhance its surface area and porosity.

2. MATERIALS AND METHODS

Hydrochar was prepared by the hydrothermal carbonization of dried leaves using a stainless-steel reactor. About 25 g of dry leaves and 150 ml of distilled water are placed in the 200 ml reactor, and the treatment was carried out for 2 hours at fixed hydrothermal carbonization temperatures of 200°C. The reactor was then allowed to cool to ambient temperature before the solid char was removed and filtered using filter paper. The char was then cleaned twice with distilled water and dried at 105 °C for 12 hours before being chemically impregnated with phosphoric acid. The dried hydrochar was recovered and dried for 5 hours in an oven at 105°C. The sample is then loaded onto crucible, which are subsequently placed into a quartz tube and placed inside a microwave. The sample was carbonised first in the presence of carbon dioxide (CO_2) using microwave at 511-Watt power for 6 minutes. The activated carbon was cooled to room temperature in the presence of CO_2. The resultant activated carbon (AC) was neutralised with hydrochloric acid (HCl) and sodium hydroxide (NaOH) before being thoroughly rinsed with distilled water until a pH of 7 is attained. Finally, the AC was dried in an oven at 120°C for 24 hours before being characterised and utilized in the adsorption experiment.

2.1. Characterization of Hydrochar

The surface characteristics of samples can be determined by BET surface area analyzer (determine the BET surface area), scanning electron microscopy (image the surface morphology and properties), and FTIR analyzer (determine the functional groups). Two samples of hydrochar were compared in this characterization study which are hydrochar before and after activating with carbon in microwave. Both hydrochar samples were chemically impregnated with phosphoric acid with a 5:1 ratio.

2.1.1. Batch adsorption of Chloramphenicol

A UV-Vis spectrometer is used to determine the concentration of CAP for each interval. Wavelength of 278 nm is used to determine the concentration against time. Eq. (1) and (2) are used to calculate the adsorption capacity and removal efficiency of CAP:

$$Adsorption\ capacity, q_e = \frac{(C_o - C_e)V}{W} \quad (1)$$

$$Removal\ efficiency\ (\%) = \frac{C_o - C_e}{C_o} \times 100 \quad (2)$$

Where;

Q_e = adsorption capacity (mg/g),

C_0 = initial concentration of CAP solution (mg/L),

C_e = equilibrium concentration of CAP solution (mg/L),

https://doi.org/10.31436/iiumecp.v1i1.2991

V = volume of solution (L)

W = mass of adsorbent (g)

3. RESULTS AND DISCUSSION

3.1 Surface Electron Microscopy (SEM)

SEM images in Fig. 1(a-d) show that for both precursors, the H_3PO_4 chemical activation leads to a morphological change, developing a porous structure. Based on the SEM images, the pores in hydrochar after activation are more visible and denser compared to before. Moreover, the size of pores can also be seen bigger in after sample due to the char undergoing activation process which increases the porous structure. These pores increase the efficiency of adsorption of CAP solution. Therefore, the larger the number or size of pores will result in better adsorption.

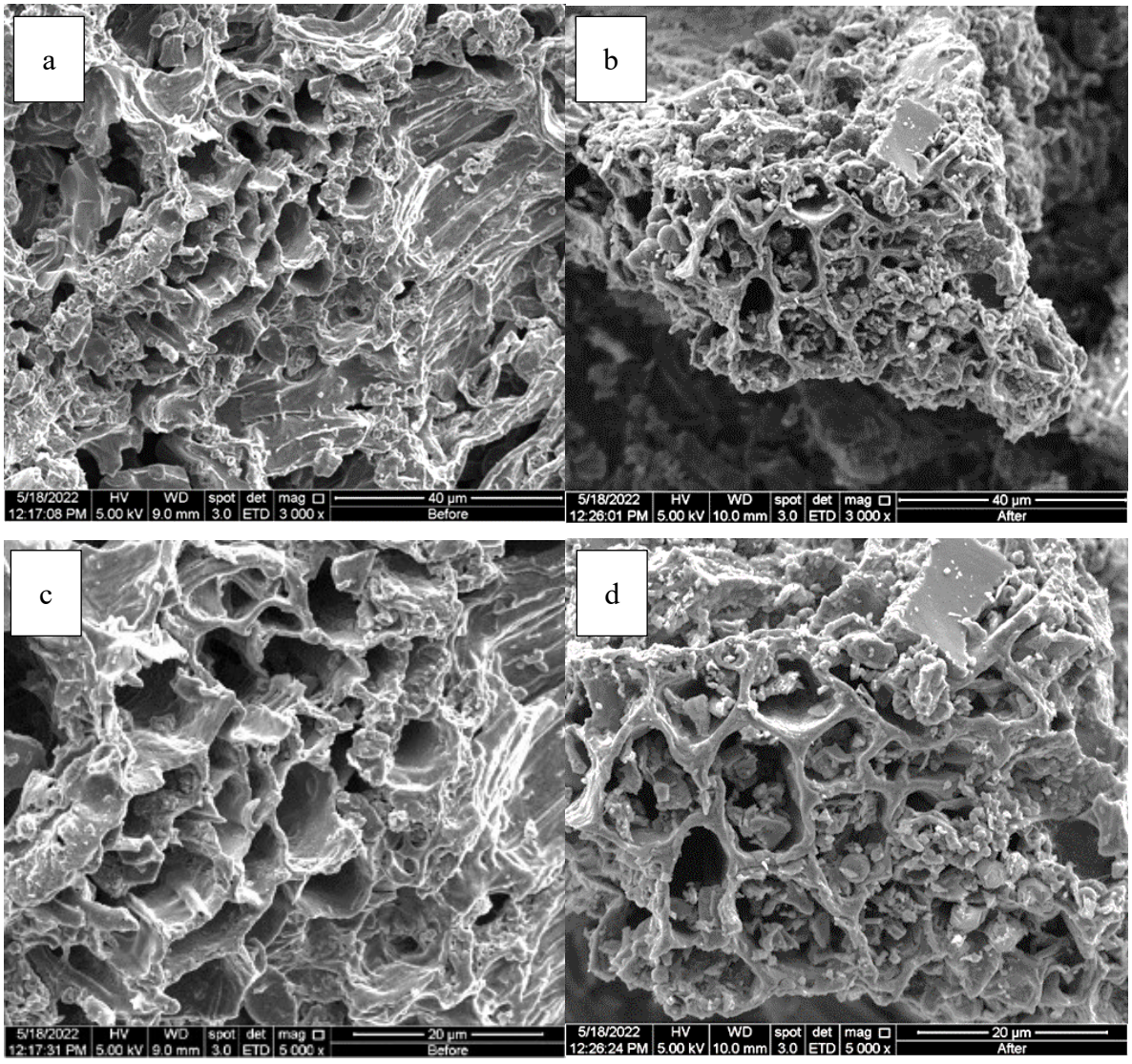

Fig. 1. SEM images before (a) and after (b) at a magnification of 3000x while (b) and (d) are before and after activation at 5000x magnification.

https://doi.org/10.31436/iiumecp.v1i1.2991

3.2 Fourier-Transform Infrared Spectroscopy (FTIR)

Fig. 2 shows the results of the functional group of hydrochar before and after the activation of carbon. For hydrochar prior to activation, the peaks (3795.91 cm^{-1} and 3402.43 cm^{-1}) indicated the presence of hydrate (H_2O), hydroxyl (-OH), ammonium, or amino, as well as oxygen-related groups such as alcohol and phenol in the plant extract. The broad peak at 2943.37 cm^{-1} was caused by aliphatic compound (C-H) stretching vibration. The peak at 2409.09 cm^{-1} indicated the presence of the triple bond (CC) in the sample. The broad peak at 1649.14 cm^{-1} was caused by the vibration of the double bond carbon (C=C), an olefinic compound, or an aromatic ring, whereas the peak at 1433.11 cm^{-1} and below was caused by (C-H) vibrations on an aromatic compound. In contrast, the peaks (3992.65 cm^{-1}, 3803.63 cm^{-1}, and 3414 cm^{-1}) observed after activation are due to (-OH) bond stretching vibration. The broad peak at 1583.56 cm^{-1} indicated the stretching of the double bond (C=C), whereas the peaks at 1409.96 cm^{-1} and below were caused by the vibrations of the (C-H) bond in the aromatic compound.

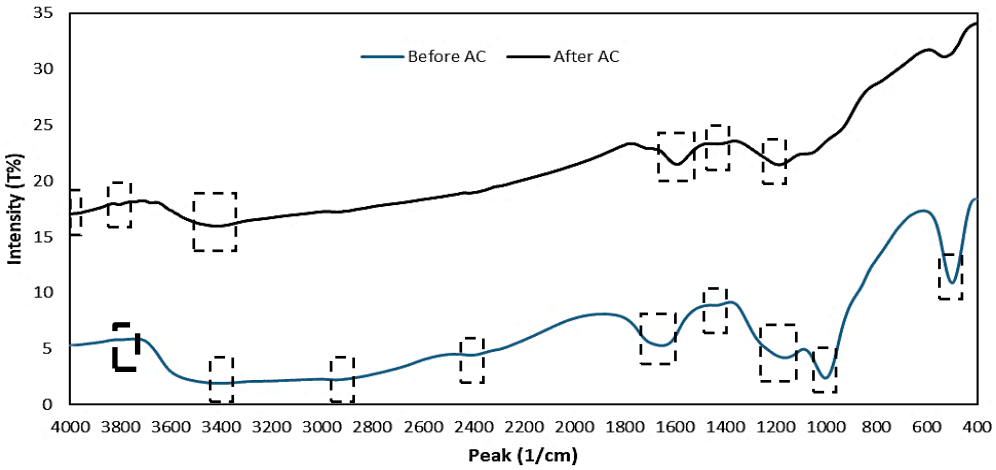

Fig. 2. FTIR result of hydrochar before and after activation.

3.3 Brunauer–Emmett–Teller (BET)

Dried leaves hydrochar derived activated carbon possessed a relatively well-developed pore structure with BET surface area of 647.88 m^2/g, Langmuir surface area of 913.14 m^2/g and total micropore volume of 0.07 cm^3/g as illustrated in Table 1. It is obvious that activation using phosphoric acid under carbon dioxide flow has altered the hydrochar significantly. The BET surface area of hydrochar after activation was higher compared to before activation as hydrochar derived activated carbon exerted the larger surface which then allowing for better removal of CAP in degradation studies.

Table 1. The properties of hydrochar before and after activation

Properties	Before (Hydrochar)	After (Activated hydrochar)
BET Surface Area (m^2/g)	5.3966	647.8754
Langmuir Surface Area (m^2/g)	18.2134	913.1442
t-Plot micropore volume (cm^3/g)	-0.0024	0.0676

https://doi.org/10.31436/iiumecp.v1i1.2991

3.4 Effect of initial concentration of CAP

Removal of CAP using dried leaves hydrochar derived activated carbon was investigated by exposing 0.2 g of adsorbent to CAP solutions with initial concentrations ranging from 10 mg/L to 50 mg/L at neutral pH and 30 °C. Manipulation of initial concentrations aids in determining the suitability of hydrochar applications in different conditions and developing cost-effective processes. At the initial stage of adsorption, the availability of more active sites on the surface of hydrochar promotes a rapid uptake of adsorbates. As shown in Fig. 3, the scenario is well represented by steeper curves observed during the first 5 minutes for each studied initial concentration. The sites are gradually occupied over time due to the competitive adsorption of CAP molecules, and only a few vacant sites are retained. At this stage, the active sites for adsorption have been saturated and difficult to be occupied because of the repulsion between the solute molecules of the solid and bulk phase [5]. The possibility of CAP desorbing from adsorbent exists if the amount of CAP absorbed on the adsorbent is in a state of dynamic equilibrium. It is worth noting that three zones were involved in the adsorption of CAP. The first zone represented fast CAP adsorption, implying rapid external diffusion and surface adsorption, while the second zone signified gradual equilibrium and the third zone denoted the equilibrium plateau. As a result, until equilibrium is reached, CAP adsorption becomes slower. Furthermore, the maximum adsorption capacity of hydrochar increased from 6.83 mg/g to 35.70 mg/g as the initial concentration of CAP solution increased from 10 mg/L to 50 mg/L. As shown in Fig. 3, the percentage of adsorption efficiency of hydrochar decreased from 96.41% to 94.89%, as the initial CAP concentration solution increased. At lower concentrations, the initial number of CAP molecules to available surface area ratio is low, and fractional adsorption becomes independent of initial concentration [6]. This could be clarified by the theory that, during the adsorption process, CAP molecules must first encounter the boundary layer effect, then diffuse from the boundary layer film onto the adsorbent surface, and finally diffuse into the porous structure of the adsorbent [7].

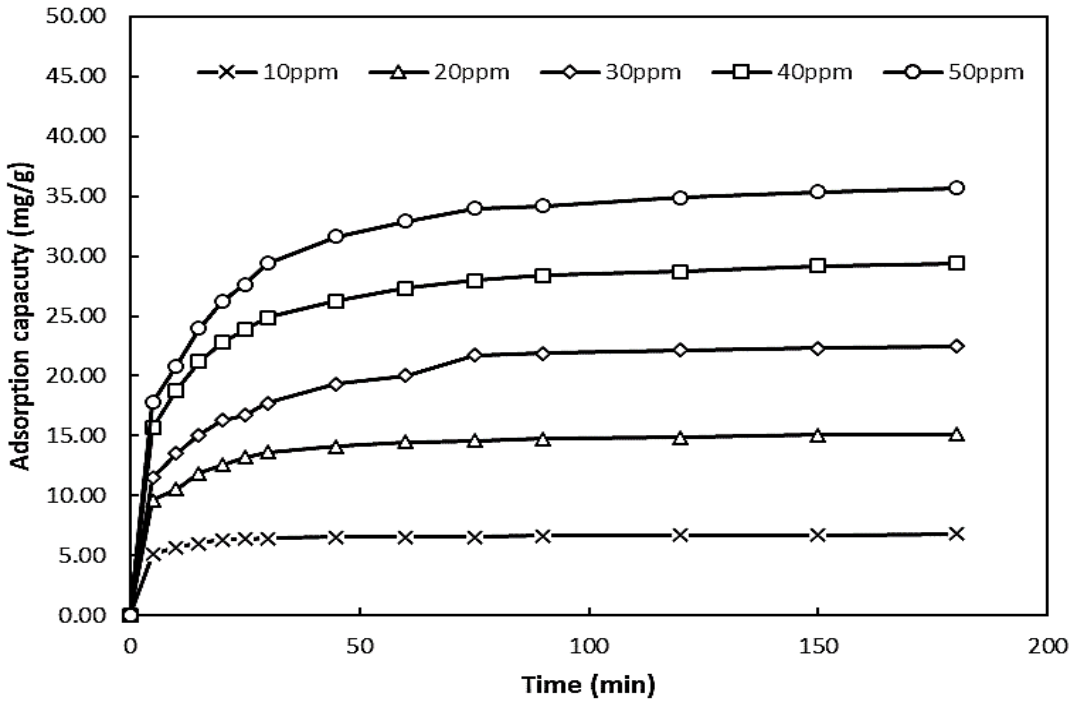

Fig. 3. CAP adsorption uptake versus adsorption time of hydrochar at different initial concentrations.

https://doi.org/10.31436/iiumecp.v1i1.2991

Furthermore, a longer equilibrium time was required for high initial concentrations. Adsorption equilibrium was reached after 180th minute for the highest initial concentration (50 mg/L), and at the 90th minute for the lowest initial concentration (10 mg/L). This is because, as the adsorbent surface becomes saturated, most of the sorbate molecules diffuse into the porous structure of hydrochar. Because the diffusion mechanism increases the mass transfer resistance to adsorption, higher initial concentrations require a longer contact time to achieve equilibrium with the adsorbent.

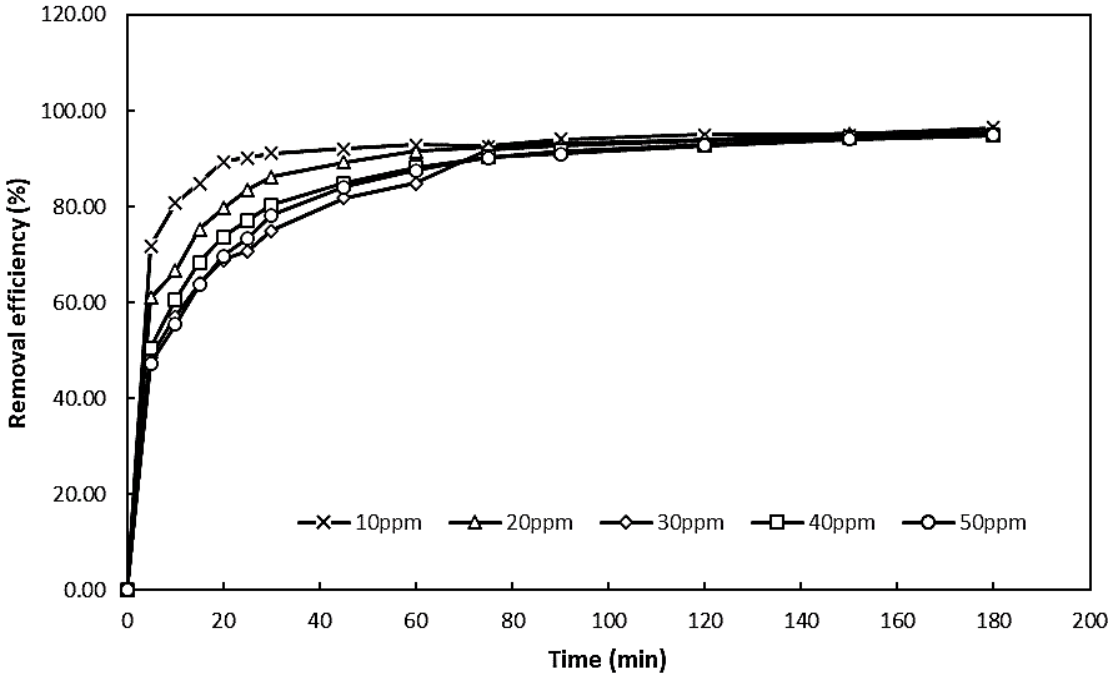

Fig. 4. CAP percentage removal versus adsorption time of hydrochar at different initial concentrations

3.5 Effect of pH of solution

To investigate the effect of solution pH on CAP adsorption, 0.2 g of hydrochar was exposed to 50 mg/L CAP solution at 30 °C at various initial pH levels ranging from pH 2 to pH 10. The pH value was adjusted accordingly by adding hydrochloric acid or sodium hydroxide solution, and the time-dependent adsorption profile is shown in Fig. 3. The adsorption performance improved with contact time until the equilibrium state was reached. Under extremely acidic conditions, CAP molecule uptake was relatively low because hydrochar had the lowest adsorption capacity at equilibrium with a value of 32.74 mg/g. This is because the cationic CAP molecules generate a strong electrostatic repulsion on the surface of hydrochar with a high concentration of H^+ ions in an acidic environment. Furthermore, according to Islam et al. [4] the presence of OH groups on the surface of hydrochar causes protonation of the OH group and creates a competition between H^+ ions and CAP molecules to bind with the active sites, resulting in a low affinity. Adsorption capacity-time curves demonstrated that adsorption increased from acidic to basic conditions, with a maximum equilibrium adsorption capacity of 35.82 mg/g at pH 10. Furthermore, the removal efficiency of CAP increases as the pH increases. The removal efficiency at most acidic condition (pH = 2) is 87.29% while at basic condition (pH =10) is 91.90%. In contrast to acidic solutions, increasing the pH of the solution enhanced the negatively charged active sites on the adsorbent surface in the presence of OH groups and improved adsorption performance. Due to the dissociation of the hydroxyl group,

https://doi.org/10.31436/iiumecp.v1i1.2991

CAP has a positive charge when dissolved in water. In alkaline solutions, it is more strongly attracted to the negatively charged surface of activated carbon. However, a slight increase in adsorption capacity was observed for solutions ranging from pH 2 to pH 8. It is easily explained that the H^+ and OH^- ions are nearly balanced within these three pH values, resulting in no noticeable competition.

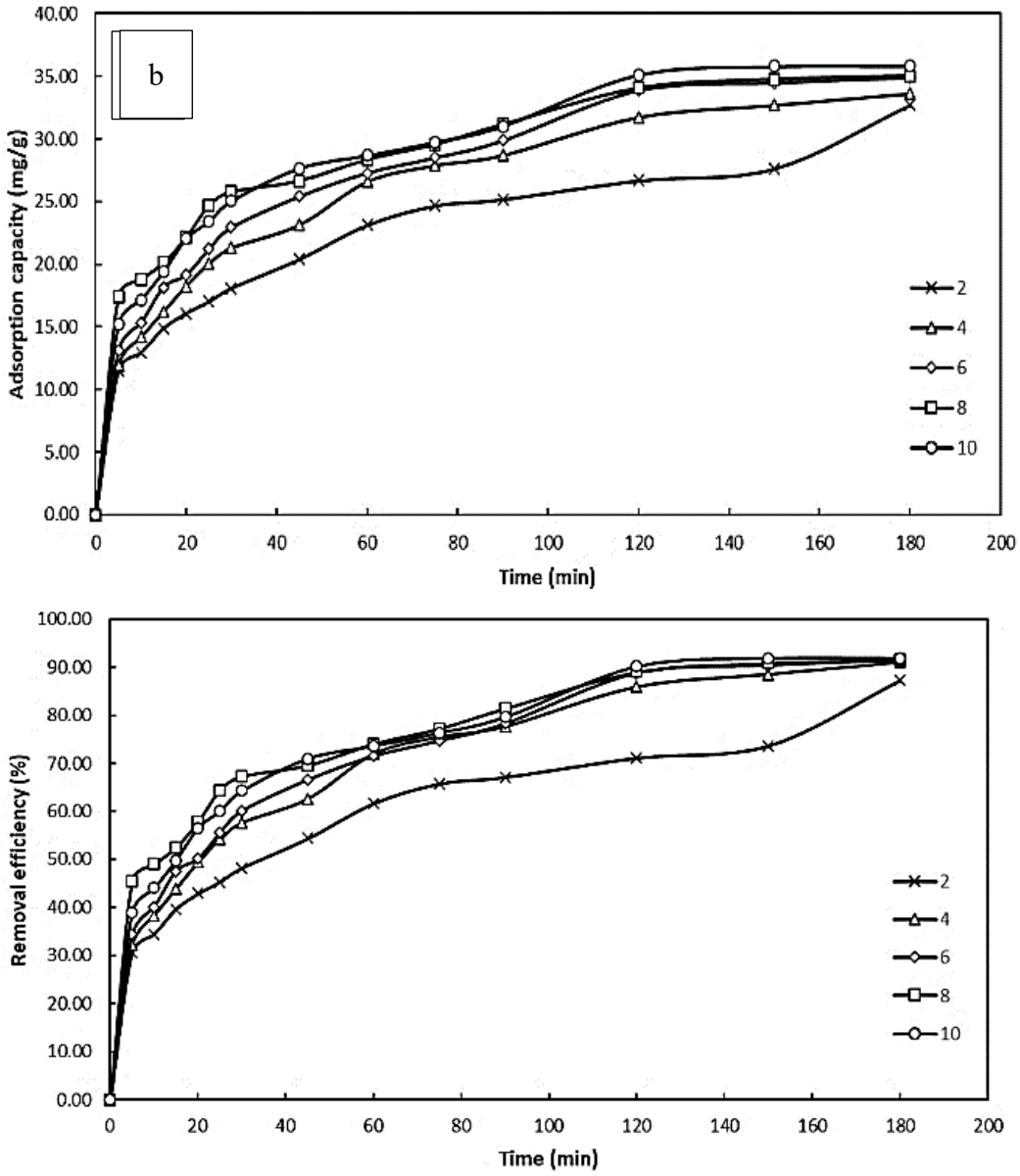

Fig. 5. CAP adsorption uptake (a) and percentage removal (b) versus adsorption time of hydrochar at different pH

3.6 Adsorption Isotherm and Kinetics

Adsorption isotherms describe the relationship between the concentration of CAP (adsorbate) molecules in the aqueous phase and the degree of adsorbed molecules on the adsorbent surface at equilibrium at constant temperature. Langmuir, Freundlich and Temkin isotherms were used as the mathematical model on the experimental data to determine the interaction of adsorbed molecules on the adsorbent surface.

https://doi.org/10.31436/iiumecp.v1i1.2991

Table 2. Adsorption isotherm parameters for CAP adsorption

Isotherm	Parameters	Values
Langmuir	q_m (mg/g)	76.92
	K_L (L/mg)	0.83
	R^2	0.9975
Freundlich	K_F (mg/g)	16.32
	n_F	1.23
	R^2	0.9996
Temkin	B	13.689
	AT (L/mg)	4.12
	R^2	0.9368

From Table 2, it can be summarized that the models showed a good fitting to the experimental data for value R^2 in order of Freundlich > Langmuir > Temkin. The Freundlich isotherm model yielded the best fit with the highest correlation coefficient (R^2) at 0.9996 since they are closer to unity. These results showed that multilayer sorption took place at the heterogenous adsorbent's surface. In addition, the Freundlich constant, n_F is found to be greater than 1, indicating the favourable condition for adsorption. From the tabulated result, it can be noticed that the maximum adsorption capacity, q_m, computed from Freundlich isotherm is close to the experimentally determined value (35.70 mg/g). Hence, the maximum adsorption capacity of CAP by dry leaves hydrochar is estimated to be 16.32 mg/g.

To investigate the adsorption mechanism and the characteristics of CAP adsorption behaviour, pseudo-first order and pseudo-second order kinetic models were fitted to the adsorption kinetics of hydrochar on CAP solution.

Table 3. Kinetic parameters

	C_o (mg/L)				
Parameters	**10**	**20**	**30**	**40**	**50**
q_{exp} (mg/g)	6.83	15.12	22.49	29.39	35.70
Pseudo First Order					
q_{cal} (mg/g)	1.30	5.61	13.14	13.97	18.61
k_1 (min^{-1})	0.02	0.03	0.03	0.03	0.03
R^2	0.7222	0.9273	0.9736	0.9573	0.9634
Pseudo Second Order					
q_{cal} (mg/g)	6.84	15.36	23.31	30.12	36.76
k_1 (g/mg.min)	0.08	0.02	0.01	0.01	0.00
R^2	0.9998	0.9996	0.9979	0.9991	0.9987

Based on the summary of kinetic models in Table 3, pseudo second order kinetic models fit the experimental data better than pseudo first order models, as this model produced higher R^2 values and was closer to unity. For the pseudo-second-order kinetic model, the R^2 values are between 0.9979 and 0.9998, whereas for the pseudo-first-order kinetic model, R^2 values are between 0.7222 and 0.9736 were obtained. Thus, it was determined that the removal of CAP by hydrochar followed pseudo-second order kinetic models. Moreover, the q_e value of the pseudo-second order for both adsorbents was considerably closer to the experimental q_e values than the q_e value of the pseudo-first-order kinetic model. The adsorption of CAP on hydrochar, as described by a pseudo second-order kinetic model, implied a chemical controlling step, indicating that the reactions involved valency forces through the sharing or exchanging of

electrons between the surface functional groups on hydrochar and CAP molecules [8]. Because the kinetic data fitted a pseudo-second-order kinetic model, Qin et al. hypothesised that chemical adsorption was the rate-controlling step of CAP adsorption on porous carbon [9]. Mohd Din et al. reported that CAP adsorption on mesoporous carbons followed a pseudo-second-order kinetic model, with a π-π interaction as a possible CAP adsorption mechanism [10]. Therefore, chemisorption explains the adsorption of CAP on hydrochar prepared in this study.

According to the results presented above, the physical adsorption of CAP by hydrochar was the primary adsorption mechanism. This was because the hydrochar had well-developed porosity and a large surface area that the CAP could occupy. Additionally, chemical interaction existed during the adsorption process. The CAP ketone, nitro, and benzene groups contained -electron-acceptors with a potent electron-withdrawing capacity. Consequently, CAP had a strong interaction with hydrochar, which possessed graphite surfaces with a high concentration of polarised -electron via - electro-donor acceptor (EDA) interaction during the adsorption process. In addition, hydrogen-bond interactions are possible between the N-H,–OH groups in CAP and the O-containing groups (COOH,-CO, etc.) on the AC surface [11]. It was proposed that the ionic/polar groups (such as phenol, amine, and alcohol) present in antibiotic molecules could interact strongly with the corresponding structural components of carbonaceous adsorbents via H-bonding. The functional groups -OH, $-CH_3$, $-NH_2$, and N-H in the two antibiotics can act as H acceptors by hydrogen bonding with the O-containing groups -COOH and C=O on the AC surface.

4. CONCLUSION

The CAP removal efficiency of 91.90% was recorded at pH 10 due to the enhancement of the negatively charged active sites on the adsorbent surface in the presence of OH groups and improved adsorption performance. The hydrochar was best characterised by the Freundlich isotherm model, indicating that multilayer CAP sorption occurred on the hydrochar's heterogeneous surfaces. In the meantime, kinetic studies revealed that the adsorbent was best described by a pseudo-second order kinetic model as opposed to a pseudo-first order kinetic model based on the correlation coefficient, R^2, which was close to unity. This indicates that the rate-controlling step of CAP adsorption on porous carbon was chemical adsorption. Thus, it is implied that dried leaves can be converted into adsorbent to remove CAP from pharmaceutical effluent wastewater.

ACKNOWLEDGEMENT

The authors are grateful to the Ministry of Higher Education Malaysia (MOHE) under the Fundamental Research Grant Scheme (FRGS//1/2020/TK0/USM/01/4) (203/PJKIMIA/ 6071482).

REFERENCES

[1] Falyouna O, Maamoun I, Ghosh S, Malloum A, Othmani A, Eljamal O, Amen TWM, Oroke A, Bornman C, Ahmadi S, Hadi DM, Hossein MA, Nasseri S, Tyagi I, Suhas, Reddy KJ. (2022) Sustainable technologies for the removal of Chloramphenicol from pharmaceutical industries Effluent: A critical review. Journal of Molecular Liquids, 368:120726. https://doi.org/10.1016/j.molliq.2022.120726.

[2] Syieluing W, Norzita N, Inuwa IM, Onn H. (2018) Recent advances in applications of activated carbon from biowaste for wastewater treatment: A short review. Journal of Cleaner Production, 175: 361-375. https://doi.org/10.1016/j.jclepro.2017.12.059.

[3] Lach J. (2019) Adsorption of CAP on Commercial and Modified Activated Carbons. Water, 11(6): 1141.
[4] Ummi SZ, Noorashrina AH. (2020) Dried Leaves as Potential Adsorbent for Removal of Methylene Blue. Journal of Engineering Technology, 11, 2:11-21.
[5] Noorashrina AH, Thineswaren ST. (2022) Physicochemical Properties of Hydrochars Produced from Khaya Senegalensis Leaves Using Hydrothermal Carbonisation. Journal of Engineering Science and Technology, 17, 3:1781-1791.
[6] Islam MA, Ahmed MJ, Khanday WA, Asif M, Hameed BH. (2017) Mesoporous activated coconut shell-derived hydrochar prepared via hydrothermal carbonization-NaOH activation for methylene blue adsorption. Journal of Environmental Management, 203:237-244. https://doi.org/10.1016/j.jenvman.2017.07.029.
[7] Demirbas A. (2009) Agricultural based activated carbons for the removal of dyes from aqueous solutions: A review. Journal of Hazardous Materials, 167: 1-9.
[8] Tan IAW, Ahmad AL, Hameed BH. (2008) Adsorption of basic dye on high surface-area activated carbon prepared from coconut husk: Equilibrium, kinetic and thermodynamic studies. Journal of Hazardous Materials, 154: 337-346.
[9] Li H, Zhang Y, Guo J, Lv J, Huan W, Li B. (2021) Preparation of hydrochar with high adsorption performance for methylene blue by co-hydrothermal carbonization of polyvinyl chloride and bamboo. Bioresource Technology, 337: 125442.
[10] Qin L, Zhou Z, Dai J, Ma P, Zhao H, He J, Xie A, Li C, Yan Y. (2016) Novel N-doped hierarchically porous carbons derived from sustainable shrimp shell for high-performance removal of sulfamethazine and chloramphenicol. J. Taiwan Inst. Chem. E, 62: 228–238.
[11] Mohd Din AT, Ahmad MA, Hameed BH. (2015) Ordered mesoporous carbons originated from non-edible polyethylene glycol 400 (PEG-400) for chloramphenicol antibiotic recovery from liquid phase. Chem. Eng. J., 260: 730–739.
[12] Zhu X, Gao Y, Yue Q, Kan Y, Kong W, Gao B. (2017) Preparation of green alga-based activated carbon with lower impregnation ratio and less activation time by potassium tartrate for adsorption of chloramphenicol. Ecotoxicology and Environmental Safety, 145: 289-294.

https://doi.org/10.31436/iiumecp.v1i1.3001

ROLE OF HYDROXYL IONS IN THE GROWTH OF 1-D ZINC OXIDE ON WIRE USING DIRECT HEATING METHOD

ANH THI LE[1,2], THI DUY HANH LE[2], NGUYEN ANH TUAN HUYNH[2], KUAN-YEW CHEONG[1], CHEE-MENG KOE[1], WAI-KIAN TAN[3], SUMIYYAH BINTI SABAR[1], SWEE-YONG PUNG[1]*

[1]*School of Materials and Mineral Resources Engineering, Engineering Campus, Universiti Sains Malaysia, 14300 Nibong Tebal, Penang, Malaysia*

[2]*Faculty of Chemical and Food Technology, Ho Chi Minh City University of Technology and Education (HCMUTE), No. 1 Vo Van Ngan, Thu Duc City, Ho Chi Minh City, Vietnam*

[3]*Institute of Liberal Arts and Sciences, Toyohashi University of Technology, Toyohashi, 441-8580, Aichi, Japan*

**Corresponding author: sypung@usm.my*

ABSTRACT: One dimensional zinc oxide (1-D ZnO) array has been utilized for various application such as photocatalytic, solar cells, and light emitting diode. Low-temperature solution-based methods including hydrothermal, chemical bath deposition, and precipitation methods have been frequently employed for the growth of 1-D ZnO nanostructures. These methods are easy to handle, less expensive, and environmental friendly. However, the main drawback of solution-based methods is the long growth duration of ZnO nanostructures varying from 2 to 12 hours. Direct heating method enables ZnO nanostructures to grow rapidly (less than 1 hour) on a metal substrate by employing the Joule heating effect. Under direct heating condition, the effect of hydroxyl ion (OH^-) on the formation of 1-D ZnO is crucial to investigate. In this work, ZnO submicron-rods were grown on kanthal wire with different OH^- concentrations. The formation of ZnO submicron-rods was verified by FESEM, TEM and XRD analyses. At low OH^- ion concentration, $Zn(OH)_2$ precipitates were formed in the bulk solution. With the increase of OH^- ion concentration, $[Zn(OH)_4]^{2-}$ complexes were formed, which initiated the nucleation of ZnO on the kanthal wire surface. After direct heating for 10 minutes using 1.2M of OH^- ion, ZnO submicron-rods were fully grown on the wire with an average diameter of 304 ± 78.6 nm. In conclusion, tailoring the OH^- ion concentration eliminated the formation of $Zn(OH)_2$ precipitates and increased the $[Zn(OH)_4]^{2-}$ complexes which was favorable for the growth of 1-D ZnO in a controlled manner using direct heating method.

KEYWORDS: *ZnO, Direct heating; Hydroxyl ion; Kanthal wire*

1. INTRODUCTION

One dimensional zinc oxide (1-D ZnO) array has been attracted much attention in advanced applications including light-emitting devices [1], solar cells [2], gas sensors [3], and photocatalysis [4]. It is known that the optical and electrical properties of ZnO nanostructure are highly dependent on shape, size, and orientation [5]. ZnO arrays has been commonly synthesized by two-steps hydrothermal with long growth duration (3h to 12h) [6]. Developing a rapid and simple method has been attracted much attention for synthesizing 1-D ZnO arrays on supportive substrate.

https://doi.org/10.31436/iiumecp.v1i1.3001

Low-temperature (65 – 95°C) solution-based methods including hydrothermal [6], chemical bath deposition [7], or precipitation [8] methods were frequently employed for the growth of ZnO nanostructures. These methods are easy to handle, low temperature (60-100°C), less expensive, and environmental friendly. However, long growth duration and randomly orientation of ZnO crystal are the main drawback of solution-based methods. Direct heating method had been adapted for growing 1-D ZnO nanorods/nanowires on printed circuit board [9], and stainless steel mesh [10]. By employing the Joule heating effect, the substrate is directly heated when the current is passing through. Under direct heating condition, the effect of hydroxyl ions (OH^-) on formation of 1-D ZnO nanostructures on the heated substrate is crucial to investigate. Thus, in this study, the structure and morphology of ZnO was examined to evaluate the role of hydroxyl ions on the growth of ZnO on kanthal wire.

2. MATERIALS AND METHODS

The materials used to synthesize ZnO were sourced from Merck including zinc acetate dehydrate (CAS-383058) and sodium hydroxide (CAS-1064981000). Kanthal wire (Vapour Tech, 20Ga, coil 30 feet) was used as a supportive substrate for the growth of ZnO.

Direct heating method was used to synthesize ZnO on kanthal wire as reported in previous study [11]. Firstly, kantal wire was cut, coiled into a string and ultrasonic cleaned using ethanol and dried at 80°C. Secondly, solutions of 0.1M zinc acetate dehydrate and sodium hydroxide with various concentrations of 0.8M, 1M and 1.2M were prepared separately using distilled water. Zinc acetate dehydrate solution was added dropwise into sodium hydroxide under vigorous stirring for 15 min at room temperature. Both ends of the kanthal coil were connected with electrical power supply of 30W. The kanthal coil was dipped into the as-prepared precursor mixture. The coil was heated up when applying the power of 30W for 10min. The temperature of the wire was measured by a digital thermometer. After 10 min of direct heating, the coil was washed with distilled water and dried at 80°C. The as-synthesized samples were designated as ZnO/wire-0.8M, ZnO/wire-1M, and ZnO/wire-1.2M corresponding to the OH^- concentration of 0.8M, 1M, and 1.2M, respectively.

The structure and morphology of as-synthesized samples were analyzed using X-ray Diffraction (XRD, Bruker D8, accelerating voltage of 40kV, Cu K_a radiation k = 1.5406 Å) and Field Emission Scanning Electron Microscope (FESEM, Zeiss Supra 35VP, WD = 5mm, accelerating voltage of 10kV, and InLens detector), Transmission Electron Microscope (TEM, Tecnai G220 S-Twin, 200kV field emission gun) analyses, respectively. The average length and diameter of ZnO rods were measured from FESEM images using ImageJ software with the sample size of 10.

3. RESULTS AND DISCUSSION

Figure 1 shows XRD spectra of bare kanthal wire and as-synthesized ZnO/wire grown at various OH^- concentration of 0.8M, 1M, and 1.2M. The bare kanthal wire had diffraction peaks of Aluminum Chromium (Al_8Cr_5, Hexagonal, ICDD. no. 98-000-0411) and Aluminum Chromium Iron ($Al_{0.5}Cr_{0.5}Fe$, Cubic, ICDD. no. 98-006-5697). After growing ZnO with OH^- concentration of 0.8M and 1M (sample ZnO/wire-0.8M and ZnO/wire-1M) most of the diffraction peaks of bare kanthal wire were suppressed. Only main diffraction peaks of Al_8Cr_5 (at 29.29° and 47.33°) and $Al_{0.5}Cr_{0.5}Fe$ (at 44.85°, 65.02°, and 82.34°) were found at ZnO/wire-1M sample. When OH^- concentration was increased to 1.2M (sample ZnO/wire-1.2M) additional diffraction peaks at 34.4°, 36.6°, and 63.1° matched the crystallographic (002), (011) and (013) planes of ZnO hexagonal Wurtzite structure (ICDD no.: 98-010-5281), respectively. Similar diffraction patterns of ZnO was reported by Amin et al. [12], where ZnO nanorods

https://doi.org/10.31436/iiumecp.v1i1.3001

were grown on silicon substrate at 90°C for 5h using hydrothermal method. The crystallographic (002) plane had the strongest diffraction peak of ZnO/wire-1.2 sample, indicating that ZnO was preferably grown in [001] direction [13].

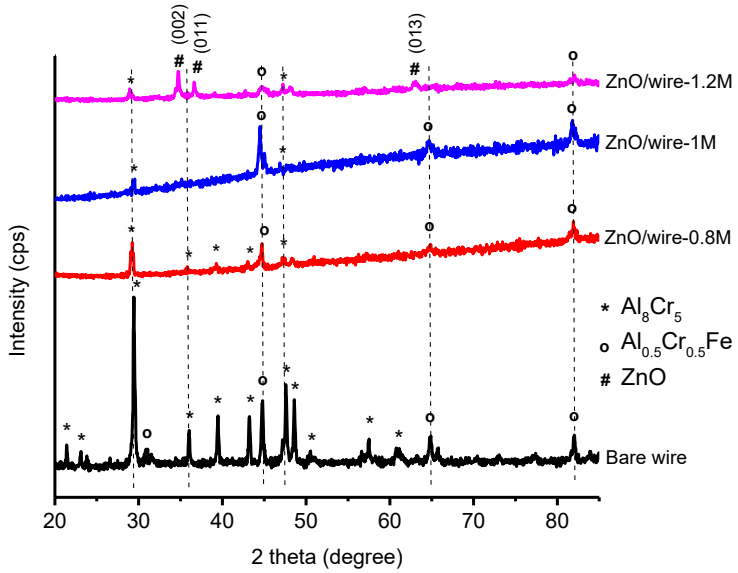

Figure 1. XRD spectra of bare kanthal wire and as-synthesized ZnO/wire grown at various OH- concentration of 0.8M, 1M, and 1.2M.

The role of OH^- ions on the growth of ZnO on kanthal wire was further investigated via morphology evolution using FESEM analysis as shown in Figure 2. After direct heating the wire at 30W for 10min the solution temperature was 73 ± 5°C. Figure 2a shows the morphology of ZnO/wire-0.8M sample, containing wo kinds of distinct products i.e., flower-like ZnO and octahedral $Zn(OH)_2$. The average diameter and length of flower-like ZnO were 67.2 ± 4.8um and 619.4 ± 180.9nm, respectively. The average size of octahedral $Zn(OH)_2$ particles was 2.7 ± 0.6µm which were aggregated from smaller microcrystals. Similar observation was found at the study of phase transformation of $Zn(OH)_2$ to ZnO particles at 80°C for 2h using hydrothermal method [14]. When the OH- concentration increased to 1M (Figure 2b), more ZnO nucleus was started growing on kanthal wire. At OH^- concentration of 1.2M, ZnO rod-shaped was fully grown on the wire surface with average diameter of 304 ± 78.6nm as depicted in Figure 2c. The FESEM images ZnO/wire-1.2M are consistent with the XRD spectra in Figure 1, showing that ZnO sub-micron rods grew on kanthal wire along [001] (c-axis) direction. Figure 2d & 2e shows TEM images of ZnO/wire-1.2M. The lattice fringes of the ZnO rods were 0.26 nm which corresponds to the (002) plane of the wurtzite ZnO. Similar lattice fringes spacing of ZnO was observed in the study of Hsu et al., in which ZnO nanorods were grown on stainless steel mesh by hydrothermal method [15].

Based on the XRD spectra, FESEM and TEM images, it can be concluded that the OH- ions play a major role for the growth of 1-D ZnO structure on kanthal wire. The OH^- ions created the super-saturation of aqueous solution of zinc acetate and sodium hydroxide, which was the key driving force for the growth of ZnO during direct heating. At relatively low OH^- concentration (0.8M), $Zn(OH)_2$ precipitates were mainly formed in the solution rather than growing on the kanthal wire surface. With the increase of OH- concentration to 1.2M, $Zn(OH)_2$ precipitates were dissolved forming soluble $[Zn(OH)_4]^{2-}$ complexes which were favorable for the nucleation of ZnO during direct heating the wire [14]. It is well known that that the hexagonal wurtzite ZnO was the polar crystal; and polar face (002) with surface dipoles were

https://doi.org/10.31436/iiumecp.v1i1.3001

thermodynamically less stable [4]. Thus, $[Zn(OH)_4]^{2-}$ ions could be adsorbed on the positively charged (002) plane of ZnO, promoting the crystal growth on [001] direction for forming 1-D ZnO submicron rod shape.

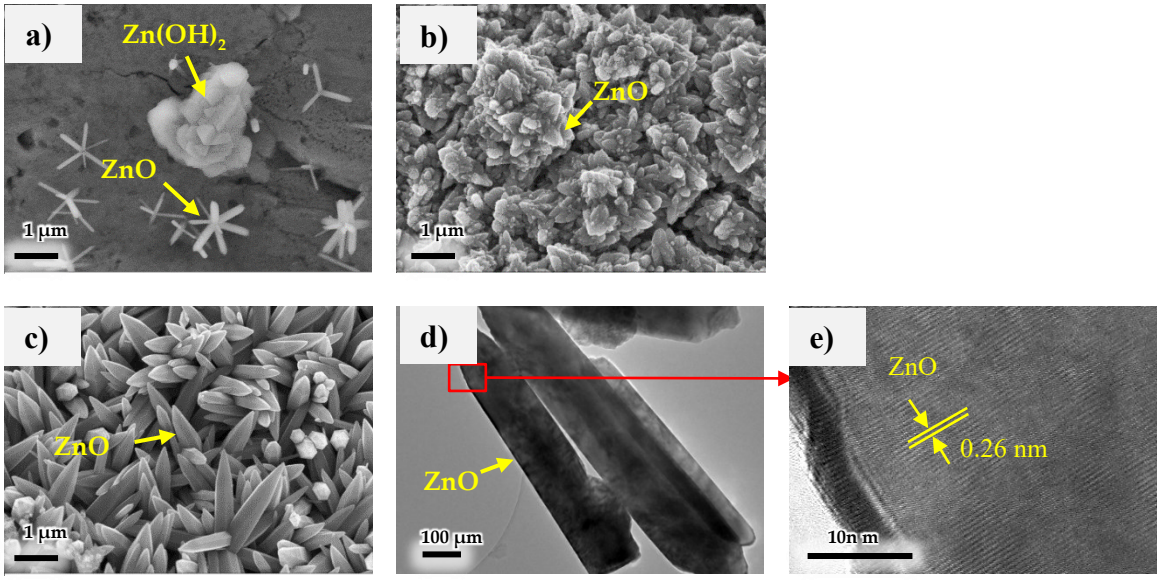

Figure 2. Morphology of ZnO/wires. a) – c) FESEM images of ZnO/wire samples synthesized at OH- concentrations of a) 0.8M, b) 1M, and c) 1.2M; and d) – e) TEM/HRTEM of ZnO/wire-1.2M

4. CONCLUSION

ZnO sub-micron rods with average diameter of 304 ± 78.6nm were fully grown on the kanthal wire by direct heating method with the control of OH^- ions concentration. At low OH- concentration, $Zn(OH)_2$ precipitates were formed in the solution rather than growing onto kanthal wire surface. With the increase of OH^- concentration, the nucleation of ZnO nuclei from $[Zn(OH)_4]^{2-}$ complex was initiated on the kanthal wire surface under direct heating. Tailoring the OH^- ion concentration eliminated the formation of $Zn(OH)_2$ precipitates and increased the $[Zn(OH)_4]^{2-}$ complexes which was favorable for the growth of 1-D ZnO in a controlled manner using direct heating method.

ACKNOWLEDGEMENT

The authors gratefully acknowledge the financial support of Ministry of Higher Education, Malaysia for providing the research funding under Fundamental Research Grant Scheme (FRGS) (FRGS/1/2020/TK0/USM/02/27) to conduct this project and the support from the USM Fellowship and Faculty of Chemical and Food Technology, HCMC University of Technology and Education.

REFERENCES

[1] Han, W., S. Oh, C. Lee, J. Kim, and H.-H. Park, (2020). ZnO nanocrystal thin films for quantum-dot light-emitting devices, ACS Applied Nano Materials, 3(8):7535-7542.

[2] Wibowo, A., M.A. Marsudi, M.I. Amal, M.B. Ananda, R. Stephanie, H. Ardy, and L.J. Diguna, (2020). ZnO nanostructured materials for emerging solar cell applications, RSC Advances, 10(70):42838-42859.

[3] Wang, C.N., Y.L. Li, F.L. Gong, Y.H. Zhang, S.M. Fang, and H.L. Zhang, (2020). Advances in doped ZnO nanostructures for gas sensor, The Chemical Record, 20(12):1553-1567.

[5] Le, A.T., T.D.H. Le, K.-Y. Cheong, and S.-Y. Pung, (2022). Immobilization of zinc oxide-based photocatalysts for organic pollutant degradation: A review, J. Environmental Chemical Engineering, 10(5):108505.

[6] Saleem, S., M.H. Jameel, A. Rehman, M.B. Tahir, M.I. Irshad, Z.-Y. Jiang, R.Q. Malik, A.A. Hussain, A.u. Rehman, A.H. Jabbar, A.Y. Alzahrani, M.A. Salem, and M.M. Hessien, (2022). Evaluation of structural, morphological, optical, and electrical properties of zinc oxide semiconductor nanoparticles with microwave plasma treatment for electronic device applications, J. Materials Research and Technology, 19(2126-2134.

[7] Zhu, Y., L. Zhou, and Q. Jiang, (2020). One-dimensional ZnO nanowires grown on three-dimensional scaffolds for improved photocatalytic activity, Ceramics International, 46(1):1158-1163.

[8] Abdulrahman, A.F., S.M. Ahmed, N.M. Ahmed, and M.A. Almessiere, (2020). Enhancement of ZnO nanorods properties using modified chemical bath deposition method: effect of precursor concentration, Crystals, 10(5):386.

[9] Yasmeen, S., F. Iqbal, T. Munawar, M.A. Nawaz, M. Asghar, and A. Hussain, (2019). Synthesis, structural and optical analysis of surfactant assisted ZnO–NiO nanocomposites prepared by homogeneous precipitation method, Ceramics International, 45(14):17859-17873.

[10] Chew, Z.J. and L. Li, (2012). Localised zinc oxide nanowires growth on printed circuit board by in-situ joule heating, Materials Letters, 76(226-228.

[11] Lee, W.C., Y. Fang, D. Commandeur, R. Qian, Z.T.Y. Al-Abdullah, and Q. Chen, (2017). Ultra rapid direct heating synthesis of ZnO nanorods with improved light trapping from stacked photoanodes for high efficiency photocatalytic water splitting, Nanotechnology, 28(35):355402.

[12] Aziz, S.N.Q.A.A., K.C. Meng, S.-Y. Pung, Z. Lockman, A. Ul-Hamid, and W.K. Tan, (2022). Rapid growth of zinc oxide nanorods on kanthal wires by direct heating method and its photocatalytic performance in pollutants removal, J. Industrial and Engineering Chemistry,

[13] Amin, G., M. Asif, A. Zainelabdin, S. Zaman, O. Nur, and M. Willander, (2011). Influence of pH, precursor concentration, growth time, and temperature on the morphology of ZnO nanostructures grown by the hydrothermal method, J. Nanomaterials, (2011)269692.

[14] Doustkhah, E., M. Esmat, N. Fukata, Y. Ide, D.A.H. Hanaor, and M.H.N. Assadi, (2022). MOF-derived nanocrystalline ZnO with controlled orientation and photocatalytic activity, Chemosphere, 303(134932.

[15] Wang, M., Y. Zhou, Y. Zhang, S.H. Hahn, and E.J. Kim, (2011). From $Zn(OH)_2$ to ZnO: a study on the mechanism of phase transformation, Crystal Engineering Communications, 13(20):6024-6026.

[16] Hsu, M.-H. and C.-J. Chang, (2014). Ag-doped ZnO nanorods coated metal wire meshes as hierarchical photocatalysts with high visible-light driven photoactivity and photostability, J. Hazardous Materials, 278:444-453.

https://doi.org/10.31436/iiumecp.v1i1.3002

QUALITATIVE METABOLITE PROFILING OF GENETICALLY MODIFIED *Escherichia coli* DURING XYLITOL PRODUCTION USING GC-MS

DAYANG NURFAIZATULQURAIN ABANG ZAIDEL, ZANARIAH HASHIM*, ROSLI MD. ILLIAS

Faculty of Chemical and Energy Engineering, Universiti Teknologi Malaysia, 81310 UTM Skudai, Johor, Malaysia

**Corresponding author: zanariahhashim@utm.my*

ABSTRACT: Many studies have been done by metabolically modifying *Escherichia coli* to produce elevated levels of xylitol. While there have been some positive results, the xylitol yield is still not at par with that produced via the chemical route. This study employed GC-MS, combined with multivariate analysis to qualitatively profile the metabolites found in genetically modified *E. coli* (Δ*pgi*+*xpdh*) for xylitol production with glucose as substrate. It was found that over time, xylitol level increased, with the peak intensity at 24h being the highest. This was parallel with the optical density (OD) value, which also increased over time, indicating that as the cell grew, more xylitol was generated. Top contributing metabolites were identified and subjected to pathway analysis, revealing that amino acids may have a significant role in xylitol production. The findings from this study provide initial metabolomics input for enhancing recombinant *E. coli* strains in the biotechnological production of xylitol, whereby glucose is employed as primary substrate.

KEYWORDS: *Metabolomics, GC-MS, Escherichia Coli, Xylitol, Amino Acid.*

1. INTRODUCTION

Xylitol is a naturally occurring 5-carbon polyol mainly used in the food industry as sugar substitute due to its similar sweetening power to sucrose but with lower caloric content among other benefits [1]. Current commercial production of xylitol via the chemical route is an extensive and unsustainable process requiring refining treatment for xylose which also makes it costly [2]. As such, continuous research has been done to produce xylitol biotechnologically by genetic modification of microorganisms, including *Escherichia coli*, which is a model microorganism for producing target compounds in laboratory settings [3] and resulted in positive outcomes [4, 5]. In terms of substrate, both xylose and glucose had been studied for xylitol production with the latter being much preferable due its price and availability [6]. Nonetheless, despite various approaches taken to increase xylitol yield including improvisation of immobilisation strategy and process parameters optimisation [7, 8], the amount of xylitol yielded is still incomparable to that of the chemical route. The metabolomics approach has proven to be successful in improving target compound production, specifically 1-butanol [9, 10, 11]. So far, none of the studies on recombinant *E. coli* producing xylitol has taken the metabolomics approach to increase xylitol yield. Therefore, this study seeks to qualitatively profile the metabolites present in recombinant *E. coli* (Δ*pgi*+*xpdh*) during xylitol production using glucose as a substrate by using GC-MS and multivariate analysis, as the first step in the metabolomics approach to improve xylitol production.

https://doi.org/10.31436/iiumecp.v1i1.3002

2. MATERIALS AND METHODS

2.1. Bacterial Strain

E. coli BL21 strain from Novagen was deleted for phosphoglucose isomerase (Δ*pgi*) gene to redirect the glucose catabolism from glycolysis to pentose phosphate pathway (PPP), and xylitol phosphate dehydrogenase (*xpdh*) gene from *Clostridium difficile* was cloned into the strain by using plasmid pET21 as vector. Insertion of *xpdh* gene was to enable the conversion of D-xylulose-5-phopshate to xylitol in PPP.

2.2. Bacterial Culture

Xylitol production took place for 24 h in a 250 mL shake flask with 50 mL LB medium (5 g/L yeast extract, 10 g/L NaCl, 10 g/L tryptone) added with 34 μg/mL chloramphenicol, induced by adding 0.1 mM isopropyl β-d-1-thiogalactopyranoside (IPTG) and 10 g/L glucose and incubated in an orbital shaker at 200 rpm and 37 ℃.

2.3. Cell Sampling and Metabolites Extraction

Cell sampling and metabolites extraction was done according to Hashim and Fukusaki [12] with slight modification. 5 mL of culture media was transferred to a fresh tube at 0, 2, 5, and 24 h. The sample was centrifuged at 4 ℃, 5000 rpm for 5 min to separate the cell pellet from the media. The media which contained extracellular metabolites was transferred to a new tube and kept at -20℃ for further analysis. Meanwhile, the cell pellet was immediately added with 2 mL of pre-cooled (-20℃) single-phase extraction solvent (methanol/chloroform/water = 5/2/2 v/v/v%) with 60 μL ribitol (0.2 mg/mL) as internal standards [12, 13]. The mixture was then left for 30 min in an incubator shaker at 200 rpm, 4 ℃. Afterwards, 1 mL of distilled water was added into the mixture, vortexed and centrifuged at 4 ℃, 16100 rcf for 3 min. Next, the upper polar phase was transferred to a new tube via syringe filtration (0.2 μm PTFE hydrophilic membrane, Hawach Scientific, Shaanxi, China) and freeze dried. Derivatisation was done by adding 75 μL of methoxyamine hydrochloride (Sigma-Aldrich, MO, USA) dissolved in pyridine (Merck, Darmstadt, Germany) to the lyophilised extracts and left in thermomixer to react at 30 ℃, 1200 rpm for 90 min in a process called oximation, followed by silylation by adding 50 μL of *N*-methyl-*N*-(trimethylsilyl)trifluoroacetamide (MSTFA) (Sigma-Aldrich, MO, USA) and the reaction was performed at 37 ℃, 1200 rpm for 30 min [13]. The derivatised samples were transferred to glass vials and analysed with GC-MS within 24 h.

2.4. Analytical Methods

2.4.1. Cell Growth

The cell growth was observed by measuring the optical density at 600 nm (OD_{600}) using a UV-1601 spectrophotometer (Shimadzu, Kyoto, Japan) at 0, 1, 2, 3, 4, 5, and 24 h. Measured values of OD_{600} were plotted on the growth curve.

2.4.2. GC-MS Analysis

GC-MS analysis was performed using GCMS-QP2010 Ultra (Shimadzu, Kyoto, Japan). The samples were separated using a BP5MS capillary column coated with 5% phenylpolysilphenylene-siloxane (30 m x 0.25 mm i.d. x 0.25 μm film thickness). One μL of sample was injected in split mode with a split ratio of 1:25. The injector, transfer line, and ion source temperature were set at 230, 250, and 200 ℃, respectively. The column flow rate was 1.12 mL/min (linear velocity 39 cm/s). The column temperature was held at 80 ℃ for 2 min,

https://doi.org/10.31436/iiumecp.v1i1.3002

raised by 15 ℃/min to 330 ℃ for 12 min. Electron ionisation (EI) was performed at 70 eV. The mass range of the detector was set to *m/z* 35 to 800 and the detector voltage (set by auto-tuning) was at 0.80 kV.

2.5. Multivariate Analysis and Statistical Analysis

The amount of each metabolite (peak intensity) was normalised to the internal standard (ribitol), mean centred and scaled to unit variance. Multivariate data analysis, such as principal component analysis (PCA), and pathway analysis was performed using MetaboAnalyst 5.0 [14].

3. RESULTS AND DISCUSSION

3.1. Bacterial Cell Growth

To determine bacterial cell growth, OD_{600} was measured using a UV-1601 spectrophotometer (Shimadzu, Kyoto, Japan). Fig. 1(a) shows the plotted growth curve for *E. coli* (Δ*pgi*+*xpdh*). It was observed that the exponential growth phase of the cell was between 1 to 4 h, with the maximum specific growth rate (μ_{max}) of 0.0.0459 h^{-1}. The cell continued to grow until the 24th hour albeit slower, indicating that the cell was starting to enter the stationary phase past 24 h.

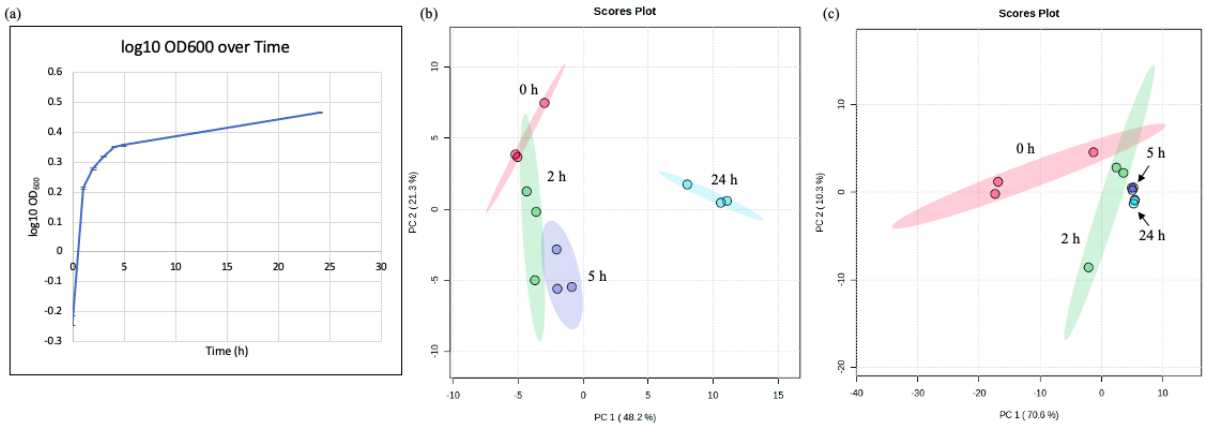

Fig. 1. (a) Growth curve of modified *E. coli* during 24 h xylitol production, and PCA score plot showing metabolite profile in (b) intracellular extracts, (c) extracellular extracts collected at 0, 2, 5, and 24 h.

3.2. Time-course Metabolite Profiling

Fig. 1(b) and 1(c) show time-course metabolite profiles of *E. coli* (Δ*pgi*+*xpdh*) at 0, 2, 5, and 24 h post-induction for intracellular and extracellular extracts respectively. It can be seen that the metabolites at 24 h are distinctly separated from the rest especially in the intracellular samples. This pattern corresponds to xylitol production which reach its peak at 24 h post-induction as can be observed in Fig. 2(a) and 2(b). The increase of xylitol is parallel with the decrease of glucose in the extracellular extracts in Figure 2(c), which tallies with the information in Fig. 1(a). It can be concluded that the genetically modified *E. coli* consumed glucose for growth and generated more xylitol as it grew.

https://doi.org/10.31436/iiumecp.v1i1.3002

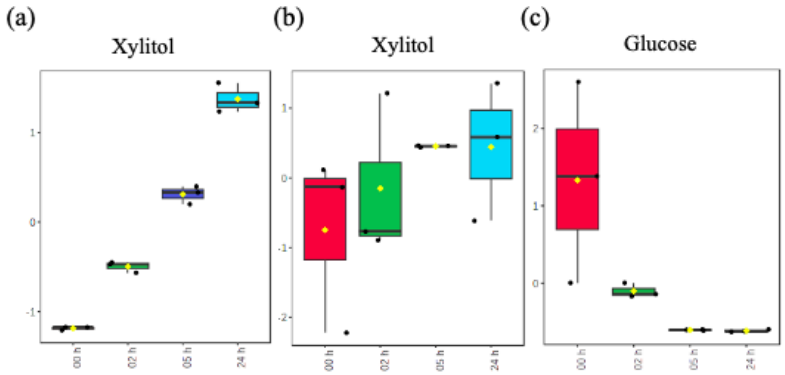

Fig. 2. Peak intensity of (a) xylitol in intracellular extracts, (b) xylitol in extracellular extracts, and (c) glucose in extracellular extracts

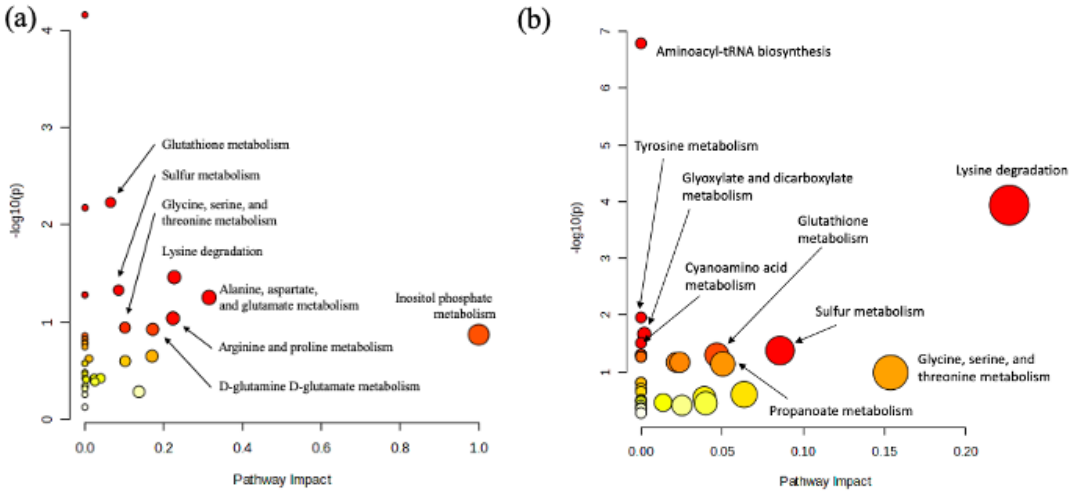

Fig. 3. Pathway analysis for top 20 most contributing metabolites in (a) intracellular samples, (b) extracellular samples

3.3. Metabolome Analysis Reveals Impacted Amino Acids Metabolisms

The most contributing metabolites in the separation of the samples were determined from the list of metabolites identified using GC-MS library and subjected to pathway analysis. The results show that in both intracellular and extracellular samples, amino acid metabolisms are mainly affected (Figure 3). This result suggested that amino acids may play a prominent role in xylitol production. This outcome is supported by a study done by Fuzi et al. [15] which demonstrated that individual supplementation of certain amino acids was able to increase the xylitol titer by nearly 50% in genetically modified *E. coli* (Δxy1AB+P21XR) whereby xylose was the main substrate and glycerol was used as carbon source. The study also concluded that amino acids may play a critical role in the production of xylitol.

4. RESULTS AND DISCUSSION

From this study, it was found that amino acid metabolisms were mainly affected in xylitol production. Further research should be done to understand the relationship between amino acids and xylitol production by comparing the metabolic profile of *E. coli* (Δ*pgi*+*xpdh*) when different amino acids were to be added to the fermentation media to learn how the amino acids affect xylitol production.

ACKNOWLEDGEMENT

This study was financially supported by UTM Transdisciplinary Research Grant (vot. 05G43) provided by Universiti Teknologi Malaysia.

REFERENCES

[1] Queiroz, S. S., Jofre, F. M., Mussatto, S. I., & Maria das Graças, A. F. (2022). Scaling up xylitol bioproduction: challenges to achieve a profitable bioprocess. Renewable and Sustainable Energy Reviews, 154, 111789.

[2] Rafiqul, I. S. M., & Sakinah, A. M. (2013). Processes for the production of xylitol—a review. Food Reviews International, 29, 2, 127-156.

[3] Yu, C., Cao, Y., Zou, H., & Xian, M. (2011). Metabolic engineering of Escherichia coli for biotechnological production of high-value organic acids and alcohols. Applied microbiology and biotechnology, 89, 573-583.

[4] Sakakibara, Y., Saha, B. C., & Taylor, P. (2009). Microbial production of xylitol from L-arabinose by metabolically engineered Escherichia coli. Journal of bioscience and bioengineering, 107, 5, 506-511.

[5] Su, B., Wu, M., Zhang, Z., Lin, J., & Yang, L. (2015). Efficient production of xylitol from hemicellulosic hydrolysate using engineered Escherichia coli. Metabolic engineering, 31, 112-122.

[6] Granström, T. B., Izumori, K., & Leisola, M. (2007). A rare sugar xylitol. Part II: biotechnological production and future applications of xylitol. Applied microbiology and biotechnology, 74, 273-276.

[7] Abd Rahman, N. H., Jahim, J. M., Munaim, M. S. A., Rahman, R. A., Fuzi, S. F. Z., & Illias, R. M. (2020). Immobilization of recombinant Escherichia coli on multi-walled carbon nanotubes for xylitol production. Enzyme and microbial technology, 135, 109495.

[8] Bedő, S., Fehér, A., Khunnonkwao, P., Jantama, K., & Fehér, C. (2021). Optimized bioconversion of xylose derived from pre-treated crop residues into xylitol by using Candida boidinii. Agronomy, 11, 1, 79.

[9] Nitta, K., Laviña, W. A., Pontrelli, S., Liao, J. C., Putri, S. P., & Fukusaki, E. (2017). Orthogonal partial least squares/projections to latent structures regression-based metabolomics approach for identification of gene targets for improvement of 1-butanol production in Escherichia coli. Journal of bioscience and bioengineering, 124, 5, 498-505.

[10] Ohtake, T., Pontrelli, S., Laviña, W. A., Liao, J. C., Putri, S. P., & Fukusaki, E. (2017). Metabolomics-driven approach to solving a CoA imbalance for improved 1-butanol production in Escherichia coli. Metabolic engineering, 41, 135-143.

[11] Nitta, K., Laviña, W. A., Pontrelli, S., Liao, J. C., Putri, S. P., & Fukusaki, E. (2019). Metabolome analysis revealed the knockout of glyoxylate shunt as an effective strategy for improvement of 1-butanol production in transgenic Escherichia coli. Journal of bioscience and bioengineering, 127, 3, 301-308.

[12] Hashim, Z., & Fukusaki, E. (2016, June). Metabolomics-based prediction models of yeast strains for screening of metabolites contributing to ethanol stress tolerance. In IOP Conference Series: Earth and Environmental Science (Vol. 36, No. 1, p. 012046). IOP Publishing.

[13] Yoshida, R., Tamura, T., Takaoka, C., Harada, K., Kobayashi, A., Mukai, Y., & Fukusaki, E. (2010). Metabolomics-based systematic prediction of yeast lifespan and its application for semi-rational screening of ageing-related mutants. Aging cell, 9, 4, 616-625.

[14] Pang, Z., Zhou, G., Ewald, J., Chang, L., Hacariz, O., Basu, N., & Xia, J. (2022). Using MetaboAnalyst 5.0 for LC–HRMS spectra processing, multi-omics integration and covariate adjustment of global metabolomics data. Nature protocols, 17, 8, 1735-1761.

[15] Fuzi, S. F. Z. M., Zahari, F. A., Puay, O. H., Oon, L. K., & Abdullah, I. (2023). Screening Effect of Amino Acid on Xylitol Production by Recombinant Escherichia coli System. Journal of Bioprocessing and Biomass Technology, 2, 1, 43-47.

https://doi.org/10.31436/iiumecp.v1i1.3003

INFLUENCE OF CONTINUOUS FLOW BEAD-MILLING PROCESS PARAMETERS ON SULFUR CURATIVE AND ITS PERFORMANCE FOR ELASTOMERIC RUBBER COMPOSITES

MOHAMAD FIRDAUS OMAR[1,2], FATHILAH ALI[1*], MOHAMMED SAEDI JAMI[1], AZLIN SUHAIDA AZMI[1], FARAH AHMAD[1], MOHD ZAHID MARZUKI[3]

[1]Department of Chemical Engineering and Sustainability, Kulliyyah of Engineering, International Islamic University Malaysia, P.O. Box 10, 50728 Kuala Lumpur, Malaysia.
[2]SC Johnson Asia Pacific Sdn. Bhd., UOA Corporate Tower, The Vertical, 8, Jalan Kerinchi, Bangsar South, 59200 Kuala Lumpur, Malaysia.
[3]Faculty of Chemical Engineering, Universiti Teknologi MARA (UiTM) 40450 Shah Alam, Selangor, Malaysia.

**Corresponding author: fathilah@iium.edu.my*

ABSTRACT: Bead-milling is an eco-friendly and feasible method for physical modification of materials that has been extensively used in many industrial applications impacting on particle size and overall products' performance. While previous studies explored various bead-milling parameters in different applications, limited research conducted on sulfur curative dispersion, necessitating a thorough investigation of its performance after bead-milling is applied. The primary objectives of the present study were to explore the influence of bead-milling process parameters, particularly rotational speed and flow rate on the sulfur curative dispersion characteristics and to analyze its behavior within the rubber elastomer matrix. Taguchi's L9 orthogonal array experimental design was employed to identify the optimal rotational speed and flow rate of a 60-L bead-milling machine on the sulfur curative dispersion. It was found that higher rotational speed (800 rpm) and lower flow rate (350 L/h) of the bead-milling process resulted in smaller sulfur particle sizes, leading to slight improvement on tensile strength of the rubber elastomer and hindered the formation of severe sulfur crystals on the casted rubber elastomer – and vice versa. This research provides valuable insights to determine the ideal bead-milling process for sulfur curative, enhancing the mechanical properties and overall performance of elastomeric rubber composites.

KEYWORDS: *bead-milling, sulfur, rubber.*

1. INTRODUCTION

Bead-milling is an eco-friendly method known for modifying materials via friction, collision, impact, and shear from milling beads and the chamber wall – altering particle size, surface properties, morphology, and functional characteristics including solubility, water absorption, swelling, pasting, and gelation of materials [1–3].

Numerous researchers have employed the bead-milling process to alter their products or materials and achieve desired attributes – such as investigations on multi-wall carbon nanotubes (MWCNTs) and bead-milling process parameters for aluminium-magnesium (Al–Mg) alloy powder which reported increasing milling time and speed yields smaller crystallite

https://doi.org/10.31436/iiumecp.v1i1.3003

sizes by 83%, enhancing MWCNT distribution and diffusion into the Al–Mg matrix [4]. A study on wheat gluten protein using bead-mill process proved significant improvements such as breakage of disulfide bonds, increased sulfhydryl groups, heightened hydrophobicity, improved foaming capacity, reduced particle size, and enhanced whiteness that diversifies the applications of wheat gluten [5]. In the context of drug nanocrystal suspensions, utilizing finer milling beads (0.1 mm yttrium stabilized zirconia) was found optimal to stabilize ultrafine drug suspensions that remain homogeneous even after refrigeration [6]. Furthermore, bead-milling enhances the stability and performance of 1.5% cesium lead bromide ($CsPbBr_3$) perovskite quantum dots/polymethyl methacrylate composite with significant performance in terms of luminous efficiency in a white light-emitting diode [7]. These studies reflected bead-milling's wide application scope across industries like chemicals, nanomaterials, food processing, and pharmaceuticals, impacting particle size, surface morphology, stability, and overall product performance.

A curing agent or "curative" is a chemical used to initiate reactions, particularly for cross-linking elastomer molecules such as rubber. Colloidal or dispersed sulfur yields fine particles that suspend well and "insoluble sulfur" is preferred over soluble to prevent "sulfur blooms" which can hinder rubber adhesion and product performance [8,9]. Extensive research explored various methods on sulfur characteristics enhancement – involving ball-milling for dispersion [10], modified sulfur for compatibility [11], and nano-additives for mechanical properties [12]. that aim to enhance sulfur's properties and dispersion within rubber which may lead to the development of high-performance elastomeric materials.

While various milling parameters' effects on products are studied, there is a relative lack of studies or exploration on sulfur dispersion, particularly on its dispersion performance after bead-milling. This research investigates how flow rate and rotational speed affect its performance in the rubber matrix – optimizing bead-milling for sulfur to yield elastomeric items with superior properties via characterizations on visual and tensile properties by using Light Emitting Diode (LED) magnifier lens and universal testing machine respectively.

2. MATERIALS AND METHODS

2.1. Sulfur Curative Preparation and Rubber Elastomer Casting

Dispersion of sulfur curative raw materials inclusive of sulfur powder, sodium salt of naphthalene-sulfonic acid (surfactant), and deionized water at weight percentage of 60%, 6% and 34% respectively was done in a 4-tonne mixing tank at 800 rpm for 30 minutes before the dispersion was pumped to the 60-Litre bead-milling machine with various rotational speed and flow rate using Taguchi's L9 orthogonal array from control factors and levels in Table 1. Yttrium-stabilized zirconia beads of 140 kg and 0.9 mm diameter were used in the milling chamber. Four sulfur samples after the bead-milling based on their particle size, D_{90} (90% of the particles in the sulfur curative having a size smaller than or equal to the reflected value) were then chosen for latex compounding where the compounding materials were obtained commercially. The compounded latices were left to mature for 48 hours and the rubber films were then casted with a pre-determined parameters setting for rubber vulcanization.

Table 1: Control factors with their respective levels for sulfur curative bead-milling

Factors	Unit		Levels	
			1	2	3
A	Rotational Speed	rpm	800	700
B	Flow Rate	L/h	750	550

https://doi.org/10.31436/iiumecp.v1i1.3003

2.2. Characterizations

The D_{90} value of sulfur curative dispersion's particle size was determined using a Particle Size Analyzer of LA-960V2 model. Total Solids Content (TSC) was calculated with the aid of oven at 100 ºC to observe water input/output to the dispersion. The dispersion's pH was measured by using pH meter while the dispersion viscosity was measured with a Brookfield viscometer. The casted elastomeric rubber samples' properties were analyzed mechanically using a universal testing machine supplied by GT Instruments Sdn. Bhd. (Model: Al-3000) to measure tensile strength with verified thickness (0.06 ± 0.005 mm), and LED magnifier lens for visual characterization.

3. RESULTS AND DISCUSSION

3.1. Sulfur Curative Properties

Table 2 shows the specifications of sulfur curatives achieved through varying bead-milling process parameters. Triplicate samples of sulfur curatives were taken and recorded their properties for each run and averaged out.

Table 2: Sulfur curative specifications results

Run No.	Rotational Speed (rpm)	Flow Rate (L/h)	pH	TSC (%)	Viscosity (cP)	Particle Size, D_{90} (µm)
1	800	750	9.5	61.31	472	7.750
2	800	550	9.5	62.99	610	6.718
3	800	350	9.6	61.63	598	6.154
4	700	750	9.7	62.05	470	8.650
5	700	550	9.9	61.84	646	7.760
6	700	350	9.5	62.31	616	6.820
7	600	750	9.7	62.43	370	9.998
8	600	550	9.7	62.69	432	8.444
9	600	350	9.5	61.89	518	7.214

It can be roughly observed that particle size and viscosity demonstrated variations across the different runs, while pH and TSC were observed to constant to less variations. This variation in particle sizes may be able to influence the resulting dispersion's stability and performance within rubber matrix.

3.2. Influence on the Resulting Rubber Elastomer

From the observations of rubber elastomer film surfaces through an LED magnifier lens, a significant presence of sulfur crystals/blooms on the rubber film surface at a lower rotational speed of 600 rpm and a higher flow rate of 750 L/h. Comparatively, sulfur produced with a higher rotational speed and lower flow rate in bead-milling, showed considerably fewer sulfur blooms on the surface.

Figure 1 illustrates the tensile strength mechanical properties of the casted rubber elastomer films across the four different sulfur curative sets, comparing their respective particle sizes. The mechanical properties underwent testing to assess the mechanical behavior of the rubber elastomer samples according to ASTM D3578 standard and remarkably passed the minimum requirement of the standard (≥ 18 MPa) [13], and the values for each set remained closely aligned, with slight improvements in tensile strength evident for Set A which featured the smallest particle size, showing the highest tensile strength value, which apparently contributed to this positive impact.

https://doi.org/10.31436/iiumecp.v1i1.3003

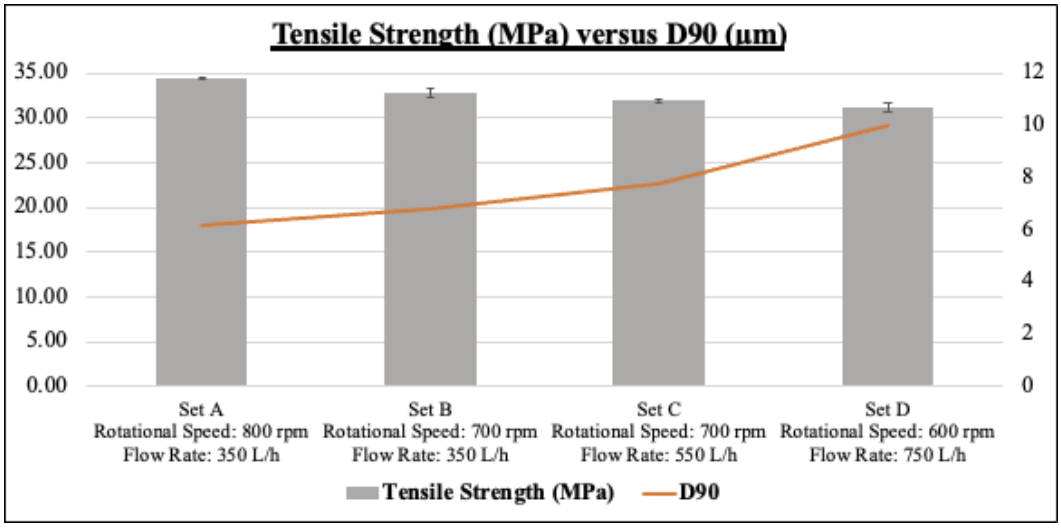

Fig. 1. Tensile strength of casted rubber elastomer films with different bead-milled sulfur curative.

4. CONCLUSION

In this study, it is proved that at the highest rotational speed (800 rpm) and lowest flow rate chosen (350 L/h) resulted in sulfur with the smallest or reduced particle size. Observations of sulfur crystals surfaced on rubber films highlighted various effects of bead-milling settings – particularly Set A with fewer blooms due to higher rotational speed and lower flow rate resulting in smaller particle size. All rubber films met the ASTM D3578 standard for strength, and the smallest sulfur particles showed the highest tensile strength and vice versa.

ACKNOWLEDGEMENT

I would like to express my sincere gratitude to all those who have contributed to the completion of this research. I am thankful for the guidance, support, and valuable insights provided by my advisors, and colleagues throughout this journey. Additionally, I would like to extend my appreciation to IIUM, Department of Chemical Engineering and Sustainability that made this work possible. Your support has been invaluable in the pursuit of knowledge and the advancement of this field.

REFERENCES

[1] Tan X, Zhang B, Chen L, Li X, Li L, Xie F. (2015) Effect of Planetary Ball-Milling on Multi-Scale Structures and Pasting Properties of Waxy and High-Amylose Cornstarches. Innovative Food Science & Emerging Technologies, 30: 198–207. https://doi.org/10.1016/j.ifset.2015.03.013.

[2] Páramo-Calderón DE, Vázquez-León LA, Palma-Rodríguez HM, Utrilla-Coello RG, Vargas-Torres A, Meza-Nieto MA, Romero-Cortes T, Aparicio-Saguilán A. (2023) Effect of High-Energy Mechanical Milling on the Physicochemical and Rheological Properties of Chayotextle (Sechium Edule Sw.) Starch. Food Chemistry, 427: 136720. https://doi.org/10.1016/j.foodchem.2023.136720.

[3] Bangar SP, Singh A, Ashogbon AO, Bobade H. (2023) Ball-Milling: A Sustainable and Green Approach for Starch Modification. International Journal of Biological Macromolecules, 237: 124069. https://doi.org/10.1016/j.ijbiomac.2023.124069.

[4] Ahmadian H, Sallakhniknezhad R, Zhou T, Kiahosseini SR. (2022) Mechanical Properties of Al-Mg/MWCNT Nanocomposite Powder Produced under Different Parameters of Ball

Milling Process. Diamond and Related Materials, 121: 108755. https://doi.org/10.1016/j.diamond.2021.108755.

[5] Liu Z, Zheng Z, Zhu G, Luo S, Zhang D, Liu F, Shen Y. (2021) Modification of the Structural and Functional Properties of Wheat Gluten Protein Using a Planetary Ball Mill. Food Chemistry, 363: 130251. https://doi.org/10.1016/j.foodchem.2021.130251.

[6] Carling C-J, Pekkari A. (2023) Bead Milled Drug Nanocrystal Suspensions FIne Enough to Pass through 0.22 Mm Sterilization FIlters. https://doi.org/https:/example.net.

[7] Liu W, Xie H, Guo X, Wang K, Yang C, Wang N, Ge C. (2023) Luminescence, Stability, and Applications of CsPbBr3 Quantum Dot/Polymethyl Methacrylate Composites Prepared by a Solvent- and Ligand-Free Ball Milling Method. Optical Materials, 136: 113398. https://doi.org/10.1016/j.optmat.2022.113398.

[8] Motavalizadehkakhky A, Shahrampour H. (2018) Determination of the Most Efficient Form of Sulfur for Use as a Natural Rubber Curing Agent by Comparison of Physical and Thermal Attributes of Cured Rubber. Petroleum Chemistry, 58: 89–93. https://doi.org/10.1134/S0965544118010048.

[9] Shahrampour H, Motavalizadehkakhky A. (2017) The Effects of Sulfur Curing Systems (Insoluble-Rhombic) on Physical and Thermal Properties of the Matrix Polymeric of Styrene Butadiene Rubber. Petroleum Chemistry, 57: 700–704. https://doi.org/10.1134/S0965544117080138.

[10] Pangamol P. (2016) Use of By-Product Sulfur from Petroleum Refinery as Vulcanizing Agent in Natural Rubber. Chiang Mai J. Sci., 43: 569–576. http://epg.science.cmu.ac.th/ejournal/.

[11] Zheng L, Jerrams S, Xu Z, Zhang L, Liu L, Wen S. (2020) Enhanced Gas Barrier Properties of Graphene Oxide/Rubber Composites with Strong Interfaces Constructed by Graphene Oxide and Sulfur. Chemical Engineering Journal, 383: 123100. https://doi.org/10.1016/j.cej.2019.123100.

[12] Duan,X, Tao R, Chen Y, Zhang Z, Zhao G, Liu Y, Cheng S. (2022) Improved Mechanical, Thermal Conductivity and Low Heat Build-up Properties of Natural Rubber Composites with Nano-Sulfur Modified Graphene Oxide/Silicon Carbide. Ceramics International, 48: 22053–22063. https://doi.org/10.1016/j.ceramint.2022.04.196.

[13] Ab Rahman MF, Norfaizal NS, Azura AR. (2019) The Influence of Sago Starch Dispersion on Mechanical Properties of Biodegradable Natural Rubber Latex Films. Materials Today: Proceedings, 17: 1040–1046. https://doi.org/10.1016/j.matpr.2019.06.507.

https://doi.org/10.31436/iiumecp.v1i1.3007

PROFILING ANAEROBIC DIGESTION STAGES FROM CAFETERIA FOOD WASTE FOR PRODUCTION OF BIOGAS

MARIATUL FADZILLAH MANSOR*, AHMAD IMAN IKMAL ADANAN, HUSNA AHMAD TAJUDDIN, AZLIN SUHAIDA AZMI

Department of Chemical Engineering and Sustainability, Kulliyyah of Engineering International Islamic University. Malaysia (IIUM), Jalan Gombak, 53100 Kuala Lumpur, Malaysia

**Corresponding author: mariatulf@iium.edu.my*

ABSTRACT: Population growth in Malaysia has led to a rise in waste production. Soon, the capacity of the sanitary landfill will not be sufficient to accommodate the daily garbage production. Therefore, biogas plants are one of the finest answers to this issue. There has been numerous research on the use of food waste (FW) to make biogas, which can then be transformed into renewable energy. Food waste constitutes the largest percentage of municipal solid waste in Malaysia (MSW). In this study, the acclimatization process was conducted to profile the stages in this process for 27 days using cafeteria food waste (CFW) as a substrate. During the process, the pH sample and biogas production was recorded. The results showed that the hydrolysis stage occurred during day 0-1, indicated by a drop in pH from 7 to 2. This was followed by the acidogenesis stage from day 2-14, with the pH remaining within the acidic range of 3.5-6.5. The acetogenesis stage took place from day 15-18, maintaining a similar acidic pH range. Lastly, the methanogenesis stage occurred during day 19-27, characterized by a significant increase in biogas production. Methanogenic archaea converted the produced acetate, hydrogen, and carbon dioxide into methane gas. Different total solid (TS) contents of CFW: 10%, 15%, and 20%, were investigated. The highest biogas production was observed with a TS content of 20%, resulting in an accumulated biogas volume of 360 ml over seven days of fermentation. Conversely, the lowest biogas production was observed with a TS content of 10%, yielding a biogas volume of 170 ml. This study demonstrates that biogas production increases with higher total solids (TS) content. Finally, this study proves that food waste is a potential feedstock for biogas production that can help to reduce the current issues of waste disposal.

KEYWORDS: *Profiling, Anaerobic Digestion, Cafeteria Food Waste, Biogas.*

1. INTRODUCTION

World populations are rising up to 64 million in 2022 [1]. The massive growth in population has a tremendous effect on natural resources. As the global population increases, the management of solid waste has become a burden for global economies and the need for more energy consumption increases. Renewable and non-renewable energy are the two types of energy that can be classified. Non-renewable energy refers to a natural resource that does not regenerate while renewable energy is obtained from ongoing replenishment through natural processes [2]. Renewable energy obtains all its different forms directly from the sun, wind, rain, ocean tides and biomass. Due to its vast access and capacity to be produced as a byproduct of numerous industrial and agricultural activities, biomass is a renewable energy source that is expanding and has a high development potential [3].

https://doi.org/10.31436/iiumecp.v1i1.3007

Biomass can be derived from forestry crops and leftovers, industrial residues, animal residues, municipal solid waste, and sewage. As of 2013, the largest share of municipal solid waste (MSW) produced in Malaysia is food waste (FW) [4]. Many nations are becoming worried about the amount of food that is wasted globally. The challenges are the annual production of FW and the quantity of food consumed. As food consumption increases, so will FW. Landfill is the primary waste disposal method in Malaysia with up to 80% utilization [5]. In addition to depleting valuable land, landfilling pollutes the air, water, and soil by releasing chemicals, pesticides, and methane into the soil, groundwater, and atmosphere. Biogenic matter, which includes all sorts of biomasses, decomposes into biogas under anaerobic circumstances.

Biogas typically refers to a gas generated by the biological breakdown of organic matter in lacking oxygen [6]. The major component of this naturally occurring biogas, methane, escapes into the atmosphere and significantly contributes to global warming. Due to the enormous environmental and financial advantages it provides, anaerobic digestion (AD) of food waste has drawn attention from all over the world. Digestion is indeed based on a reduction process consisting of a few biochemical events occurring in anoxic settings, which is why anaerobic digestion is frequently thought of as a complex process [7].

Anaerobic digestion produces methane through four distinct processes: hydrolysis, acidogenesis, acetogenesis, and methanogenesis. By profiling each stage of acclimatization process for AD, we can understand the dynamics of microbial populations and their role in the degradation of FW. Production of biogas requires anaerobic digestion to be limited to one of the crucial factors such as total solid (TS) content of the food waste. The TS content of a sample is the mass of solids remaining after a sample has been dried divided by the original mass of the sample. Previous studies showed that the high-solids system was found to produce more methane production rate but there is also a study that found out the total methane production decreased with total solid (TS) content increasing from 10% to 25% [8]. Thus, this study was concentrated on profiling anaerobic digestion stages of cafeteria food waste for production of biogas. Furthermore, the TS content was also optimized to increase biogas production.

2. MATERIALS AND METHODS

Cafeteria food waste (CFW) used as a substrate was collected from Mahallah Faruq Cafeteria in IIUM Gombak campus. It consisted of leftover foods such as vegetables, meats, fish, rice, fruits, and sauces. The source of mixed culture sludge (MCS) used as inoculum in this experiment was Palm Oil Effluent (POME) collected from Biogas Plant in Pahang.

2.1. Sample Preparation

A food blender was used to homogenize the cafeteria food waste (CFW) into particles that are smaller than 2 mm in diameter. The CFW was blended with distilled water with the ratio of (4 g:1 ml) (CFW: distilled water). Prior to usage, the blended CFW was stored in a refrigerator at 4°C. The CFW was further diluted again with the same proportion of (4 g:1 ml) (CFW: distilled water) before being used in the experiment.

Three different samples were prepared in this project. The three samples differ in terms of total solid (TS) content of the cafeteria food waste (CFW). The sample preparation for each content is shown in Table 1.

https://doi.org/10.31436/iiumecp.v1i1.3007

Table 1: Sample preparation of each total solid (TS) content

TS content (%)	Ratio (CFW: Distilled Water)
20	20 g:100 ml
15	15 g:100 ml
10	10 g: 100 ml

2.2 Acclimatization of Mixed Culture Sludge

The modified Schott bottle with a working volume of 1000 ml was used as a reactor. In this study, the total volume in the reactor was at proportion (50:50) (CFW: MCS). The initial pH of the mixture was adjusted to pH 7. The daily production of biogas and the pH of the mixture was recorded for twenty-seven days. Besides, this seed was used as an inoculum for anaerobic digestion (AD) process.

2.3 Optimization Total Solid Content

For this experiment, 100 ml of acclimatization sample was added into 100 ml of the sample with TS content of 20%. The biogas production and pH were recorded for 7 days. Total carbohydrates of the samples were also analyzed. This step was repeated for TS content of 15% and 10%. Previous studies [8] and practical experiences have shown that anaerobic digestion tends to exhibit favorable performance within the 10-20% TS content range.

3. RESULTS AND DISCUSSION

3.1 Acclimatization of Mixed Culture Sludge

The cumulative biogas collected and pH value throughout the acclimatization process was plotted in Figure 1. From biogas produced, it can be indicated that from day 0-1 is considered as hydrolysis stage (S1) where the initial pH observed dropped from pH 7 to pH 2. The pH drop signifies the start of the acidogenesis stage in the acclimatization process. During hydrolysis stage, complex organic molecules in the substrate such as proteins, carbohydrates, and lipids are converted into smaller compounds such as sugars, amino acids, and fatty acids by hydrolysis bacteria.

Once hydrolysis occurs, the acidogenesis stage (S2) took place from day 2-14 where the pH of the substrate remains within the acidic pH range. The acidogenic bacteria take over and convert the simpler organic compounds produced in the hydrolysis stage into organic acids, alcohols, and other volatile fatty acids. During acidogenesis, pH decreases due to acidification, and VFAs accumulate. The production of VFAs is accompanied by the release of carbon dioxide and hydrogen gas, contributing to initial biogas production. However, biogas production during acidogenesis is relatively low compared to the later stages of acetogenesis and methanogenesis.

From day 15-18, with pH within the acidic range of 3.5-6.5, biogas production increases and further metabolizes the organic acids and volatile fatty acids produced in the acidogenesis stage (S3) into acetic acid, hydrogen and carbon dioxide. This stage is crucial for generating acetate, which is a key precursor for methane production in the next stage.

The final stage of the acclimatization process, which is methanogenesis (S4), occurred between day 19-27 where methanogenic archea converts the acetate, hydrogen and carbon dioxide into methane gas or biogas. This stage is marked by a significant increase in biogas production and low concentrations of VFAs can also be observed.

https://doi.org/10.31436/iiumecp.v1i1.3007

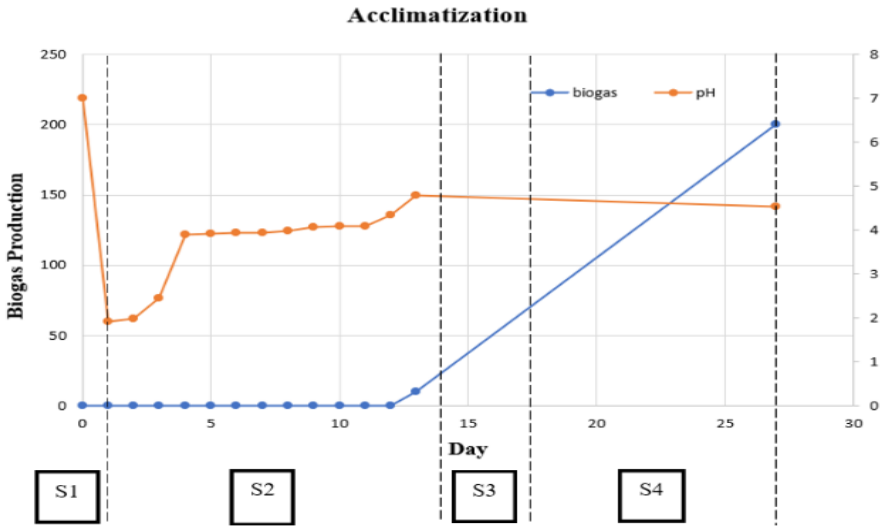

Figure 1: Biogas production and pH value for each stage in the acclimatization process

3.2 Optimization Total Solid Content

The accumulation of biogas in mL for different TS content of CFW was recorded as in Figure 2. The cumulative biogas produced by TS content of 20%, 15%, and 10% accounted to 360 ml, 250 ml, and 170 ml. Hence, biogas production showed an increasing trend with increasing TS content of CFW.

The acclimatization process aims to enhance biogas production in the anaerobic digester by ensuring efficient conversion of organic matter. This leads to higher biogas yields, stability, and sustainability. As a result, the cafeteria food waste (CFW) with 20% total solids (TS) content produced the highest biogas volume, as predicted by the initial total carbohydrates (TC) analysis. The results obtained were similar to previous study [8] in which substrates with higher TS content showed higher biogas production in the batch anaerobic digestion of CFW.

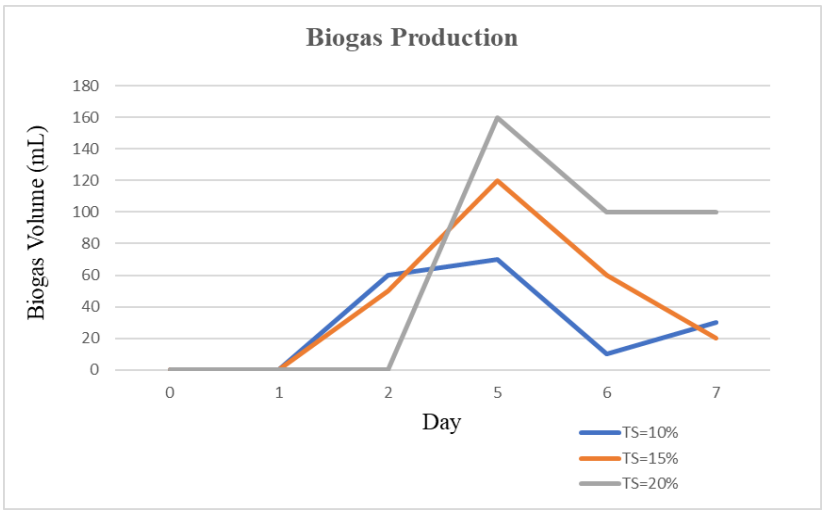

Figure 2: The cumulative biogas production for different (TS) content of CFW

https://doi.org/10.31436/iiumecp.v1i1.3007

It is well known that FW is a high degradable substrate for anaerobic digestion. For TS content of 5%, 10% and 20% at a fixed 7 days of solid retention time (SRT), increased TS content of CFW meant higher applied organic loading rate (OLR) and larger proportion of easily degradable substrate of microorganism, which results in higher volumetric biogas [10]. OLR indicates the quantity of organic material that is being fed into an anaerobic digester. High OLR can improve the processing efficiency of AD, while it might inhibit biogas production [11]. In this study, it is difficult to determine if the high OLR inhibited the biogas production, but the biogas produced showed an increasing trend with increasing TS content of CFW. So, it can conclude that high OLR in CFW improved the efficiency of AD process.

It is also clear that in Figure 2, the highest biogas production for all TS content was on day 5. It is difficult to point out a single factor affecting this, but one of the main factors is the peak concentration of carbohydrates just before day 5 of biogas production as shown in Figure 3. During anerobic digestion (AD), carbohydrates are significant components of organic matter that can be degraded by microorganisms. As the concentration of carbohydrates increases, there is typically more substrate available for microbial fermentation, leading to enhanced biogas production.

In the initial stages of anaerobic digestion, the total carbohydrates analysis value of food waste increases over time [12]. This rise occurs during hydrolysis and acidogenesis, where complex carbohydrates are broken down into sugars and fermented into volatile fatty acids (VFAs) like acetic acid, propionic acid, and butyric acid. These processes release soluble carbohydrates and VFAs into the digester, elevating the total carbohydrates analysis value. As digestion progresses, acetogenesis and methanogenesis take place. Acetogenic bacteria convert VFAs into acetic acid, hydrogen gas, and carbon dioxide, while methanogenic archaea utilize these compounds to produce methane gas. During acetogenesis and methanogenesis, some carbohydrates and VFAs are further broken down, resulting in a decrease in the total carbohydrates analysis value of the remaining digestate and higher biogas production.

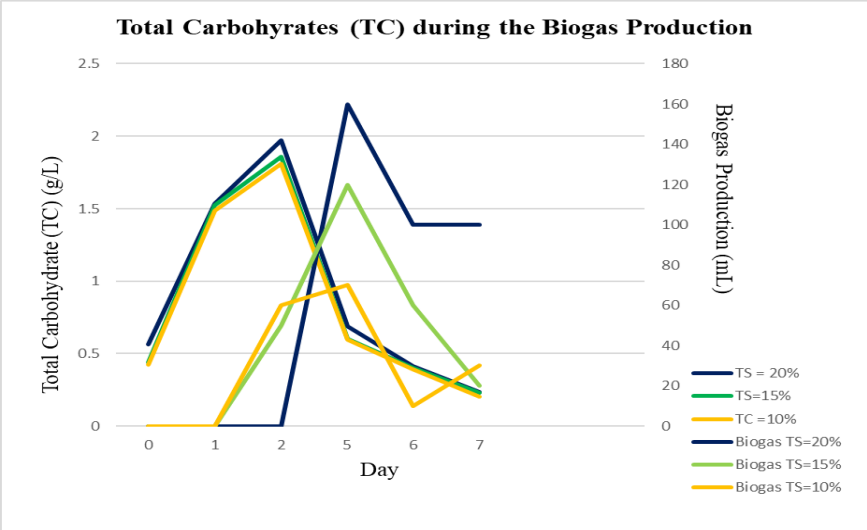

Figure 3: Total carbohydrate content during biogas production

Table 2 shows the pH values of substrates during AD. The average pH value for TS content of 20%, 15%, and 10% are 5.32, 5.31 and 5.30, respectively. These pH values were

not within the optimal range for AD which is between pH 6.8- pH 7.4. This may be due to organic acid accumulation. During the AD process, organic acids are produced as intermediate products. If the digestion process is not well-balanced, the accumulation of organic acids can cause a drop in pH. This can occur if the SRT is too short. At low SRT, conversion of feedstock is limited, and organic acids are the main fermentation products [13].

Table 3: pH values of substrates for each TS during AD

Day	pH Value		
	TS = 20%	**TS = 15%**	**TS = 10%**
0	7.00	7.00	7.00
1	4.85	4.93	4.88
2	4.90	4.95	4.98
5	5.07	5.06	5.03
6	5.05	4.99	4.96
7	5.04	4.95	4.95

4. CONCLUSION

The AD of CFW was studied by profiling the stages in the acclimatization process between the CFW and MCS and investigating the feasibility of biogas production using different TS content of CFW. The profiles of anaerobic digestion were shown in this study; however, it is suggested to prolong the fermentation time for a better profiling stage. While biogas production showed an increasing trend with increasing TS content. This proved that the biogas production is highly dependent on the TS content of CFW undergoing the process of AD.

ACKNOWLEDGEMENT

The authors thanked the research grant FRGS/1/2021/TK0//UIAM/02/19 and the Ministry of Higher Education Malaysia for supporting this work.

REFERENCES

[1] Current world population. Worldometer. https://www.worldometers.info/world-population/

[2] Dhir, R. (2023, June 2). Nonrenewable resource: Definition, features, and examples. Investopedia. https://www.investopedia.com/terms/n/nonrenewableresource.asp

[3] Perea-Moreno, M. A., Samerón-Manzano, E., & Perea-Moreno, A. J. (2019). Biomass as Renewable Energy: Worldwide Research Trends. Sustainability 2019, Vol. 11, Page 863, 11(3), 863. https://doi.org/10.3390/SU11030863

[4] Noor, Z. Z., Yusuf, R. O., Abba, A. H., Abu Hassan, M. A., & Mohd Din, M. F. (2013). An overview for energy recovery from municipal solid wastes (MSW) in Malaysia scenario. Renewable and Sustainable Energy Reviews, 20, 378–384. https://doi.org/10.1016/J.RSER.2012.11.050

[5] Chen, H. L., Nath, T. K., Chong, S., Foo, V., Gibbins, C., & Lechner, A. M. (2021, March 8). The Plastic Waste Problem in Malaysia: Management, recycling and disposal of local and global plastic waste - SN Applied Sciences. SpringerLink. https://link.springer.com/article/10.1007/s42452-021-04234-y

[6] Bhatia, S. C. (n.d.). *Advanced Renewable Energy Systems*. ScienceDirect. https://www.sciencedirect.com/book/9781782422693/advanced-renewable-energy-systems

[7] Adekunle, K. F., & Okolie, J. A. (2015). A Review of Biochemical Process of Anaerobic Digestion. Advances in Bioscience and Biotechnology, 06(03), 205–212. https://doi.org/10.4236/ABB.2015.63020 S. A. Muyibi and L. M. Evison. "Coagulation of Turbid Water and Softening of Hard Water with Moringa oleifera Seeds," Intern Journ. Environmental Studies, 1996, Vol. 49, pp 247-259, 1996.

[8] Duan N, Dong B, Wu B, Dai X (2012) High-solid anaerobic digestion of sewage sludge under mesophilic conditions: feasibility study. *Bioresour Technol* 104: 150–156.

[9] Brack, P., Dann, S., Wijayantha, K. G. U., Adcock, P., & Foster, S. (2016, August 17). *A simple, low-cost, and robust system to measure the volume of hydrogen evolved by chemical reactions with aqueous solutions*. Journal of visualized experiments : JoVE. https://www.ncbi.nlm.nih.gov/pmc/articles/PMC5091921/

[10] Yi, J., Dong, B., Jin, J., & Dai, X. (n.d.). Effect of increasing total solids contents on anaerobic digestion of food waste under mesophilic conditions: Performance and Microbial Characteristics Analysis. PLOS ONE. https://journals.plos.org/plosone/article?id=10.1371%2Fjournal.pone.0102548

[11] Pearse, L. F., Hettiaratchi, J. P., and Kumar, S. (2018). Towards developing a representative biochemical methane potential (BMP) assay for landfilled municipal solid waste – a review. Bioresour. Technol. 254, 312–324. doi: 10.1016/j.biortech.2018.01.069

[12] Al-Wahaibi, A., Osman, A. I., Al-Muhtaseb, A. H., Alqaisi, O., Baawain, M., Fawzy, S., & Rooney, D. W. (2020, September 24). Techno-economic evaluation of biogas production from food waste via anaerobic digestion. Scientific reports. https://www.ncbi.nlm.nih.gov/pmc/articles/PMC7515879/

[13] Silva, I. M. O., & Dionisi, D. (2020, June 8). Effect of the operating conditions on the anaerobic digestion of wheatgrass for chemicals and energy production - biomass conversion and Biorefinery. SpringerLink. https://link.springer.com/article/10.1007/s13399-020-00735-9

https://doi.org/10.31436/iiumecp.v1i1.3008

ENHANCED REMOVAL OF MULTI-METAL ION BY GRAPHENE OXIDE POLYETHERSULFONE NANOCOMPOSITE ADSORPTIVE MEMBRANE

NIK-RASHIDA NIK-ABDUL-GHANI*, MOHAMMED SAEDI JAMI , MD ZAHANGIR ALAM, NURUL SAKINAH ENGLIMAN

Department of Chemical Engineering and Sustainability, Faculty of Engineering, International Islamic University Malaysia, Jalan Gombak, 53100 Kuala Lumpur, Malaysia

**Corresponding author: nikrashida@iium.edu.my*

ABSTRACT: Water pollution due to natural and human activities is a critical issue of global concern. Moreover, rapid population growth that led to urbanization, industrialization and intensification of agricultural activities has rendered to the accumulation of pollutants in water and wastewater. Heavy metals were identified as one of the inorganic pollutants found in significant amounts in industrial effluent discharges. Therefore, this study aims to evaluate the efficiency of graphene oxide polyethersulfone nanocomposite (GPN) adsorptive membrane in a synthetic multi-metal ion system using dead-end filtration process. GO powder was incorporated with a polymer solution to fabricate the GPN membrane. After that, simulated industrial wastewater was prepared based on the real waste content including lead (Pb), iron (Fe), copper (Cu) and aluminum (Al) at pH 3.4±0.2. Then, the dead-end filtration was conducted using the prepared simulated wastewater at 3 bar of transmembrane pressure. The final concentration of the metals in the permeate demonstrated that the removal of multi-metal ions was in the descending order of Al > Pb >Cu > Fe and Pb > Al > Cu > Fe for Type 1 and 2, respectively. For Type 1 simulated wastewater (mining industry), the removal percentages were about 62, 40, 61 and 81% for Pb, Fe, Cu and Al, respectively. Meanwhile, for Type 2 simulated wastewater (semiconductor industry), the removal percentages were 93, 43, 63 and 67% for Pb, Fe, Cu and Al, respectively. The results exhibited that metal ions compete for these interactions and behave differently when they come into contact with the GPN membrane. The final concentration of the metals in the permeate demonstrated an enhanced removal of multi-metal ions. Therefore, it is suggested that this GPN membrane is suitable for industrial use and could be verified with real wastewater effluent in the future.

KEYWORDS: *Modified graphene oxide, Adsorptive membrane and Multi-metal ion removal.*

1. INTRODUCTION

Heavy metal contamination in water is a significant environmental issue that poses serious threats to human health and the ecosystem. While these metals have various industrial and commercial applications, their improper disposal and release into the environment can lead to water pollution. Once heavy metals enter water systems, they can persist for extended periods and accumulate in the environment. As a result, they are often found in elevated concentrations in rivers, lakes, and groundwater. These elevated levels can have harmful effects on aquatic life, plants, and humans [1,2]. To date, the incorporation of nanomaterials in membrane fabrication has been proven to improve membrane performance and fouling resistance as well

https://doi.org/10.31436/iiumecp.v1i1.3008

as provide innovative systems for novel adsorptive/filtration membranes for improving wastewater treatment [3]. Graphene oxide (GO), a highly oxidized form of the graphene sheet, has been investigated due to easy dispersion in an aqueous solution as these oxygen moieties make GO hydrophilic [4-8]. This study explores the application of an effective membrane utilizing GO as the main nanomaterial of a nanocomposite adsorptive membrane for heavy metals removal known as graphene oxide polyethersulfone nanocomposite (GPN) membrane. In general, industrial effluent contains a variety of pollutants which is more than one of heavy metals. As a result, incorporating other heavy metals would serve as simulated real-world wastewater, allowing the hindrance of other metal ions to be determined utilizing the GPN membrane. However, only a few studies of the GPN have been tested on multi-metal ion rejection and no study has evaluated the simulated wastewater based on the wastewater effluent from mining/semiconductor industries. Therefore, the aim of this study was to investigate and validate the applicability of GPN for enhanced removal of multi metal ions and elucidation of its mechanism. This research envisages that heavy metals containing wastewater effluents that are currently discharged into the water environment could be efficiently treated and subsequently control the water pollution issues by integrating nanomaterials and adsorptive membrane systems. an attempt to make formatting easy, you can use the style menu just under the standard menu.

2. MATERIALS AND METHOD

All reagents used for the experiment were analytical grade. Lead nitrate (PbNO3: 99%), and iron sulfate (FeSO4: 98%) were purchased from R&M Chemicals. Copper sulfate (CuSO4: 98%) was supplied from Ajax Finechem and aluminum sulfate (Al2(SO4)3: 98%) was purchased from HmbG Chemicals. The synthesized graphene oxide according to Hummers' method and the fabricated GPN membrane as described elsewhere [9], were used throughout the experiment utilizing graphite powder (particle size < 50 μm) which was supplied by R&M Chemicals, Canada.

2.1. Simulated wastewater

In this study, the simulated industrial wastewater was prepared based on the real waste content as reported previously [10,11] and tested for the applicability of the GPN. The lead (Pb) ion concentration was mixed with other metals including iron (Fe), copper (Cu) and aluminum (Al) and the pH was 3.4±0.2, where the pH of the solution remains similar to that of the acidic real wastewater. The components of simulated wastewater from industrial wastewater were prepared according to previous findings from mining (Pb-100; Fe-30; Cu-70; Al-200 mg/L) and semiconductor (Pb-1.5; Fe-3.5; Cu-2; Al-3 mg/L) industries pertaining to the multi-metal ions system. Finally, the final concentration of the multi-metal elements was determined using ICPMS and the removal efficiency was observed.

2.2 Dead-end filtration

The dead-end filtration experiments were conducted on GPN membrane using simulated wastewater containing multi-metal ions as inlet feed. The filtration experiment was conducted according to [9] with slight modification using a hand-made dead-end membrane filtration set-up with constant transmembrane pressure (TMP) and a variation of filtration time. The compaction step was carried out for 15 min at a pressure of 3 bars to obtain a steadier solution flux and to remove residual chemicals. The permeate flux was calculated using the Equation(1).

https://doi.org/10.31436/iiumecp.v1i1.3008

$$J = \frac{\Delta V}{A \Delta t} \quad (1)$$

where J is the measured permeate flux (L/m^2 h), ΔV is the permeate cumulative volume (L), A is the effective membrane surface area (m^2), and Δt is the filtration duration (h).

3. RESULTS AND DISCUSSION

3.1 Multi-metal ions rejection

The dead-end filtration experiments were conducted on GPN membrane using multi metal ions as inlet feed. The removal percentage of multi metal ions were obtained using ICPMS and analyzed. Type 1 simulated wastewater is based on the mining industry with high concentration of heavy metals content, while the Type 2 of simulated wastewater is based on the semiconductor industry which contains low concentration of heavy metals. The permeation flux of both sets is shown in Fig. 1 below. The fluxes values are 412 L/m^{2}h and 240 L/m^{2}h for low and high concentration of simulated wastewater, respectively. From the results, the flux is decreased with increasing concentration. This is suggested that membrane resistance increases linearly with increasing initial feed concentration [12]. However, it can be clearly seen that both attained steady flux in 30 minutes.

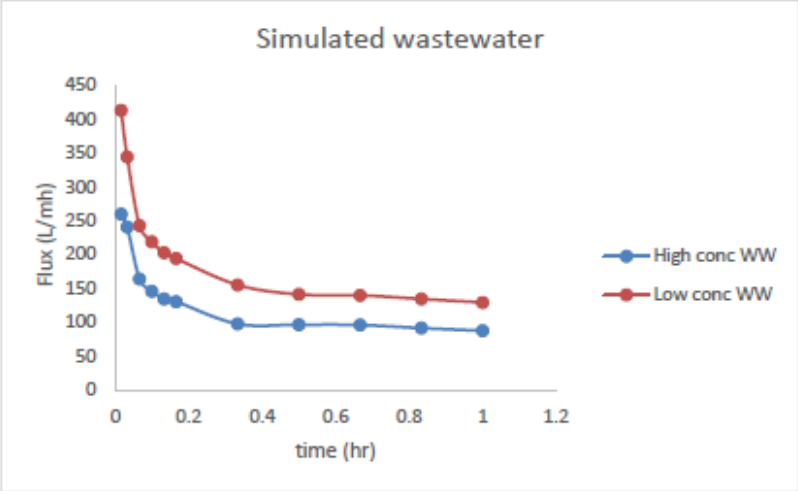

Fig. 1. Flux vs time plot for simulated wastewaters at 3 bar of TMP and acidic conditions (pH 3.2±0.2).

The percentages removal for heavy metals were shown in Figure 2. The multi metals ion rejection was determined using ICPMS analysis. The final concentration of the metals in the permeate demonstrated that the removal of multi-metal ions was in the descending order of Al > Pb >Cu > Fe and Pb > Al > Cu > Fe for Type 1 and 2, respectively. For Type 1 simulated wastewater (mining industry), the removal percentages were about 62, 40, 61 and 81% for Pb, Fe, Cu and Al, respectively. Meanwhile, for Type 2 simulated wastewater (semiconductor industry), the removal percentages were 93, 43, 63 and 67% for Pb, Fe, Cu and Al, correspondingly. From the results, it is revealed the rejection percentage for heavy metals did not follow an orderly trend, but it appeared to follow these manners which removal of Pb and Al was higher than the others for semiconductor and mining industry, respectively.

https://doi.org/10.31436/iiumecp.v1i1.3008

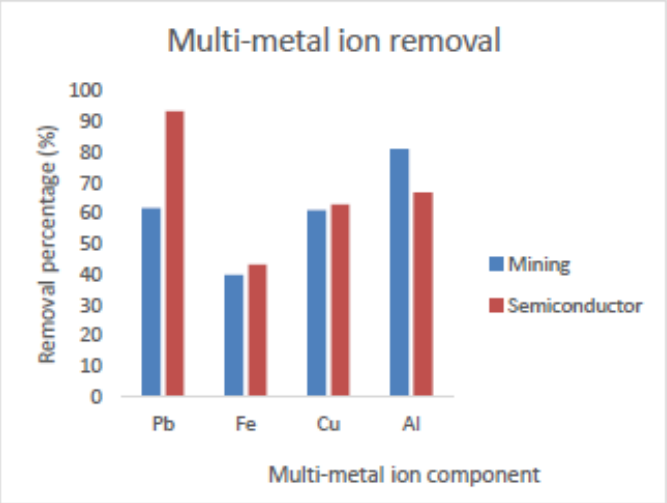

Fig. 2. Removal percentage of multi metal ions component through GPN membrane at 3 bar of TMP and acidic condition (pH 3.2±0.2)

The removal of metal ions from aqueous solutions is attributed to two types of interactions: electrostatic and Van der Waals interactions [5]. Metal ions compete for these interactions and behave differently when they come into contact with the GPN membrane. It is suggested that the metal ions can be coordinated due to the presence of OH and COOH groups in GO and the electrostatic interaction between the functional group in GPN membrane and metal ions are responsible for this selective permeation [5,13]. In addition, metal ions are removed with a three-step mechanism involving the external diffusion of metal ions, diffusion into the nanocomposite and adsorption in the nanocomposite as well as a synergetic effect [5,14].

4. CONCLUSION

The validation of the GPN applicability towards the simulated wastewater containing multi-metal ions is well achieved where the GPN membrane can be utilized to remove multi-metal ions from the wastewater. The final concentration of the metals in the permeate demonstrated an enhanced removal of multi-metal ions. Therefore, it is suggested that this GPN membrane is suitable for industrial use and could be verified with real wastewater effluent in the future.

ACKNOWLEDGEMENT

This work was partially supported by the Ministry of Higher Education (MOHE) Malaysia through a Fundamental Research Grant Scheme [grant number FRGS/1/2019/TK02/UIAM/01/1] and Research Cluster Research Initiative Grant Scheme [grant number RC-RIGS 20-004-0004].

REFERENCES

[1] Assi MA, Hezmee MNM, Haron AW, Sabri MYM, Rajion MA. (2016). The detrimental effects of lead on human and animal health. Veterinary World, 9(6):660–671. https://doi.org/10.14202/vetworld.2016.660-671

[2] Tiwari S, Tripathi IP, Gandhi M, Gramoday C, Tiwari H. (2013). Effects of Lead on Environment. International Journal of Emerging Research in Management and Technology, 2(6):1–5. https://doi.org/10.11468/seikatsueisei1957.28.190

[3] Khulbe KC, Matsuura T. (2018). Removal of heavy metals and pollutants by membrane adsorption techniques. Applied Water Science, 8(19):1-30. https://doi.org/10.1007/s13201-018-0661-6

[4] Nasir AM, Goh PS, Abdullah MS, Ng BC, Ismail AF, He M, Wang L, Lv Y, Wang X, Zhu J, Zhang Y, Liu T, Zarei F, Marjani A, Soltani R. (2019). Adsorptive nanocomposite membranes for heavy metal remediation: Recent progresses and challenges. Chemical Engineering Journal, 389(13):96–112. https://doi.org/10.1016/j.cej.2020.124452

[5] Marjani A, Nakhjiri AT, Adimi M, Jirandehi HF, Shirazian S. (2020). Effect of graphene oxide on modifying polyethersulfone membrane performance and its application in wastewater treatment. Scientific Reports, 10(1):1–11. https://doi.org/10.1038/s41598-020-58472-y

[6] Luque-Alled JM, Abdel-Karim A, Alberto M, Leaper S, Perez-Page M, Huang K, Vijayaraghavan A, El-Kalliny AS, Holmes SM, Gorgojo P. (2020a). Polyethersulfone membranes: From ultrafiltration to nanofiltration via the incorporation of APTS functionalized-graphene oxide. Separation and Purification Technology, 230 (115836):1-12. https://doi.org/10.1016/j.seppur.2019.115836

[7] Huang ZQ, Cheng ZF. (2020). Recent advances in adsorptive membranes for removal of harmful cations. Journal of Applied Polymer Science, 137(13):1-12. https://doi.org/10.1002/app.48579

[8] Vo TS, Hossain MM, Jeong HM, Kim K. (2020). Heavy metal removal applications using adsorptive membranes. Nano Convergence, 7(36):1-26. https://doi.org/10.1186/s40580-020-00245-4

[9] Nik-Abdul-ghani NR, Sulaiman SS, Tahreen A, Jami MS. (2021). Polyether sulfone-graphene oxide-polyvinyl pyrrolidone nanocomposite adsorptive membrane for arsenic removal from wastewater. Journal of Water and Environmental Nanotechnology, 6(2):121–137. https://doi.org/10.22090/jwent.2021.02.003

[10] Peligro FR, Pavlovic I, Rojas R, Barriga C. (2016). Removal of heavy metals from simulated wastewater by in situ formation of layered double hydroxides. Chemical Engineering Journal, 306:1035–1040. https://doi.org/10.1016/j.cej.2016.08.054

[11] Wong YC, Moganaragi V, Atiqah NA (2013). Physico-chemical investigations of semiconductor industrial wastewater. Oriental Journal of Chemistry, 29(4):1421–1428. https://doi.org/10.13005/ojc/290418

[12] Mohammadi T, Kazemimoghadam M, Saadabadi M. (2003). Modeling of membrane fouling and flux decline in reverse osmosis during separation of oil in water emulsions. Desalination, 157(1–3):369–375. https://doi.org/10.1016/S0011-9164(03)00419-3

[13] Joshi RK, Alwarappan S, Yoshimura M, Sahajwalla V, Nishina Y. (2015). Graphene oxide: the new membrane material. Applied Materials Today, 1(1):1–12. https://doi.org/10.1016/j.apmt.2015.06.002

[14] Nure JF, Nkambule TTI. (2023). The recent advances in adsorption and membrane separation and their hybrid technologies for micropollutants removal from wastewater. Journal of Industrial and Engineering Chemistry,126:92-114. https://doi.org/10.1016/j.jiec.2023.06.034

https://doi.org/10.31436/iiumecp.v1i1.3009

EFFECT OF POLYLACTIC ACID (PLA) CONCENTRATIONS ON TENSILE PROPERTIES FOR TRANSDERMAL PATCH

ASMA KHERCHI[1], FATHILAH ALI [1], FARAH AHMAD[1], AZLIN SUHAIDA AZMI[1], HAZLEEN ANUAR[2]

[1]Department of Chemical Engineering and Sustainability. Faculty of Engineering, International Islamic University Malaysia, Jalan Gombak, 53100, Kuala Lumpur, Malaysia
[2]Department of Manufacturing and Materials Engineering, Faculty of Engineering, International Islamic University Malaysia, Jalan Gombak, 53100, Kuala Lumpur, Malaysia.

**Corresponding author: fathilah@iium.edu.my*

ABSTRACT: The usage of petrochemical-based polymers is tremendous, and this is partially due to excellent mechanical properties and durability. However, with the continuous usage and development of materials, the after-use of these materials is causing huge problems for the environment. As it is non-degradable and lasts long for hundreds of years, it remains in the environment surrounding us. Conventional patches used in transdermal patches are made from non-degradable polymeric materials, thus, research on biodegradable polymers such as polylactic acid (PLA) is crucial for the usage as a patch. To achieve the requisite flexible properties for transdermal patches, the selection of appropriate materials should be considered. In this study, a fabricated semi-automated patch machine was utilized for the preparation of PLA film. Thus, it is crucial to optimize the PLA concentrations using this device. The tensile properties were examined with various polylactic acid (PLA) concentrations. The goal is to identify the ideal concentration that balances the flexibility and strength of the PLA film. Tensile testing was conducted on PLA films at five different concentrations (7%, 10%, 13%, and 15%) (w/v %). Key factors such as Young's Modulus, ultimate tensile strength (UTS), and strain at break were assessed on these PLA films. According to preliminary findings, the concentration of PLA has a significant impact on the mechanical behavior of PLA films. For transdermal and cosmeceutical patches to have the right flexibility and strength, choosing the best PLA concentration is essential. A sustainable and environmentally responsible alternative to traditional non-degradable polymers can be provided by incorporating these mechanical behavior discoveries into the creation of biodegradable patches. Our research advances environmentally friendly approaches to medicine delivery and material science.

KEYWORDS: *Polylactic Acid (PLA), Flexibility, Ultimate Tensile Strength, Transdermal Patch.*

1. INTRODUCTION

The scope of research on immunology kits, biosensors, and drug delivery devices has greatly expanded over the past three decades. With the development of new pharmacological dosage forms, it is now possible to duplicate the adverse effects of conventional dosage forms by introducing chemicals into the body through the skin [1]. Transdermal drug delivery system (TDDS) or, more commonly, transdermal patches refer to a method of administering medications topically in the form of patches that, when applied to the skin, release the

https://doi.org/10.31436/iiumecp.v1i1.3009

medication at a controlled and predetermined rate throughout the skin to improve therapeutic efficacy and reduce side effects. For an effective transdermal drug delivery system, the drug must be able to easily enter the skin and reach the target site [2].

The main supporting structure (matrix) of a transdermal patch is the polymer. It regulates how the drug diffuses from the patch [3]. The polymer utilized as a matrix must be guaranteed to be secure for skin contact and approved by the US Food and Drug Administration (USFDA) [4,5]. However, the main cause of pollution in the land, air, soil, and water is from non-biodegradable trash [6]. So, degradable polymers have since gained popularity in drug delivery applications. Due to their biocompatibility and degradability qualities [7].

The most widely researched and promising biopolymer is Polylactic acid (PLA), used in transdermal patch development, which has drawn a lot of interest because of its biocompatibility, fully biodegradable, nontoxic, and adaptable mechanical properties.[5]

The purpose of this study is to determine how varying PLA concentrations affect patches' flexibility.

2. MATERIALS AND METHODS

Polylactic acid (Ingeo biopolymer 3251 D) was purchased from Nature Works LLC, Minnetonka, MN, USA with an average molecular weight (Mw) of 148000 g/mol. Chloroform was purchased from HmbG chemicals (analytical grades, Germany) and used as it is.

2.1. Preparation of polylactic acid (PLA) film in various concentrations

PLA beads were oven-dried for 24 hours at 40 ℃ before using it. Then, PLA beads were dissolved in chloroform to create a solution that had a different concentration, the selected range was (7% to 15% (w/v) as it is shown in Table 1. The solution of PLA and chloroform was left on the stirring plate for four (4) hours. Following the dissolution of the PLA, the solution of the polymer was poured into a clean glass plate, and then cast using the semi-automated patch fabricator and allowed to dry all night. Glass plates are suitable since they have a smooth, clean surface that will make it simpler to peel the patch once the produced film has entirely dried.

Table 1: Selected Range of PLA Concentration

Sample Code	Volume of Chloroform (ml)	Concentration of PLA (w/v) %	Mass of PLA beads (g)
PLA 7	60	7%	PLA 7
PLA 10	60	10%	PLA 10
PLA 13	60	13%	PLA 13
PLA 15	60	15%	PLA 15

2.2. Universal Tensile Test

Elongation at break, Yield strength, and Young's modulus were determined using a Universal Testing Machine (Shimadzu, AGS-X, Japan). Samples were prepared in the laboratory, cut into 1 cm x 5 cm according to the America Society for Testing and Materials (ASTM D-882 type -V) with a crosshead speed of 5 mm/min. The results were taken as an average of five tests.

https://doi.org/10.31436/iiumecp.v1i1.3009

3. RESULTS AND DISCUSSION

2.1. Mechanical properties

properties in terms of mechanical strength. The test shows how a material reacts to the force applied in strain. As observed from Figure 1, PLA10 film is more flexible and less likely to fail during application and usage because it has a higher elongation at break, which means it can withstand greater deformation without breaking.

The tension at which a material switches from elastic to plastic deformation is known as the yield point. The yield point for the PLA10 concentration is at X = 3.344% and Y = 20.31 MPa, indicating a balanced behavior. The PLA10 film has a moderate yield point, which shows that it can withstand tension before deforming plastically. This makes it resilient and less likely to experience substantial deformation under normal conditions.

The 15% PLA concentration (PLA15) demonstrates the largest elongation at break (27.81%), showing good flexibility, but it also displays a higher Ultimate Tensile Strength (UTS) value (28 MPa). The material may be somewhat hard and less flexible under stress at high UTS. The film's excessive stiffness may result in decreased conformability and a higher chance of patch separation. The 7% (w/v%) PLA concentration (PLA7), on the other hand, shows lower elongation at break (7.4%) and UST (7.4 MPa), which indicates decreased flexibility and probable brittleness.

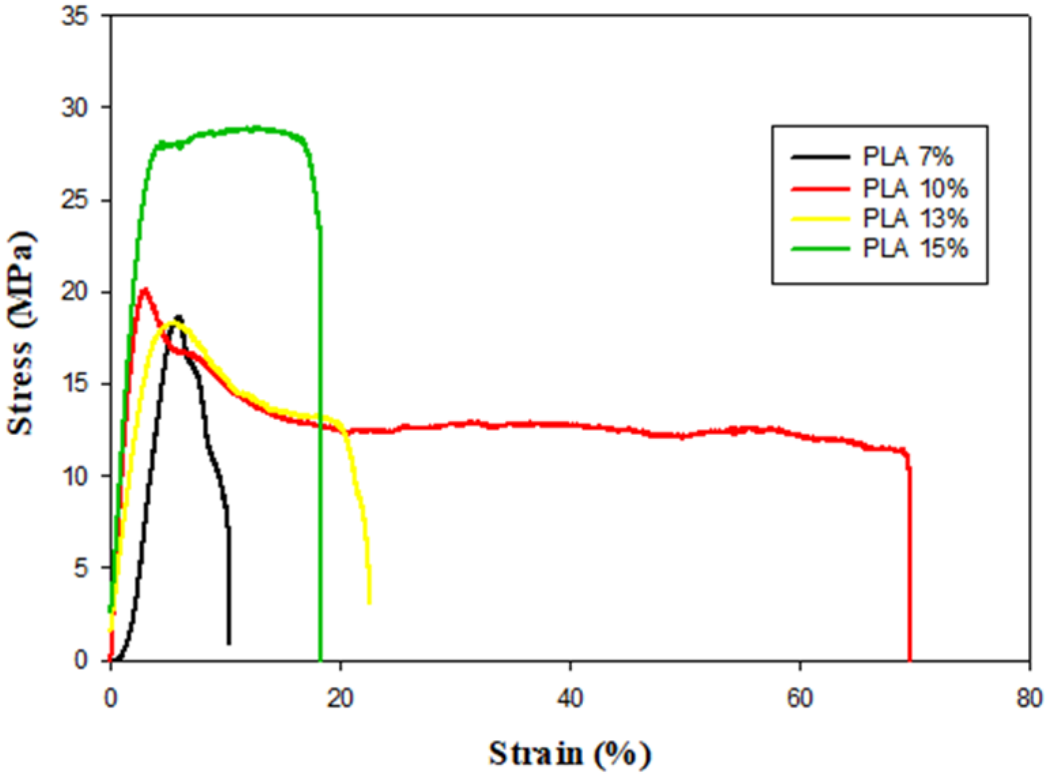

Fig. 1. Effect of PLA concentration on mechanical performance: strain-stress behavior study.

https://doi.org/10.31436/iiumecp.v1i1.3009

The ability of a material to stretch and deform before breaking is determined by a mechanical feature called the elongation at break [9]. The elongation at break of polylactic acid (PLA) films made at different concentrations (7%, 10%, 13%, and 15%) (w/v %) for the creation of flexible transdermal patches was examined in this study. Stress-strain curves generated from tensile testing of the PLA films were used to calculate the elongation at break values [5,9].

Figure 2 represents the elongation at break data for each PLA concentration. Based on the data it can be deducted from this figure that elongation at break increases up to 10% (w/v%) PLA concentration and decreases at 7% (w/v). Chain alignment, entanglement, and amorphous morphology are likely best balanced around 10% PLA concentration, allowing for improved chain mobility and deformability. The astounding elongation shown for the 10% (w/v%) concentration is the outcome of this.

Due to the lower concentration of PLA chains, the 7% (w/v%) PLA concentration's restricted elongation at break may be caused by insufficient chain alignment and tangling. With an intermediate elongation value and a 15% (w/v%) PLA content, there may be a balance between some flexibility and growing stiffness, maybe because of increased crystallinity [10].

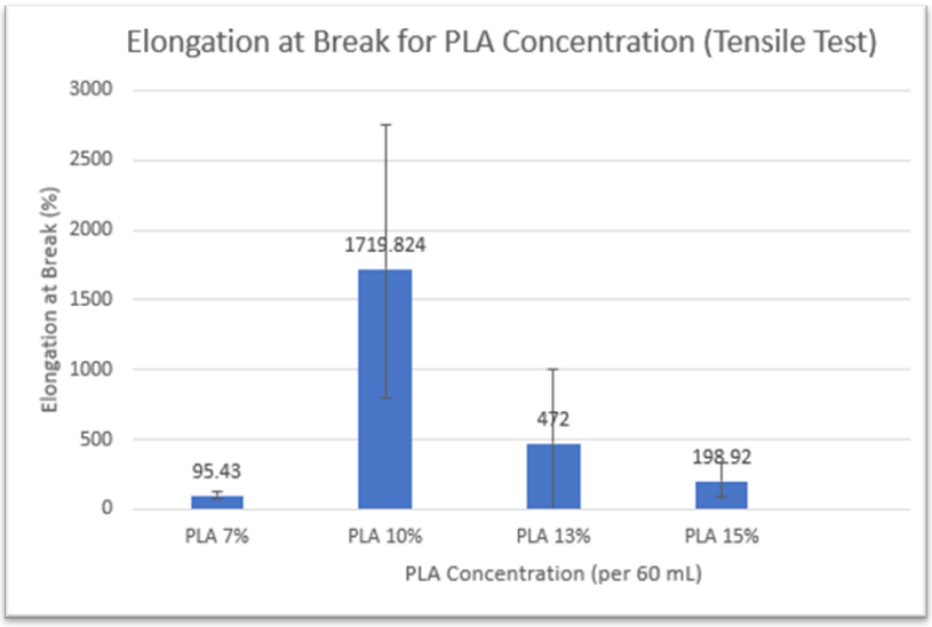

Fig. 2. Elongation at break of films prepared at different PLA concentrations.

4. CONCLUSION

The maximum elongation at break (1719.8%) was seen at the 10% (w/v%) PLA concentration, demonstrating remarkable stretchability and flexibility. The 10% (w/v%) PLA concentration was the most flexible of the investigated concentrations due to decreased Young's modulus and yield stress. Lower elongation at break was observed at the 7% (w/v%) and 15% (w/v %) concentrations, indicating reduced stretchability because of inadequate chain alignment and increased crystallinity, respectively. Overall, flexible PLA films with a 10% (w/v %) PLA concentration showed the best tensile properties to be used as a patch.

ACKNOWLEDGEMENT

The authors would like to thank the International Islamic University Malaysia (IIUM) and Kulliyyah of Engineering for their support in terms of lab facilities.

REFERENCES

[1] A. S. Morozova, E. N. Vilchevskaya, W. H. Müller, and N. M. Bessonov, "Models for drug release of gentamicin in a polylactic acid matrix," Mathematics and Mechanics of Complex Systems, vol. 8, no. 4, pp. 307–320, 2020, doi: 10.2140/MEMOCS.2020.8.307.

[2] M. Orthofer *et al.*, "Identification of ALK in thinness," *Cell*, vol. 181, no. 6, pp. 1246-1262.e22, Jun. 2020, doi: 10.1016/j.cell.2020.04.034.

[3] S. Johnson Udaya Chander, S. J. Johnson Udaya Chander, and M. T. Sidheek, "FORMULATION AND EVALUATION OF SALBUTAMOL TRANSDERMAL MEMBRANES USING POLYETHYLENE GLYCOL AS PERMEATION ENHANCER Article in WORLD JOURNAL OF PHARMACY AND PHARMACEUTICAL SCIENCES

[4] "Drugs@FDA Glossary of Terms | FDA." https://www.fda.gov/drugs/drug-approvals-and-databases/drugsfda-glossary-terms (accessed Jan. 19, 2023).

[5] S. A. Adli, F. Binti Ali, A. S. Azmi, H. Anuar, and R. Hasham, "BIODEGRADABLE POLYMER COMPOSITE FOR COSMETIC PATCH," 2019.

[6] J. S. C. Lo et al., "Optimization of polylactic acid-based medical textiles via electrospinning for healthcare apparel and personal protective equipment," Sustain Chem Pharm, vol. 30, p. 100891, Dec. 2022, doi: 10.1016/J.SCP.2022.100891.

[7] P. Goel, R. Arora, R. Haleem, and S. Kr. Shukla, "Advances in Bio-degradable Polymer Composites-Based Packaging Material," Chemistry Africa, pp. 1–21, 2022.

[8] S. S. Nair, "POLYVINYL ALCOHOL BASED TRANSDERMAL DEVICES FOR ENHANCED SKIN PERMEATION," 2019, doi: 10.26479/2019.0501.09.

[9] D. J. Patel, A. M. Vyas, S. G. Rathi, and S. K. Shah, "Formulation and Evaluation of Transdermal Patch of Apixaban," Int. J Pharm Sci Rev Res, vol. 69, no. 2, Aug. 2021, doi: 10.47583/ijpsrr. 2021.v69i02.009.

[10] T. T. Li et al., "Preparation and property evaluations of PCL/PLA composite films," Journal of Polymer Research, vol. 28, no. 5, pp. 1–9, May 2021, doi: 10.1007/S10965-021-02439-8/METRICS.

https://doi.org/10.31436/iiumecp.v1i1.3011

MODELING OF *E. COLI* GROWTH, GLUCOSE CONSUMPTION, AND RECOMBINANT COLLAGEN-LIKE PROTEIN FORMATION KINETICS

ABEIR HUSSEIN MOHAMED GAMEIL, FARIDAH YUSOF*, AZLIN SUHAIDA AZMI, NOOR ILLI MOHAMAD PUAD

Dept. of Chemical Engineering and Sustainability,
International Islamic University Malaysia, Kuala Lumpur, Malaysia

**Corresponding author: yfaridah@iium.edu.my*

ABSTRACT: Mathematical modeling of the kinetics of fermentation processes is crucial to understand complex microorganism behavior and identify problems. To investigate growth kinetics, as well as glucose utilization and recombinant collagen-like protein formation kinetics, *E. coli* BL21 (DE3) harboring a collagen-like protein from *Rhodopseudomonas palustris* (RPCLP) was cultivated in M9-casamino acids medium containing glucose (10 g/L). OD_{600} and a glucose assay kit were used to monitor the biomass concentration and glucose depletion, respectively. The RPCLP concentration was measured via a fluorometric assay. Results show that the maximum biomass achieved was 8.25 g/L, whereas the maximum RPCLP yield was 2 mg/L. Growth data was then fitted into unstructured models- Monod model and logistic model. The Luedeking-Piret model was used for the substrate utilization and product formation data. Kinetic parameters were determined by nonlinear regression and ANOVA analyses were done to determine the significance of each fit. While the growth data fitted both the Monod and the logistic model well, with significant coefficients of determination (R^2 values 0.96 and 0.99, respectively), the Luedeking-Piret models did not represent the substrate utilization and product formation well (correlation coefficients ≤ 0.7). The study suggests that the production is mixed-growth associated and modification of the model is required.

KEYWORDS: *Fermentation Kinetics, Kinetic Modelling, Escherichia coli, Recombinant Protein, Collagen.*

1. INTRODUCTION

Interest in alternative sources of collagen has risen over the past several decades, primarily due to the demand for collagen in various sectors and in part due to disadvantages with the current sources, namely bovine and porcine sources. Collagens are a family of proteins that are ubiquitous in the mammalian body and are indispensable due to their numerous uses in the body. Many species of bacteria have been discovered to produce collagen-like protein sequences, and the production of recombinant collagen-like proteins from a few selected species has been studied at the shake flask culture level, using recombinant *E. coli*. The current literature has supported the viability of recombinant bacterial collagen-like protein production as a sustainable source of Halal, vegan, and non-immunogenic collagen-like peptides. To our best of knowledge, none of these studies have considered fermentation kinetics. Prior to any scale-up attempts, the laboratory scale production must first be characterized via a kinetic study to investigate and mathematically model *E. coli* growth kinetics, as well as substrate utilization

https://doi.org/10.31436/iiumecp.v1i1.3011

and recombinant collagen-like protein formation kinetics. Mathematical modeling of the kinetics of fermentation processes sheds light on the metabolic regulation of the microbe and in process control. Furthermore, it has techno-economic and physiological implications in the reactor design and optimization of operation conditions. By understanding the growth kinetics of the microbe of interest, the fermentation process can be designed to achieve optimum product concentration. In this study, a collagen-like protein from *R. palustris* (RPCLP) has been successfully expressed in recombinant *E. coli*. This recombinant collagen-like protein production aims to yield Halal, high purity, non-immunogenic, collagen-like proteins that could be modified to suit various applications and cater to the ever-growing collagen demands of the pharmaceutical, biomedical, and food industries in a sustainable manner. To facilitate its scaleup, insight into the fermentation kinetics is necessary. Therefore, the objective of this work was to evaluate the data using unstructured models and estimate the values of relevant kinetic parameters.

2. MATERIALS AND METHODS

Strains, Medium and Batch fermentation

Genetically engineered *E. coli* BL21 (DE3) carrying pColdII (Takara Bio) containing a collagen like protein-coding gene from *R. palustris*, an ampicillin-resistance gene, and temperature-sensitive promoter. The *E. coli* was cultivated in a complex M9-casamino acid medium that had been optimized for *R. palustris* collagen-like protein (RPCLP) expression using *E. coli* BL21 (DE3). This medium consists of D-glucose (10 g/l), 1X M9 salts, casamino acids, trace elements, magnesium sulfate, thiamine, calcium chloride, and ampicillin (50 µg/ml).

Inoculum (2.5 ml, OD_{600} ~ 3-5) was transferred into 250 ml unbaffled Erlenmeyer flasks containing 50 ml M9-casamino acid medium, supplemented with ampicillin (50 µg/ml). The flasks were cultured at 37 ℃ temperature and 250 rpm agitation speed. Sampling was done every 30 minutes until induction, and then hourly until the end of the fermentation (24 hours). Induction was carried out at the mid-log phase by lowering the temperature to 20 ℃, increasing the agitation speed to 300 rpm, and adding IPTG solution to attain a final concentration of 1 mM [1]. The cells were harvested via centrifugation at 4696 x g, at 4°C, for 30 minutes (Heraeus Multifuge X1R, Thermo Scientific, USA), and cell pellets were stored at -20 ºC. Cell pellets were resuspended with ice-chilled lysis buffer (20 mM sodium phosphate pH 7.4, 0.5 M sodium chloride) and lysed by sonication using 5-minute burst cycle, with 0.5 second pulse, at 40% amplitude (Labsonic M, Sartorius, Germany) [1]. The resultant lysed cells were clarified via centrifugation at 12, 000 rpm, 4°C, for 30 minutes (Heraeus Multifuge X1R, Thermo Scientific, USA).

Analysis Methods

Cell density was analyzed turbidometrically at 600 nm optical density (OD_{600}) using a spectrophotometer (Biophotometer, Eppendorf, Germany). Cell wet weight (CWW) and dry cell weight (DCW), in g/l, were also determined using established calibration curves. A colorimetric glucose assay kit (Cell Biolabs Inc, USA) was used to determine the glucose concentration during fermentation. A glycine-based, fluorometric collagen assay was used to determine collagen-like protein concentration as described by Yasmin and colleagues, measured at $\lambda_{\text{excitation/emission}}$ = 375/465 nm [2].

https://doi.org/10.31436/iiumecp.v1i1.3011

Modeling and Statistical Analysis

Unstructured batch kinetic models, based on either Monod model of growth and the logistic model of growth, combined with Luedeking-Piret equations for substrate utilization and product formation were employed in this study [3, 4]. These models are hereafter referred to as the Monod-Luedeking Piret (MLP) and the Logistic-Luedeking Piret (LLP), respectively. Unsegregated and unstructured models based on the Monod equation are often used to describe the overall substrate-dependent cell growth and fermentation kinetics in batch, fed-batch, or continuous microbial processes [5]. As such, the simple Monod model was selected. Sometimes, information on the limiting carbon substrate is not available, due to use of complex media, and in such cases, substrate-independent growth kinetics can be determined by applying models like the Logistic model or modifications to the Monod model such as the Contois equation [6]. To consider the effect of substrate consumption, the logistic model of cell growth was chosen for comparison. The Monod model for specific growth rate, μ, is expressed as follows:

$$\mu = \mu_{max} \frac{S}{Ks+S} \quad (1)$$

where μ_{max} is the maximum specific growth rate, S is substrate (glucose) concentration (g/L), and K_S is the half-saturation constant for glucose.

The logistic model equation is:

$$\mu = k\,(1 - (\frac{X}{Xmax})) \quad (2)$$

$$\frac{\Delta X}{\Delta t} = \mu . X \quad (3)$$

The Luedeking-Piret model equations for rates of substrate consumption ($\frac{\Delta S}{\Delta t}$) and product formation ($\frac{\Delta P}{\Delta t}$) are:

$$\frac{dS}{dt} = -m\frac{dX}{dt} - n.X \quad (4)$$

$$\frac{dS}{dt} = -\frac{1}{YXS}\frac{dX}{dt} - \frac{1}{YPS}\frac{dP}{dt} - k_e X \quad (5)$$

$$\frac{dP}{dt} = \alpha\frac{dX}{dt} + \beta X \quad (6)$$

where X represents biomass concentration (g/L), P is collagen-like protein concentration (g/L), α is the growth associated collagen-like protein production constant, β is the non-growth associated collagen-like protein production constant, m is growth associated glucose consumption constant (g g^{-1}), and n is the non-growth associated glucose consumption constant (g g^{-1} g^{-1}), k_e is the maintenance coefficient for cells (g/g.h), Y_{XS} is the yield of cell mass from substrate , Y_{PS} is the yield coefficient of product from substrate, k is initial specific growth rate (h^{-1}), and X_{max} is the maximum cell concentration (g/L).

Initial estimation of kinetic parameters and yield constants was accomplished using Microsoft Excel software, wherein experimental data was keyed in and the OD_{600} values were plotted against time. The slope of the resulting linear regression line was taken as μ_{max} [5]. These values were then used as initial guesses for solving the ordinary differential equations. MATLAB software (R2022a, MathWorks, USA) was used to generate plots of experimental data and pass initial values of kinetics parameters into sets of ordinary differential equations which were solved by using the *ode45* function and the Levenberg-Marquardt method of the *lsqcurvefit* function. The coefficient of determination (R^2) was then estimated to evaluate the

https://doi.org/10.31436/iiumecp.v1i1.3011

accuracy of the estimated parameters achieved by fitting the experimental data to the kinetic models [6].

3. RESULTS AND DISCUSSION

The pattern of growth of the recombinant *E. coli* follows typical bacterial growth curve composed of a short lag phase, a log phase of exponential increase in biomass, and a stationary phase. Similar growth patterns were observed in protein-producing fermentations employing recombinant *E. coli* [3]. The profile of substrate concentration over time shows a sharp decrease in substrate concentration after inoculation. The product concentration profile with time shows accumulation of product, but the increase is inconsistent with expected results. Induction of the protein expression with IPTG starts at the mid-log phase, after hours of inoculation, which means that product accumulation should gradually increase after the induction. However, this is not reflected well in the product concentration curve (refer to Fig. 1-2). The kinetic parameters were approximated by the respective models as in Table 1.

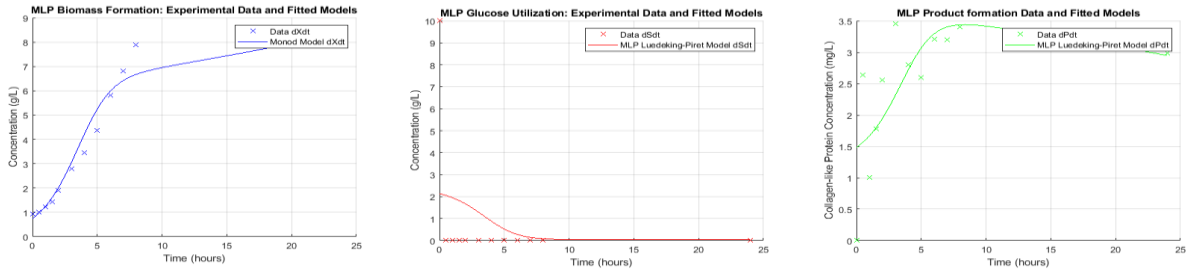

Fig. 1 Monod-Luedeking Piret (MLP) model experimental data and fitted models.

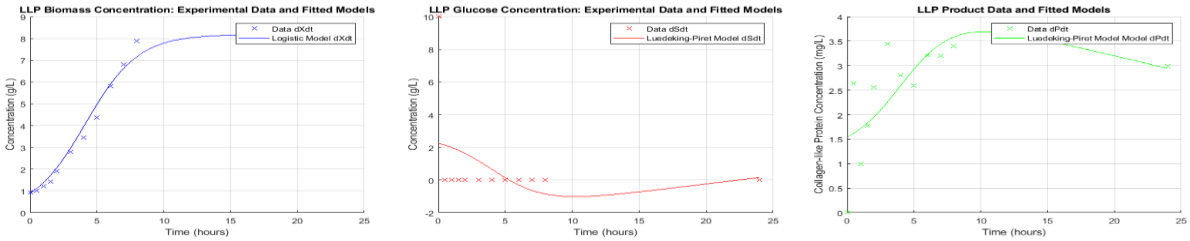

Fig. 2 Logistic-Luedeking Piret (LLP) model experimental data and fitted models.

Table 1 Estimated Kinetic Parameters of Respective Models

Model	μ_{max} **[/h]**	K_S **[g/L]**	Y_{XS} **[g X/g S]**	Y_{PS} **[g P/ g S]**	α **[g P/g X]**	β **[g P/g X h]**	k_e **[g S/g X h]**	X_{max} **[g/L]**	k **[h^{-1}]**
MLP	1.75	4.82	2.69	0.02	0.0004	-0.000009	-0.00483	-	-
LLP	-	-	1.80	0.02	0.00037	-0.000008	-0.01224	8.18311	0.507

Of the two models studied, it can be observed from Figure 1 that biomass concentration is best described by the Monod model. Even though the Monod-Luedeking Piret and Logistic-Luedeking Piret substrate utilization and product formation models studied did not fit the experimental data well, the Monod model for biomass accumulation fitted the data very well (Figure 1). This is further supported by the Monod kinetic parameter values of μ_{max} = 1.75 and K_S = 4.82 g/l, which were acceptable, compared to those reported in the literature for *E. coli* [7]. As for the logistic model (Figure 2), it can be observed that it fits the experimental data for growth

https://doi.org/10.31436/iiumecp.v1i1.3011

but was unable to attain a good fit for substrate utilization and product formation. Factors such as hydrodynamics, oxygen partial pressure, agitation speed, pH, and temperature can affect the fermentation process by a large margin. While the growth data fitted both the Monod and the logistic model well, with significant coefficients of determination (R^2 values 0.96 and 0.99, respectively), the Luedeking-Piret models did not represent the substrate utilization and product formation well (correlation coefficient ≤ 0.7).

4. CONCLUSION

Both the Monod model and logistic model provided a good fit of the growth experimental data. The growth-associated and non-growth associated constants, α and β, suggest that the production is mixed growth associated, and as the Luedeking-Piret model was not a good fit for the product formation and substrate consumption, further modification of the model is required. As there is limitation to the control of parameters such as pH and oxygen partial pressure, in the shake flask culture, it is recommended that the kinetics are evaluated at the 2 L bioreactor culture for comparison. Overall, the kinetic parameters obtained provide useful indicators for the fermentation process optimization and its scale-up.

ACKNOWLEDGEMENT

This study is funded by the Ministry of Higher Education, Malaysia, via the Transdisciplinary Research Grant Scheme (TRGS/1/2018/UIAM/01/1/3). We would like to express our gratitude towards the Institute of Halal Research and Training (INHART), IIUM, for the use of the INHART Lab facility.

REFERENCES

[1] Xu C, Yu Z, Inouye M, Brodsky B, Mirochnitchenko O. (2010) Expanding the family of collagen proteins: recombinant bacterial collagens of varying composition form triple-helices of similar stability. Biomacromolecules, 11(2), 348-356.

[2] Yasmin H, Kabashima T, Rahman MS, Shibata T, Kai M. (2014) Amplified and selective assay of collagens by enzymatic and fluorescent reactions. Sci Rep, 4, 4950.

[3] Ariff AB, Nelofer R, Abdul Rahman RNZR, Basri M. (2015). Kinetics and modelling of batch fermentation for the production of organic solvent tolerant and thermostable lipase by recombinant E. coli Turkish Journal of Biochemistry, 40(4).

[4] Garnier A, Gaillet B. (2015). Analytical solution of Luedeking-Piret equation for a batch fermentation obeying Monod growth kinetics. Biotechnol Bioeng, 112(12), 2468-2474.

[5] Doran PM. (2013) Bioprocess Engineering Principles. Academic press, Waltham, MA.

[6] Ali MK, Serge H, Nawel O, Radia C, Noreddine, KC. (2017). Kinetic models and parameters estimation study of biomass and ethanol production from inulin by Pichia caribbica (KC977491). African Journal of Biotechnology, 16(3), 124-131.

[7] Limoes S, Rahman SF, Setyahadi S, Gozan M. (2018) Kinetic study of Escherichia coli BPPTCC-EgRK2 to produce recombinant cellulase for ethanol production from oil palm empty fruit bunch. IOP Conf. Ser.: Earth Environ. Sci., 141 012016.

https://doi.org/10.31436/iiumecp.v1i1.3006

EFFECT OF STABILITY AND BACTERIAL INHIBITION ACTIVITY OF MELASTOMA MALABATHRICUM LINN LEAVES PLANT EXTRACT IN A WATER-BASED EMULSION

NUR ATHIRAH ABDUL RAHMAN, NORASHIKIN AHMAD ZAMANHURI*

School of Chemical Engineering, College of Engineering,
Universiti Teknologi MARA, Selangor, Malaysia

**Corresponding author: shikin.zamanhuri@uitm.edu.my*

ABSTRACT: *Melastoma malabathricum Linn*. (MB) is a herbal plant that has benefits in treating scars from smallpox, pimples and black spots on the skin. The active ingredient in MB leaves can produce a quality and effective product which can inhibit bacterial development. Therefore, this study was to identify the effect of stability and bacterial inhibition activity in based-water emulsion after it had been added with the extraction of MB leaves. The water-based emulsion containing 1% of MB extraction in different storage conditions showed its stability when viscosity and pH at 4 °C, 25 °C, and 58 °C slightly changed much from the initial after 21 days. The colour of emulsion MB extract at 58 °C changes from yellowish to brown due to the degradation of chlorophyll in extract when it exposes to high temperature. Viscosity from different pH showed that pH 6 was the most stable viscosity during the storage period which this pH was in the range of skin pH. This study shows that the emulsion MB extract was most stable at lower temperature, 4 °C and pH around 6. Thus, this emulsion MB extract suitable to use on the skin. Besides that, the emulsion MB extraction did not show antibacterial activity against *Escherichia coli.*

KEYWORDS: *emulsion MB extract, stability, viscosity, pH, bacterial*

1. INTRODUCTION

Melastoma malabathricum Linn. is a widespread herb or shrub that originates primarily in the moist tropics, specifically India, Thailand, and Malaysia, where it grows as a small tree between 12 and 13 feet in height, occasionally reaching 20 feet. The leaves of this plant have been used for a variety of medicinal purposes, including the treatment of dysentery and diarrhea, the reduction of the appearance of scars, and as an anti-infection [1]. Additionally, herbs can be utilised to treat dehydration and skin irritation. Therefore, we will use the active ingredient of *Melastoma malabathricum Linn*. leaves because this plant is well known in Malaysia for its advantages in the treatment of different diseases and ailments as the leaves of this plant can treat scars, pimples, and black spots on the skin [2].

Plant extracts from herbs are widely used in cosmetics products as people seek a more holistic, natural approach to health and wellness. Water-based emulsions like emollients and moisturisers are used to treat and prevent dry skin because they help seal moisture deep inside the skin, which can keep it soft and supple. Moisturizing creams with natural ingredients are currently popular since they are likely to be effective, harmless, and skin-friendly. According to a study by Leelapornpisid et al. [3], the extraction of the freshwater macroalgae in a cream base proved safe and showed the same moisturising properties as hyaluronic acid via humectants, followed by an occlusive effect that can keep skin hydration

https://doi.org/10.31436/iiumecp.v1i1.3006

for a longer period of time. Aside from that, a cream containing *Moringa oleifera* leaves extract demonstrated efficiency in enhancing skin hydration by avoiding UV radiation due to ascorbic acid in *Moringa oleifera* leaves, which provides photoprotection and inhibits inflammation, and UVB-induced immune suppression when applied topically [4].

The warm humid conditions of a tropical environment are ideal for the development of microorganisms, which are the causes of several infectious diseases and the spoilage of cosmetics and medicines. There is a possibility that if there are too many bacteria at any point during the product's shelf life, they could cause the product's physical state to get worse. The risk of this occurring is higher with many present-day moisturizing creams and lotions, which contain special additives (including plant extracts, fatty acids and vitamins) that could increase the growth of bacteria [3]. In order to obtain a stable extract cream, a physical stability test must be conducted so that the cream is safe to use and does not cause skin damage such as irritation, allergies, dark spots, and discolouration. A stable cream is one whose physical qualities and characterization remain within acceptable limits during the storage and use period. Several factors influence the stability of cream, including the stability of the active ingredient, the interaction of the active ingredient with additives, and the temperature at which additives and raw materials are heated during production. For bacterial inhibition activity, tannins and other phytochemicals have been shown to have antibacterial activity, suggesting they can greatly reduce the risk of wound infections. Tannins, an astringent and antibacterial compound found in the plant, may help accelerate the wound-healing process by reducing inflammation and promoting the formation of new skin cells (epithelium) [5]. Active compounds like flavonoids, alkaloids, tannins and saponins have antibacterial activity against various bacteria, one of which is *Staphylococcus aureus*. This Gram-positive bacterium can cause skin infection, resulting in a variety of skin diseases, including acne [6].

From previous studies, the active ingredient the *Melastoma malabathricum Linn*. plant can be used for a variety of beneficial purposes. Che Omar et al. [1] conducted a study on the growth of pathogenic bacteria from flower and fruit extract of *Melastoma malabathricum Linn.* Whereas a study on leaves of *Melastoma malabathricum Linn*. to evaluate the antioxidant, antihyperlipidemic and antidiabetic activity has been conducted by Kumar et al. [7]. Therefore, this study was done to identify the effect of leaves extraction of *Melastoma malabathricum Linn.* (MB) in the water-based emulsion on stability and bacterial inhibition activity.

2. MATERIALS AND METHODS

2.1. Materials

Leaves of *Melastoma malabathricum Linn*. as Fig. 1 were collected from Kampung Balok, Kuantan, Pahang, Malaysia. The leaves were cleaned with tap water and a portion was dried in a hot oven at 100 ◦C for 1h 30 minutes. The dried samples are ground and passed through a sieve (30 mesh). The powders were kept in sealed containers and protected from light until used. The water-based emulsion was purchased from a local vendor for use in this research project (Fig. 2).

2.2 Soxhlet extraction of dried leaves

The dried powdered leaves were separately placed into a thimble and extracted with 60% ethanol (1:20, w/v) in a Soxhlet apparatus [8]. Extraction is carried out for 7 to 8 h. The combined extract from the extraction method is separately filtered through a Whatman No. 1

https://doi.org/10.31436/iiumecp.v1i1.3006

filter paper. The filtrate was dried under reduced pressure at 50 °C using a rotary vacuum evaporator. The crude extract is weighed and kept in a tight container protected from light [9].

Fig. 1. *Melastoma malabathricum Linn.* plant

Fig. 2. Water-based emulsion

2.3. Phytochemical screening

In a test of tannin, 0.5 g of the extract is heated in 10 mL of distilled water and filtered. The filtrate was diluted with distilled water until it was colourless and adds 1-2 drops of $FeCl_3$ 1% to form a blue/dark blue or blackish-green colour [10].

2.4. Stability test at different temperatures and pH

10g of an emulsion 1% MB extract mixture of was stored for 21 days for rapid stability tests. For this purpose, the samples were kept at different temperatures: 4 °C, 25 °C (at room temperature) and 58 °C. At the same time, 10g of an emulsion 1% MB extract was stored at room temperature, 25 °C. The pH of the sample was adjusted to pH 5, 6, 7, and 8, respectively by using 0.3M HCl and 0.1M NaOH solution [3]. These tests were to observe the change of colour by using a chromameter (Konica Minolta Chroma meter), pH by using a pH meter and viscosity by using a rheometer (HAAKE RheoStress 6000) during the storage period.

2.5. Antibacterial activity

The agar diffusion method was used to determine bacterial inhibition activity. Petri dishes containing nutrient agar (Tryptone Soya Broth) were inoculated with bacteria (*Escherichia coli*). Then, filter paper disks with a diameter of 6mm, containing MB extract and mixture of water-based extract were placed on the agar surface. The petri dishes were then incubated at 37°C for 24 h and observed for growth or inhibition. The diameter of zone inhibition presented in discs is recorded [1].

https://doi.org/10.31436/iiumecp.v1i1.3006

3. RESULT AND DISCUSSION

3.1. Phytochemical screening

The colour change of MB extract solution from yellow to blackish-green colour (Fig. 3b). The colour change of MB extract solution from yellow to deep yellow colour then gradually becomes colourless showed the presence of flavonoids (Fig. 4c). *Melastoma Malabathricum Linn* leaves extract was found to contain tannins and flavonoids. Tannins can help protect the skin from damage caused by free radicals [5]. Free radicals are unstable molecules that can damage cells and contribute to the ageing process. According to Shamsudin et al. [6], pyrogallol structure in the flavonoids is an important structural feature for the manifestation of good antibacterial activity. Pyrogallol work by disrupting the cell membrane of bacteria which cause them to die [11].

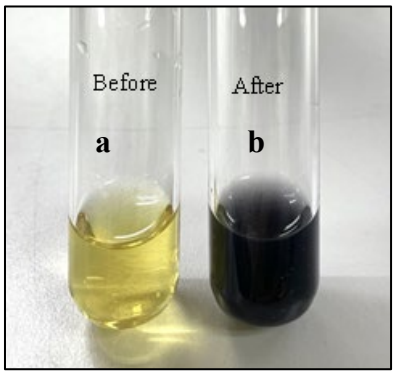

Fig. 3. Melastoma extract before add $FeCl_3$ (a) and presence of tannins after add $FeCl_3$ (b)

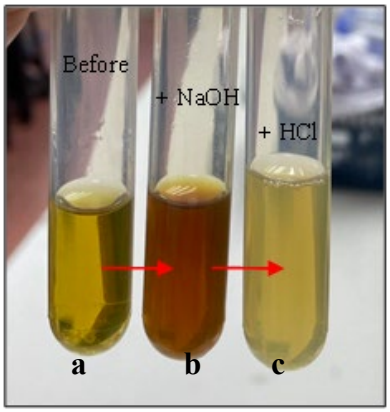

Fig. 4. Melastoma extract before add NaOH (a), after add NaOH (b) and the presence of flavonoids after gradually add HCl (c)

3.2. Stability test at different temperatures

The stability test for water-based emulsions MB extract was examined and it was found that the emulsion MB extract was stable at storage conditions (4 °C, 25 °C and 58 °C) for 21 days. Table 1 showed the value pH of emulsion MB extract for these three conditions was between 6.47-6.65. According to Muhammad et al. (2014) pH of human skin typically ranges from 4.5 to 6 but for skin care product like moisturizer, the common pH range between 5-7 [12]. Therefore, the emulsion MB extract must be in moisturizer pH range because this range is preferable for dry and sensitive skin [13].

https://doi.org/10.31436/iiumecp.v1i1.3006

The viscosity of emulsion MB extract at these different storage conditions is represented in Fig. 5. Viscosity is a useful process to indicate the quality and check the stability of the emulsion [14]. The viscosity of emulsion MB extract maintained stable conditions for 21 days without liquefaction. However, the emulsion MB extract at 4 °C showed an increase in viscosity while the emulsion MB extract for 58°C had the lowest viscosity after 21 days. Increasing the temperature would decrease the viscosity of the emulsion MB extract. Baily and Davey [15] stated that high temperatures can cause an increased frequency of droplet collisions due to an increase in kinetic or thermal energy. Therefore, when the attractive binding energy in the emulsion decreases, the viscosity decreases. Meanwhile, the viscosity increases due to the less mobile of molecules in the oil droplets at lower temperatures, so they are more likely to stick together.

Table 1: Stability test of water-based emulsion 1% MB extract and without extract at 4 °C, 25 °C and 58 °C for 21 days.

Temperature			0 Day	7 Day	14 Day	21 Day
4 °C	pH	WOE	6.58	6.35	6.41	6.62
		WE	6.47	6.31	6.38	6.65
	Viscosity	WOE	4.804	4.073	5.073	5.8
		WE	4.615	4.758	5.327	5.334
	Colour	WOE	white	white	white	white
		WE	yellowish	yellowish	yellowish	yellowish
25 °C	pH	WOE	6.58	6.55	6.61	6.49
		WE	6.47	6.53	6.43	6.53
	Viscosity	WOE	4.804	4.740	4.72	4.729
		WE	4.615	4.453	4.886	4.668
	Colour	WOE	white	white	white	white
		WE	yellowish	yellowish	yellowish	yellowish
58 °C	pH	WOE	6.58	6.44	6.6	6.45
		WE	6.47	6.36	6.5	6.6
	Viscosity	WOE	4.804	4.5	5.381	5.514
		WE	4.615	3.817	4.527	4.159
	Colour	WOE	white	white	white	white
		WE	yellowish	Olive-brown	Olive-brown	Brown

* WOE = without extract, WE = with extract

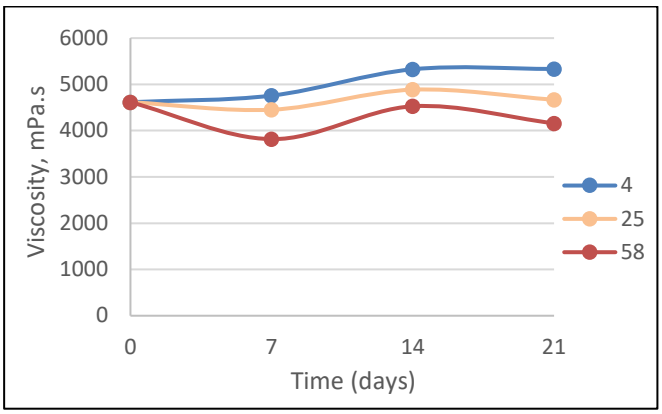

Fig. 5.Viscosity of emulsion MB extract at 4 °C, 25 °C and 58 °C

https://doi.org/10.31436/iiumecp.v1i1.3006

The colour of the emulsion MB extract after 21 days showed yellowish colour for samples that store at 4 °C and 25 °C. Meanwhile, the sample at 58 °C became brown colour after 21 days. The colour of the sample changes at high temperature due to the degradation of chlorophyll in the MB extract. When chlorophyll is exposed to high temperatures, it can be degraded [16]. The loss of the green colour in the degradation process of chlorophyll results in the formation of other pigments, such as pheophytin. Pheophytin is a brown pigment that is responsible for the brown colour [17]. The colour change has been shown in Fig. 6a, 6b, 6c and 6d.

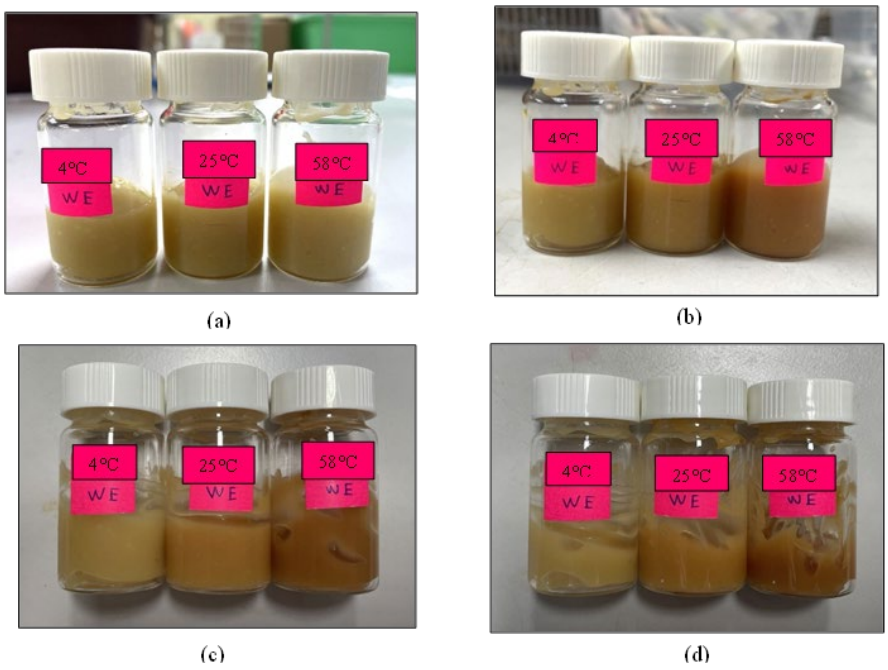

Fig. 6. (a) Colour of emulsion at initial. (b) Colour of emulsion after 7 days. (c) Colour of emulsion after 14 days. (d) Colour of emulsion after 21 days.

3.3. Stability test at different pH

At different values of pH 8,7,6 and 5, the viscosity was vary (Fig. 7). At pH 8 and 7, the viscosity was higher compared to acidic samples, pH 6 and 5. Viscosity at pH 6 and pH 5 become lower due to the presence of water when the sample mix with the HCl. Ingredients in emulsion like polyoxyethylene make the hydroxyl groups (-OH) react with the hydrogen ions (H+) of HCl to form ester which then loses a water molecule [18]. pH 8 and 7 had higher viscosity because the interaction between NaOH and surfactant in the emulsion can cause the surfactant molecule to clump together [19]. All samples of emulsion MB extract at pH 8,7 and 6 stable during storing period because still in range of standard lotion which is 2000-50000 mPa.s except sample at pH 5 [20].

The sample of emulsion MB extraction for pH 8,7,6 and 5 was stored at 25 °C (room temperature). The colour of the sample at pH 8,7,6 and 5 on day 21 slightly changed from the initial (Fig. 8a and 8b).

3.4. Antibacterial test

On the antibacterial activity test, the MB extract, and emulsion MB extract showed no inhibition zone against *E. coli*. This illustrated that *Melastoma malabathricum Linn* leaves were not effective in inhibiting the growth of *E. coli* bacteria (Fig. 9). The concentration of the

https://doi.org/10.31436/iiumecp.v1i1.3006

extract in the water-based emulsion is 1%. The result studied by Fares et al. [21] showed that no inhibition zones were found for the lower concentrations (25% or 50%) of the extract. Therefore, the concentration must be more than 50% of the extract or higher. Other than that, *E. coli* is gram-negative bacteria. According to Biswas et al. [10], the Gram-negative bacteria's resistance can be attributed to its unique cell wall structure, which includes an effective permeability barrier. This barrier comprised a thin lipopolysaccharide exterior membrane, which could restrict the penetration of the extruding plant extract. The study from Cortis Maigoda & Nisak, [22] stated that the antibacterial action of *Melastoma malabathricum Linn* leaves extract was more effective against Gram-positive bacteria than Gram-negative bacteria.

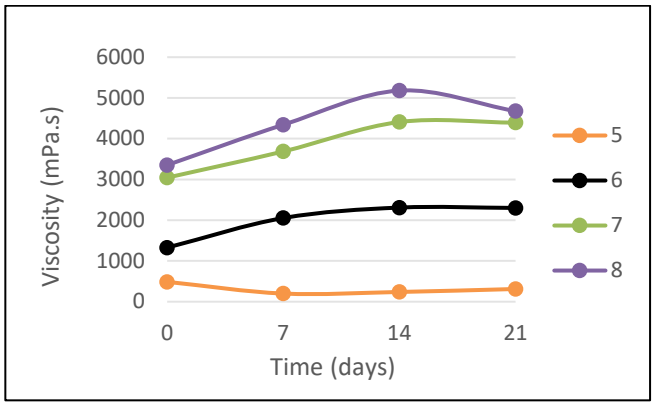

Fig. 7.Viscosity of emulsion MB extract at pH 8,7,6,5

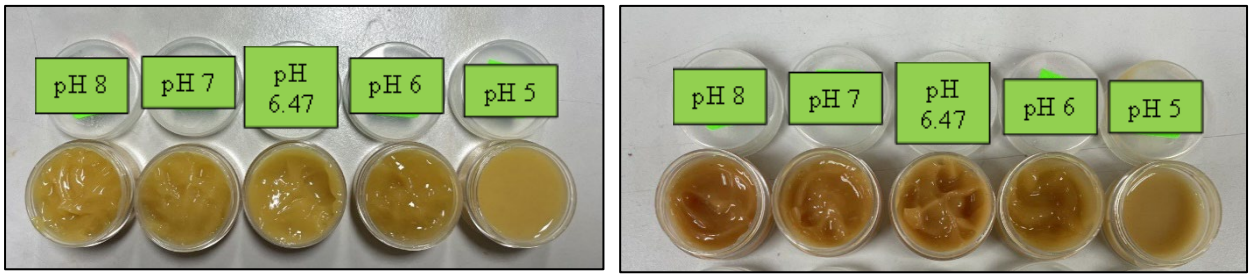

(a) (b)

Fig. 8. (a) Colour emulsion at different pH at initial. (b) Colour emulsion at different pH after 21 days

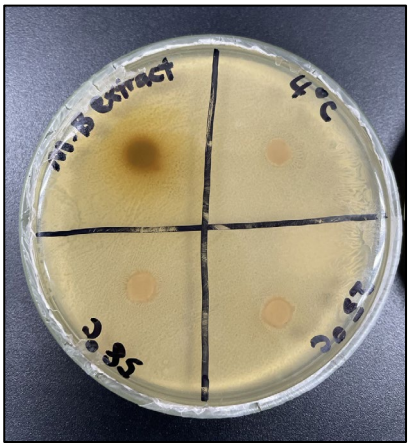

Fig. 9. Emulsion MB extract against E. coli.

4. CONCLUSION

This study showed that an emulsion containing 1% *Melatoma Malabathricum* (MB) extract maintained its viscosity, pH, and colour stability at various storage conditions for 21 days. No significant change in pH indicates that it is safe to use on the skin. The colour of emulsion MB extract at 4 °C after 21 days did not change from its initial colour. The suitable pH for the emulsion MB extract that maintained its viscosity for 21 days was pH 6. The antibacterial test showed no inhibition zone in MB extract and emulsion MB extract against Escherichia coli. From the above study, the most stable emulsion MB extract was the emulsion at pH around 6 and to keep its effectiveness of emulsion must be stored at 4 °C.

ACKNOWLEDGEMENT

The authors gratefully acknowledge the School of Chemical Engineering, Universiti Teknologi MARA, Shah Alam, Selangor, Malaysia.

REFERENCES

[1] S. N. Che Omar, J. Ong Abdullah, K. A. Khairoji, S. Chin Chin, and M. Hamid, "Effects of flower and fruit extracts of Melastoma malabathricum Linn. on growth of pathogenic bacteria: Listeria monocytogenes, Staphylococcus aureus, Escherichia coli, and salmonella typhimurium," Evidence-based Complementary and Alternative Medicine, vol. 2013, 2013, doi: 10.1155/2013/459089.

[2] S. M. Joffry et al., "Melastoma malabathricum (L.) smith ethnomedicinal uses, chemical constituents, and pharmacological properties: A review," Evidence-based Complementary and Alternative Medicine, vol. 2012. 2012. doi: 10.1155/2012/258434.

[3] P. Leelapornpisid, L. Mungmai, B. Sirithunyalug, S. Jiranusornkul, and Y. Peerapornpisal, "A Novel Moisturizer Extracted from Freshwater Macroalga [Rhizoclonium hieroglyphicum (C.Agardh) K tzing] for Skin Care Cosmetic," 2014. [Online]. Available: http://epg.science.cmu.ac.th/ejournal/

[4] A. Ali et al., "Moisturizing effect of cream containing Moringa oleifera (Sohajana) leaf extract by biophysical techniques: In vivo evaluation," Journal of Medicinal Plants Research, vol. 7, no. 8, pp. 386–391, 2013, doi: 10.5897/JMPR012.504.

[5] R. G. Daré, C. V. Nakamura, V. F. Ximenes, and S. O. S. Lautenschlager, "Tannic acid, a promising anti-photoaging agent: Evidences of its antioxidant and anti-wrinkle potentials, and its ability to prevent photodamage and MMP-1 expression in L929 fibroblasts exposed to UVB," Free Radic Biol Med, vol. 160, pp. 342–355, Nov. 2020, doi: 10.1016/j.freeradbiomed.2020.08.019.

[6] N. F. Shamsudin et al., "Antibacterial Effects of Flavonoids and Their Structure-Activity Relationship Study: A Comparative Interpretation," Molecules, vol. 27, no. 4, p. 1149, Feb. 2022, doi: 10.3390/molecules27041149.

[7] V. Kumar, D. Ahmed, P. S. Gupta, F. Anwar, and M. Mujeeb, "Anti-diabetic, anti-oxidant and anti-hyperlipidemic activities of Melastoma malabathricum Linn. leaves in streptozotocin induced diabetic rats," 2013. [Online]. Available: http://www.biomedcentral.com/1472-6882/13/222

[8] O. R. Alara, N. H. Abdurahman, and C. I. Ukaegbu, "Soxhlet extraction of phenolic compounds from Vernonia cinerea leaves and its antioxidant activity," J Appl Res Med Aromat Plants, vol. 11, pp. 12–17, Dec. 2018, doi: 10.1016/j.jarmap.2018.07.003.

[9] B. Vongsak, P. Sithisarn, S. Mangmool, S. Thongpraditchote, Y. Wongkrajang, and W. Gritsanapan, "Maximizing total phenolics, total flavonoids contents and antioxidant activity of Moringa oleifera leaf extract by the appropriate extraction method," Ind Crops Prod, vol. 44, pp. 566–571, Jan. 2013, doi: 10.1016/j.indcrop.2012.09.021.

[10] B. Biswas, K. Rogers, F. McLaughlin, D. Daniels, and A. Yadav, "Antimicrobial activities of leaf extracts of guava (psidium guajava L.) on two gram-negative and gram-positive bacteria," Int J Microbiol, vol. 2013, 2013, doi: 10.1155/2013/746165.

[11] Y.-L. Chew, C. Arasi, and J.-K. Goh, "Pyrogallol Induces Antimicrobial Effect and Cell Membrane Disruption on Methicillin-Resistant Staphylococcus aureus (MRSA)," Curr Bioact Compd, vol. 18, no. 1, Jan. 2022, doi: 10.2174/1573407217666210526121512.

[12] S. Saraf, S. Sahu, C. D. Kaur, and S. Saraf, "Comparative measurement of hydration effects of herbal moisturizers," Pharmacognosy Res, vol. 2, no. 3, p. 146, 2010, doi: 10.4103/0974-8490.65508.

[13] N. Ijaz, A. I. Durrani, S. Rubab, and S. Bahadur, "Formulation and characterization of Aloe vera gel and tomato powder containing cream," Acta Ecologica Sinica, vol. 42, no. 2, pp. 34–42, Apr. 2022, doi: 10.1016/j.chnaes.2021.01.005.

[14] A. Naveed, B. A. Khan, T. Mahmood, and H. M. Shoaib Khan, "Formulation development and moiturising effects of a topical cream of Aloe vera extract Assessment of Bakery Products View project," 2011. [Online]. Available: https://www.researchgate.net/publication/286481326

[15] R. Davey and S. Baily, "How does Temperature Change Viscosity in Liquids and Gases? ," Sep. 23, 2013.

[16] D. Indrasti, N. Andarwulan, E. H. Purnomo, and N. U. R. Wulandari, "Stability of chlorophyll as natural colorant: A review for suji (dracaena angustifolia (medik.) roxb.) leaves' case," Current Research in Nutrition and Food Science, vol. 6, no. 3. Enviro Research Publishers, pp. 609–625, Dec. 01, 2018. doi: 10.12944/CRNFSJ.6.3.04.

[17] L. Kusmita, I. Puspitaningrum, and L. Limantara, "Identification, Isolation and Antioxidant Activity of Pheophytin from Green Tea (Camellia Sinensis (L.) Kuntze)," Procedia Chem, vol. 14, pp. 232–238, 2015, doi: 10.1016/j.proche.2015.03.033.

[18] P. Y. Stergiou et al., "Advances in lipase-catalyzed esterification reactions," Biotechnology Advances, vol. 31, no. 8. pp. 1846–1859, Dec. 2013. doi: 10.1016/j.biotechadv.2013.08.006.

[19] C. Zhao, Y. Jiang, M. Li, T. Cheng, W. Yang, and G. Zhou, "The effect of NaOH on lowering interfacial tension of oil/alkylbenzene sulfonates solution," RSC Adv, vol. 8, no. 11, pp. 6169–6177, 2018, doi: 10.1039/c7ra11287d.

[20] D. Fransiska et al., "Characteristics of Oil in Water (o/w) Type Lotions Incorporated with Kappa/Iota Carrageenan," in IOP Conference Series: Earth and Environmental Science, IOP Publishing Ltd, Apr. 2021. doi: 10.1088/1755-1315/715/1/012050.

[21] M. M. Fares, S. K. Radaydeh, and H. M. AlAmeen, "Green tannins /Avocado oil composites; suncare and skincare materials," Arabian Journal of Chemistry, vol. 16, no. 6, Jun. 2023, doi: 10.1016/j.arabjc.2023.104764.

[22] T. Cortis Maigoda and B. Nisak, "Diabetic Wound Healing and Antimicrobial Activities of Gels Melastoma malabathricum L. and Psidium guajava L. in Sprague Dawley Rats (Penyembuhan Luka Diabetes dan Aktivitas Antimikroba dari Gel Ekstrak Melastoma malabathricum L. dan Psidium guajava L. pada Tikus Sprague Dawley)," Jurnal Ilmu Kefarmasian Indonesia, vol. 21, no. 1, 2023.

https://doi.org/10.31436/iiumecp.v1i1.3013

A REVIEW: ESTABLISHMENT AND APPLICATIONS OF STARCHY CROPS CELL SUSPENSION CULTURES

NUR SYAZWANI NADHIRAH MOHD SOFRI[1], NOOR ILLI MOHAMAD PUAD[1]*, SARINA SULAIMAN[1], YUSILAWATI AHMAD NOR[1], FAZLENA HAMZAH[2]

[1]Bioprocess and Molecular Engineering Research Unit (BPMERU), Department of Chemical Engineering and Sustainability, Kulliyyah of Engineering, International Islamic University Malaysia, Malaysia
[2]Faculty of Chemical Engineering, Universiti Teknologi MARA (UiTM), 40450 Shah Alam, Selangor Darul Ehsan

**Corresponding author: illi@iium.edu.my*

ABSTRACT: Starchy crops are crops that contain starch which is the main source of dietary energy for the world's population. Starchy crops include rice, sweet potato, cassava, soybean, corn, wheat and more. Plant tissue culture offers many advantages including the regeneration of whole plants from plant cells that have been genetically modified, the production of medicinal compounds and a convenient tool for molecular levels studies. The purpose of this paper is to review the latest progress in cell suspension culture for starchy crops. Different types of starchy crops require different parameters for the optimum growth rate which depends on the purpose of establishing them. The main parameters that affect the growth of cell suspension culture are the type of media used and growth conditions such as inoculum size and agitation rate. The procedures for establishing cell suspension culture are generally similar for all types of plants. As of now, reports on cell suspension cultures for starchy crops focus more on the regeneration of plants and the transformation of plant cells for enhancing plant traits. In conclusion, the culture parameters for starchy crop cell suspension growth differed based on its application and purpose.

KEYWORDS: *starchy crops, cell suspension culture, culture parameters*

1. INTRODUCTION

Starch, which is found in starchy plants, provides most of the world's population with dietary energy. Starch is the biggest compound of carbohydrate-rich food and carbohydrate is known as an important food component. Starchy crops include rice, sweet potato, cassava, soybean, corn, wheat and more [1]. Food and industrial economies are mostly based on starch, but due to the rising population and a lack of fertile land, the food situation in the majority of tropical developing nations is deteriorating faster [2]. This resulted in high demand for starch in the food, medicinal, and industrial sectors.

Alternatively, biotechnological studies have been carried out to understand the fundamental processes in starchy plants such as in vitro experimental studies by using callus and cell suspension culture [3]. Plant cell cultures offer a promising option that is less

https://doi.org/10.31436/iiumecp.v1i1.3013

expensive, more scalable, needs less infrastructure investment upfront, permits post-translational modification, and is stable in storage [2]. It also can regenerate complete plants from plant cells that have undergone genetic modification, manufacture medicinal compounds, and be an effective tool for molecular-level study.

Cell suspension cultures (CSC) are helpful experimental methods in the study of plant sub-proteome composition, including both intracellular and extracellular sub-proteomes, as well as differential gene expression in response to both biotic and abiotic stress factors [3]. CSC is defined as a multiplication or division of single cells or cell aggregates when the liquid medium is agitated. This CSC starts from the subculture of friable callus. A successful callus formation will be used to generate the CSC by adding the callus into the liquid medium. It is required to optimize the growth, maintenance and production of liquid media to produce a higher number of natural products [4]. Optimized conditions of culture medium environment can give the integrity and stability of the specific production of natural products. This review aims to evaluate the most recent developments related to the cell suspension cultures of starchy crops.

2. APPLICATIONS OF STARCHY CROPS

Starchy crops have many applications in food, industrial and pharmaceutical productions [5]. Table 1 shows the applications of starch from different starchy crops.

Table 1: Applications of starch in various industries

Starchy crops	Applications	References
Rice starch	Orodispersible (ODF) film former	[6]
Cassava starch	• Thickening agent • Textiles • Paper • Sweeteners	[7]
Purple sweet potato	• Food like noodles, breads, jams • Cosmetics like lipstick, rouge and shampoo • Pharmaceutical–coloured tablets	[8]
Sorghum	• Beverages like grain tea • Snacks like cookies • Animal feed	[9]

3. ESTABLISHMENT OF CELL SUSPENSION CULTURE

Growth of cells in starchy crop suspension cultures required different parameters according to their variation and purpose of establishment. A successful CSC depends on the optimization of growth media and growth conditions. The most common parameters that affect the growth of CSC are the type of media used and growth conditions such as inoculum size and agitation rate. Table 2 summarizes the establishment of CSC from different starchy crops such as rice (Oryza sativa L.), sweet potato and sorghum. Different starchy crops have different requirements of growth conditions and carbon sources, PGRs, inoculum size and agitation rate are significant parameters in the growth of CSC.

Carbon source is important for the in vitro cultures to provide energy and control the osmotic potential of the medium [13]. Sucrose and glucose are normally used for the CSC [13]. Fructose may be used but it can result in a slower growth of cells. This is due to the nature of plants that commonly absorb glucose faster including hydrolysis of sucrose

https://doi.org/10.31436/iiumecp.v1i1.3013

compared to fructose [13]. Generally, the optimal concentration of sucrose for the growth of callus or cell suspension culture is between 20 – 40 g/L as shown in Table 2. However, for morphogenesis and plantlet development, this optimal concentration may not be suitable [14]. This is due to a large number of interaction elements in plants like mechanical stimuli, biochemical signalling or genetic prerequisites. Thus, experiments based on a statistical approach are recommended to study the optimal type and concentration of carbon sources [13]. As stated in Table 2, the most frequently supplied carbon source is sucrose with a concentration of 30 g/L.

Table 2: Establishment of cell suspension culture from different starchy crops

Starchy crops	Applications of CSC	Type of medium	Carbon source	PGRs	Inoculum size	Agitation rate	Reference
Oryza sativa L.	Genetic engineering	N6 medium	30 g/L sucrose	• 2.0 mg/L 2,4-D • 0.02 mg/L Kinetin	10%	100 rpm, dark, 28 °C	[2]
Oryza sativa L.	Genetic engineering	N6 medium	30 g/L sucrose	• 2.0 mg/L 2,4-D • 0.02 mg/L Kinetin	10%	100 rpm, dark, 28 °C	[10]
Sweet potato (*Ipomoea batatas L.*)	Molecular biology	MS medium	20 g/L sucrose	• 0.5 mg/L 2,4-D • 0.3 mg/L Kinetin	50%	120 rpm, dark, 25 °C	[11]
Sorghum bicolor L.	*In vitro* plant regeneration	MSMO	30 g/L sucrose	• 3 mg/L 2,4-D • 2.5 mg/L NAA	40%	130 rpm, orbital shaker, dark, 27 °C	[3]
Oryza sativa L.	Molecular biology	MS medium	60 g/L sucrose	• 60 mM 2,4-D • 2.5 mM 2-(N-morpholino) ethanesulfonic acid (MES).	50%	100 rpm, dark, 23 °C	[12]

PGRs are usually needed in the growth or production media since they affect the management of vegetative and reproduction growth of plants [13] [15]. Concentrations of PGRs during cell division, expansion, and differentiation have an impact on how quickly and fully plants grow and develop. The end products can also be affected by the presence of PGRs, the development stage of the target cells or tissues, the concentration of other PGRs, the target plant's health, nutrition, and water status, as well as the physical environment. The most used PGRs for the growth and development of plants are auxin and cytokinin. The auxin is used for the stimulation of root formation while cytokinin is used to stimulate the shoot formation [15]. The PGRs can either be used separately or combined for the cell's growth. Examples of auxins are indole-3-acetic acid (IAA, a natural auxin) and the synthetic auxins, 1-naphthaleneacetic acid (NAA) and 2,4-dichlorophenoxyacetic acid (2,4-D) while cytokinins are kinetin, zeatin and benzylaminopurine. The concentration range can be between $10 - 7$ and $10 - 5$ M [5]. From Table 2, 2,4-D is the most used for different types of starchy crops and their applications in combination with another PGR.

This is due to the important roles of 2,4-D in stimulating the cell dedifferentiation process, organogenesis, and callus culture maintenance [16].

For any plant species, the initial inoculum density is crucial for generating a cell suspension culture. This is due to interactions that take place both between individual cells and the culture media, which have an impact on the cultures' biological environment [13]. To maintain active cell development after subculture, the inoculum density must stay above the minimal cell density. It is a fact that cell growth does not take place when the minimum cell density is reached or when there is a growth lag phase. The minimal cell density can be influenced by the cell line, components of the culture medium, and cell growth rate, whereas the optimal inoculum density depends on the species. Generally, a high cell density is created by a large inoculum size to establish the growing cell suspension culture. However, a low inoculum density also can initiate cell suspension culture when a conditioned medium is used. A conditioned medium is a medium that contains the cells' secreted components that are required for another set of cells [17]. The inoculum size of cells can be either 0.1 g (low) or 2.0 g (high) per 33–50 mL of medium [13]. Table 2 shows the difference in inoculum size which was between 10 – 50 %. The difference in the inoculum size may be due to the number of cells needed to be subcultured into a new media [18]. A suitable size of inoculum can prevent a "staling" that affects the growth of cells and increases nutrient depletion in media. Thus, the minimum inoculum size needed for the cell suspension culture are depending on the species and its culturing conditions.

The final parameter is agitation speed which functions to increase the multiplication rate of cell growth by increasing the gaseous exchange. This agitation is used to supply oxygen for the proliferation of cells as well as promote homogeneity in terms of nutrient supply and cell biomass due to cell dispersion [13]. High shaker speeds may be detrimental to the viability of plant cells because they may be susceptible to shear [15]. The size of cell aggregates produced as well as the amount of oxygen supplied can be affected by the agitation frequency. The most optimal shaker speed used for tissues in suspension culture is around 30 – 150 rpm while for CSC, the optimal agitation speed required is around 90 – 125 rpm [13]. From Table 2, the most used agitation speed is 100 rpm under room temperature with different purposes of study. This can be due to the physical characteristics of the studied cells like the size, thick cellulose–based cell wall or the presence of a large vacuole leading to the hydrodynamic stress on the cells caused by the agitation of cells [19].

4. CONCLUSION

In conclusion, culture parameters play an important role in starchy crops' cell suspension culture based on their application and purpose. Different plants require different establishment cell suspension culture protocols that help in the growth of cells and achieving the objectives of establishment. Understanding the culture parameter's role can help in generating an optimized condition for initiation of cell suspension culture.

ACKNOWLEDGEMENT

We would like to acknowledge the Ministry of Higher Education Malaysia for funding this project under the Fundamental Research Grant Scheme (FRGS/1/2021/STG01/UIAM/02/2).

REFERENCES

[1] Lal, M. K., Singh, B., Sharma, S., Singh, M. P., & Kumar, A. (2021). Glycemic index of starchy crops and factors affecting its digestibility: A review. Trends in Food Science and Technology, 111(March), 741–755. https://doi.org/10.1016/j.tifs.2021.02.067

[2] Islam, M. R., Kim, N. S., Jung, J. W., Kim, H. B., Han, S. C., & Yang, M. S. (2018). Spontaneous pepsin C-catalyzed activation of human pepsinogen C in transgenic rice cell suspension culture: Production and characterization of human pepsin C. Enzyme and Microbial Technology, 108(May 2017), 66–73. https://doi.org/10.1016/j.enzmictec.2017.09.006

[3] Ramulifho, E., Goche, T., Van As, J., Tsilo, T. J., Chivasa, S., & Ngara, R. (2019). Establishment and Characterization of Callus and Cell Suspension Cultures of Selected Sorghum bicolor (L.) Moench Varieties: A resource for gene discovery in plant stress biology. Agronomy, 9(5). https://doi.org/10.3390/agronomy9050218

[4] Marisol Ochoa-Villarreal, Howat, S., Hong, S. M., Jang, M. O., Jin, Y. W., Lee, E. K., & Loake, G. J. (2016). Plant cell culture strategies for the production of natural products. BMB Reports, 49(3), 149–158. https://doi.org/10.5483/BMBRep.2016.49.3.264

[5] Ivanova, N., Gugleva, V., Dobreva, M., Pehlivanov, I., Stefanov, S., & Andonova, V. (2016). We are IntechOpen , the world ' s leading publisher of Open Access books Built by scientists , for scientists TOP 1 %. Intech, i(tourism), 13.

[6] Limpongsa, E., & Jaipakdee, N. (2020). Physical modification of Thai rice starch and its application as an orodispersible film former. Carbohydrate Polymers, 239(March), 116206. https://doi.org/10.1016/j.carbpol.2020.116206

[7] Tan, S. L. (2015). Cassava – Silently, The Tuber Fills. UTAR Agriculture Science Journal, 1(2), 12–24.

[8] Li, A., Xiao, R., He, S., An, X., He, Y., Wang, B., Shi, X., & He, I. (2019). Molecules-24-03816.

[9] Xiong, Y., Zhang, P., Warner, R. D., & Fang, Z. (2019). Sorghum Grain: From Genotype, Nutrition, and Phenolic Profile to Its Health Benefits and Food Applications. Comprehensive Reviews in Food Science and Food Safety, 18(6), 2025–2046. https://doi.org/10.1111/1541-4337.12506

[10] Van Giap, D., Jung, J. W., & Kim, N. S. (2019). Production of functional recombinant cyclic citrullinated peptide monoclonal antibody in transgenic rice cell suspension culture. Transgenic Research, 28(2), 177–188. https://doi.org/10.1007/s11248-019-00113-w

[11] Volk, G. M., & Caspersen, A. M. (2017). Cryoprotectants and components induce plasmolytic responses in sweet potato (Ipomoea batatas (L.) Lam.) suspension cells. In Vitro Cellular and Developmental Biology - Plant, 53(4), 363–371. https://doi.org/10.1007/s11627-017-9834-5

[12] Liu, D., Ford, K. L., Roessner, U., Natera, S., Cassin, A. M., Patterson, J. H., & Bacic, A. (2013). Rice suspension cultured cells are evaluated as a model system to study salt responsive networks in plants using a combined proteomic and metabolomic profiling approach. Proteomics, 13(12–13), 2046–2062. https://doi.org/10.1002/pmic.201200425

[13] Kong, E. Y. Y., Biddle, J., Foale, M., & Adkins, S. W. (2020). Cell suspension culture: A potential in vitro culture method for clonal propagation of coconut plantlets via somatic embryogenesis. Industrial Crops and Products, 147(October 2019), 112125. https://doi.org/10.1016/j.indcrop.2020.112125

[14] Marconi, M., & Wabnik, K. (2021). Shaping the Organ: A Biologist Guide to Quantitative Models of Plant Morphogenesis. Frontiers in Plant Science, 12(1). https://doi.org/10.3389/fpls.2021.746183

[15] Mustafa, N. R., De Winter, W., Van Iren, F., & Verpoorte, R. (2011). Initiation, growth and cryopreservation of plant cell suspension cultures. Nature Protocols, 6(6), 715–742. https://doi.org/10.1038/nprot.2010.144

[16] Nasution, N. H., & Nasution, I. W. (2019). The Effect of Plant Growth Regulators on Callus Induction of Mangosteen (Garcinia mangostana L.). IOP Conference Series: Earth and Environmental Science, 305(1). https://doi.org/10.1088/1755-1315/305/1/012049

[17] Systems, C. guidance. (2020). Conditioning cell culture media. https://www.cellgs.com/blog/conditioning-cell-culture-media.html

[18] Martínez, M. E., Jorquera, L., Poirrier, P., Díaz, K., & Chamy, R. (2023). Effect of Inoculum Size and Age, and Sucrose Concentration on Cell Growth to Promote Metabolite Production in Cultured Taraxacum officinale (Weber) Cells. Plants, 12(5). https://doi.org/10.3390/plants12051116

[19] Singh, M., & Chaturvedi, R. (2012). Evaluation of nutrient uptake and physical parameters on cell biomass growth and production of spilanthol in suspension cultures of Spilanthes acmella Murr. Bioprocess and Biosystems Engineering, 35(6), 943–951. https://doi.org/10.1007/s00449-012-0679-3

https://doi.org/10.31436/iiumecp.v1i1.3010

CO_2 SOLUBILIZATION IN ALKALINE SOLVENTS

SOUMAYAT ALI IBRAHIM MZE[1], AZLIN SUHAIDA AZMI[1*], NOOR ILLI MOHAMAD PUAD[1], FARAH AHMAD[1], FIRDAUS ABD WAHAB[1], SYARIFAH NOR FAIZAH SY ABD RAHMAN[2]

[1]Department of Chemical Engineering and Sustainability, Kulliyyah of Engineering,International Islamic University. Malaysia, Jalan Gombak, 53100 Kuala Lumpur, Malaysia.
[2]Petronas Research Sdn. Bhd. Lot 3288 & 3299, off Jalan Ayar Itam, Kawasan Institusi Bangi, 43000 Kajang, Selangor Darul Ehsan, Malaysia.

**Corresponding author: azlinsu76@iium.edu.my*

ABSTRACT: CO_2 removal by chemical reaction of sodium carbonate (Na_2CO_3), and aqueous ammonia (NH_3) shows promising absorption quality for CO_2 removal and sequestration. Nevertheless, the solubility of CO_2 by those alkaline solutions has been reported to be highly dependent on the temperature and the pH drop. This study focuses on screening the different solvents used for maximum CO_2 solubility using pure CO_2 based on 2 sets of experiments: First identifying the optimum temperature for distilled water which is considered as control under 3 different temperatures (20, 30 and 40°C). The Second was to identify the maximum CO_2 capture from the solvents under two factors: the type of solvent used (Na_2CO_3, NH_3), and their concentration (1-5%). The solubility behaviours of the CO_2 in the solvents will be analysed according to pH change, CO_2 capture rate, and CO_2 capture efficiency using the water displacement method. The experimental results show that the control condition provided higher solubility than the proposed solvents; the CO_2 removal using water value at 99.49% at 30°C while at the same condition, the highest removal efficiency for Na_2CO_3 value at a concentration of 3% 99.12% and NH_3 at a concentration of 5%, 98.54% respectively.

KEYWORDS: *carbon dioxide (CO_2) capture, sodium carbonate, aqueous ammonia*

1. INTRODUCTION

Reducing the emission of greenhouse gases, particularly carbon dioxide (CO_2), is crucial in addressing global warming and achieving carbon neutrality by 2050[1]. Much research has been performed on CO_2 capture from various industrial gas streams in order to reduce the contribution of CO_2 to global warming. Among those methods, chemical absorption through amine reaction has proven to be the most employed method nowadays. Nonetheless, the chemical absorption process based on amines such as monoethanolamine (MEA) is still too expensive to apply for large CO_2 sources like power plants [2,3]. The amine process is commonly associated with drawbacks such as absorbent degradation due to acidic compounds and oxygen in the gas stream, high energy usage, and equipment corrosion[1]. Alternatively, an alkaline solution such as aqueous ammonia (NH_3) and sodium carbonate (Na_2CO_3) seems to provide good CO_2 removal efficiency and less toxicity[1–3]. Recent research has proven that the aqueous NH_3 and Na_2CO_3 have a larger capacity of CO_2 compared to the amine solution, low regeneration energy required, low material cost, and potential ability to capture acidic gases in flue gas[1–3].

https://doi.org/10.31436/iiumecp.v1i1.3010

Yeh and Bai[4]'s experiments using ammonia and MEA to capture CO_2 in a bubble reactor proved that NH_3 is a superior absorbent to MEA in removing CO_2 from flue gas systems. With a CO_2 removal efficiency of up to 99% under optimal conditions and an absorption capacity of over 1.0 kg CO_2 kg NH_3, NH_3 outperformed MEA, which had a maximum CO_2 removal efficiency of 94% and an absorption capacity of 0.4 kg CO_2 kg. These findings indicate that NH_3 is more efficient option for CO_2 capture in industrial settings[1,5,6]. Similar results were obtained with Na_2CO_3. Barzagli et al.[3] studied the removal efficiency of CO_2 by Na_2CO_3 at different concentrations (5.43% to 13.81%), and it was found that 8.12% could provide a CO_2 removal of 80%. Additionally, due to their low toxicity, and capability to react at moderate conditions, both solvents can be used to turn CO_2 into chemicals with an economic value and a commercial scale utilization such as calcium carbonate, and ammonium carbonate as sources for fertilisers[7,8]. It is also allowed to be coupled with biological absorption to provide sustainable CO_2 fixation and valorisation of biomass[7,9].

In view of all those advantages this paper studied the removal of CO_2 by aqueous ammonia and Na_2CO_3 solutions were carried out in a laboratory-scale reactor by comparing them to the CO_2 absorption profile of water (control solution). The effects of several operating parameters such as absorbent temperature, and absorbent concentration, on the CO_2 removal efficiency were studied as it seems that the solubility of CO_2 by those alkaline solutions has been reported to be highly dependent on the temperature and the pH drop.

2. MATERIALS AND METHODS

2.1. Materials

The chemical reagents used in this project are ammonia solution (25%) A.R from R&M chemicals and sodium carbonate anhydrous (Na_2CO_3) from HmBG chemicals. The compressed gas was measured using the GM CO2 flow meter Regulator.

2.2. CO_2 capture experimental set-up.

An airlift photobioreactor with a 2L working volume was used as the absorption reactor of this project. All inlets of the bioreactor were covered except for the gas inlet and vented gas outlet. To adjust the reaction temperatures, a circulating water bath was connected to the jacketed reactor. Both solvents, aqueous NH_3 and Na_2CO_3, were introduced to the reactor at three different concentrations (1%, 3%, and 5%). CO_2 gas was injected at a flow rate of 1ml/min from the pure CO_2 cylinder for 2 min at room temperature and pressure.

A simple water displacement method was used to measure the vented CO_2 from the process as illustrated in Figure 1. The method consists of measuring the displacement of water inside an inverted graduated measuring cylinder inside a water bath every 30 seconds in order to identify the flow rate of the outlet gas.

2.2. Experimental design

The study consisted of two sets of experiments. The first set consisted of determining the optimum temperature for CO_2 dissolution in distilled water (control solution) based on 3 different temperatures (20°C-40°C) using pure CO_2 at a flow rate of 1 Lpm. The second set was based on two factors which are the solvent used (Na_2CO_3 and NH_3) and the concentration of the solution (1%-5%) at the optimum temperature found previously. Table 1 presents the design summary of the experiments. The effect of those variables was tested through the records of the change in pH, and CO_2 removal efficiency.

https://doi.org/10.31436/iiumecp.v1i1.3010

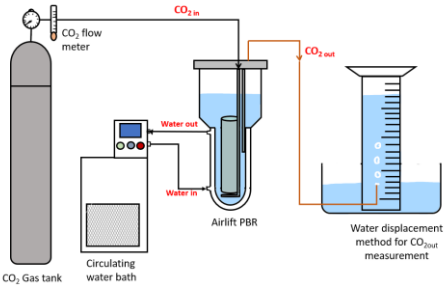

Fig. 1. Experimental set up of the experiment

The pH, which is considered an indication of the dissolution of CO_2 gas, was measured at the beginning and end of the experiment, after 60 min of run. The percentage of absorption was calculated according to the capture efficiency, as it varies with temperature, solvent concentration and reaction time, by the relation indicated in Equation 1.

$$\eta = \frac{V_{in} - V_{out}}{V_{in}} \times 100 \quad (1)$$

Where η is the dissolution efficiency V_{in} is the inlet gas flow rate (1 Lpm), and V_{out} is the outlet gas flow rate.V_{in} which was obtained from the standard curve of the water displacement method.

Table 1. The design of the experiments

No	Fixed variables	Manupilated variables	Responses
1	Solvent: Water Flow rate: 1L/min or 16.67mL/s Duration of CO_2 supply: 2min Duration of the experiment: 60 min	Temperature: 20, 30 and 40 °C	pH change CO2 out (mL/s) Solubility efficiency (%)
2	Solvent: Sodium carbonate (Na_2CO_3) Temperature: 30°C Flow rate: 1L/min or 16.67mL/s Duration of CO_2 supply: 2min Duration of the experiment: 60 min	Solvents concentrations: 1%, 3% and 5%	pH change CO2 out (mL/s) Solubility efficiency (%)
3	Solvent: aqueous ammonia (NH_3) Temperature: 30 °C Flow rate: 1L/min or 16.67mL/s Duration of CO_2 supply: 2min Duration of the experiment: 60 min	Solvents concentrations: 1%, 3% and 5%	pH change CO2 out (mL/s) Solubility efficiency (%)

3. RESULTS AND DISCUSSION

3.1. Effect of temperature on the CO_2 dissolution by water

Table 2 shows the CO_2 dissolution efficiency profile of water under different temperatures (20°C,30°C,40 °C) of the experiment. The temperature of the solution affects the reaction rate of CO_2 and water ultimately reducing the removal efficiency of CO_2 in water at 30°C provided higher removal efficiency with 99.49 % compared to 20°C and 40°C with 90.22% and 97.98 % respectively. These findings opposed the results obtained previously as they concluded that higher temperatures decrease the reaction of CO_2 [8,10,11]. Research conducted by Duan and Sun[10] shows that as temperature increases from 0°C to 90°C, the solubility of CO_2 in water decreases from 0.0693 mol/kg to 0.036 mol/kg. Wolfbeis[11] conducted a separate study using pure CO_2 and found that at temperatures ranging from 5°C to 35°C, the solubility decreased from 2982 to 1173 ppm. While our findings differ from other studies, it is important to note

https://doi.org/10.31436/iiumecp.v1i1.3010

that CO_2 solubility can increase under high pressure and with increasing temperature. Additional research by Erfan Muhammadian et al, [12] indicates that at higher pressures (1-400 atm), CO_2 solubility increases with temperature (0-2.25 mol/kg). Nevertheless, all research shows a very low solubility of CO_2 in water, (CO_2< 30%), opposing the results obtained in this research. This could be due to the use of the water displacement method to measure the CO_2 leaving the system. The water used for the water displacement method was from regular tap water which pH was towards alkaline value[13]. Thus, when passing through the measuring cylinder, more CO_2 was absorbed leading to the low volume of CO_2 gas released in the measuring cylinder.

Related to the pH change in the system, it showed that all solutions turned to acidic validating the CO_2 capture data obtained. Water becomes acidic since a part of the water will react to become carbonic acid (H_2CO_3). Its hydrogen ions make the water acidic. Equation (2) presents the reaction taking place between water and CO_2 [14].

$$CO_2(g) + H_2O(l) \leftrightarrow H_2CO_3(aq) \quad (2)$$

The difference observed between the trend of the pH value and CO_2 capture is due to in the initial pH of the water in the experiment. Indeed, all solutions have different initial pH values. When the initial pH of water is higher, the CO_2 solubility is more favourable due to the forward reaction (2) is faster. However, after reaching equilibrium, the reverse equation will take place, and more CO_2 will be released instead of absorbed. Thus, by having a high initial pH (pH>7,8), CO_2 was easily absorbed and reached equilibrium faster. It became highly acidic and started releasing CO_2 which in turn increase the pH of the solution. Nonetheless, because of the highest removal efficiency at 30°C temperature, the comparison of the aqueous NH_3 and Na_2CO_2 was performed at 30°C.

Table 2. Comparison of the CO_2 capture efficiency based on the temperature in water.

Temperature (°C)	pH initial	pH final	pH change	CO_2 in (mL/s)	CO_2 out (mL/s)	Dissolve CO_2 (mL/s)	Efficiency (%)
20	7.82	5.78	2.04	16.67	1.63	15.04	90.22
30	7.23	5	2.23	16.67	0.0845	16.58	99.49
40	7.84	4.62	3.22	16.67	0.3357	16.33	97.98

3.2. Effect of the concentration of the solvent on the CO_2 dissolution by Na_2CO_3 and NH_3

The influence of the concentration of the absorbent solution on the removal efficiency of CO_2 was investigated. Figure 2 and Table 3 show that Na_2CO_3 has the highest CO_2 capture at a concentration of 3% (99.12% capture efficiency) followed by aqueous ammonia at 5% (98.54% efficiency). The ammonia results followed the results obtained by other studies since its removal profile increases as the concentration increases[1,4–6]. Nonetheless, Table 3 clearly indicates that both solvents have a lower CO_2 capture rate than water (99.49%). However, this directly contradicts previous research. Barzagli et al[3] studied the effect of concentration of the solvent (5.43 wt%-13.81 wt%) on the CO_2 capture by Na_2CO_3. It was found that with 15% CO_2, the higher the sodium carbonate concentration, the higher the CO_2 capture (with a capture rate > 80%), however, to reduce the excess use of solvent 8.12 wt% of Na_2CO_3 was considered as the optimum concentration. Similar results were observed with CO_2 dissolution by aqueous ammonia (5% to 15%) at room temperature. Liu et al,[14] reported that the higher the ammonia concentration, the higher the CO_2 capture (with a capture rate > 90%)., However, to avoid

https://doi.org/10.31436/iiumecp.v1i1.3010

volatilization of the ammonia, a concentration below 10% should be able to achieve similar results. It is possible that the variance observed in our results could be attributed to the analytical approach chosen for scrutinizing the CO_2 emitted from the system. The experiment employed a displacement method that did not differentiate between the various gases collected, which may have impacted the obtained measurement. Additionally, the water used for the displacement method was ordinary tap water that was not degassed and potentially contained unidentified gases, resulting in an overestimation of the gas emitted from the system. Besides that, the temperature was monitored from the circulating water instead of the direct measurement of the temperature of the solution. However, Barzagli [3] reported that the reaction between CO_2 and aqueous NH_3 and Na_2CO_3 is exothermic. This could have resulted in the release of NH_3 gases if the temperature increased above 35°C leading to an increase in the volume of gas vented to the measuring cylinder for the 3% NH_3.

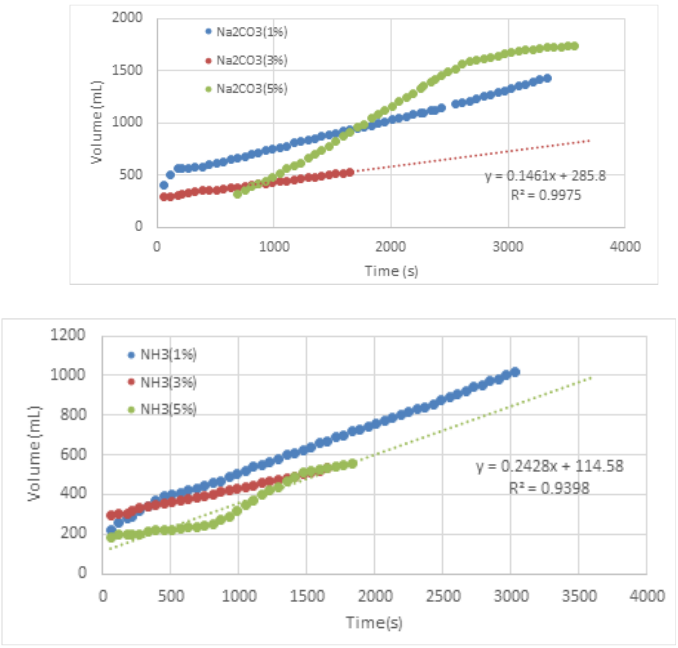

Fig. 2. Release CO_2 based on Na_2CO_3 and NH_3 concentration.

Table 3. Comparison of the CO_2 capture efficiency based on the solvents used.

Experimental condition	pH initial	pH final	pH change	CO_2 in (mL/s)	CO_2 out (mL/s)	Efficiency (%)
water (30°C)	7.23	5	2.23	16.67	0.08	99.49
Na_2CO_3 (1%)	10.3	9.28	1.02	16.67	0.28	98.32
Na_2CO_3 (3%)	10.21	9.73	0.48	16.67	0.15	99.12
Na_2CO_3 (5%)	10.19	9.81	0.38	16.67	0.49	97.07
NH_3(1%)	10.93	9.24	1.69	16.67	0.25	98.49
NH_3(3%)	11.28	10	1.28	16.67	0.54	96.75
NH_3(5%)	11.44	9.68	1.76	16.67	0.24	98.54

https://doi.org/10.31436/iiumecp.v1i1.3010

4. CONCLUSION

The results of the experiment at current setup and condition revealed that a temperature of 30°C and distilled water to be the best conditions for CO_2 dissolution. Distilled water provided higher CO_2 dissolution than chemical absorption by alkaline solvent, with almost 99.94% of CO_2 being removed. For the alkaline solvent, Na_2CO_3 had the highest CO_2 capture at a concentration of 3%, amounting to 99.12% removal efficiency, followed by aqueous ammonia at concentration of 5%, with 98.54% removal efficiency. These findings do not align with previous research in this field, which could be due to differences in CO_2 gas outlet measurement. Further research is necessary to provide conclusive reasons for the high CO_2 dissolution in water when using pure CO_2 gas. To enhance the study of CO_2 capture, it is highly recommended to select a fast and effective CO_2 capture analysis that specifically targets CO_2 gases.

ACKNOWLEDGEMENT

The authors thank Petronas Research Sdn.Bhd. (PRSB) for its financial support through SPP22-122-0122.

REFERENCES

[1] Hamouda A S, Eldien M S and Abadir M F. (2020) Carbon dioxide capture by ammonium hydroxide solution and its possible application in cement industry. Ain Shams Engineering Journal. 11 1061–7

[2] Liu J, Wang S, Zhao B, Tong H and Chen C. (2009) Absorption of carbon dioxide in aqueous ammonia Energy Procedia 1 933–40

[3] Barzagli F, Giorgi C, Mani F and Peruzzini M. (2017) CO2 capture by aqueous Na2CO3 integrated with high-quality CaCO3 formation and pure CO2 release at room conditions Journal of CO2 Utilization 22 346–54

[4] Yeh A C and Bai H. (1999) Comparison of ammonia and monoethanolamine solvents to reduce CO greenhouse gas emissions 2 Sci Total Environ 228 121133

[5] Liu J, Wang S, Zhao B, Tong H and Chen C. (2009) Absorption of carbon dioxide in aqueous ammonia Energy Procedia 1 933–40

[6] Yeh J T, Resnik K P, Rygle K and Pennline H W. (2005) Semi-batch absorption and regeneration studies for CO2 capture by aqueous ammonia Fuel Processing Technology 86 1533–46

[7] Dubey A and Arora A. (2022) Advancements in carbon capture technologies: A review J Clean Prod 373 133932

[8] Asif M, Suleman M, Haq I and Jamal S A. (2018) Post-combustion CO2 capture with chemical absorption and hybrid system: current status and challenges Greenhouse Gases: Science and Technology 8 998–1031

[9] Sharma A K, Sahoo P K, Singhal S and Patel A. (2016) Impact of various media and organic carbon sources on biofuel production potential from Chlorella spp. 3 Biotech 6

[10] Duan K and Sun R. (2003) An improved model calculating Co2 solubility in pure water and aqueous NaCL solutions from 273 to 533K and from 0 to 2000bar. Chem Geol 193 257–71

[11] Wolfbeis O S, Kovács B, Goswami K and Klainer S M. (1998) Fiber-Optic Fluorescence Carbon Dioxide Sensor for Environmental Monitoring. Mikrochim Acta 129 181–8

https://doi.org/10.31436/iiumecp.v1i1.3010

[12] Mohammadian E, Hadavimoghaddam F, Kheirollahi M, Jafari M, Chenlu X and Liu B. (2023) Probing Solubility and pH of CO2 in aqueous solutions: Implications for CO2 injection into oceans. Journal of CO2 Utilization 71 102463

[13] Chapoy A, Burgass R, Terrigeol A and Coquelet C. (2016) Water Content of CO 2 -rich Mixtures: Measurements and Modeling using the Cubic-Plus-Association Equation of State. Journal of Natural Gas Engineering 1 85–97

[14] Liu J, Wang S, Zhao B, Tong H and Chen C. (2009) Absorption of carbon dioxide in aqueous ammonia. Energy Procedia 1 933–40

https://doi.org/10.31436/iiumecp.v1i1.3019

THE IMPACTS OF COVID-19 ON MUNICIPAL AND CLINICAL SOLID WASTE GENERATION IN SELANGOR THROUGHOUT 2019-2021

NURUL IMAN MOHD DAUD[1], HUSNA AHMAD TAJUDDIN[1*], MUHAMMAD SYAHMI AMRA[1], MARIATUL FADZILLAH MANSOR[1], NOOR FAIZUL HADRY NORDIN[2]

[1]Department of Chemical Engineering and Sustainability, Kulliyyah of Engineering, International Islamic University Malaysia (IIUM), Jalan Gombak, 53100 Kuala Lumpur, Malaysia.
[2]International Institute for Halal Research and Training (INHART), International Islamic University Malaysia (IIUM), Jalan Gombak, 53100 Kuala Lumpur, Malaysia.

**Corresponding author: dr_husna@iium.edu.my*

ABSTRACT: Selangor, like many other Malaysian states, experienced various disruptions due to the COVID-19 pandemic. In addition to health and economic challenges, the populous state also faced notable issues regarding waste production. The pandemic has led to a dramatic rise in solid waste generation especially in its two largest sources, municipal solid waste (MSW) and clinical solid waste (CSW). Though, it is unclear which waste source is more affected by the pandemic. In the present study, the trend of solid waste generation in Selangor during the pandemic was investigated. A comparative statistical analysis was also made between the annual generation rates of both MSW and CSW, particularly spanning the period from 2019 to 2021. After collecting relevant numeric data from respective resources, the data is recorded into Microsoft Excel to generate graphs. The analysis uncovered that MSW exhibited an average annual generation rate of 4.52%, whereas CSW demonstrated a higher average generation rate of 33.03%. An upward trend was seen in both MSW and CSW generation in Selangor from 2019 to 2021, with CSW demonstrating a significantly higher generation rate. The increased generation of CSW during the COVID-19 pandemic emphasises the need for adhering to appropriate waste management practices. Failure to do so can result in serious consequences, including environmental harm.

KEYWORDS: *COVID-19, Pandemic, Municipal Solid Waste and Clinical Solid Waste.*

1. INTRODUCTION

The COVID-19 pandemic refers to the global spread of the coronavirus disease [1]. In an effort to end the pandemic, the Malaysian government executed strict measures such as movement control orders (MCOs) and a national recovery plan (NRP) [2]. At this point, Malaysians were forced to adapt their lifestyles to the new normal. Goods were delivered as people remained at homes [3], increasing municipal solid waste (MSW) production. Additionally, medical staff worked extended hours to care for infected patients [4], escalating clinical solid waste (CSW) generation. This spike in Malaysia's waste production is particularly pronounced in Selangor, the most populous state of the country [5].

Solid waste is defined as any discarded solid items from human activities [6]. MSW comprises everyday materials produced by the public [7]; its management is under the control of KDEB Waste Management Sdn. Bhd. (KDEBWM). Conversely, CSW is infectious waste

https://doi.org/10.31436/iiumecp.v1i1.3019

generated by medical centres [8]; its handling is directed by private companies, namely Radicare (M) Sdn. Bhd. and Cenviro Sdn. Bhd., which is monitored by the Department of Environment (DoE). The surge in Selangor's waste production during the COVID-19 pandemic calls for the need of proper waste management practices to avoid threatening issues to the public and the environment.

The COVID-19 widespread has led the country to implement various measures, namely MCO and NRP. These measures resulted in a rise in Selangor's waste generation, specifically MSW and CSW. During the period of the COVID-19 pandemic, MSW management in the state is overseen by KDEBWM. As for CSW management, it is controlled by Radicare (M) Sdn. Bhd. and Cenviro Sdn. Bhd.. However, it remains uncertain which waste source has been more impacted by the pandemic. The aim of this study is to investigate the trends of both MSW and CSW generation in Selangor during the COVID-19 period, from 2019 until 2021. Additionally, it aims to conduct a comparative statistical analysis on their generation rates to identify which waste source is more affected by the COVID-19 pandemic.

2. MATERIALS AND METHODS

In this study, Microsoft Excel is utilised. To construct graphs using this software, five steps are involved: data preparation, data selection, graph insertion, graph subtype choosing and final checking [9].

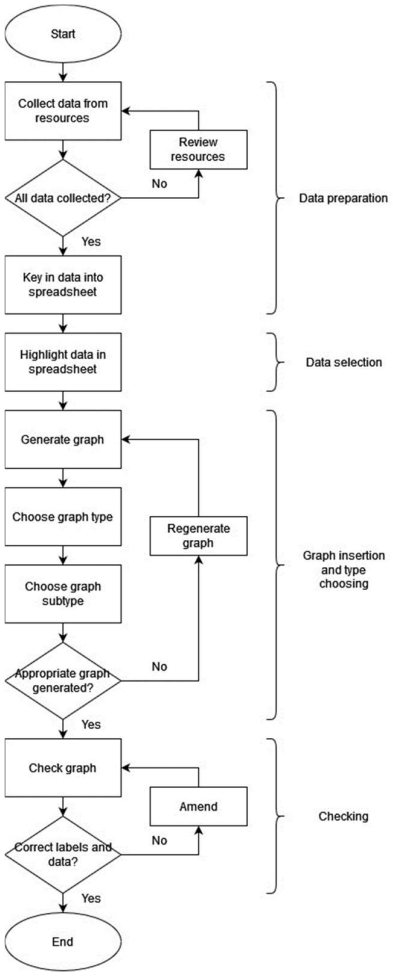

Fig. 1. Steps in generating a graph (Soni, 2022).

https://doi.org/10.31436/iiumecp.v1i1.3019

3. RESULTS AND DISCUSSION

This chapter discusses the study's outcomes. Sections 3.1 and 3.2 investigated the trends in MSW and CSW production in Selangor amid the COVID-19 pandemic. Section 3.3 then highlights which waste source is more notably impacted by the pandemic.

3.1. Municipal Solid Waste (MSW)

This section elaborates on the yearly MSW generation in Selangor, from 2019 to 2021 [10]. In 2019, the production of MSW was relatively low. However, with the onset of the pandemic in 2020, there was a 4.99% increase in the state's MSW production from 2019. This escalation was attributed to the pandemic-related circumstances. The wide use of single-use items in 2020 to curb the spreading of the disease led to an upsurge in waste production. In 2021, a further rise of 4.05% from 2020 was seen. This increase can be attributed to the reopening of businesses and the implementation of delivery services. The disposal of packaging materials, in particular, played a role in contributing to the overall generation of MSW.

3.2. Clinical Solid Waste (CSW)

Section 3.2 examines the annual CSW generation within the state, covering the timeframe from 2019 to 2021 [11]. In the absence of the virus in 2019, there was a comparatively low production of CSW. With the start of the pandemic in 2020, there was a 32% rise in CSW generation from 2019. This increase was driven by the increasing number of patients in healthcare facilities. Consequently, high volumes of COVID-19-related CSW were generated. Transitioning to 2021, a growth of 33.91% from 2020 was observed. This surge can be linked to the introduction of COVID-19 vaccinations, which led to an increase in the use of single-use medical instruments, further heightening the CSW generation.

3.3. Comparison Of Generation Rates

This section compares the generation rates of MSW and CSW of Selangor from 2019 to 2021. To facilitate this comparison, a graph is created to illustrate the rates over the three-year period (Figure 2).

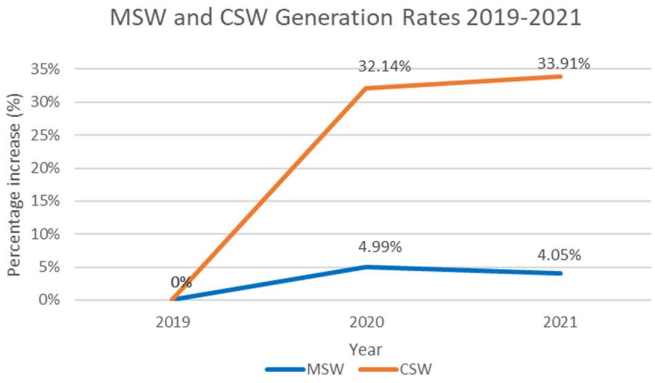

Fig. 2. Comparison of MSW and CSW annual generation rates 2019-2021.

It is evident that the MSW generation rate remained relatively low within the range of 4-5% from 2019 to 2021; its average generation rate is 4.52%. On the other hand, the rate of CSW generation exhibited a sharper incline of 32-34% in the same timeframe; its average generation rate is 33.03%. Comparing the average generation rates, it is evident that CSW exhibits a 28.51% greater variance when compared to MSW. The heightened rate of CSW generation is linked to the exceptional conditions happening during the COVID-19 pandemic. Medical practitioners were disposing of clinical disposables around the clock as they attended

patients. Furthermore, numerous doses and boosters of COVID-19 vaccinations were administered. This constant disposal led to a significant increase in CSW generation, surpassing the growth of MSW.

4. CONCLUSION

From 2019 until 2021, a spike in generation was seen in both MSW and CSW. The average annual growth rate of MSW production is 4.52%, while CSW production is 33.03%. Though production of both waste sources was affected, CSW generation clearly had a more significant impact from the pandemic. This may be attributed to the fact that CSW such as used protective personal equipment (PPE), swab kits and COVID-19 vaccination wastes were only generated during the pandemic crisis, with no production prior to that. This proves that identifying effective CSW management practices is of higher importance. It is recommended that Selangor's CSW management companies take definite measures such as transport route optimisation, employee training and equipment investing. Transport route optimisation will not only reduce time, but it will minimise greenhouse gas emissions as well. Besides, employee training will raise awareness on the impacts of poor waste management, ultimately reducing environmental pollution. Lastly, investing in environmentally friendly equipment will greatly decrease harmful emissions towards the environment during waste disposal processes.

ACKNOWLEDGEMENT

The authors are thankful to the Department of Chemical Engineering and Sustainability at the Kulliyyah of Engineering, International Islamic University Malaysia (IIUM) and the Ministry of Higher Education Malaysia for their assistance. The ministry funded this research through the IIUM-UMP-UiTM Grant Scheme (research grant no.: SRCG20-011-0011).

REFERENCES

[1] World Health Organisation. (2023). Coronavirus Disease (COVID-19). World Health Organisation. https://www.who.int/health-topics/coronavirus#tab=tab_1
[2] Prime Minister's Office of Malaysia. (2021). National Recovery Plan.
[3] Bernama. (2020, March 18). Malaysia's Covid-19 crisis sees 30% jump in delivery orders | Free Malaysia Today (FMT). Free Malaysia Today. https://www.freemalaysiatoday.com/category/leisure/2020/03/18/malaysias-covid-19-crisis-sees-30-jump-in-delivery-orders/
[4] Jarrar, M., Ali, N. B., Shahruddin, R., Al-Mugheed, K., Aldhmadi, B. K., Al-Bsheish, M., Alsyouf, A., Albaker, W., & Alumran, A. (2023). The Impact of the Working Hours Among Malaysian Nurses on Their Ill-Being, Intention to Leave, and the Perceived Quality of Care: A Cross-Sectional Study During the COVID-19 Pandemic. Journal of Multidisciplinary Healthcare, 16, 119–131. https://doi.org/10.2147/JMDH.S394583
[5] Department of Statistics Malaysia. (2022). Current Population Estimates, Malaysia, 2022.
[6] United States Environmental Protection Agency. (2023). Criteria for the Definition of Solid Waste and Solid and Hazardous Waste Exclusions. United States Environmental Protection Agency. https://www.epa.gov/hw/criteria-definition-solid-waste-and-solid-and-hazardous-waste-exclusions
[7] United States Environmental Protection Agency. (2016). Municipal Solid Waste. United States Environmental Protection Agency. https://archive.epa.gov/epawaste/nonhaz/municipal/web/html/
[8] Choi Yi, T., & Muhammad Noor Hazwan, J. (2021). Overview of Clinical Waste Management in Malaysia. In Review Article (Vol. 1, Issue 1).
[9] Soni, P. (2022, April 15). How to Make A Line Graph In Excel With Two Sets Of Data. Career Karma. https://careerkarma.com/blog/how-to-make-a-line-graph-in-excel-with-two-sets-of-data/

https://doi.org/10.31436/iiumecp.v1i1.3019

[10] KDEB Waste Management. (2023, April 5). KDEB Waste Management - Contact. KDEB Waste Management. https://www.kdebwm.com/contact/
[11] Department of Environment. (2022). Department Of Statistics Malaysia 2022 Statistik Alam Sekitar Environment Statistics. www.dosm.gov.my

https://doi.org/10.31436/iiumecp.v1i1.3004

ADVERSE IMPACT ANALYSIS OF BLOCKCHAIN APPLICATION ON SUSTAINABILITY FOR CHEMICAL INDUSTRY

MD RAFIQUL ISLAM

[1]*Department of Mechatronics, International Islamic University Malaysia, Kuala Lumpur, Malaysia*
[2]*Dept. of Information Technology Division, Bengal Commercial Bank Ltd, Dhaka, Bangladesh*

**Corresponding author: engrrafiqul@gmail.com*

ABSTRACT: Due to security, transparency, traceability, and efficiency, blockchain technology has become more popular in the financial, healthcare, education, and industrial sectors as well. However, before the commercial use of this technology for the chemical industry, the adverse impact of the same should be considered carefully. A study of detailed adverse impact analysis of blockchain applications on the sustainability of the chemical industry has been highlighted in this paper. This research complies with accepted publication standards, in particular, the Preferred Reporting Items for Systematic Reviews and Meta-Analyses (PRISMA) recommendations. A variety of primary and supplemental databases are used in our research. Scopus and Science Direct are two well-known databases that we have accessed, along with Emerald Insight, IEE Explore, and Google Scholar as other sources. After comprehensive adverse impact analysis on sustainability from chemical production to blockchain application has been considered such as 1) Environmental: Higher energy use and CO_2 emissions linked to the blockchain, 2) Social: The adoption of blockchain technology that may extend the digital divination in society who have less technological privilege, and 3) Economical: Resource-constrained businesses entities may face difficulties due to the costs of developing and integrating blockchain technology in business. This paper will help the stakeholders in the chemical production business to make wise decisions on the adoption of blockchain applications to maximize the benefits by identifying potential risks, developing mitigation strategies, and ensuring that blockchain applications align with sustainable development goals and practices.

KEYWORDS: *Blockchain, Chemical Industry, Proof-of-Work, sustainability.*

1. INTRODUCTION

The chemical industry, which is a pillar of contemporary civilization, plays a crucial role in supplying the materials and compounds required for a vast array of activities in our everyday lives. Numerous industries have undergone substantial change because of the quick development of technology where blockchain technology has an emerging potential to be used for increasing transparency, and real-time monitoring systems that may ultimately help to produce quality goods in fertilizers, pharmaceuticals, polymers, and numerous industrial chemicals in chemical industries [1]. However, the advantages this business offers frequently come at a price, with unfavorable environmental effects that pose serious problems for sustainability. Innovative technologies have arisen as possible change agents as the world struggles with the urgent need for more ethical and environmentally conscientious behavior.

https://doi.org/10.31436/iiumecp.v1i1.3004

Though there are several benefits of blockchain application, a mentionable number of negative influences on sustainability due to environmental pollution, climate change, ecosystem, CO_2 emission, excessive electricity consumption, etc. cannot be ignored [2, 3]. The main objective of this study is to identify the adverse impacts of blockchain applications on sustainability in the chemical industry. Besides the adverse impact analysis, this paper also maps the relationship between environmental pollution, social, and economic impacts, and Sustainable Development Goals (SDGs) by answering the following research questions and hence presents the research gap analysis.

- RQ1: What are the negative effects of blockchain applications on the chemical industry's sustainability owing to CO_2 emissions?
- RQ2: What connection exists between SDG and the negative effects of blockchain applications in the chemical industry?

1.1 Present Work and Research Gap

In the review article [4], the authors clearly explained the negative impacts of blockchain technology on the environment, society, and economy. They also explained the impact of CO_2 on the environment as well as inequality in social life and they mapped the impacts with SDGs. In the research papers [5], [6], [7], and [8], the authors briefly highlighted the negative impacts on sustainability due to using PoW protocol and excessive use of electricity which generated extensive amounts of CO_2 in the environment. The authors in articles [9], [10], and [11] highlight how the environment can be affected by emitting CO_2 where they mentioned electricity consumption, air pollution, and climate changes. In this paper, the impact of using blockchain applications in chemical industries has been discussed in detail with related properties of environment, social, and economic as well as mapping of these effects with SDGs.

2. METHODOLOGY

The main objective of this study is to find out the adverse ecological effects of blockchain implementations on the chemical industry's sustainability, particularly concerning carbon dioxide (CO2) emissions. Additionally, this research also finds out how the Sustainable Development Goals (SDGs) relate to the negative effects of the chemical industry's implementation of blockchain technology. Systematic studies and literature reviews have been conducted based on the following criteria: 1) Relevant research work and articles related to blockchain applications in the chemical industry, 2) Sustainability and environmental impacts, 3) Related peer-reviewed journals, and 4) The information searched from 2018 to 2023. This systematic literature review was conducted based on the searching data from academic databases which included Scopus journals, Web of Science, newspapers, and online related articles. The peer-reviewed articles published in the journals, conferences, books, or symposiums that have been selected to search the databases. The Search strings such as "blockchain" and ("chemical industry*" or "SDGs*" or "environmental effects*" or "social*" or "economical*") have been used to collect the articles. It also analyzed several factors, including the effects on the environment (air, water, soil, climate, ecosystem), the effects on society (health, inequality, migration trends), and the effects on the economy (healthcare expenses, costs related to climate change, industrial costs).

2.1. Paper Screening Process

The databases were searched for articles with titles that were almost equivalent to this research report. Titles were taken into consideration, and publications that did not match the reviews were discarded. Retrieved papers were discarded if their titles made it very evident

https://doi.org/10.31436/iiumecp.v1i1.3004

that they were not pertinent to this paper. The search protocol produced some papers, some of which were eliminated since they had nothing to do with the use of blockchain in the chemical industry. When a paper's relevance could not be quickly inferred from its title, it was moved on to the following stage for additional screening. Reading the abstracts of the papers that made it past the first step of screening made up the second phase of the screening process. Sometimes it was required to study a paper's opening and conclusion as well to see if it met our exclusion standards.

According to our exclusion criteria, we have to ignore the following: (1) Non-peer-reviewed papers, such as press releases and interviews, (2) Papers without full access, (3) Papers whose primary focus is unrelated to the use of blockchain technology in the chemical industry, (4) Duplicate papers, (5) Non-English papers, and (6) Retracted papers. The systematic literature review as per PRISMA [12] has been used to screen and select the records which is shown in Fig. 1.

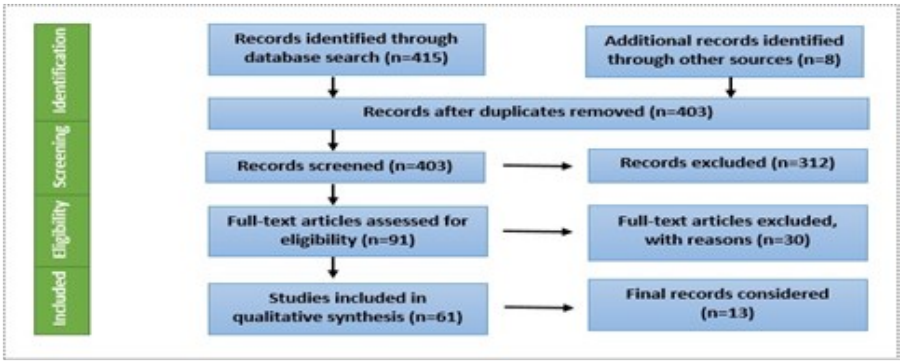

Fig. 1. Process flow diagram of screening and selection records.

3. ADVERSE IMPACT ANALYSIS ON SUSTAINABILITY

The adoption of blockchain applications in the chemical sector has major negative implications on sustainability, in contrast to the positive effects of blockchain technology on the Sustainable Development Goals (SDGs). These consist of areas: 1) Impact on the environment: The use of blockchain networks may result in higher energy use and resultant CO_2 emissions. This increased energy requirement for blockchain operations presents a problem for the environment because it could increase carbon emissions. 2) Social implications: The adoption of blockchain technology may make digital inequality worse. People with restricted access to technology can find it harder to participate in society, which could widen the digital divide. 3) Economic considerations: The expenditures involved with the development and integration of new blockchain technology into operations may provide challenges for companies operating on a limited budget. Smaller companies in the business can be financially burdened even more because of these costs.

3.1 Respone of RQ1 and RQ2

Table 1 provides an adverse impact analysis of the negative effects of blockchain applications on Sustainable Development Goals (SDGs). This research has highlighted the detrimental effects in this table based on the three main goals of the environmental, social, and economic sectors. This comprehensive analysis not only captures pertinent features but also offers mappings to SDG targets. We learn that blockchain applications may have an impact on SDGs spanning several fields, which has broad consequences. SDGs 3 (Good health and well-being), 6 (Clean water and sanitation), 9 (Industry, innovation, and infrastructure), 10 (Reduced inequalities), 11 (Sustainable cities and communities),13 (Climate action), 14 (Life below

https://doi.org/10.31436/iiumecp.v1i1.3004

water), and 15 (Life on land) are at risk from these negative effects. Further investigation reveals that these effects also apply to several specific SDG targets, such as SDGs 3.1(Reduce Maternal Mortality*),* 3.8 (Achieve universal health coverage), 3.9 (Reduce illnesses and deaths from hazardous chemicals and pollution), 6.3 (Improve water quality, wastewater treatment, and safe reuse), 9.1(Develop sustainable, resilient and inclusive infrastructures), 10.2 (promote universal social, economic and political inclusion), 10.4 (Adopt fiscal and social policies that promote quality), 10.7 (Responsible and well-managed migration policies*),* 11.6 (Reduce the environmental impacts of cities), 13.1 (Strengthen resilience and adaptive capacity to climate-related *disasters),* 13.2 (Integrate climate change measures into policy and planning), 14.3 (Reduce ocean acidification), and 15.4 (Ensure conservation of mountain ecosystems) [13].

Table 1: Adverse impact analysis of blockchain applications on SDGs

Impact on		Adverse impact on sustainability	Effect on SDG and its Targets [13]
Environmental Pollution	Air	The planets become worm-like as the amount of CO_2 in the atmosphere rises, changing the temperature and ultimately harming people and other living things.	3 (3.9), 11 (11.6)
	Seawater	The concentration of CO_2 in the atmosphere increases the temperature and acidification of the ocean surface, rising sea levels, and melting glaciers which affect the safety and drinking water, ecosystem system, and aquatic life.	6 (6.3), 14 (14.3).
	Soil	Increasing CO_2 in the air influences to increase in the soil pH level which ultimately influences the rate of weathering and plant nutrients.	3 (3.9)
	Climate change	CO_2 is one of the main concerns of global warming and climate change where it functions as a greenhouse gas by heating the earth and increasing the temperature.	13 (13.1, 13.2)
	Ecosystem	The emission of CO_2 adverse impact on biodiversity and ecosystems. Increasing temperature disrupts and changes the distribution and behavior of species and the ecosystem like in polar regions as well as coral Islands.	15(15.4)
Social	Health	Once CO2 levels are high enough in the atmosphere, it affects temperature rise, which can cause climate change, heat waves, floods, storms, and fatalities.	3 (3.1,3.8, 3.9)
	Inequality	CO_2 emissions are not only affected by the atmosphere, but they also enhance to differentiation of low-income people, indigenous communities, and developing nations. It also leads to an increase in the poverty level and food scarcity in daily social life.	10 (10.2, 10.4)
	Migration tendency	The increase in CO_2 leads the changes in climate, sea levels, natural disasters, and weather which may insist on forced migration from different geographical locations to comparatively better geographical locations, and the overall result may be harmful to society.	10 (10.7)
Economical	Healthcare cost	Climate change may have an impact on diseases like malaria, cancer, dengue fever, and mental illness, among others, due to CO_2 emissions. On the other hand, breathing contaminated air can cause a variety of respiratory and cardiovascular conditions, which can increase the cost of medical care, insurance, and other related expenses.	3 (3.1, 3.8)
	Climate changes cost	Emissions of CO_2 lead to climate change which also exacerbates the extreme weather impacts such as floods, hurricanes, and draughts that may losses extra costs to recovery as well as resiliency costs. The extra budget needs to be allocated for these unseen events.	13 (13.1, 13.2)
	Industry cost	Emissions of CO_2 and climate change may interrupt the chemical industries directly. Due to climate changes, forestry, marine life, tourism, and other sectors. The production, maintenance, and employee health and safety costs will be increased significantly.	9 (9.1)

It depicts the connections between negative effects and several SDGs because of the Proof-of-Work (PoW) blockchain protocol and excessive CO_2 emissions. Blockchain has many benefits for SDGs. It is critical to recognize and solve these unfavorable effects within the chemical business. Understanding and minimizing these negative effects are crucial for ensuring the ethical and long-lasting use of blockchain technology.

4. CONCLUSION

The analysis of the negative effects of blockchain applications on SDGs for the chemical production industry highlights the importance of taking a thorough and cautious approach. While blockchain technology may provide advantages like security and transparency, its implementation must consider the adverse impacts on sustainability such as environmental, social, and economic including their properties with continuous monitoring and adaptation of essential technology for maximizing its benefit.

REFERENCES

[1] Zhou, X. ev Kraft, M., (2022). Blockchain Technology in the Chemical Industry, Annual Review of Chemical and Biomolecular Engineering, Rev. Chem. Biomol. Eng. 13, 347–71.

[2] Sankaran, K. (2019). Carbon Emission and Plastic Pollution: How Circular Economy, Blockchain, and Artificial Intelligence Support Energy Transition? The Articles Content is of the Author's exclusive responsibility, 7, 4, ISSN- 2183-0606.

[3] Jian, T., Song, J., ev Yu, Y., (2022). The influencing factors of carbon trading companies applying blockchain technology: evidence from eight carbon trading pilots in China, Environmental Science and Pollution Research, 29, 28624–28636.

[4] Shanshan, J., Kine, J., Jonas, B., ve Jingyue, L., (2022). A Tertiary Review on Blockchain and Sustainability with Focus on Sustainable, IEEE Access, 10, 11476-115006

[5] Esmaeilian, B., Sarkis, J., Lewis, K., & Behdad, S. (2020). Blockchain for the future of sustainable supply chain management in Industry 4.0. Resources, Conservation and Recycling, 163, 105064.

[6] Thalhammer, F., Schöttle, P., Janetschek, M., ev Ploder, C., (2022). Blockchain Use Cases Against Climate Destruction, Cloud Computing and Data Science, Universal Wiser Publisher, 22-38.

[7] Pan, Y., Zhang, X., Wang, Y., Yan, J., Zhou, S., Li, G., ev Bao, J., (2018). Application of Blockchain in Carbon Trading, Preceding of 10th International Conference on Applied Energy (ICAE2018), 22-25 August 2018, Hong Kong, China, 158 (2019) 4286–4291.

[8] Islam, M. R., Rashid, M. M., Rahman, M. A., Mohamad, H. S. B. Embong, ev Abd. H. B., (2022). International Journal of Advanced Computer Science and Applications, Vol. 13, No. 4.

[9] Qin, M., Su, C., Lobonţ, O., ev Umar, M. (2023). Blockchain: A carbon-neutral facilitator or an environmental destroyer? International Review of Economics & Finance, 86, 604-615.

[10] Erdogan, S., Ahmed, M. Y., ev Sarkodie, S. A., (2021). Analyzing asymmetric effects of cryptocurrency demand on environmental sustainability, Environmental Science and Pollution Research, 29-31723–31733.

[11] Borowski, P. F., (2021). Digitization, Digital Twins, Blockchain, and Industry 4.0 as Elements of Management Process in Enterprises in the Energy Sector, energies, 14, 1885.

[12] Moher, D., Liberati, A., Tetzlaff, J., Altman, DG., (2009). PRISMA Group, Preferred reporting items for systematic reviews and meta-analyses: the PRISMA statement, 151(4), 264-9.

[13] United Nations, Sustainable Development, the 17 goals. Available: https://sdgs.un.org/goals.

https://doi.org/10.31436/iiumecp.v1i1.3012

STRATEGIES FOR IMPROVING PHOTOTHERMAL CONVERSION CAPABILITIES IN HYDROGEL POLYMER MATERIALS FOR SOLAR VAPOR GENERATION

FLORA SERATI [1], SYAZWANI MOHD ZAKI[2*], AHMAD AKID[3]

[1]Department of Electrical and Computer Engineering, Kulliyah of Engineering, International Islamic University Malaysia,PO Box 50728 Kuala Lumpur, Malaysia
[2]Department of Manufacturing and Materials Engineering, Kulliyah of Engineering, International Islamic University Malaysia,PO Box, 50728 Kuala Lumpur, Malaysia

**Corresponding author: syazwani_mohdzaki@iium.edu.my*

ABSTRACT: Solar evaporation is a promising technology that has garnered attention due to the renewable nature of the sun as an energy source, which can facilitate the sustainable advancement of human society. This technology relies on easily obtainable water sources and uncomplicated structures, while also benefiting from significant enhancements in conversion efficiency through the utilization of advanced photothermal materials and effective thermal management techniques. This review provides a brief summary of recent research conducted on hydrogel polymers utilized in solar vapor generation. The primary goal of this review is to explore multiple strategies aimed at optimizing light absorption, hence enhancing the overall efficiency of the design. We present the photothermal management in hydrogel polymer with proper solar absorber selection, tuning the thermal conductivity via porosity of hydrogel and the incorporation of a layered structural design that leads to a greater photothermal conversion efficiency.

KEYWORDS: *Hydrogels, polymer,solar vapor generation*

1. INTRODUCTION

Water is a fundamental component necessary for the sustenance of life and crucial for the existence of all living beings. Water resources are considered valuable assets due to their significance in sustaining various aspects of human life and the environment. Consequently, the practice of water conservation is imperative, given the prevalent occurrence of water crises on a global scale. According to the United Nation Development Programme, a significant proportion of the global population, exceeding 40%, currently experiences the adverse effects of water shortages. This figure is of great concern and is projected to escalate further in tandem with the anticipated rise in temperatures. It is predicted a minimum of 25% of the global population is predicted to encounter recurring water scarcity by the year 2050. The escalation in population pressure, shifting water consumption patterns, and the impact of climate change are expected to heighten the challenge of sustaining appropriate levels of water use.[1] The predominant proportion of water present on the Earth's surface, amounting to more than 96%, is composed of saline water found in the oceans. Freshwater resources, encompassing precipitation and subsequent flow into various hydrological systems, including streams, rivers, lakes, and groundwater, play a vital role in meeting the daily water requirements for human sustenance.[2] Therefore, desalination has become the predominant way to overcome the water crisis, and is the main source of drinkable water. Desalination is a procedure that involves the

https://doi.org/10.31436/iiumecp.v1i1.3012

division of saline water into two distinct components: freshwater, characterized by a reduced concentration of dissolved salts, and brine concentrate, which exhibits a significantly higher concentration of dissolved salts compared to the original feed water.[3] However, the process of water desalination is characterized by high costs, complex technology and a significant demand for energy.[4] Due to this complexity researcher has been came up with a simple preparation, low-cost, non-toxic, and mechanically strong approached which is through the process of desalination by utilizing a three-dimensional network of hydrogel polymer materials. Hydrogel is a three-dimensional cross-linked hydrophilic polymer network, that may expand and deflate reversibly in water and retain huge amounts of liquid. [5] Polymeric networks with strong water absorption and pollutant immobilization capacities are the most promising hydrogels for water purification. Hydrogels polymer possess a remarkable capacity to effectively sequester and retain various pollutants present in water through the process of adsorption. Because of that hydrogel has been studied based on its available functional groups, which expected to remove the contaminant via adsorption for water purification [6] In order to further enhance the efficacy of hydrogel polymer for the purpose of generating clean water, researchers have introduced an innovative and economically viable technology for desalinating seawater. This technology incorporates a solar vapor generation (SVG) system, which combines the utilization of solar energy and water, both of which are abundant resources. SVG can directly transfer heat to facilitate evaporation is an effective method of collecting solar energy and purifying water.[7] The SVG system utilizes hydrogel networks to convert seawater into potable water. The device successfully harnesses solar energy and enhances the efficiency of freshwater conversion and overall device performance. In essence, SVG and hydrogel function similarly to the natural convection of water bodies, such as seas or rivers. Natural convection is a process of heat and mass transport in which a water body absorbs heat from solar radiation. The primary focus of SVG design revolves around two key aspects, namely the system structure and the evaporation surface. The system's architecture relies on the presence of an insulating layer positioned at the bottom of the hydrogel, as well as the photothermal material's capacity to effectively absorb incident light. The evaporation efficiency of the merged SVG with hydrogel polymers ranges from 60 to 94%, which is equivalent to 1-3 kg $m^{-2}\ h^{-1}$ under 1 sun irradiation.[8] As solar radiation is the only source of power for vapour generation, a variety of materials, such as ultra-black absorbers, plasmonic nanoparticles, and thermal-concentrating ceramics, have been employed to improve the conversion efficiency.[9-11] Nonetheless, inefficient utilization of converted heat presents an additional obstacle from these materials such as water heating, parasitic thermal loss, and water evaporation. Also, poor solar absorption and large heat losses due to the placement of the light absorber at the bottom of the water source severely limit the practical application of traditional solar evaporation approaches, which typically deliver a low photothermal conversion efficiency of 30%-45%.[12] Additionally, black inorganic semiconductors like $Cu_7\ S_4$ nanocrystals, TiOx nanoparticles, etc., have been studied as a potential new class of solar-thermal absorbers because of their low cost and low toxicity.[13-14] However, their practicality is limited by the difficulties of producing large-scale samples. Efforts have been made to improve photothermal efficiency by increasing light absorption and minimizing heat loss by combining materials to create a microporous structure with dispersed pores. The recent development of interfacial solar evaporation systems that position the light absorber at the water-air interface has made it possible to heat only the air-liquid interface as opposed to the bulk water, resulting in a significant increase in photothermal efficiency.[15] Typical components of a double-layered interfacial solar evaporation system include a light absorber, substrate, bulk water reservoir, incident light, and condensate. The light absorber absorbs incident light and converts it to heat. In parallel, water is absorbed by the substrate and transported to the evaporative surface via

https://doi.org/10.31436/iiumecp.v1i1.3012

capillary forces and interconnected water pathways. The generated heat raises the water's temperature on the evaporative surface, which powers the continuous evaporation process with an unlimited water supply. Nonetheless, a portion of the generated heat is always lost to the surrounding environment via conduction to bulk water and air, radiation to air, and convection to bulk water, resulting in a less-than-perfect evaporation efficiency. The ratio of the thermal energy contained in the generated vapor to the incoming solar flux can be used to calculate the evaporation efficiency.[16]

$$\eta = \frac{\dot{m}\, h_{LV}}{P_{in}} \qquad (1)$$

where, ṁ is denotes as the mass flux, $h_{LV}$is the total enthalpy of liquid vapor transformation, and P_{in} is the rate of solar energy incident. The marking point as an ideal number to achieve highly efficient SVG is $1 kW m^{-2}$ (typically ~50% to higher than 80%) under 1 sun or even weaker natural daylight.

In this short review, we provide insights to a few strategies for tuning the light absorption in particular emphasis on hydrogel polymer materials with solar absorbers in enhancing the thermal efficiency of SVG design for high water transport.

2. MECHANISM OF PHOTOTHERMAL EFFECT FOR POLYMER BASED MATERIALS IN SOLAR VAPOR GENERATION

In solar evaporation devices, photothermal materials and thermal-insulating and water-transporting materials are essential components. These materials' properties largely determine the efficacy of solar evaporation. For solar absorber design, strong light absorption across the entire solar spectrum range of 0.3 to 2.5 μm, as well as high light-to-heat conversion efficiency, are of equal importance, whereas for substrate material design, thermal insulation and water transport properties are desired. There are three types of photothermal mechanisms involved in SVG plasmonic localized heating, electron-hole generation and relaxation, and thermal vibration of molecules as illustrated in Fig.1. In general, one type of photothermal material uses a single mechanism to convert light to heat. In some instances, however in a specific photothermal material, one or more of these photothermal mechanisms can convert light into heat. Here, the emphasis is on polymeric materials with a photothermal mechanism based on the thermal vibration of molecules. Under irradiation, the photothermal effect has been observed in organic materials (such as polymers) [17] that convert incident light into thermal energy. A photothermal process is a direct conversion of solar light that can achieve the highest possible energy conversion efficiency in comparison to other solar energy utilization technologies.

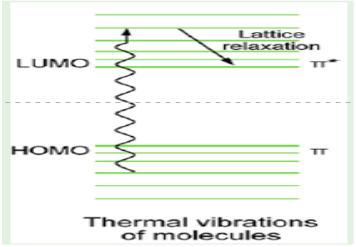

Fig.1. Thermal vibration of molecules of the photothermal effect [18]

When incident light energy matches the electronic transition energies in molecules, loosely held electrons can be excited from the ground state to higher-energy orbitals. Under irradiation, for instance, the electron can transition from the highest occupied molecular orbital (HOMO) to the lowest unoccupied molecular orbital (LUMO). The photoexcited electrons then return to

https://doi.org/10.31436/iiumecp.v1i1.3012

their ground state via electron-vibration coupling, causing molecules to generate heat. Due to their abundant conjugated π bonds, which can facilitate electron excitation from π to π* orbitals even with low irradiation energy, carbonaceous and certain polymeric materials (typically black polymers) [18] with strong light absorption can convert solar energy into thermal energy through the thermal vibration mechanism. In addition, the energy disparity between the LUMO and HOMO can become lower as the number of π bonds rises. Polymers have utility in solar evaporation applications due to their high light absorption across a broad spectrum of wavelengths, relatively low cost, and stability as solar absorbers for high-efficiency solar evaporation, such as polypyrrole (PPy) [8], PEGDA-polyaniline (PANi) [19], polyvinyl alcohol (PVA), and chitosan/PPy[20] have recently been utilized. However, their selection is more limited if compared to carbon materials. Polymers, particularly polymer hydrogels, possess a number of advantageous properties, such as the ability to bind with water to facilitate evaporation.

3. STRATEGIES TO INFLUENCE THE THERMAL BEHAVIOR IN HYDROGELS POLYMER FOR HIGH EFFICIENCY IN SOLAR VAPOR GENERATION

Water evaporation and thermal insulation are commonly regarded as two fundamental roles that the substrate must accomplish. Efficient water transport and evaporation need the presence of both excellent wetting qualities and continuous routes. Enhanced thermal insulation can be achieved through the utilization of materials with low heat conductivity and porous architectures. The pore structure has a significant role in facilitating water transport and thermal insulation. It is important to find a balance between effective water transport, which necessitates water-filled holes, and thermal insulation, which requires air-filled pores. Hydrogel materials, characterized by their hydrophilic nature, porous structure, and thermal insulation properties, have been extensively studied in accordance with established criteria. The objective of these investigations is to enhance water transport capabilities and optimize heat management, hence rendering hydrogels suitable as substrates for solar evaporation. PVA and chitosan hydrogels demonstrate remarkable hydrophilicity, low thermal conductivity, and ample hierarchical porosity, hence ensuring adequate water transport/evaporation and appropriate heat management capabilities for solar evaporation. [20] For the occurrence of evaporation at the interface between liquid and vapor, the material must possess certain properties based on the principle of heat localization. These properties include a high capacity for absorbing solar radiation in the volumetric range, low thermal conductivity, the ability to float on the liquid surface, and the capability for continuous or rapid fluid transport to the liquid-vapor interface. A considerable body of research has been dedicated to the advancement of hydrogel materials in conjunction with photothermal materials, mostly from a theoretical perspective. In the context of thermal structure design, the fundamental ideas revolve around the minimization of heat loss and the optimization of heat concentration on the evaporative surface. This section will examine a few main strategies employed in material and structural engineering to enhance the evaporation performance.

3.1. Photothermal materials

Materials employed as light absorbers must have the crucial attribute of strong absorption in the solar spectrum for solar heat localization, allowing the hydrogel to be integrated with the SVG system. The chosen material must be efficient in absorbing light across the full range of the solar spectrum, which is roughly 300 nm to 2500 nm, as illustrated in Fig. 2 [21] When photothermal material incorporated to other polymer material it may resulted with improvement across solar spectral irradiation wavelength due to the chemical interaction

https://doi.org/10.31436/iiumecp.v1i1.3012

between two materials. In an investigation examining the influence of polyaniline (PANi) on chitosan, the study successfully observed the structural, conductivity, and dielectric properties of chitosan [22]. The protonation of chitosan material was achieved through the acid-induced protonic doping effect of PANi within the chitosan structure, as depicted in Fig. 3. Fig 4 illustrates the depiction of the protonation process involving two forms of polyaniline (PANi), respectively emeraldine base (EB) and emeraldine salt (ES). Basically, emeraldine is considered to be a comparatively more stable form of PANi, which may occur in two distinct forms: emeraldine base (neutral), characterized by its insulating properties, and emeraldine salt, which exhibits conductivity due to the protonation of its imine nitrogen through the process of doping with acids.[23] When acid is introduced to the PANi, protons (H+) from the acid start to attached to the nitrogen-hydrogen (NH bonds) in the polymer chains. This protonation makes the nitrogen atom to become positively charge, which is known as polaronic sites. It acts as a carrier in the polymer, it can accept and donate electrons which allowing the movement of electric charge within the materials, i.e., the movement of proton along the NH bonds or called electron hopping. Through this additional charge carrier via protonic doping, it furthered increase the electrical conductivity of chitosan with incorporation of PANi. The result of the PANi doping in chitosan can be seen in Fig. 5 where the incorporation resulted with 551 nm peak in visible range of solar spectral due to the polaron formation. This optical energy is due to the Pi-to-Pi star transition from the valence band to the conduction band at 389 nm due to the common doped state of PANi.

Table 1: Proposed hydrogel polymer with photothermal materials for SVG applications

Hydrogel type and Photothermal Material	**Structure Design**	**Evaporation Rate**	**Evaporation Efficiency, %**	**Advantages for SVG applications**	**Reference**
Pegda hydrogel and Polyaniline	Cellulose-wrapped EPE foam with 2D water supply via capillary force	1.40 $kg\ m^{-1}h^{-1}$ under 1 sun illumination	91.5	Strong light absorption, layered structures design, 2D water transport	Yin et al. (2018)
PVA hydrogel and Polypyrrole	Buoyancy by tuning density and porosity by the molecular mesh	3.2 $kg\ m^{-1}h^{-1}$ under 1 sun illumination	94	Direct contact with water, improving water diffusion without layered, facile synthesis	Zhao et al. (2018)
Chitosan hydrogel Carbon dots	Buoyancy via porous network	1.4 $kg\ m^{-1}h^{-1}$ under 1 sun illumination	89	Broadband absorption, lightweight	Singh et al. (2019)
PVA, Chitosan hydrogel with Polypyrrole	Buoyancy by tuning density and porosity by the molecular mesh	3.6 $kg\ m^{-1}h^{-1}$ under 1 sun illumination	92	Water transport rate efficiency via porosity, facile synthesis, temperature management via porosity	X. Zhao et al. (2019)
Chitosan hydrogel with Molybdenum Carbide/Carbon-Based	Buoyancy by tuning density and porosity by the molecular mesh	2.19 $kg\ m^{-1}h^{-1}$ under 1 sun illumination	96.15	Broadband absorption, facile synthesis	Yu et al. (2020)
PVA, chitosan hydrogel with CNP	PVC foam and cotton wipe	2.28 $kg\ m^{-1}h^{-1}$ under 1 sun illumination	66.7	Broadband absorption, layered structure, 2D water transport	Zhu et al. (2022)

https://doi.org/10.31436/iiumecp.v1i1.3012

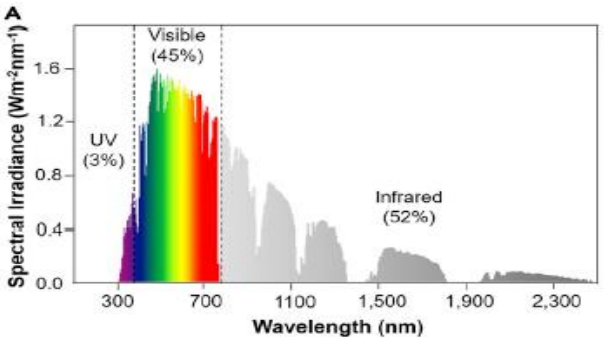

Fig.2. Solar spectral irradiation across a wavelength range of 300 nm to 2.5 mm [21]

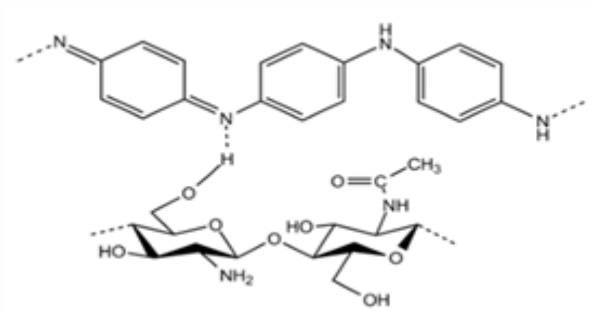

Fig.3. Schematic for PANi-chitosan interaction [22]

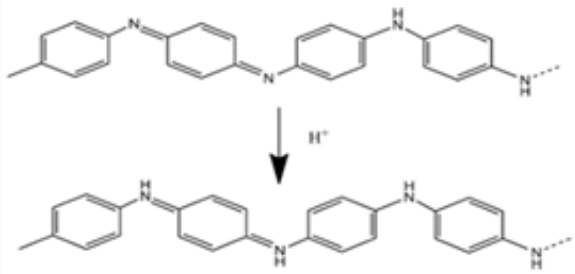

Fig.4. Protonation of emeraldine base to emeraldine salt upon acid introduction [22]

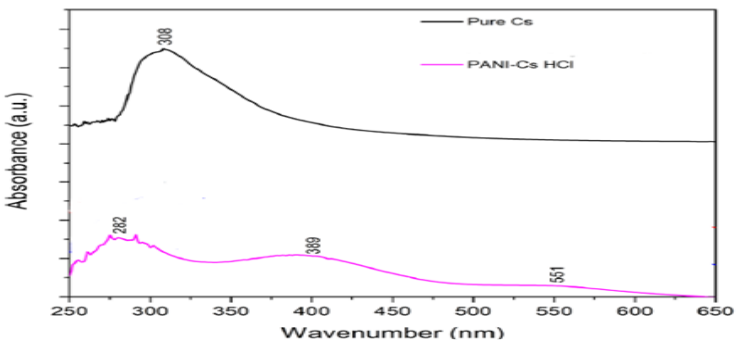

Fig.5. UV-VIS absorbance spectra of chitosan and PANi-chitosan sample with acid dopant [22]

Furthermore, when photothermal materials are added to the other material, it will produce a significant difference in physical observation. The observation of Fig.6 reveals the investigation of the integration of PANi into a hydrogel composed of poly (ethylene glycol) diacrylate (PEGDA). The hydrogel exhibits a noticeable visual transformation, transitioning

https://doi.org/10.31436/iiumecp.v1i1.3012

from a transparent state with invisible porous to a darkened appearance with rich in porosity upon the inclusion of PANi. This change of color is due to the absorption of molecular or delocalization Pi electron in conductive PANi.[19] Based on this discovery, it can be inferred that the integration of a solar absorber into a hydrogel polymer enhances the mechanical stability of the hydrogel. This is evident from the presence of a well-developed macroporous structure in the hydrogel containing PANi. The hydrogel's porous structure is recognized for its robustness, resembling that of a sponge. Also, this characteristic allows for efficient water absorption, hence potentially enhancing the water transport rate in SVG.[24] The combination of these materials also showing a high light absorption in visible range as shown in Table 2, as hydrogel with rough and porous surface naturally traps light, which cuts down on repeated scattering and reflection. PEGDA-PANi hydrogel also recorded a high SVG efficiency of 91.5% with 1.40 $kg\,m^{-1}h^{-1}$ water transport, under 1 sun illumination making it a suitable candidate for SVG design.

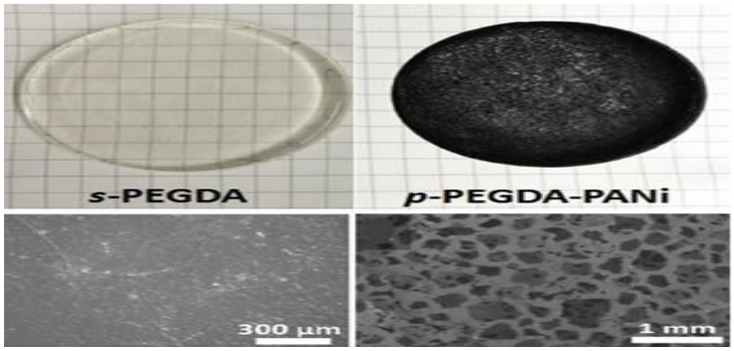

Fig. 6. Representative of hydrogel with and without the incorporation of solar absorber [19]

Table 2: Proportion of light absorption in different spectral regions of solid-PEGDA and PEGDA-PANi [19]

Sample	Total absorption	UV (< 400 nm)	Visible (400-700 nm)	NIR (700-2500 nm)
Solar Spectrum	100%	5.40%	54.7%	39.90%
s-PEGDA	32.61%	4.25%	17.29%	11.07%
PEGDA-PANi	98.48%	5.22%	54.02%	39.24%

3.2. Tuning density of hydrophilic polymer

Tuning density refers to quantifying chemical connections that connect polymer chains, subsequently influencing thermal vibration. Typically, an increase in density results in a hydrogel that exhibits greater stiffness due to a decrease in chain mobility, leading to a reduction in thermal vibration. The work conducted by Zhao et al. [8] demonstrates that altering the ratio of polymer density has a discernible impact on the structural characteristics of hydrogels as shown in Fig.7, where the hydrogel porosity changes with different amount of ratio. The efficiency of localized heating on the hydrogel surface is dependent upon the size and shape of the hydrogel. When the hydrogel polymer porosity does not have homogenous porosity, it will interfere with the temperature distribution on the hydrogel surface. The ineffective localization of the hydrogel surface has the potential to decrease the thermal

https://doi.org/10.31436/iiumecp.v1i1.3012

conductivity of the material, resulting in reduced heat loss to the bulk water and its surrounding environment. X.Zhao et al. [20] improved their hydrogel by changing the ratio of their hydrophilic polymer of PVA and chitosan with water content, which resulted with altered internal gaps within the hydrogel as depicted in Fig.8. The internal gaps within hydrogel may efficiently transport water to the hydrogel surface in timely manner.[24] However, the hydrophilic polymer of PVA/chitosan with highest concentration resulted in the highest saturated water content, as depicted in Fig.9. This highest amount of water saturation with the highest concentration of hydrophilic polymer results in a higher demand for energy during the process of water heating, thereby diminishing the part of usable energy that can be utilized for water vaporization. Although the enthalpy of vaporization is relatively low, the presence of a high level of saturated water content hinders energy utilization and restricts the rate of SVG. In essence, the reason the hydrogel with the highest concentration does not have the highest evaporation rate is due to the continual presence of highly saturated water within the polymer networks, which keeps the internal gaps moistened and heats the water instead. Therefore, from this observation it can be inferred that achieving a balance between the volume and concentration of hydrophilic polymer is essential for increasing the rate of water evaporation. It can be seen in Fig. 10 by tuning the density of hydrophilic polymer, resulted with localize heating in the middle of hydrogel surface, and the bulk water temperature remain low and stabilize within 1 hour period, as an indicator of efficient temperature distribution within the hydrogel network.

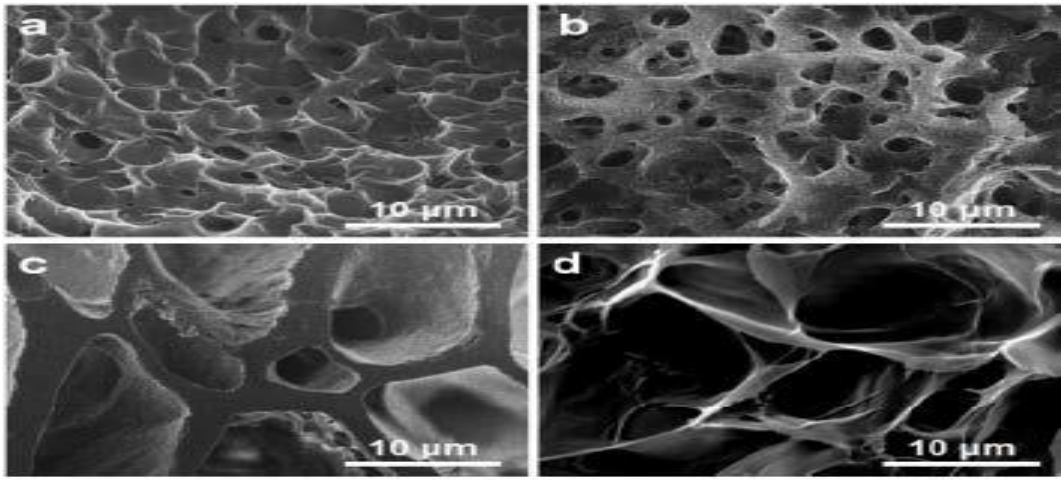

Fig. 7. Porous structure different shape with different ratio of PVA and ppy[8]

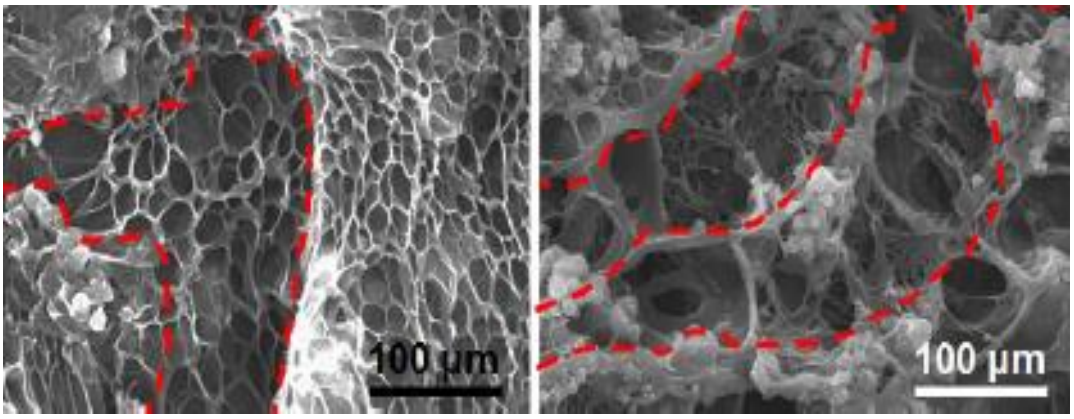

Fig. 8. Internal gaps within hydrogel after tuning the density of hydrophilic polymer [20]

https://doi.org/10.31436/iiumecp.v1i1.3012

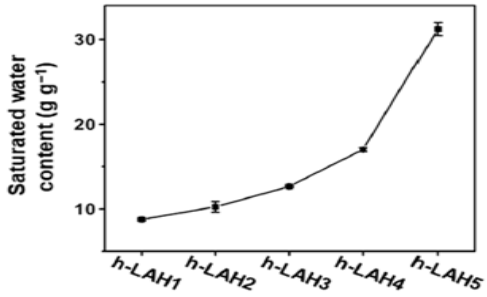

Fig. 9. Saturated water content with different concentration of hydrophilic polymer [20]

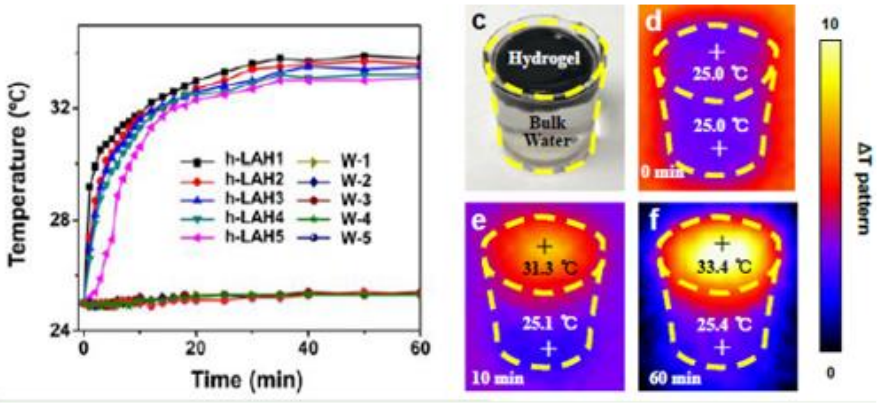

Fig.10. Low temperature to the bulk water and effective localize heating at the hydrogel surface [20]

3.3 Thermal conduction via structural design

Hydrogel is known to have higher density than water, therefore, in new SVG design it is necessary for the hydrogel to be able to float in water surface as opposed to traditional evaporation design where the absorber is immersed in the water.[8] Hence, in order to enable the hydrogel's buoyancy, researchers proposed the integration of an insulator material to regulate the heat conductivity of the SVG design. This approach also serves to provide structural support for the hydrogel, which functions as a light absorber and is positioned atop the structural design. As demonstrate in Fig. 11, Yin et al. [19] proposed a design that consist of the cellulose-wrapped expanded polyethylene (EPE) foam, which serves as thermal insulation and also as water supply between the hydrogel and the bulk water. By placing EPE foam around the hydrogel material, it acts as a thermal barrier, minimizing heat transfer to the surroundings and maintaining a higher temperature within the system. This insulation helps improve the overall energy efficiency of the system by reducing heat losses during the vapor generation process that resulted with 91.5% solar thermal efficiency. Another simple design proposed by Zhu et al. [15] as illustrated in Fig. 12, where the design is composed of polyvinyl chloride (PVC) foam as heat insulation in the bottom layer and then a cotton wipe is act as water pipe between hydrogel and bulk water, which the water will be transfer from PVC surrounded to the cotton and then absorbed by the hydrogel, this design resulted with 66.7% solar thermal efficiency.

https://doi.org/10.31436/iiumecp.v1i1.3012

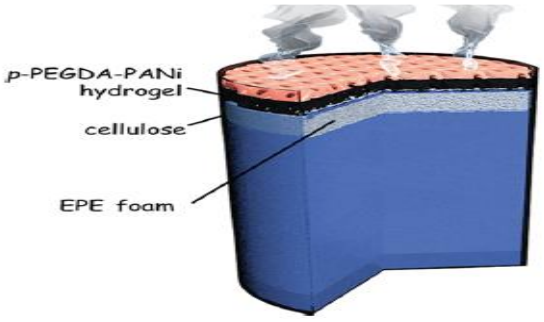

Fig. 11. Structural design using EPE foam and Cellulose with hydrogel [19]

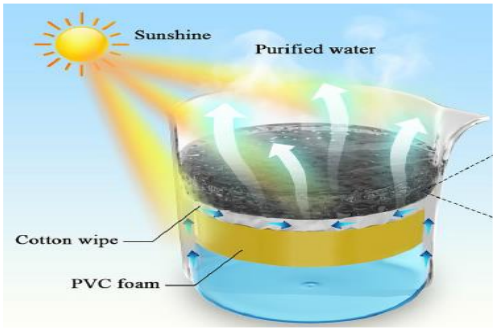

Fig. 12. Structural design using PVC foam and cotton wipe with hydrogel [15]

4. CONCLUSION

This review article has provided a brief summary of a few strategies in hydrogel polymer with SVG. It discusses three primary strategies that have significantly enhanced the efficiency of SVGs through the utilization of hydrogel polymers. These strategies include the careful selection of solar absorber materials, the optimization of hydrophilic polymer properties to improve temperature management, and the incorporation of hydrogel into the SVG design. Hydrogel polymer possess a significant benefit in terms of water purification and water transport. The optimization of light absorption strategies to enhance the compatibility between SVG and hydrogel materials, resulting in improved water delivery and solar energy utilization efficiency, holds significant promise for future societal benefits. These approaches are characterized by their simplicity, cost-effectiveness, and ability to achieve higher water rates. As a result, the integration of these two technologies facilitates the effective utilization of solar energy, presenting a feasible and enduring solution to mitigate the challenge of limited energy resources. Furthermore, the intricate nature of hydrogel polymers allows them to serve as a medium for harnessing solar energy. Additionally, they can function as an external control mechanism for manipulating temperature, particularly when combined with various unexplored materials. Notably, the morphology of hydrogel polymers exhibits promising characteristics that undergo changes when impregnated with others emerging polymer materials, photothermal materials, and different methods of producing the hydrogels. Through the process of further integration with diverse other materials and new structural designs, the functionalized hydrogel polymer that exhibits synergistic properties demonstrates the potential to perform many functions tailored to water transport and water purification applications.

ACKNOWLEDGEMENT

This research was funded by a grant from the Ministry of Higher Education of Malaysia (FRGS Grant FRGS/22-259-0868/UIAM). The authors also would like to express an appreciation thanks to the International Islamic University Malaysia and, Majlis Amanah Rakyat (MARA) for their technical and financial support.

REFERENCES

[1] Schewe, J., Heinke, J., Gerten, D., Haddeland, I., Arnell, N. W., Clark, D. B., Dankers, R., Eisner, S., Fekete, B. M., Colón-González, F. J., Gosling, S. N., Kim, H., Liu, X., Masaki, Y., Portmann, F. T., Satoh, Y., Stacke, T., Tang, Q., Wada, (2014). Multimodel assessment of water scarcity under climate change. Proceedings of the National Academy of Sciences of the United States of America, 111(9), 3245–3250

[2] Green, T. R., Taniguchi, M., Kooi, H., Gurdak, J. J., Allen, D. M., Hiscock, K. M., Treidel, H., & Aureli, A. (2011). Beneath the surface of global change: Impacts of climate change on groundwater. Journal of Hydrology, 405(3-4), 532-560. https://doi.org/10.1016/j.jhydrol.2011.05.002

[3] Buros, O. K. (2000). The ABCs of desalting (p. 30). Topsfield, MA: International Desalination Association.

[4] M. El Haj Assad, M. Nooman AlMallahi, M. A. Abdelsalam, M. AlShabi and W. N. AlMallahi, "Desalination Technologies: Overview," 2022 Advances in Science and Engineering Technology International Conferences (ASET), Dubai, United Arab Emirates, 2022, pp. 1-4, doi: 10.1109/ASET53988.2022.9734991.

[5] Ahmed, E. M. (2015). Hydrogel: Preparation, characterization, and applications: A review. Journal of Advanced Research, 6(2), 105-121. https://doi.org/10.1016/j.jare.2013.07.006

[6] Ozay, Ozgur & Aktas, Nahit & Sahiner, Nurettin. (2011). Hydrogels as a Potential Chromatographic System: Absorption, Speciation, and Separation of Chromium Species from Aqueous Media. Separation Science and Technology. 46. 1450-1461. 10.1080/01496395.2011.560918

[7] Qiblawey, H. M., & Banat, F. (2008). Solar thermal desalination technologies. Desalination, 220(1-3), 633-644. https://doi.org/10.1016/j.desal.2007.01.059

[8] Zhao, F., Zhou, X., Shi, Y. (2018) Highly efficient solar vapour generation via hierarchically nanostructured gels. _Nature Nanotech_ 13, 489–495

[9] Wang J, Li Y, Deng L, Wei N, Weng Y, Dong S, Qi D, Qiu J, Chen X, Wu T. (2017) High-Performance Photothermal Conversion of Narrow-Bandgap Ti2 O3 Nanoparticles. Adv Mater. ;29(3)

[10] Zhou, L., Tan, Y., Wang, J., Xu, W., Yuan, Y., Cai, W., Zhu, S., & Zhu, J. (2016). 3D self-assembly of aluminium nanoparticles for plasmon-enhanced solar desalination. Nature Photonics, 10(6), 393-398. https://doi.org/10.1038/nphoton.2016.75

[11] Ni, George, Gabriel Li, Svetlana V. Boriskina, Hongxia Li, Weilin Yang, TieJun Zhang, and Gang Chen. “Steam Generation Under One Sun Enabled by a Floating Structure with Thermal Concentration.” Nature Energy 1, no. 9 (August 22, 2016): 16126

[12] Kabeel, A., & El-Agouz, S. (2011). Review of researches and developments on solar stills. Desalination, 276(1-3), 1-12. https://doi.org/10.1016/j.desal.2011.03.042

[13] Zhang, C., Yan, C., Xue, Z., Yu, W., Xie, Y., & Wang, T. (2016). Shape-Controlled Synthesis of High-Quality Cu7 S4 Nanocrystals for Efficient Light-Induced Water Evaporation. Small (Weinheim an der Bergstrasse, Germany), 12(38), 5320–5328. https://doi.org/10.1002/smll.201601723

[14] Ye, M., Jia, J., Wu, Z., Qian, C., Chen, R., Sun, W., Dong, Y., & Ozin, G. A. (2017). Synthesis of Black TiOx Nanoparticles by Mg Reduction of TiO2 Nanocrystals and their Application for Solar Water Evaporation. Advanced Energy Materials, 7(4), 1601811. https://doi.org/10.1002/aenm.201601811

[15] Zhu, M., Liu, X., Tian, Y., Caratenuto, A., Chen, F., & Zheng, Y. (2022). Dome-arrayed chitosan/PVA hydrogel-based solar evaporator for steam generation. Scientific Reports, 12(1), 1-8. https://doi.org/10.1038/s41598-022-08589-z

[16] Ghasemi, H., Ni, G., Marconnet, A. M., Loomis, J., Yerci, S., Miljkovic, N., & Chen, G. (2014). Solar steam generation by heat localization. Nature Communications, 5(1), 1-7. https://doi.org/10.1038/ncomms5449

[17] Gao, Zhu, L., Peh, C. K., & Ho, G. W. (2019). Solar absorber material and system designs for photothermal water vaporization towards clean water and energy production. Energy & Environmental Science, 12(3), 841–864. https://doi.org/10.1039/c8ee01146j

[18] Chen, Qiaomei & Pei, Zhiqiang & Xu, Yanshuang & Li, Zhen & Yang, Yang & Wei, Yen & Ji, Yan. (2017). A durable monolithic polymer foam for efficient solar steam generation. Chemical Science. 9. 10.1039/C7SC02967E.

[19] Yin, X., Zhang, Y., Guo, Q., Cai, X., Xiao, J., Ding, Z., & Yang, J. (2018). Macroporous Double-Network Hydrogel for High-Efficiency Solar Steam Generation Under 1 sun Illumination. ACS applied materials & interfaces, 10(13), 10998–11007. https://doi.org/10.1021/acsami.8b01629

[20] Zhou, X., Zhao, F., Guo, Y., Rosenberger, B., & Yu, G. (2019). Architecting highly hydratable polymer networks to tune the water state for solar water purification. Science Advances. https://doi.org/aaw5484

[21] Lewis N. S. (2016). Research opportunities to advance solar energy utilization. Science (New York, N.Y.), 351(6271), aad1920. https://doi.org/10.1126/science.aad1920

[22] Santos, Nicole & Pulido, Maria Teresa & Tumacder, Doebner Von & Taaca, Kathrina Lois. (2021). Effect of Polyaniline on the Structural, Conductivity, and Dielectric Properties of Chitosan. Carbohydrate Polymer Technologies and Applications. 2. 100129. 10.1016/j.carpta.2021.100129.

[23] Goswami, S., Nandy, S., Fortunato, E., & Martins, R. (2022). Polyaniline and its composites engineering: A class of multifunctional smart energy materials. Journal of Solid State Chemistry, 317, 123679. https://doi.org/10.1016/j.jssc.2022.123679

[24] Guo Y, Zhou X, Zhao F, Bae J, Rosenberger B, Yu G. Synergistic Energy Nanoconfinement and Water Activation in Hydrogels for Efficient Solar Water Desalination. ACS Nano. 2019 Jul 23;13(7):7913-7919. doi: 10.1021/acsnano.9b02301